INFLUENCE OF MICROSTRUCTURAL AND LOAD WAVE FORM

CONTROL ON FATIGUE CRACK GROWTH BEHAVIOR OF

PRECIPITATION HARDENING STAINLESS STEELS .

A Dissertation

Presented to

the Faculty of the Graduate School

University of Missouri

In Partial Fulfillment

of the Requirement for the Degree

Doctor of Philosophy

by

Kevin Richard Kondas

July 1976

Dissertation Supervisor   Professor David W. Hoeppner

107475

ACKNOWLEDGEMENT

in pursuing the research effort, thanks are extended to Messers Jack Yahl, Daryl Carpenter, Edward Bruemmer and Arthur Braun.

Finally, the author extends a very special appreciation to his patient wife, Lois, who always believed he would finish and who worked many long hours assembling and proofing this paper.

NOMENCLATURE

a	Crack length, (in or cm)
a_i	Initial crack length, (in or cm)
A_{cl}	Horizontal line; eutectoid reaction, (°F or °C)
a_{cr}	Critical crack length, (in or cm)
a_f	Final crack length (precracking), (in or cm)
a/W	Crack length ratio, or dimensionless crack length, (in/in, or cm/cm)
B	Thickness of specimen, (in or cm)
b	Slope of regression line
C	Compliance or reciprocal of stiffness, (in/lb, or cm/nt) Constant in Paris equation (empirical)
c	Total crack length, (in or cm)
CEB	Dimensionless compliance
COD	Crack opening displacement, also δ, (in or cm)
CT	Compact tension
Da/DN	Crack Growth Rate, also H, (in/cycle, or mm/cycle)
E	Young's modulus, (lb/in^2, or nt/cm^2)
e	Weibull threshold parameter
e_0	Elastic elongation, (in or cm)
EBn/P	Dimensionless compliance, also CLB
F	$\Delta K/K_b$, (ksi/ksi, or MPa/MPa)
$F(a/W)$	K calibration factor, (in/in, or cm/cm)

f   Function

G_I Crack extension force, (lb/in, or nt/cm), also energy release rate (lb-in/in^2, or nt-cm/cm^2) normal to flaw propagation

G_c Critical crack extension force, (ksi or MPa)

H   Da/DN, (in/cycle, or mm/cycle)

H/W   CT specimen heighth to width ratio, (in/in, or cm/cm)

K   Stress intensity, (ksi $\sqrt{in}$, or MPa $\sqrt{m}$)

K_b Final stress intensity for fitting relations, (ksi $\sqrt{in}$, or MPa $\sqrt{m}$)

K_c Critical plane stress fracture toughness, (ksi $\sqrt{in}$, or MPa $\sqrt{m}$)

K_I Plane strain stress intensity, (ksi $\sqrt{in}$, or MPa $\sqrt{m}$)

K_{Ic} Critical plane strain fracture toughness, (ksi $\sqrt{in}$, or MPa $\sqrt{m}$)

K_{max} Maximum stress intensity, (ksi $\sqrt{in}$, or MPa $\sqrt{m}$)

K_{min} Minimum stress intensity, (ksi $\sqrt{in}$, or MPa $\sqrt{m}$)

K_{th} Stress intensity threshold, (ksi $\sqrt{in}$, or MPa $\sqrt{m}$)

k   Weibull parameter for curve shape

ksi   Kilo-pounds per square inch (1 ksi = 6.895 MPa)

LVDT   Linear variable differential transformer

MPa   Mega Pascal, or 10^6 Pascal (unit of pressure or stress)

M   Spring constant, (in/lb, or cm/nt)

m   Empirical Rate exponents

P   Load, (lb or nt)

R	Stress ratio (S_{min}/S_{max}), $(lb/in^2$, or $nt/cm^2)$
r	Sample coefficient of correlation, also R
r*	Risk function
S_{max}	Stress maximum, $(lb/in^2$, or $nt/cm^2)$
S_{min}	Stress minimum, $(lb/in^2$, or $nt/cm^2)$
U	Stored linear strain energy, (in-lb, or cm-nt)
v	Weibull characteristic value for specimen type
w	Weibull parameter, 1/k
WOL	Wedge open loading
Y	Polynomial expression
Δ	Difference; Range; Area of triangle, $(in^2$ or $cm^2)$
δ	COD, deflection of crack opening, (in or cm)
ξ_0	Elliptical parameter, non-dimensional
ϵ	Strain and increments, (in/in, or cm/cm)
$\bar{\epsilon}$	True fracture strain, (in/in, or cm/cm)
ϵ_c	Critical strain, (in/in, or cm/cm)
ϵ_p	Plastic strain, (in/in, or cm/cm)
γ	Surface energy, (lb/in, or dyne/cm)
ρ	Radius of curvature, (in or cm)
μ	Micrometer ($= 10^{-6}$ m)
ν	Poisson's ratio
2σ	Statistical scatter in the vertical direction
$\bar{\sigma}$	Uniformly applied normal stress, $(lb/in^2$, or $nt/cm^2)$

$\bar{\sigma}$ True fracture stress, (lb/in^2, or nt/cm^2)

σ^* Critical value of stress, (lb/in^2, or nt/cm^2)

σ_{ts} Tensile strength,(lb/in^2, or nt/cm^2)

σ_{ys} Yield strength, (lb/in^2, or nt/cm^2)

τ Shear stress, (lb/in^2, or nt/cm^2)

TABLE OF CONTENTS

LIST OF FIGURES

LIST OF TABLES

ABSTRACT

Consumers are recognizing the need for close control in high
performance designs, materials, and structures when operating
within the realm of rational continuum or sharp flaw mechanics.
This is evidenced by the increasing use of Structural Integrity
Technology in advanced high performance designs. In order to
implement a Structural Integrity plan, fundamental understanding of
subcritical crack growth rates is needed. To achieve this, it is
essential to increase the data base accuracy and relate physical
boundary conditions of the fatigue-crack growth process to life
prediction models. The scientific hypothesis and major conclusion
of this work is that microstructure when acted upon by load and
environment determines the fatigue-crack growth rates or life of a
component.

The experimental approach varied the heat treatment of two
precipitation hardening martensitic alloys, 17-4 PH and 15-5 PH.
Fatigue-crack growth data was correlated between materials cycled
under wave forms of 10 Hz sine frequency and trapezoidal one minute
hold-time for different stress range ratios and environments.

The data are represented through four parameters of a unique
functional curve, not a straight line, that precisely applies
mathematical boundary conditions to the physics of the fatigue-
crack growth process. This contemporary Weibull-type mathematical
method has been demonstrated to be applicable to the quantification

of microstructural effects on fatigue-crack growth.

It is the judgment of this author that a key to future advancement of technology utilization of fatigue-crack growth data lies in its application and interpretation for structures in accordance with physical boundary conditions under the operational conditions of interest.

Chapter 1

INTRODUCTION

In recent years, materials' properties and structural design requirements have increased as high performance technology was explored and pursued. Using performance as a standard, materials are being used at their limits not only in strength and toughness, but also in fatigue resistance. Attempts are being made to extend these limits through improved alloying, microstructural control, and quality control. In certain areas, changing materials have given way to a more refined approach that studies component or structural operation, expected life, and maintenance schedule versus its desired material response.

These trends have placed extensive demands upon the designer and materials engineer, for he must know with precision and confidence the factors that describe materials, the operational environments, and the anticipated structural response. Achieving this demand does not lie solely in more thorough data collection techniques, in data reduction processes, or in approaches that advocate only refinement of previous techniques but in recognizing the physics of the event. The reason is that neither materials' properties nor operational environments are presently subject to unique description. These factors must be quantized as a function of the physical interactions limiting structural life. The import of this approach can be considered pro-

portional to the structure's mission, risk, and cost.

As a consequence of the probabilistic nature of materials and operational environments, a new design philosophy has been cultivated. Through a natural progression of events, (e.g. structural in-operability, failures, and performance derating) a limited number of people have become advocates of a philosophy termed Structural Integrity to produce a needed engineering capability for extending or assuring design life. The uniqueness of this approach lies in combining established disciplines such as statistics, stress analysis, material science and fracture mechanics, to produce this capability. The combination will benefit certain disciplines more than others depending upon the situation, however, the resultant capability of Structural Integrity is the main concern.

There are several objectives of this work which evaluates the interaction of metallurgy, stress range, flaw type, load profile, and environment under fatigue-crack propagation testing of precipitation hardened (PH) stainless steels. Testing these alloys under various conditions, may provide immediate application of Structural Integrity to the U.S. Navy high performance hydrofoil program, PHM, where major structural elements are fabricated from these materials (Bauman, 1974).

Chapter 2

OBJECTIVE

This study was directed toward achieving the following specific
technical objectives:

i. To evaluate the effect of fatigue-crack growth behavior
of two precipitation hardened (PH) stainless steels (i.e.
17-4 and 15-5) in two different heat treated conditions
(i.e. H 1050 and H 1100 conditions.)

ii. To explore the effect of wave form in terms of increasing
or decreasing the rate of fatigue-crack growth.
Prime importance will be placed on the hold-time at maxi-
mum load.

iii. To determine environmental effects when combined with wave
form under hold-time conditions.

iv. To consider the effects of stress range ratio with specific
regard to internal residual stresses.

v. To provide an approach and data to observe if traditional
methods for fatigue-crack growth testing that have con-
sidered the influence of operational load time profiles are
capable of describing component life, maintenance, or mor-
tality time frame.

As indicated, the primary materials in this study are 17-4 PH
and 15-5 PH stainless steels. They are used in a high strength
salt water application. Both base materials will be studied over a

3

narrow yield strength level as controlled by the final heat treatments. The program was formulated around the concepts of fracture mechanics using a modified compact tension specimen called a wedge open loading (WOL) test specimen of type I design (i.e. load normal to crack growth.)

It is anticipated that through this program the following achievements can be realized:

(a). Provide a satisfactory technical rationale for critical resolution of the effect of environment, wave form, stress ratio, and material condition on fatigue-crack growth of 17-4 PH and 15-5 PH stainless steels.

(b). Close control and observation of microstructures, multi-laboratory data acquisition, and a contemporary procedure for fatigue-crack growth data reduction may provide a more decisive mechanism in describing and relating microstructural response to service applications.

(c). Determine the feasibility, through physically definable data reduction and fractography, of a technique for assessing a metals' ability for stress relaxation in fatigue-crack growth tests or field operational applications.

Chapter 3

TECHNICAL DISCUSSION

3.1 HISTORICAL REVIEW OF FRACTURE MECHANICS

Considering fracture mechanics as a function of crack behavior, metal damage can be partitioned into three selected areas (Hoeppner, Fall 1975):

1. initiation

2. acceleration

3. unstable crack growth

Traditionally, each of these areas has been studied independently even though all areas may be present during a single physical event. Depending upon the situation, fracture initiation may carry the main import of crack growth. Assuming this is appropriate, the first outgrowth could represent total failure, however, in other situations this is not the case. A succinct overview of these areas is warranted considering their interpretation and interaction.

3.1.1 Flaw Initiation

Usually fracturing begins from a small discontinuity in what is considered a homogeneous, continuous material. The imperfection, termed defect, flaw, inclusion, or void, can be found throughout a structure and will initiate fracture if a complex combination of factors, not as yet fully understood, exist. These factors include size and shape of the imperfection, local stress and strain fields,

micro- and macroscopic material characteristics, component load history, and environment. These factors may be evaluated for the simple case but one must consider the controlling element, fracture criterion. This criterion is the road map for overall consideration of individual factors that predicate when fracture will occur. For a simple case, the most widely known criterion is that put forth by A. A. Griffith (1921). His realization that strain energy in a cracked brittle plate decreases as the crack grows has promulgated most of the modern work in fracture. The resulting relationship between increased energy associated with the generation of new crack surfaces and decrease of input strain energy has been developed into functional form and applied to complex situations that can predict final metal failure beyond that of basic brittle materials. Aware that an energy transfer and balance exists, the factors affecting the rate of crack development or crack acceleration must be considered.

2.1.2 Acceleration

As a crack begins to grow through the material its growth rate becomes important. If the controlling microstructural parameters provide resistance to crack growth, the crack acceleration may be low enough so that operational equipment could be maintained over its design lifetime. However, if crack extension occurs by bursting through preferred microstructure paths in the material, then the potential decrease in component life must be considered. How these

accelerations interface in fatigue loading and crack growth rates requires knowledge of events after initiation of fracture (Hoeppner, 1973-1976) and recognition of impact to life prediction and time to terminal or unstable fracture.

3.1.3 Unstable Crack Growth

As crack growth instability occurs there is an acceleration to a constant velocity that is controlled by the material's inherent ability to absorb strain. In materials with a high propensity toward cleavage, a less energetic fracture process, the velocity is approximately equal to one-third of the dilatational wave velocity (5000 ft/sec or 1524 m/sec) (Swedlow, 1922). The importance of the speed of unstable crack propagation can be seen in the difference between static and dynamic (steady state) stress fields as applied to "crack arrestor" design in wings, fuselages, tanks, and piping systems.

3.2 FRACTURE CRITERION

As a composite of loads are placed on a specimen, a component with a small flaw, for example, fracture may begin. Assuming it has initiated and a definition of initiation has been agreed upon, Griffith considered two questions:

1) What type of mathematical model of the event can be applied?

2) What defines the critical load that made the fracture begin for a simple model material?

3.2.1 Griffith Model

Griffith's mathematical model was required to describe a physical situation by way of providing necessary information and be in a form such that analytical techniques could be applied to the model. Besides geometry and loading parameters, other factors that deserved consideration were material characteristics such as metallurgy versus elastic values, residual stress, load history, and environment (Hoeppner et al, 1974). However, the abundance of physical factors met with limited analytical techniques such as dislocation theory, plasticity, elasticity, finite elements and statistics. Even though elasticity does not consider chemical composition, heat treat or environment, the continuum viewpoint which was most familiar was to be the basis of the model in spite of idealization.

The Griffith model was a flat plate of linearly elastic, isotropic, homogeneous material that followed the relationships of classical elastomechanics. An infinitely long and wide plate containing a crack 2a long through its thickness was selected. Its stress and strain fields were considered invariant with respect to thickness constraint. The perimeter of the plate was equipollently stressed.

3.2.2 Interpretation

Since the flaw has been represented by a perfectly sharp crack, fracturing was considered a linear extension of the crack, i.e. 2a to 2(a + $\cdot$a). The condition for extension could have been a value of

stress as identified by maximum shear or octahedral shear or some limit of strain. However, these parameters were not applicable due to the stress field's position with respect to the crack tip (Swedlow, 1972).

In lieu of setting governing parameters in a spurious manner a key physical factor and necessary condition was conservation of energy. The function, as previously stated, maintains a balance of relative energy change between new surface energy and strain energy for a crack incremental extension. As applied to this model the condition has become known as Griffith's criterion for brittle fracture (Griffith, 1921).

Griffith's work is based on three salient points, definition of stress field at the crack, mode of crack growth, and criterion. The first element is extracted from the work of Inglis (1913) where he computed the stresses in a plate with an elliptically shaped hole. The describing equation with foci of the ellipse on the x-axis at $x = \pm a$ is:

$$\frac{x^2}{(a \cosh \zeta_0)^2} + \frac{y^2}{(a \sinh \zeta_0)^2} = 1 \qquad (1)$$

where ζ_0 is a non-negative parameter that when approaching zero, shrinks the ellipse to a line length 2a along the x-axis. Succinctly, Inglis found the stress field for various loadings; he located the highest stress at the end of the major x-axis. The stress was approximated by applied stress $\bar{\sigma}$ times $2\sqrt{a/\rho}$, where ρ the radius of curva-

ture is expressed as

$$\rho = a \sinh \xi_0 \tanh \xi_0 \qquad (2)$$

For a crack, as ξ_0 goes to zero all components of stress have magnitudes inversely proportional to the square root of the distance from the crack tip. This characteristic stress is either infinite or singular and the strain is similar as calculated by linear elasticity. At the crack tip, the displacements are bounded (Williams, 1957). Thus, limiting factors of stress or strain as fracture criteria were inappropriate for this model.

The potential strain energy due to a crack is mathematically integrable, thus a finite quantity directly proportional to $(a^2 \sigma^2 / E)$, per unit plate thickness. Computing the total potential energy of the cracked plate Griffith added a factor $4a\gamma$ where γ equals surface energy. Assuming fracture was attributed to crack extension the total energy was to remain unchanged. The result is a critical value of $\bar{\sigma}$ designated by σ^* and given by:

$$\sigma^* = \left(\frac{2E\gamma}{\pi a (1-\sigma^2)} \right)^{1/2} \qquad (3)$$

for plane strain

$$\sigma^* = \left(\frac{2E\gamma}{\pi a} \right)^{1/2} \qquad (4)$$

for plane stress

Griffith's criterion predicts a relationship between critical stress, geometry, and elastic properties of an idealized plate. It

can be stated that $\sigma^* \sqrt{a}$ is equal to a me··· ·, constant.

As Griffith's criterion was developed and derived from work with glass as a model material it was promoted later for application to more common engineering materials. A discrepancy was observed when under restrictive conditions the value $\sigma^* \sqrt{a}$ was not close to a constant. It was hypothesized that creation of new surfaces was not a total representation of energy interchange for elastic strain energy an aspect Griffith recognized as a physical reality that would have to be considered. Traditionally, Orowan (1952) and Irwin (1948) are credited with amending Griffith's original formula to reflect plasticity conditions. Their modification attempts to account for plastic strain energy and flow at the crack tip absorbing or dissipating some potential energy. The amended formula can be stated as:

$$\sigma^* = \left(\frac{EG_{Ic}}{\pi a(1-\nu^2)} \right)^{1/2} \tag{5}$$

where G_{Ic} (1 is the opening mode normal to crack) is an energy release rate with crack extension, replacing 2_γ and measured directly from a fracture test. Presently, there are approximate solutions for the energy dissipation due to crack tip plasticity, but because all microstructural variables and physical fracture processes are not uniquely described, exact solutions considering material compatibility and equilibrium conditions are not available (Hoeppner, 1973-1976).

3.2.3 Stress Intensity Consideration

Basic equations of linear elastic fracture mechanics relate G_{Ic} to the elastic stress and flaw size conditions necessary for fracture. These equations are utilized in the practical sense only for the case of plane strain, because of strong dependence of G_{Ic} on specimen dimensions and materials' properties. For plane strain, as noted by Irwin and others, G_{Ic} is related to the critical stress intensity factor K_{Ic} by $K_{Ic}^2 = G_{Ic}E$ where E is Young's Modulus (Judy, 1972). Using a simple model from previous publications of Inglis (1913) and Williams (1957), and deleting crack-tip plasticity effects, Irwin was able to analyze the stress state at a point remote from the crack tip (Figure 1). In these relations, K_1 is proportional to $\sigma\sqrt{a}$; with all other components of the equations pertaining to geometry. It is important to notice that the stress intensity factors are not dependent on the coordinates, r and 0; hence they control the intensity of the stress fields and reflect the redistribution of stress in a body due to a crack. Thus, K_I is a measure of intensity of stress singularity, deduced from an appropriate analysis of the local elastic stress fields (Williams, 1957), and it has nothing whatever to do with fracture of materials per se. Simply stated, the Griffith-Irwin work defines an equation relating stress intensity, K, flaw size, a, and applied stress, S:

$$K = S \sqrt{a\pi} \, C \tag{6}$$

Figure 1   Model and Equations for Describing the Stress Field near the Crack Tip in a Body. In these equations the relation $K \sim \sigma\sqrt{a}$ is obvious; all other parts of the equation pertain to geometry.
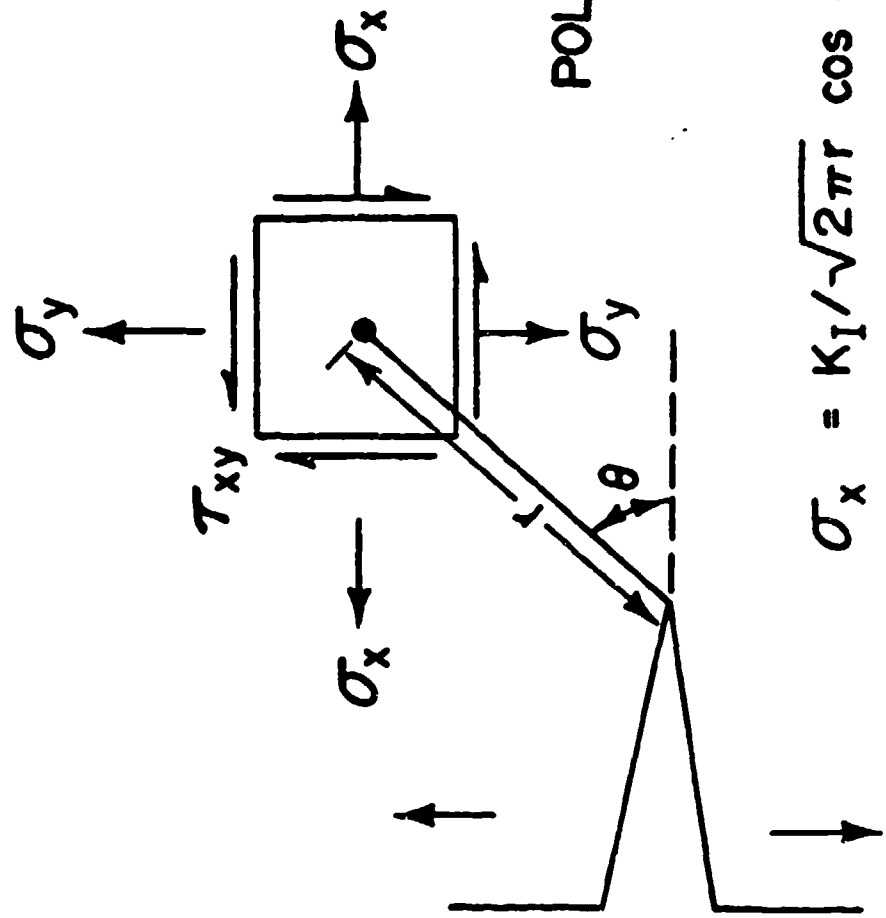
POLAR COORDINATES

$$\sigma_x = K_I / \sqrt{2\pi r} \; \cos \theta/2 \; (1 - \sin \theta/2 \; \sin 3\theta/2)$$

$$\sigma_y = K_I / \sqrt{2\pi r} \; \cos \theta/2 \; (1 + \sin \theta/2 \; \sin 3\theta/2)$$

$$\tau_{xy} = K_I / \sqrt{2\pi r} \; \sin \theta/2 \; (\cos \theta/2 \; \cos 3\theta/2)$$

where C considers geometry, plasticity approximations and other effects (Hoeppner, Fall 1975).

However, critical values of K describe characteristics of material. For brittle materials, the point in the energy balance system, proposed by Griffith, where the onset of crack extension is reached is a point, G_{Ic}. The same point, described by critical stress intensity, K_{Ic}, has specific meaning in that it is a material property measuring propensity of a specific material to fracture. It is considered an invariant quantity within reasonable limits. Similarly, G_{Ic} is a material property. However, applied G and K connote totally different ideas. The term that describes available energy is G where the term describing stress state is K. The two terms are then related only at points where crack extension takes place and both apply only for initiation of cracking.

3.2.4 Fracture Mechanics to Fatigue

It is beneficial to summarize certain factors that encompass the field of fracture mechanics and their use in achieving the capabilities of Structural Integrity.

In a flawed or cracked material an evaluation of the flaw tolerance (i.e. fracture toughness) is required. An analysis of stress state for the loading condition, nature of crack growth, and fracture criterion must be considered if performance or life prediction are desired. Stress analysis, and particularly stress intensity factors, are evaluated generally by either analytical and/or numerical methods

(Paris et al, 1965).

After obtaining a suitable representation of K_I, its critical value K_{Ic} must be determined. Unlike Griffith's work, where $\sigma*\sqrt{a}$ and $\sqrt{E\gamma}$ were measured independently, K_{Ic} is identified for most engineering materials by a prescribed fracture test. The reason is that G_{Ic} cannot be measured independently as Griffith had done for γ.

Obtaining a material's fracture toughness value permits a distinct application in design. If design stresses can be accurately determined for the structural material application then calculation of the largest tolerable flaw size can be established. Inspection to verify that no flaws larger than this size would exist frequently becomes very necessary and difficult. Conversely, the minimum inspectable flaw size can be used to set the allowable load limits for the structure. It would be ideal if flaws in structures could be detected prior to ultimate failure, however, this is not always the case. An arbitrary division of the three toughness regions with their associated functional failure modes are cited below:

	Failure Mode	Toughness Region
a.	Overload, plastic yielding	Plastic
b.	Yielding before break	Elastic-Plastic
c.	Brittle fracture	Plane Strain

The respective consequences, dependent on application, could be:

a. Maintenance, repair and overhaul

b. Environmental contamination, possible structural loss

c. Human disaster, catastrophic failure

In many designs the probable failure mode is secondary to the number of cycles to failure, however, it does control the severity of failure and remains the primary factor in assuring failure-safe design.

Crack or fracture toughness is definitely a material property used to evaluate structural integrity of a material providing mode of crack growth and Griffith's concept is applicable. Due to inconsistencies in internal microstructure, deviations from the expected have occurred. Because engineering materials are often non-glass like and G_{Ic} cannot be measured independently, much work has been directed to repeating Griffith's analysis for materials that are not perfectly elastic, brittle bodies. It is preferable to describe fracture or crack toughness in terms of diverse energy spreading mechanisms with accompanying geometry and loading. Progress to this goal has been slow due to limited analytical methods, however, many achievements have been attained due to precise interpretation of experimental results.

Knowing the final fracture condition with its attendant parameters is important in identifying the mortality of a structure. However, pursuing a positive aspect, establishing the nature of crack growth provides information with respect to maintenance cycles thus, extending time to component wear out (Freudenthal, December 1973 and Hoeppner, 1973-1976). This study on 17-4 PH and 15-5 PH is concerned primarily with this point as it explores crack growth under a loading condition termed fatigue.

3.3 FATIGUE

The fatigue failure process is discussed throughout this section to develop the concept of fatigue-crack growth. Fatigue failure occurs when a material is subjected to repeated applied cyclic force. However, fracturing is produced by a force-amplitude that is far below the force associated with fracture under a single load application. This amplitude decreases with increasing number of repetitions. If the number is relatively large, fracture occurs well within the range of stresses and deformations that can be considered elastic on a "macroscopic" scale. These fatigue fractures usually occur without noticeable macroscopic permanent deformation and have been produced under the following test conditions:

-fatigue at constant load amplitude,
-fatigue at constant strain amplitude,
-fatigue under spectrum loading,
-fatigue at positive or negative mean loads.

Conventionally, these tests have been conducted with notched or un-notched specimens under sinusoidally constant amplitude load cycles until failure occurred. A curve of stress versus number of cycles to failure was plotted for the test population results.

Recognizing that fatigue from design discontinuities and/or in-herent material or manufacturing inconsistencies progressively damages the material, study of the fatigue-crack mode was undertaken. The fatigue crack grows incrementally after starting from a stress

concentration and spreads gradually by mechanisms of slip, cleavage, twinning and delamination. When the remaining cross section can no longer withstand even a single further application of the cyclic force, fracture by momentary overload begins. It is at this stage that the crack propagation mechanism associated with unstable fracture under a single rapid load application becomes relevant with respect to final fatigue fracture (Freudenthal, 1958). Here, the incremental crack extension γa is plotted against the number of cycles (N) to yield the a-N curve (Figure 2) which then can be differentiated to establish a crack growth rate: Da/DN.

Reflecting on section 3.2.2, it can be observed how the study of fatigue-crack growth relates the stress intensity parameter, K_I, to fatigue-crack propagation rates until fracture where, if valid, K_{Ic} is achieved.

3.3.1 Fatigue-Crack Propagation

Crack growth processes in fatigue can be expressed as a function of the fracture mechanics crack tip stress intensity factor, K or ΔK, versus the empirically determined crack growth rates (Da/DN). Complete description of the fatigue stress cycle for simple wave forms is characterized by a maximum stress, S_{max}, and a minimum stress, S_{min}, corresponding to a stress range $\Delta S = (S_{max} - S_{min})$. Now, associating this with $(K_{max} - K_{min}) = \Delta K$ permits evaluation of the effective stress intensity. Additionally, a stress range load ratio $(R = \dfrac{S_{min}}{S_{max}})$ can be computed for the applied stresses and used for

Figure 2 Crack Growth (Flaw Size) Versus Number of Cycles Illustrates
Effect of Environment and Frequency. Note that when environ-
ment is influential the final crack size, a_c, may be reduced
(Hoeppner, 1975).

FLAW SIZE, a, inch (mm)

Final Crack Size, a_c

Environment and Frequency Effect

Base-Line

Inspectable Flaw Size

a_i

NUMBER OF CYCLES, N
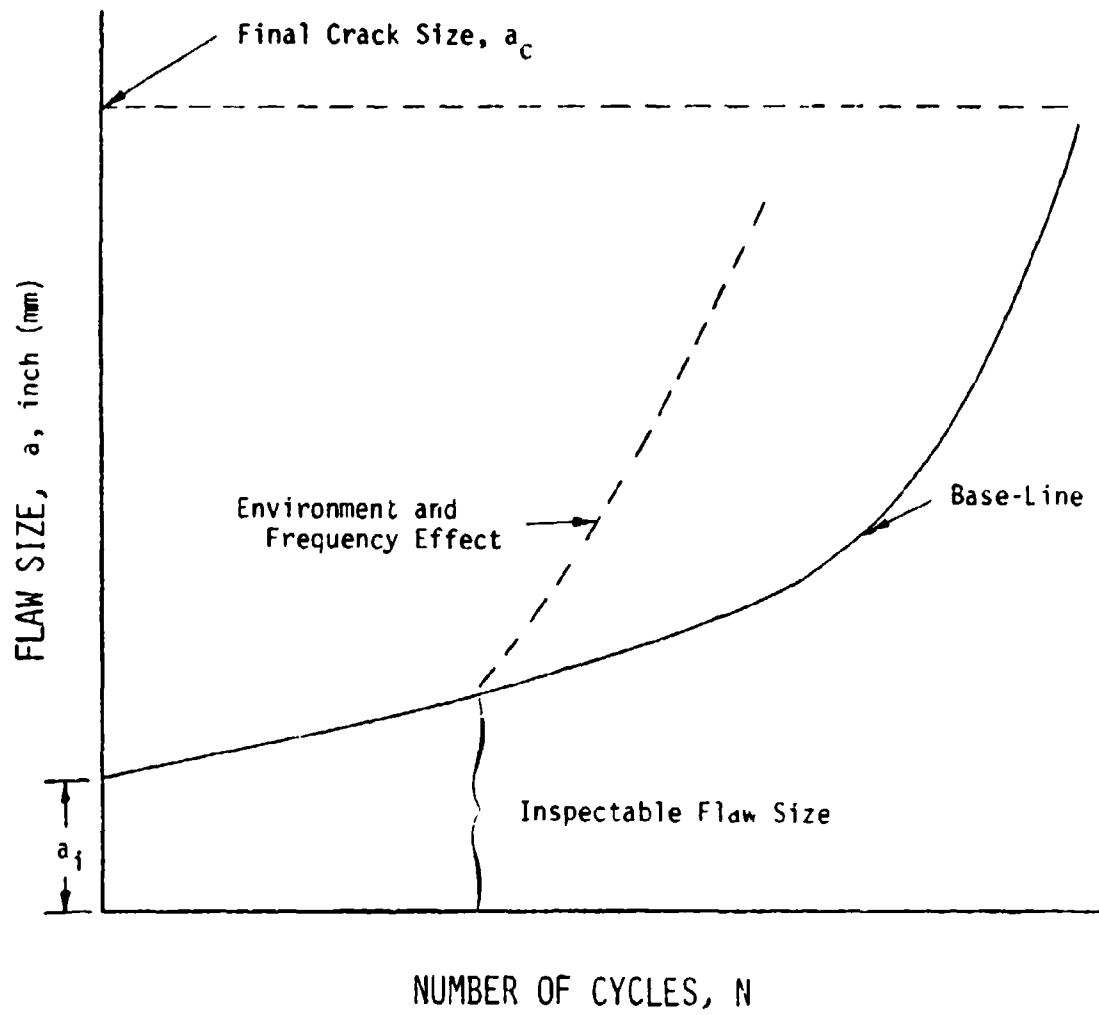
identification of crack growth rates. For zero-to-tension cycling,
R=0, in a non-aggressive environment, the crack propagation generally
follows a typical logarithmic plotted sigmoidal curve (Figure 3).
Traditionally, one of many ways the second region (transition) of
the curve has been described is assuming a linear semi-empirical
relationship referred to as the power-law or relation.

$$Da/DN = C(\Delta K)^m \qquad (7)$$

The curve, bounded by region 1, illustrates nonpropagating fatigue
cracks when $Da/DN \to 0$ at some low ΔK_1. Above region 3, crack growth
accelerates unstably to eventual failure at some high ΔK_3.

The parameters C, m, ΔK_1 and ΔK_3 are sensitive to the material.
The exponent (m) generally varies approximately between 2 and 5 for
steels, and in some materials is as high as 18 for different ma-
terial conditions, load spectra and test environments. Generally,
a small value of (m) leads to optimum fatigue-crack growth resis-
tance, although there are definite exceptions.

The value (C) is considered to be primarily dependent on Young's
Modulus (E) (Crooker, 1972). However, values of (C) may vary sub-
stantially with changes in alloy groups and the value of (m). Often
when comparing (Da/DN) versus (ΔK) curves of two materials, the curves
will intersect and the benefit of each material must then be judged
for its intended application. Consideration should be given to the
minimum ΔK values that apply to the structural situation under in-
vestigation. Then only that part of the curve above the minimum ΔK

Figure 3   Sigmoidal Crack Growth Rate Curve for Engineering Materials
or Engineering Alloys Plotted on Log Paper (Crooker, 1973
and Kondas, 1974).

LOG FATIGUE CRACK GROWTH RATE, da/dN

$$\frac{da}{dN} = C(\Delta K)^m$$

REGION 1:
SLOWLY GROW-
ING FATIGUE
CRACKS

REGION 2:
POWER - LAW
RELATIONSHIP PERMITS
FATIGUE LIFE
CALCULATIONS

REGION 3:
RAPID
UNSTABLE
CRACK
GROWTH

ΔK_1 ΔK_3

LOG STRESS-INTENSITY FACTOR RANGE, ΔK
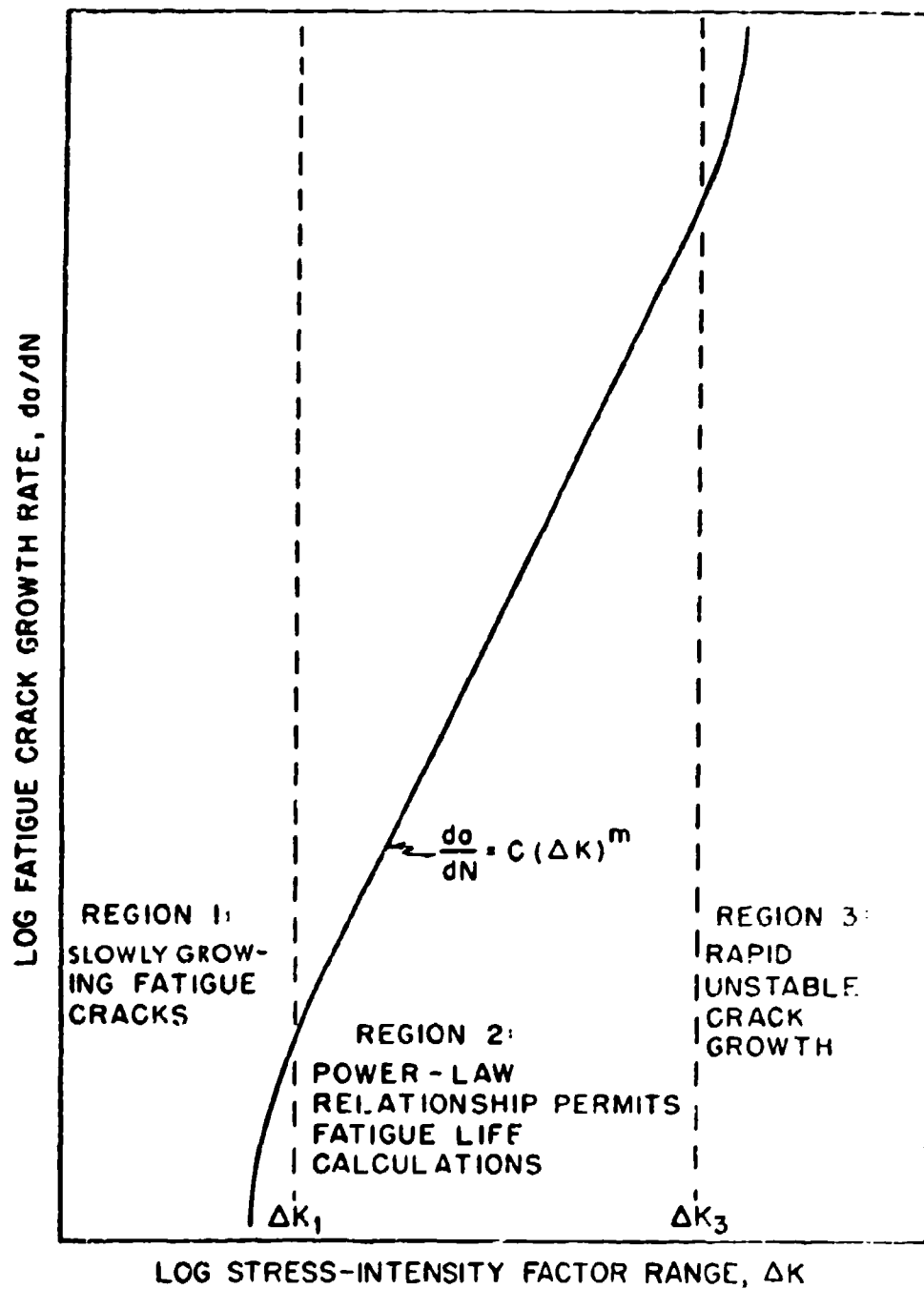
should be used for further comparison. This type of approach is important in highly stressed structures where the flaw detection capability is limited and resulting ΔK levels are in a region of medium to fast crack growth rates.

There are other parameters that can influence the shape of the curve in Figure 3. Some of these are environment (Figure 4), stress ratio (Figure 5), and load wave form and frequency. In general, environment has its greatest effect at low stress intensities and low operational frequencies (Hoeppner, 1964, 1971 and Crooker, 1972), but exceptions are available. There are many combinations of the above factors with effects that are variable. Some of the combinations will be investigated in this work.

Presently, to determine an optimum alloy for a fatigue application, a materials trade-off may be conducted using conventional parameters such as n', $\bar{\epsilon}_f$, $\bar{\sigma}_f$, σ_{ts}, K_{Ic}, σ_{ys} (Feltner et al, 1967). However, this approach is restrictive because it lacks the necessary technique to optimize or indicate those parameters that could be improved to increase the fatigue resistance of a new metal (Grosskreutz, 1972). This must be done by examining, identifying and relating microstructures to specific fatigue resistance. Frequently, when we have attempted to improve the fatigue resistance by raising the fatigue limit, we have inadvertently decreased the flaw tolerance of the material. In addition, the material's resistance to environmentally enhanced subcritical flaw growth has decreased, creating a maintenance problem.

Figure 4 Typical Effect of Corrosive Environment. At low frequencies
the dashed curve shifts to the left and generally increases.
Maximum effect is at low ΔK values (Hoeppner, 1964-1971,
Crooker, 1973 and Kondas, 1974).

EFFECT OF CORROSIVE ENVIRONMENT ON FATIGUE CRACK PROPAGATION

LOG CRACK GROWTH RATE, da/dN

LOG STRESS-INTENSITY FACTOR RANGE, ΔK

CORROSIVE ENVIRONMENTS

NON-CORROSIVE ENVIRONMENTS
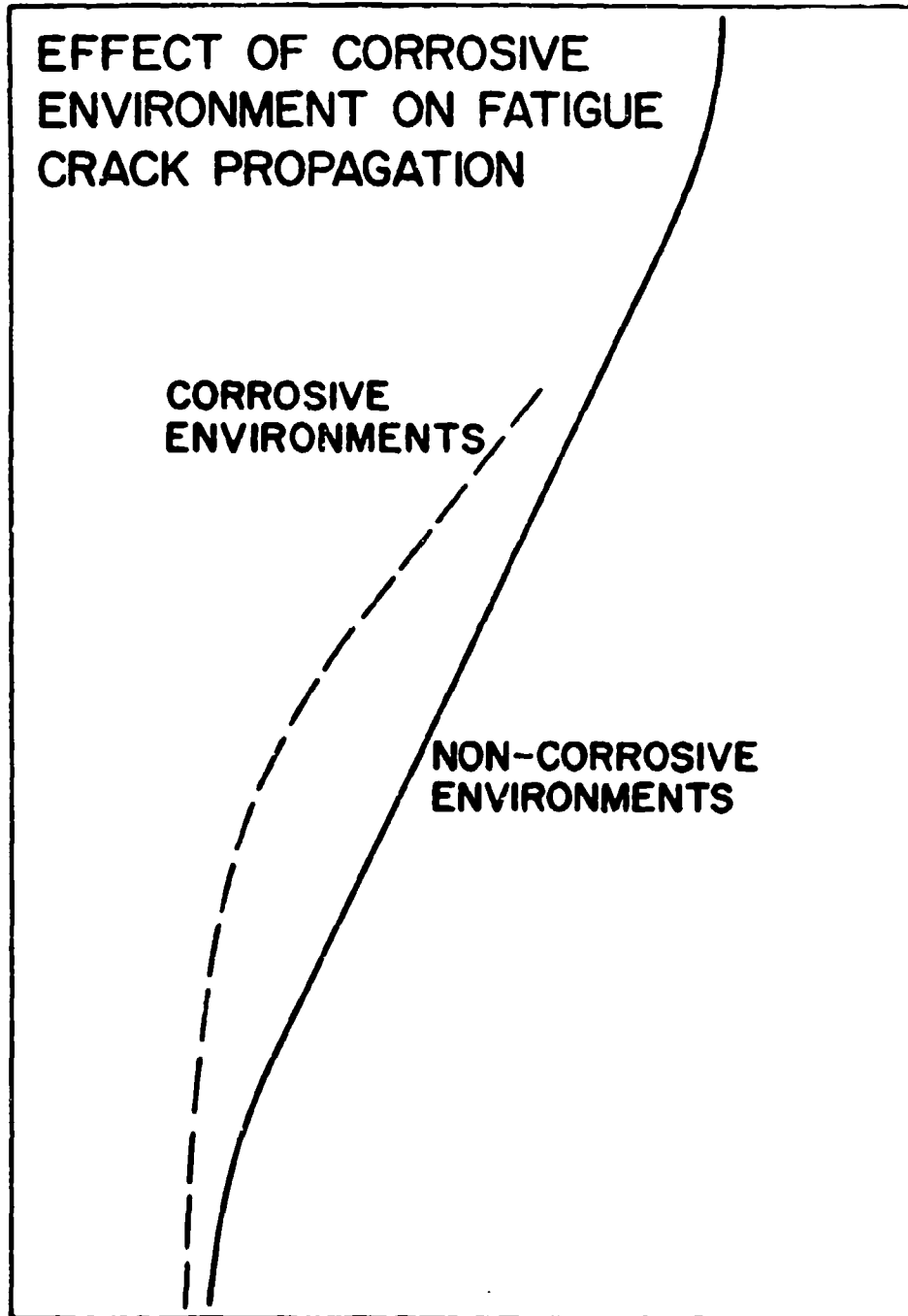
Figure 5 Effect of Stress Ratio, R, (S_{min}/S_{max}) on Fatigue-Crack Propagation (Pettit et al, 1973).

EFFECT OF STRESS-RATIO ON FATIGUE CRACK PROPAGATION

LOG CRACK GROWTH RATE, da/dN

R>0

R=0
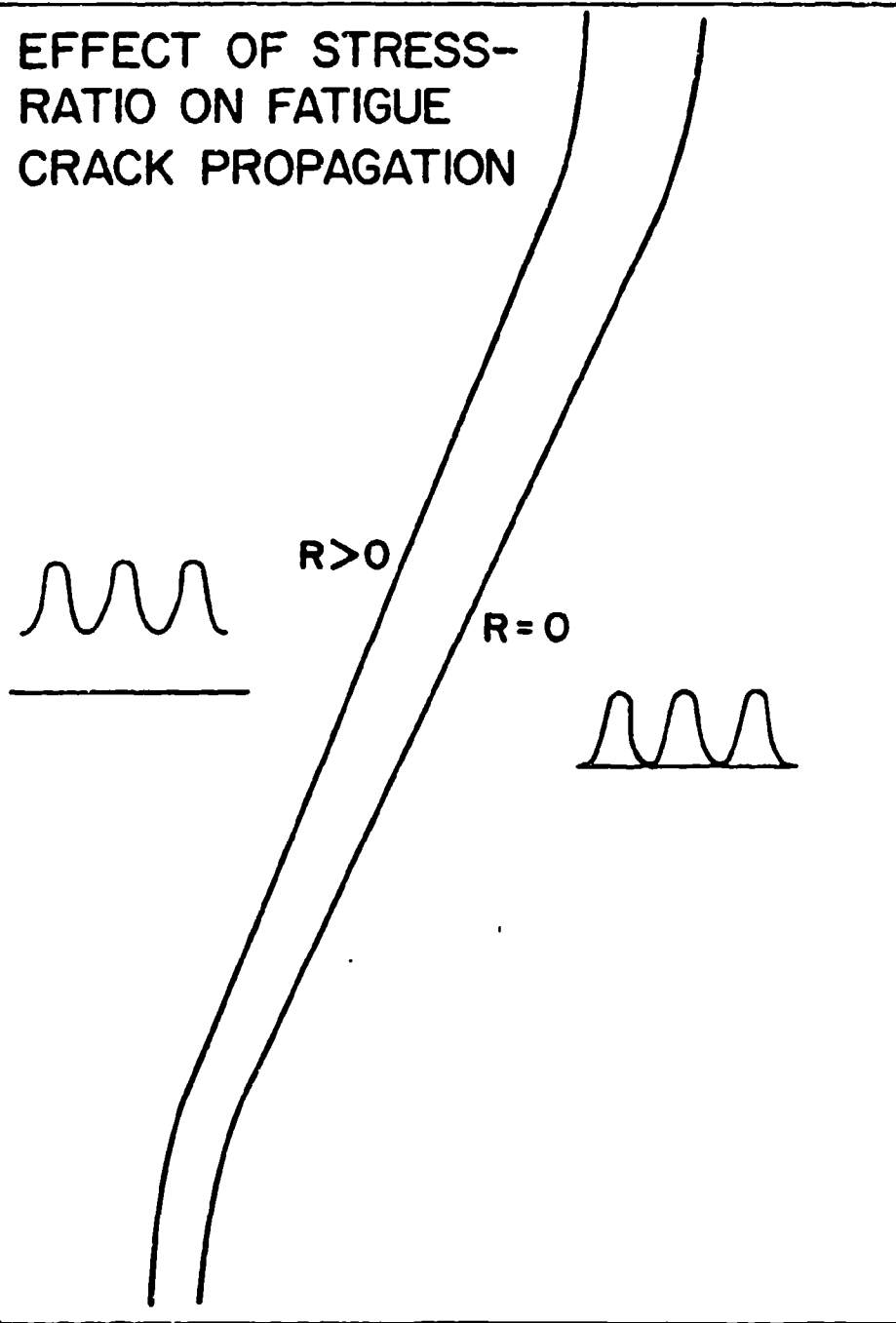
LOG STRESS-INTENSITY FACTOR RANGE, ΔK

It has been assumed (Grosskreutz, 1972 and Laird, 1967) that due to high stress concentrations present under high crack growth rates (i.e. greater than 4.0×10^{-5} in/cycle or 10.2×10^{-5} mm/cycle) fatigue resistance is unaffected by microstructural conditions (i.e. second phase precipitates, residual stresses, etc.).

However, to alter growth rates, inclusions in the matrix have been observed to provide initiation sites for cracks in the matrix (Harrigan, 1973 and Hoeppner, 1969, 1975). Thus, if the inclusion or interstitial content was decreased, leaving a cleaner alloy matrix, the fatigue-crack growth rates should decrease. Further, Hoeppner (1963) has maintained that the grain boundary misorientation angles are crack direction mechanisms of primary influence in initiating flaws by controlling the energy potential to its least value thus, developing slip, cleavage or twinning as a result. Outgrowth of this thinking is observed in areas such as microstructural and mechanical texture and subgrain boundary cell development and effect. As expected grain size has been observed to be influential. Grain size effect can be allied with slip or glide mode and stacking fault characteristics as presented by Hoeppner (1963 and 1967) and Laird (1967). If the metal has a high stacking fault energy (i.e. wavy slip) the flow stress (static or dynamic) is essentially independent of grain size. It appears that such materials form a characteristic dislocation cell structure that depends on strain amplitude and test temperature. These cells are much smaller than the grains. Materials of low stacking fault energy (i.e. planar slip) show a distinct de-

pendence of fatigue-crack growth on grain size. The reason is that in
these materials dislocation cells do not form at high cyclic strains
but a uniformly banded structure develops. The grain size effect is
considered as most influential for planar slip mode materials such as
the steels being examined in this study (i.e. 17-4 and 15-5). How-
ever, when decreasing grain size, fatigue-crack growth rates decrease
only to a point depending on the thermal process and microstructural
configuration (Feltner et al, 1970).

3.3.2 Materials and Mechanics; Orientation and Direction

To achieve an increase in fatigue life by decreasing fatigue-
crack growth rates, an optimum approach would be to design requisite
metal quality through microstructural modifications in the surface,
grain size, phase distribution, texture and metal cleanliness.
Figure 6 graphically diagrams factors to be reviewed in the metal
damage process. The ability to relate specific microstructures with
fatigue resistance has been explored minimally, and the present
state-of-the-art does not permit accurate predictions of the above
mentioned for optimum fatigue response. This field will have to be
explored by asking the right questions and utilizing chemistry and
physics to relate to exact phenomenological events referred to for
fatigue resistance processes.

Figure 6   Impacting Factors on the Physical Process of Crack Growth
          Under Fatigue. The metal quality or microstructure is
          the focal point from where fatigue performance diverges.

CRACK

ϵ_c

ϵ_c

f METAL QUALITY

ϵ_c

ϵ_c

PROCESS ZONE

PLASTIC ZONE (DETERMINES TOTAL ENERGY)

ELASTIC

PLASTIC

ADVERSE IMPOSED FACTORS

METAL QUALITY FACTORS
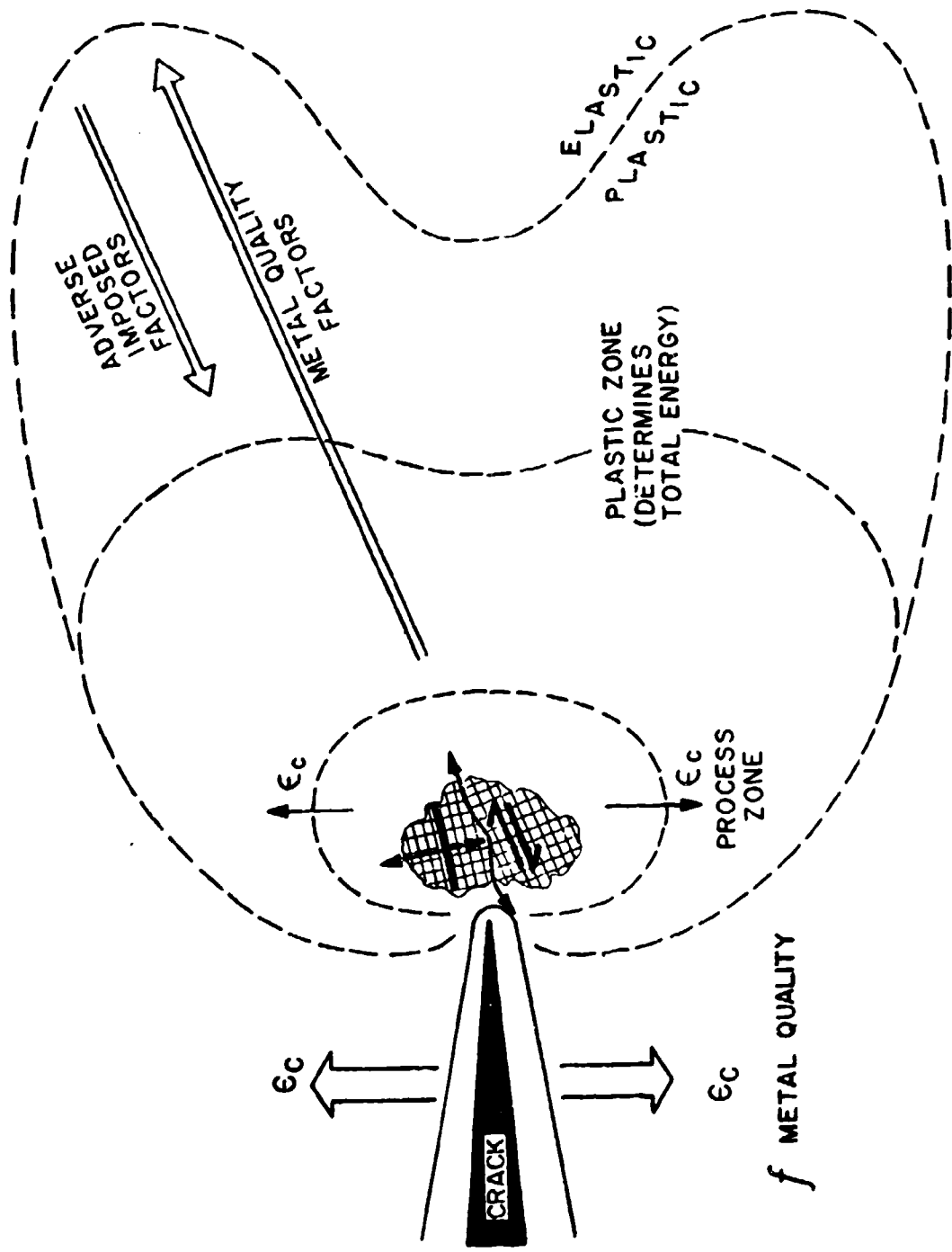
Chapter 4

PROGRAM PLAN

4.1 TEST PROGRAM PURPOSE AND APPROACH

The design and construction of Naval Advanced High Performance
ships (AHPS) presents technological similarities to the airframe
industry where minimum weight constraints and high performance re-
quirements dictate use of higher strength materials.

Traditionally, design of ship structural components is conser-
vative to keep service stresses below allowable macroscopic
material property limits, such as ultimate strength and 0.2 percent
yield stress. The alloy selection process sometimes considers other
macroscopic properties such as fracture toughness and ductility.
Rarely, however, are these included in design principally because
"traditional" design methodology does not consider these quantities.
The "traditional" engineering design practice while reasonable, could
be improved by developing a methodology for further mechanical prop-
erty considerations.

This study investigated the existence of a specific parameter,
dynamic hold-time, in structural material applications and attempted
to identify its effect and micro-mechanism. Generally, the hold-
time parameter is not considered, but it has been found to be a key
factor in fatigue-crack propagation behavior (Hoeppner et al, 1968,
Popp et al, 1969, and Ryder et al, 1973). Unfortunately, neither an

individual nor combined macroscopic material property characteriza-
tion of conventional design properties has produced evidence to
indicate hold-time to be a culprit in numerous service condition
cracking incidents in the aviation industry. However, relatively
simple laboratory scale fatigue-crack propagation tests can reveal
interactions between applied loads, external environment, and mic-
rostructural phenomena and help forewarn of deterioration in crack
growth resistance under service conditions. The generalized concept
for use of fracture mechanics is to provide a couple between idealized
laboratory and in-service fatigue-crack propagation behavior to enhance
the accuracy of life prediction procedures.

The objective of this study in part was to qualify whether existing
circumstances as applied to candidate alloys of hydrofoil and strut
structures produce an increase in the fatigue-crack propagation rate
when hold-times typical of service operation are considered.

During service operation, the structures experience variations
in steady loading conditions. In the hull borne mode, the foils
and struts may be raised or lowered for a prolonged time, contingent
on ship operation. Thus creating an increased or decreased steady
loading on a certain area of the structure. Continuous steady loads
can develop also in foil-borne mode through biaxial loading and drag
bending. If cavitation occurs, a low noise ringing, similar to hollow-
blade turbine problems, will result in an internal friction condition
if not properly damped (Bowie, 1974-1976).

To simulate this type of load behavior, fatigue-crack propagation tests were conducted with various hold-times at peak loads. These loads and stress intensities can be acquired from the structural analysis of the hydrofoils and struts providing applicability of results. In stress analysis of foil and strut structures continuous perturbation with changes in temperature gradients, typical of turbines, is not a predominant concern. However, in view of fit-up, welding constraint, heat treatment and flame straightening, the stress field is not necessarily reduced to trivially low values under a constant temperature and at-rest conditions. Some portions of the structure can have locked-in or residual stress fields of magnitude approaching the material yield strength. Accordingly, fatigue-crack propagation tests will be performed with consideration of residual stress variability (R-ratio) as a impacting feature. The R-ratio will be patterned after that in the relevant and applied Navy spectrum.

4.2 DETAILED DESCRIPTION

4.2.1 Rationale

The fatigue-crack propagation tests were conducted in two modes. First, sine wave tests performed at 10 Hz determined base-line, then trapezoidal wave "hold-time" test were conducted. The wave form difference is seen in Figures 7a and 7b.

Figure 7a   Sinusoidal Wave Form Illustrating P_{max} and P_{min}.

Figure 7b   Trapezoidal Wave Form with One Second Rise Time and One
Minute Hold-Time.

P, LOAD

P_{MAX}

P_{MEAN}

P_{MIN}

TIME

P, LOAD

HOLD
PERIOD

P_{MAX}

P_{MIN}

1.0
SEC
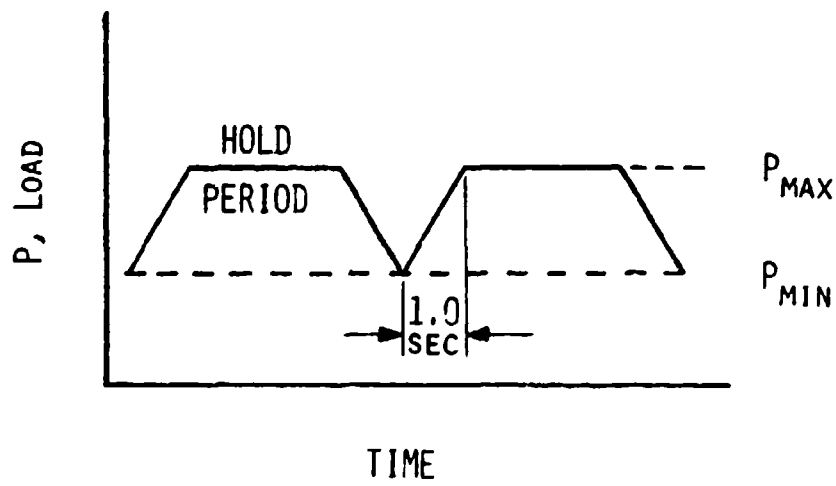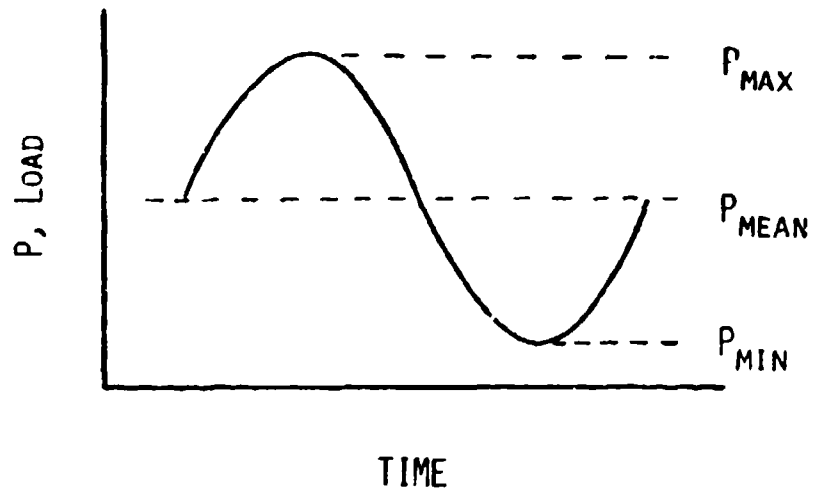
TIME

The hold-time and stress ratio (R) are evaluated in accordance with the test schedule (Table I). This study has been integrated with programs at Naval Research Laboratory and Lockheed Rye Canyon Advanced Design and Research Laboratory to provide the utmost benefit to the U.S. Navy on a Fleet Support level.

The dynamic loading procedure used in testing hold-time enhancement of fatigue-crack propagation should not be confused with static loading procedures of sustained load (cracking) flaw growth that, among other things, consider material susceptibility to stress corrosion cracking (SCC) at a given stress intensity (K_{Iscc}). Mechanistically, the two events may be similar or diametrically opposite. It has been demonstrated that alloy response to stress corrosion cracking (SCC) is sensitive to microstructure (Krupp and Hoeppner, 1973). Whether a microstructure can be conditioned to prohibit (SCC) and mitigate or eliminate hold-time effect in fatigue is an area of ongoing research.

The hold-time effect would not be overly important if the "initiation of cracks" was difficult and thus a major part of component life spent at low growth rates and low stress intensity levels. However, if cracks are part of the fabricated structure in the form of weld suck-back, heat treatment cracks, etc., then, the time spent in "crack initiation" is lost and larger initial cracks would be subject to relatively high stress intensity levels. Thus, the effect of hold-time would become quite important.

TABLE I   TEST MATRIX FOR EACH MATERIAL
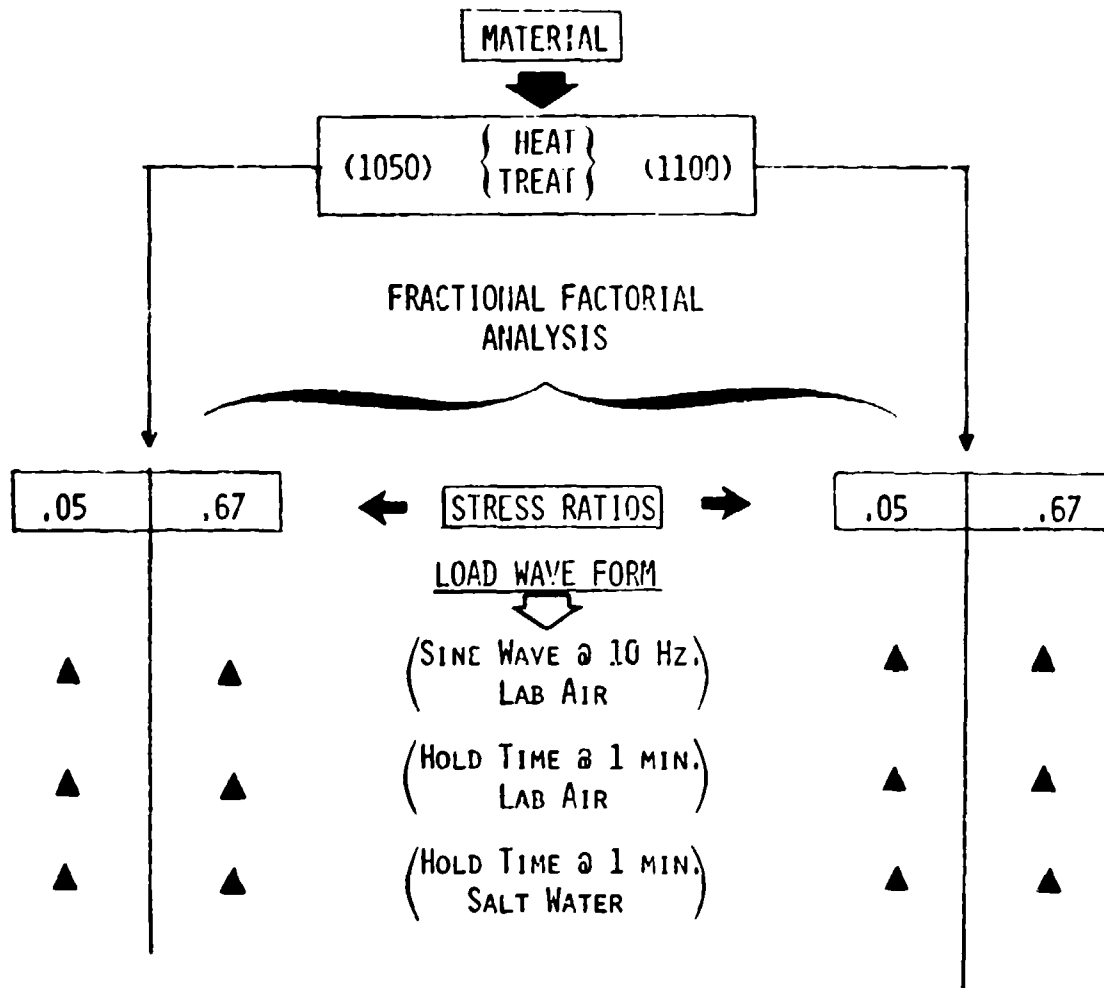
Multiple cracking frequently observed ahead of the main crack during this type of fatigue-crack propagation and in stress corrosion tests indicates an interesting cracking phenomena. Such multiple cracking is possibly indicative of severe multiple cracking under service conditions where small cracks couple; yielding larger cracks, higher propagation rates, and reduced time between maintenance periods.

4.2.2 Materials and Heat Treatments

Metals that deform plastically by slip can have resistance to slippage increased by any treatment that will harden and strengthen the metal. There are numerous ways of "hardening" metals such as cold-working, diffusion hardening, and precipitation hardening (PH). Since PH steels are the subject of this work a discussion of the hardening process and heat treatment process used on them follows.

Precipitation hardening is caused by myriad submicroscopic particles being deposited on slip planes throughout the alloy. These particles strengthen the alloy by increasing slip resistance.

Not all alloys are hardenable by precipitation hardening. Alloys that do harden by this mechanism have only one thing in common, this is, a decreasing solubility for one phase on cooling.

The 17-4 PH and 15-5 PH alloys are martensitic PH stainless steels owing their properties (Table II) to a combination of two interacting metallurgical phenomenon--the transformation of austenite (Face-centered Cubic) to martensite (Body-centered Tetragonal) and precipitation

TABLE II. MECHANICAL PROPERTIES

	17-4 PH		15-5 PH	
	H 1050	H 1100	H 1050	H 1100
Ultimate Strength, KSI (MPa)	167 (1151)	150 (1034)	167 (1151)	150 (1034)
Yield Strength, KSI (MPa)	154 (1062)	135 (930.8)	153 (1089)	135 (930.8)
Elong. % in 2"	16	17	16	17
Reduction of Area, %	57	58	62	58
Hardness (Rockwell)	c37	c34	c37	c34
Impact (Charpy-V) FT-LBS (NT-M)	33 (51.5)	45 (61.0)	40 (54.2)	45 (61.0)

Room Temperature

hardening. A precipitation hardening heat treatment, that hardens by precipitation of a copper-rich phase within the matrix and tempers the matrix structure gives these alloys their properties.

The complete heat-treating sequence consists of two steps, viz;

1. Solution Treatment - 1900 F + 25 F (1038 C $\pm$ 13.9 C) for 30 minutes, then air cooled.

2. Precipitation Harden - in a range from 900 F to 1150 F (482 C to 621 C) for 1 to 4 hours, then air cooled.

The microstructure of these alloys is controlled by chemical composition and heat treatment. The constituents that comprise the alloys (Table III and Figure 8) can be classified as ferrite formers, austenite formers, and austenite stabilizers within the ranges indicated in Table III. The balance between these elements insures a predominant martensitic microstructure with some delta ferrite present in 17-4 PH and virtually no delta ferrite in 15-5 PH. Carbon and nitrogen are carefully controlled due to their strong influence on the austenite's stability to insure a full martensitic transformation and develop properties to their fullest.

At the solutionizing temperature (1900 $\pm$ 25 F or 1038 C $\pm$ 13.9 C) the metallurgical structure of 17-4 PH and 15-5 PH is austenite with dispersed islands of delta ferrite. The solution heat treatment dissolves copper, the hardening element in the austenite. Upon cooling from this temperature, transformation from austenite to martensite begins at approximately 270 F (133 C) and usually is complete by

TABLE III. MATERIALS COMPOSITION

ELEMENTS	17-4 PH*	15-5 PH*
	WEIGHT PERCENT	
C	0.07 MAX	0.07 MAX
Mn	1.00 MAX	1.00 MAX
P	0.04 MAX	0.04 MAX
S	0.03 MAX	0.03 MAX
Si	1.00 MAX	1.00 MAX
Cr	15.5 - 17.5	14.0 - 15.5
Ni	3.0 - 5.0	3.5 - 5.5
Cu	3.0 - 5.0	2.5 - 4.5
Cb + Ta	0.15 - 0.45	0.15 - 0.45
Fe	BALANCE	BALANCE

*VACUUM-ARC REMELTED

Figure 8   Diagrammatic Representation of Chemical Compositions for 17-4
            PH and 15-5 PH.

ELEMENTS

15-5   17-4

Cu

Ni

Cr

WEIGHT PERCENT

0   5   10   15   20
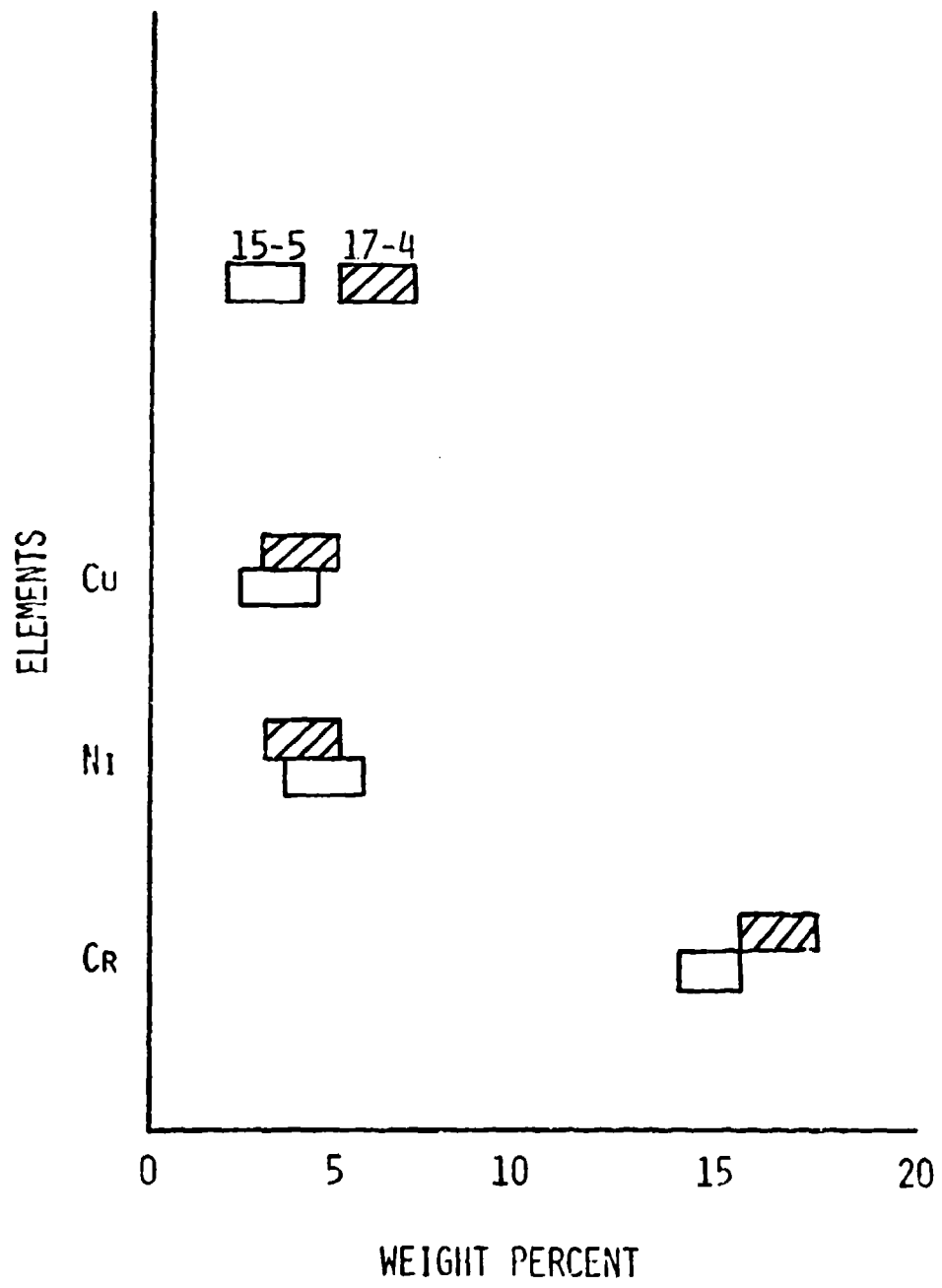
90 F (32.2 C). Treatments at temperatures below 1875 F (1024 C) will
result in reduced tensile and yield strength properties because the
copper hardening element is not completely dissolved. Treatments at
temperatures above 1925 F (1052 C) cause excessive grain growth re-
sulting in lower tensile ductility and reduced impact strength.

After solutionizing, the martensite that is formed on cooling is
super-saturated with copper. Subsequent heating to temperatures
below the A_{c1} precipitates a copper-rich phase within the martensite
increasing hardness and strength. The stress relieving effect due
to tempering of martensite combined with precipitation hardening is
important in terms of increasing ductility and toughness of the alloy.
Heating at temperatures above A_{c1} causes increasingly more au
to form. The austenite formed at these temperatures (1150-15°
621 - 816 C) does not transform to martensite upon cooling due to
the excessive carbon in solution stabilizing the austenite (Armco
Steel Co., 1969).

4.2.3 Test Specimen and Preparation

Figure 9 shows the modified compact tension specimen used in this
study. It is referred to as a wedge open loading (WOL) specimen.
Note that this specimen is slightly longer and higher than the com-
pact tension specimen normally used for K_{Ic} testing. The WOL height
to width ratio is H/W = 0.486 versus H/W = 0.600 for the standard K_{Ic}
specimen (ASTM E399-1972). The longer specimen (WOL - ASTM 1975) is

Figure 9   Dimensioned Wedge Open Loading (WOL) Specimen Used in Fatigue-Crack Growth Testing.

3.200 ±.031

2.550 ±.015

2.480 ±.02

.500 ±.005

.16

.16

≡ A .002
⊥ B TIR

40° ± 2°

.001
.003 P

B

63

63

.0938
.550 ±.005

1.100 ±.005

1.240 ±.005

A

0.500 Dia ± .005   II A .002 TIR
2 Holes   ⊥ B Spec Thickness
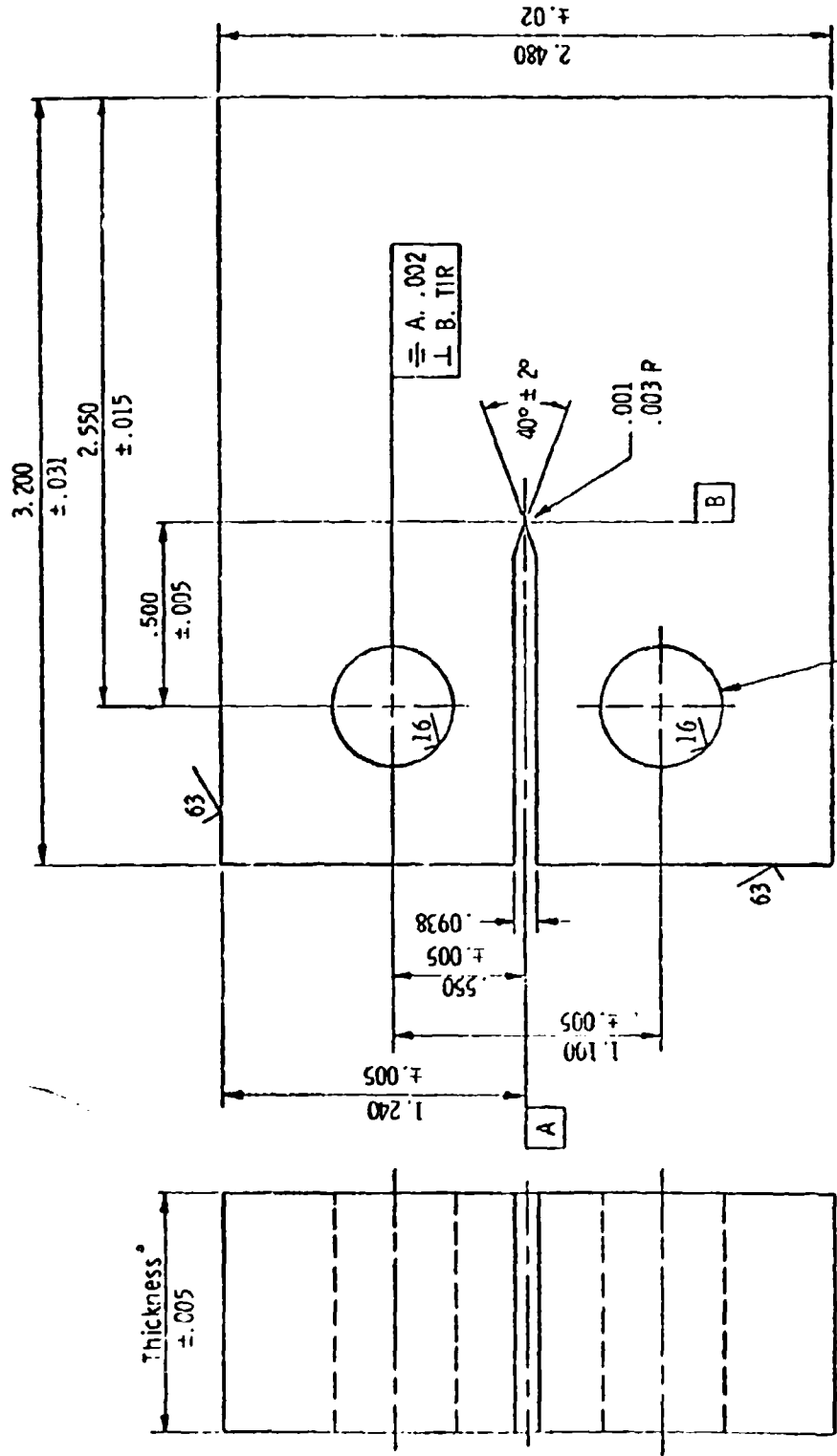
Thickness* ±.005

• Thickness To Be 0.250 or 1.000

preferred for crack growth testing because the rate of change in K_I with crack length is not as rapid as in smaller specimens. This slower rate of change makes more accurate crack growth rate measurements possible.

All test specimen blanks were cut from one inch (2.54 cm) thick plates such that the direction of crack propagation is parallel to the rolling direction (T-L orientation). In addition, a random distribution of specimen blanks were used to eliminate possible ordering effects associated with specimen location. Figure 10 shows the orientation of the specimen blanks in the as-received plate.

After solutionizing all test specimen blanks within an argon atmosphere the blanks were final machined before precipitation.hardening, again under argon. A careful examination was made to certify dimensional control on these specimens.

4.3 EXPERIMENTAL TEST EQUIPMENT

4.3.1 Fatigue Testing Equipment

A 20 kip (88,960 nt) closed loop, servo-controlled electro hydraulic test machine was used for these tests. The machine operated in a load control mode. An amplitude measurements system and an oscilloscope were available for continuous monitoring of load during testing. When crack opening displacement (COD) was monitored the load versus COD was autographically recorded. The output signals to the recording device were $\pm$ 10 volts full scale, single amplitude.

Figure 10 Fracture Plane Identification where L = Direction of Grain
            Flow, S = Short Transverse Grain Direction, and T = Trans-
            verse Grain Direction.

42

LONGITUDINAL

L

LENGTH
LONGITUDINAL DIRECTION
ROLLING DIRECTION
EXTRUSIOF FORGING
AXIS OF

S
THICKNESS
SHORT TRANSVERSE

T
WIDTH
LONG TRANSVERSE

S-T

L-S

S-L

T-S

L-T

T-L
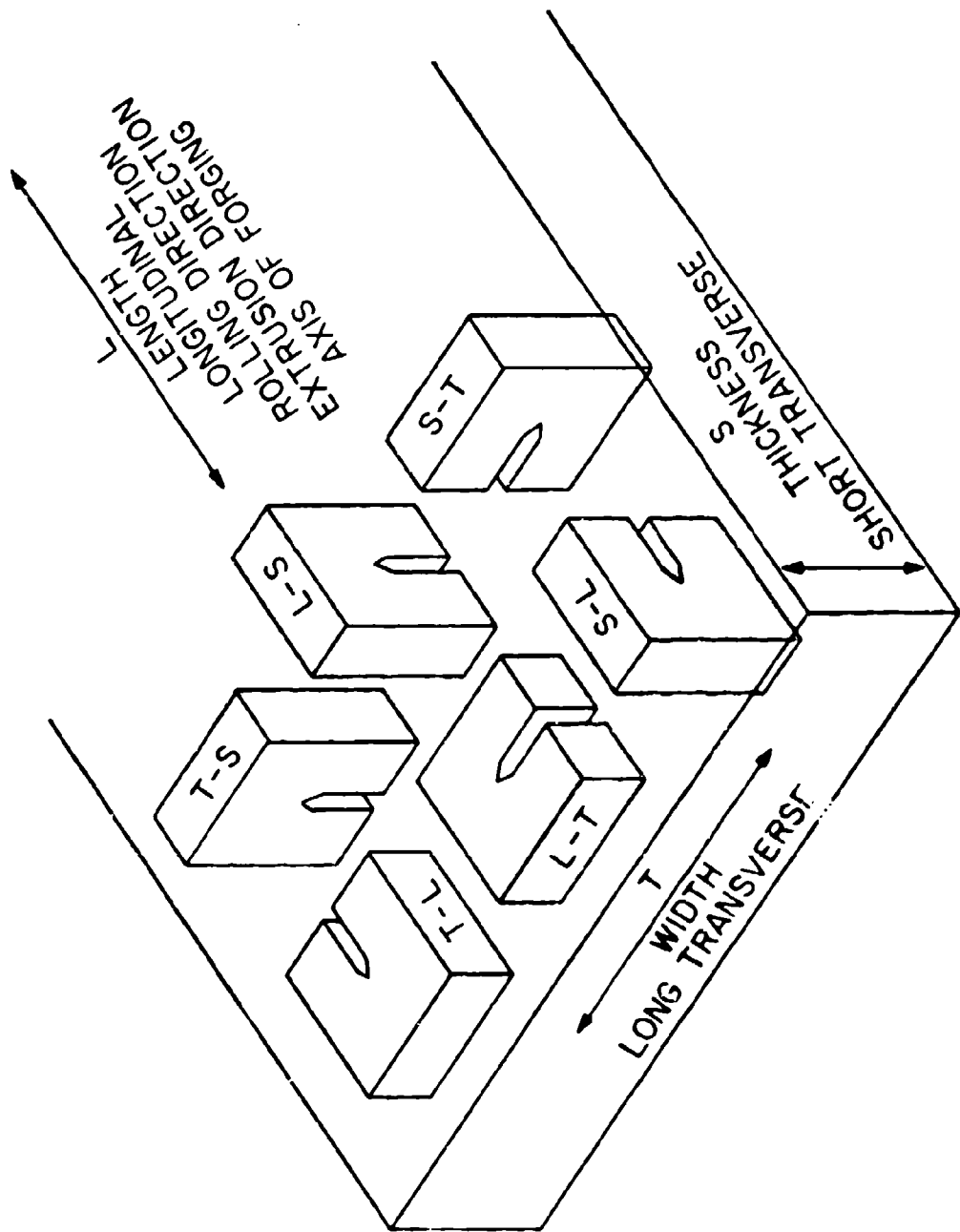
The closed loop MTS system diagram (Figure 11) shows the load frame, hydraulic power supply, load cell, control console and function generator. Note that the oscilloscope and x-y recorder are included in the test assembly (Figure 12).

The hydraulic pumping unit output of approximately 3 gpm (11.4 l/min) under pressure of 3000 psi ($2072 \ nt/cm^2$) is used to drive the hydraulic actuator. The actuator, similar to the human heart, accepts high pressure fluid on one side of the piston actuator, driving it in the opposite direction. The control of the actuator is developed through a servovalve and a controller that compares a command reference signal with a feedback signal. After both are satisfactorily summed and amplified an error signal is generated, inverted and sent to the servovalve, metering the overall flow quantity and direction. The entire system is looped closed with the aid of feedback signal from the load cell. Their output voltages are balanced in the controller to achieve the desired response profile.

4.3.1.1 Load Cell Transducer

The force applied to the test specimen was measured with a load cell transducer that is fatigue rated and temperature compensated. The sensing element is hermetically sealed within the load cell body and consists of resistance strain gages electrically connected to form a balanced wheatstone bridge. The signal output is free from the effects of drift, creep, ambient temperature changes, hysteresis, or resonance from static load+ : 4 to 50 Hz.

Figure 11   Scaled Drawing of Material Test System Used in Compliance
and Fatigue-Crack Growth Testing.
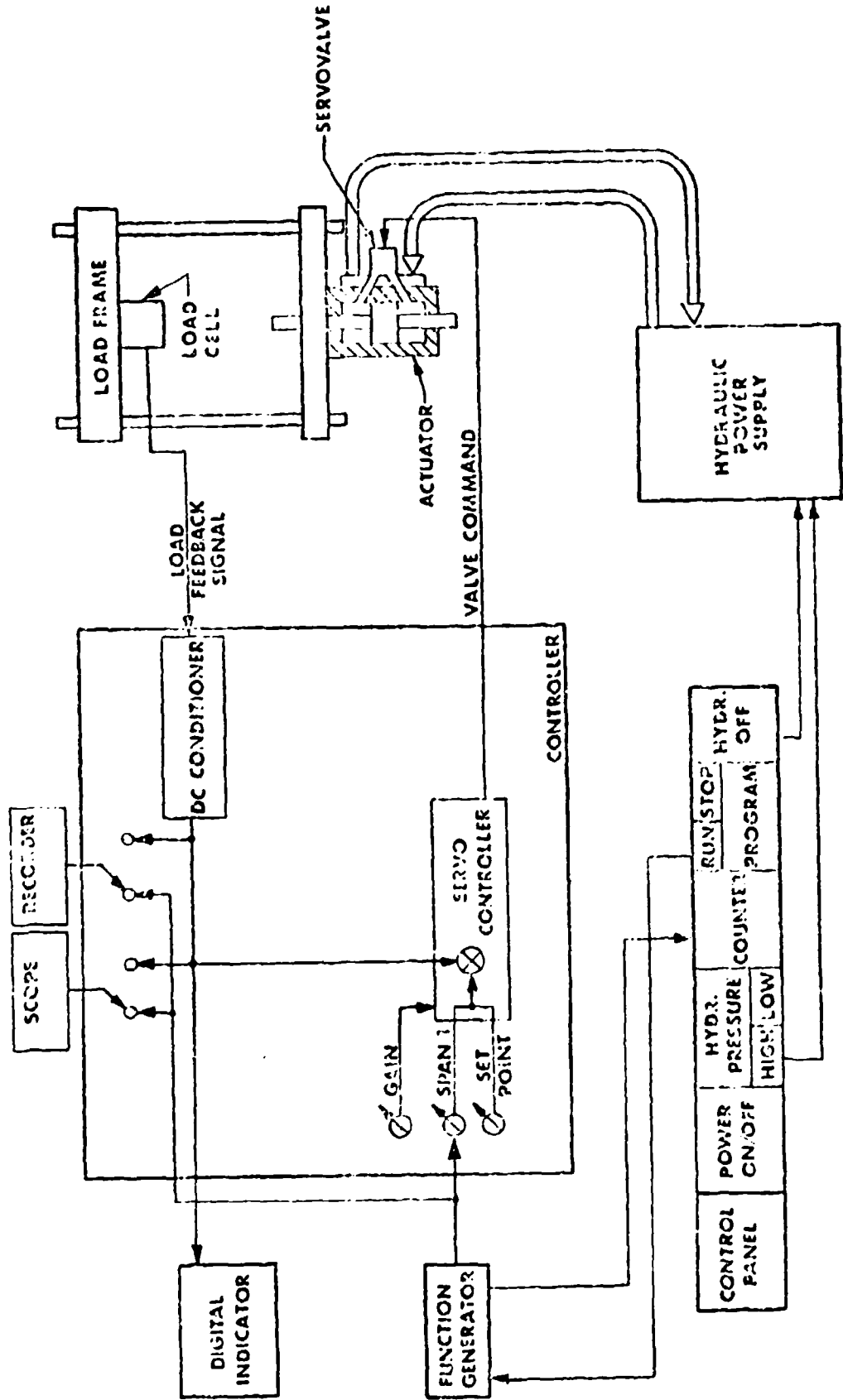
Figure 12   Material Test System (MTS) Equipment for Closed Loop Fatigue Testing.
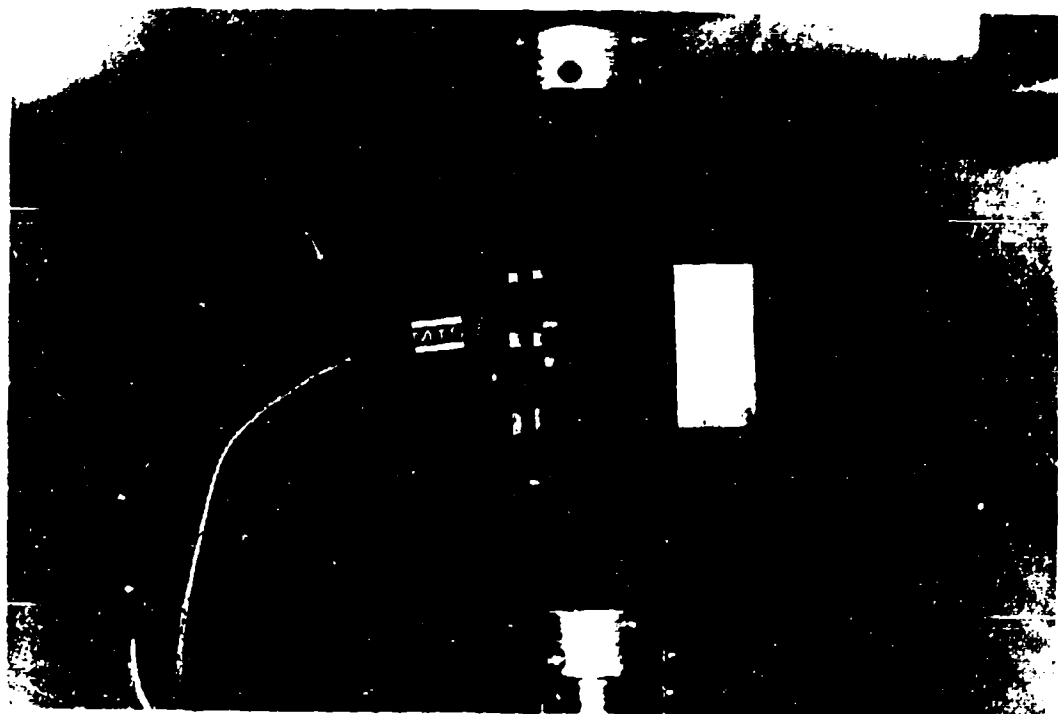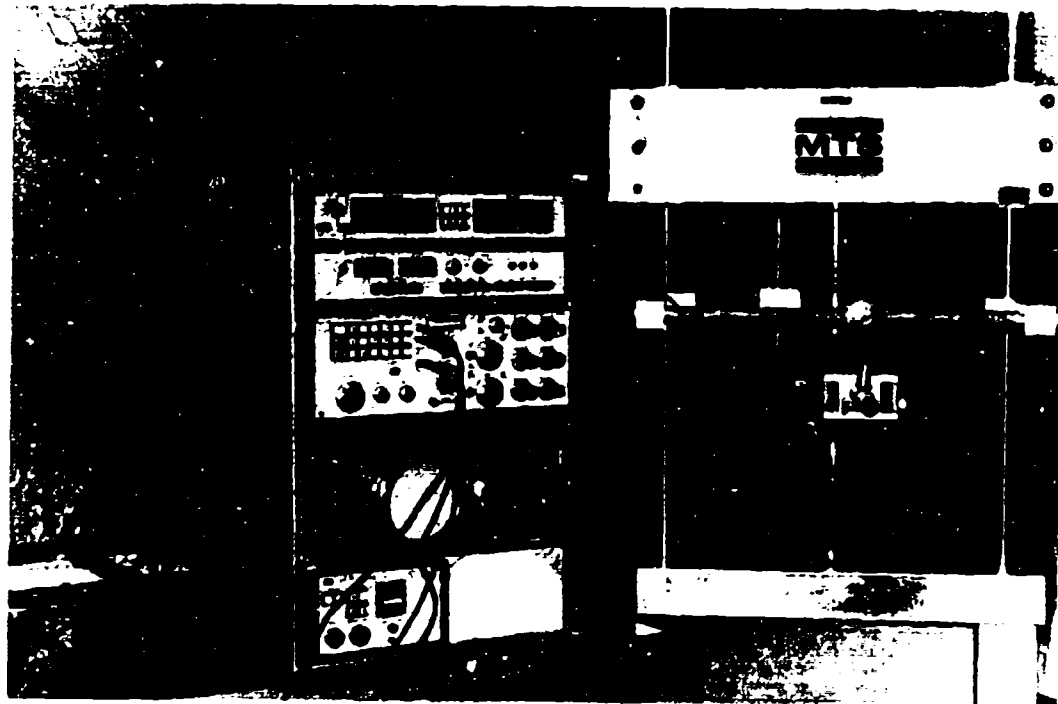
4.3.1.2 Test System Calibration

The test system was calibrated prior to the start of test and at four month intervals during testing. Calibration was performed whenever a transducer or test system component is changed or anytime a testing error occurs that could cause the system to exceed transducer limitations. The system was calibrated as a complete unit from the point of input to the transducer to final signal output at the recorder. The calibration standards that are used are traceable to the National Bureau of Standards.

The load and the COD measuring channels were calibrated in 10 equal increments for the ranges being used. Either shunt resistance calibration techniques or master load cell calibration techniques were used to calibrate the load weighing system. COD system calibration was performed with a frame micrometer with 0.0001 inch (0.000254 cm) or less thimble graduations. The maximum allowable error at the test system recorder was $\pm$ 0.5% of full scale single amplitude at each of the 10 increments. The COD gage was calibrated at the temperature and the environment in which the testing was performed. The load cell was adequately protected to ensure that ambient conditions exist at the load cell during all testing.

4.3.2 Accessories for Fatigue Testing

4.3.2.1 Clevises

The load was applied to the test specimen with two matched clevises. The load line went through the center of each clevis. The

loading holes were 0.50 inch (1.27 cm) diameter with load pins not less than 0.484 inch (1.23 cm) diameter. The clevis was capable of maintaining specimen vertical alignment with spacers between the specimens and clevis inside walls.

4.3.2.2 Crack Opening Displacement Gage

The edge crack opening displacement (COD) was measured with a double-cantilever, resistance strain gaged, clip-on displacement gage transducer. The gage was similar to the displacement gage described in reference (ASTM E399-1972). However, during the data reduction the thickness of the knife edges used to mount the COD gage was taken into account.

4.3.2.3 Gaertner Microscope

This microscope was used at 33x magnification and mounted in a micrometer slide for optical recording of crack extension. Due to the motion of the system and the specimens, scribe marks were placed at every 0.100 inch (0.254 cm) from the crack tip to crack run length. These markings assist the crack reading accuracy because of decreased transit from a known point to the crack tip. The definition of crack tip location is known to be a function of crack tip displacement, test material, condition of specimen surface and lighting source. For this reason these factors were of primary concern during testing.

4.4 TEST PROCEDURES

All test specimens were precracked under sinusoidal cyclic load-
ing prior to generating the crack growth data. The maximum stress in-
tensity factor during precracking did not exceed 17 ksi $\sqrt{in}$ (18.7
MPa $\sqrt{m}$) with the corresponding stress ratio (R) equal to 0.05. The
test frequency used for precracking was 10-15 Hz. The modified com-
pact tension specimens were precracked approximately 0.050 to 0.075
inches (0.127 to 0.190 cm) beyond the end of the machined notch.

After precracking to an acceptable length, a variation in the
cyclic loading or frequency was required to produce a beach mark at
the precrack front to evaluate this crack front eccentricity or bowing
shape after final fracture.

Following precracking and marking the crack front, fatigue-
crack growth testing was conducted. Crack growth data (a vs. N)
was recorded optically for both back and front crack extensions.
Crack length measurements were made at crack growth intervals not
exceeding 0.01 inch (0.025 cm). Both sides of crack length did not
have a difference exceeding 0.05 inch (0.127 cm) at any time during
testing.

For testing in a salt water environment, the specimens were
placed in a sealed plastic bag or for horizontal load frames the
specimens were dipped into the salt water tank (Figure 13).

The test region of the specimen was immersed in a solution of
3.5% NaCl in deionized water which was maintained at a constant flow-

Figure 13 The Portion of the Specimen to be Exposed to the Salt Water
Environment is Illustrated in Position within the Tank.
The water is fed through and drained without reuse.

INPUT

DRAIN
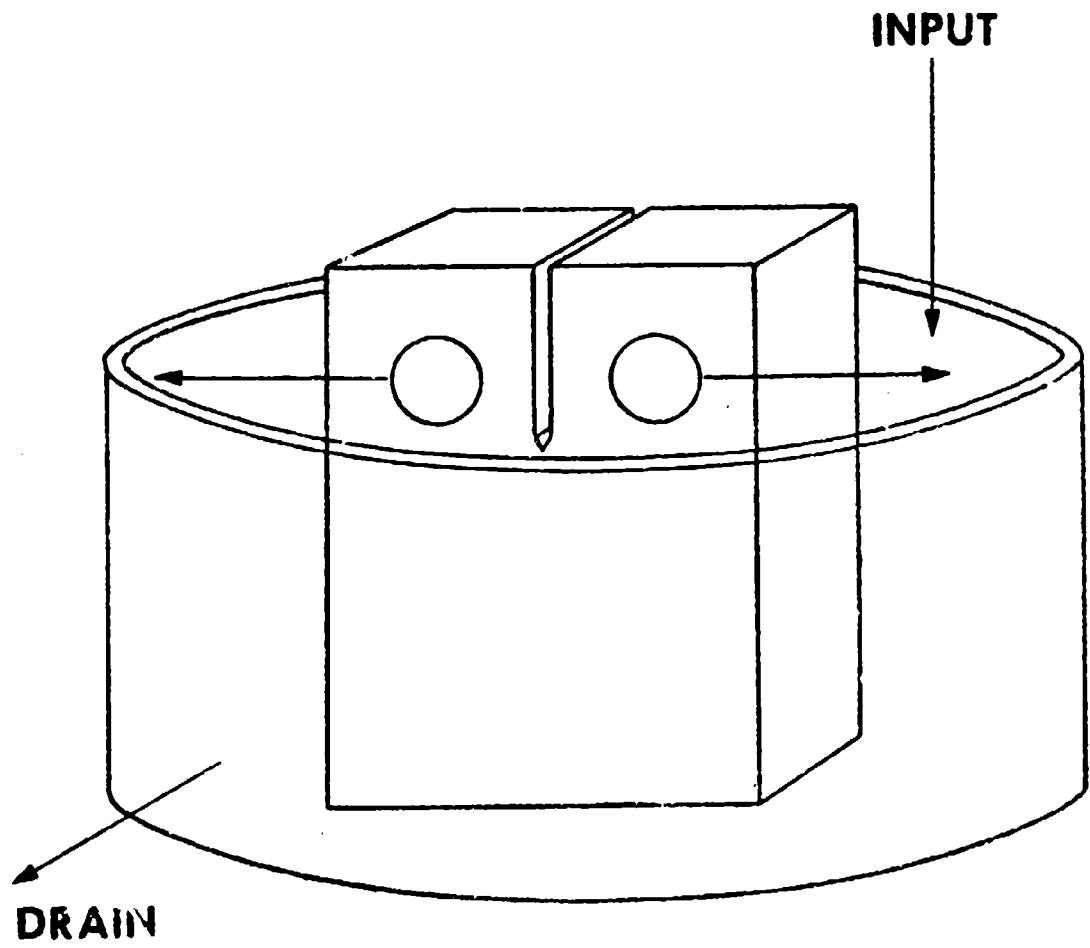
through rate of approximately one half pint per hour (0.214 1/hr). The solution was not reused.

Test interruptions were avoided where practical, since transient periods of crack growth retardation have been observed following these interruptions.

The maximum and minimum load excursions were monitored continuously during the test by a memory circuit. This was able to detect and record load spikes which might arise from extraneous electrical or mechanical sources even though limit detectors wiil monitor gross deviations for shut-down.

During the test, specimen compliance was deveioped by measuring crack opening displacement, COD. The process will be discussed more thoroughly in chapter 5.

The mathematical relationships for the specimen's stress intensity calibration will be explored in chapter 5 as twu types of approaches are considered. The Wilson polynomial and Weibull exponential equations comprise the two data reduction techniques considered for this work. The rationale for these techniques will be discussed in the following section.

Chapter 5

EXPERIMENTAL DATA REDUCTION DESIGN AND PROCEDURES

5.1 WEIBULL'S SURVIVORSHIP FUNCTION

Deviations of the Weibull survivorship function, termed the
third asymptotic distribution of smallest values, are given in
Gumbel's text (1958). Weibull's classic paper in 1949 was the pro-
genitor for present applications to statistical representation of
fatigue failures. Analytical procedures for estimating the three
parameters of the Weibull survivorship function were summarized
in 1963 (ASTM 1963).

The rationale as to why the Weibull function has been pursued
may be obvious with a succinct overview of existing expressions and
their inherent difficulties. The most common is attributed to Paris
(1965)

$$Da/DN = C(\Delta K)^m \qquad (8)$$

where C and m are acquired from the data plot. Here, a significant
deviation occurs as the data does not conform to the equation at low
and high Da/DN values. It also tends to mask effects due to material,
frequency, environment, load spectrum, and stress ratio. The most
common formulation for stress ratio correction used for Da/DN has
been proposed by Forman (1967):

$$Da/DN = \frac{C(\Delta K)^2}{K_c - K_{max}} \tag{9}$$

Even though applicable at higher crack growth rates, it tends to
be in error at low cracking rates where the largest impact occurs
to long life structure (Bowie et al, 1974). Another expression
for stress ratio effect was explored by Walker (1970):

$$\Delta\sigma = (\sigma_{max})^{1-m_2} \Delta\sigma^{m_2} = \sigma_{max}(1-R)^{m_2} \tag{10}$$

This approach gives a good fit to the data at low crack growth
rates. However, as K_{max} increases to a critical value and environ-
mentally assisted cracking effects are considered, the equations will
be in error (Jaske et al, 1973).

Overall, a number of curve fitting numerical relations have been
proposed to assist the graphical mechanics of fatigue-crack propaga-
tion. However, no single relation has gained acceptance by the fa-
tigue and fracture mechanics community.

The fitting power of Weibull's relation is demonstrated by ob-
serving the weaknesses in the data fitting for traditional poly-
nomial stress intensity calibrations. This evaluation, will be
explored in the following section using compliance measurements.
Additionally, benefits and physical rationale are suggested for the
fatigue-crack growth life predictions approach.

5.2   COMPLIANCE MEASUREMENT

5.2.1 Theoretical Derivation of Compliance

An entirely new relationship for the representation of compliance measurements is considered herein. The relationship incorporates a Weibull type function with the associated Weibull parameters k, e, and v. Before discussing the approach, a brief review of the historical mathematics for compliance calibration to supplement section 3.2.1 will be given. Examining specific energistic relationships of the G-concept (i.e. crack extension energy), compliance determination may be considered. Assuming a center cracked panel or a single-edge notch configuration (Figure 14a) where:

$$c = 2a \text{ total crack length}$$
$$\delta c \text{ crack extension}$$
$$e_o \text{ elastic elongation}$$

The increment of energy consumed in crack extension, δc, is the change of strain energy with crack extension for fixed grip conditions. Plotting load (P) versus displacement (e_o) (Figure 14b) results in an energy relation

$$u = 1/2 \, Pe_o \tag{11}$$

Approaching the problem by utilizing a spring constant, M, beyond the free length to insure linear response yields:

Figure 14a A Representation of Configurations for Single-Edge Notch and Center-Cracked Panel Assuming a Fixed Grip Position in Compliance Analysis.

Figure 14b Plot of Load (P) Versus Displacement (e_o) for Compliance.

FIXED

a

C + δC

PLASTIC
ZONE

C

e_0

P = LOAD

P

U

e_0
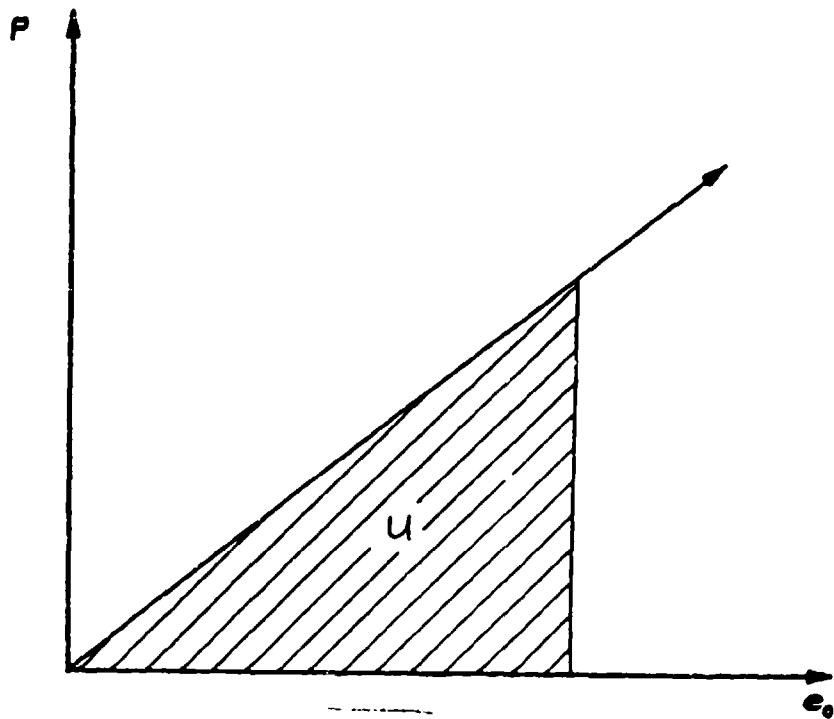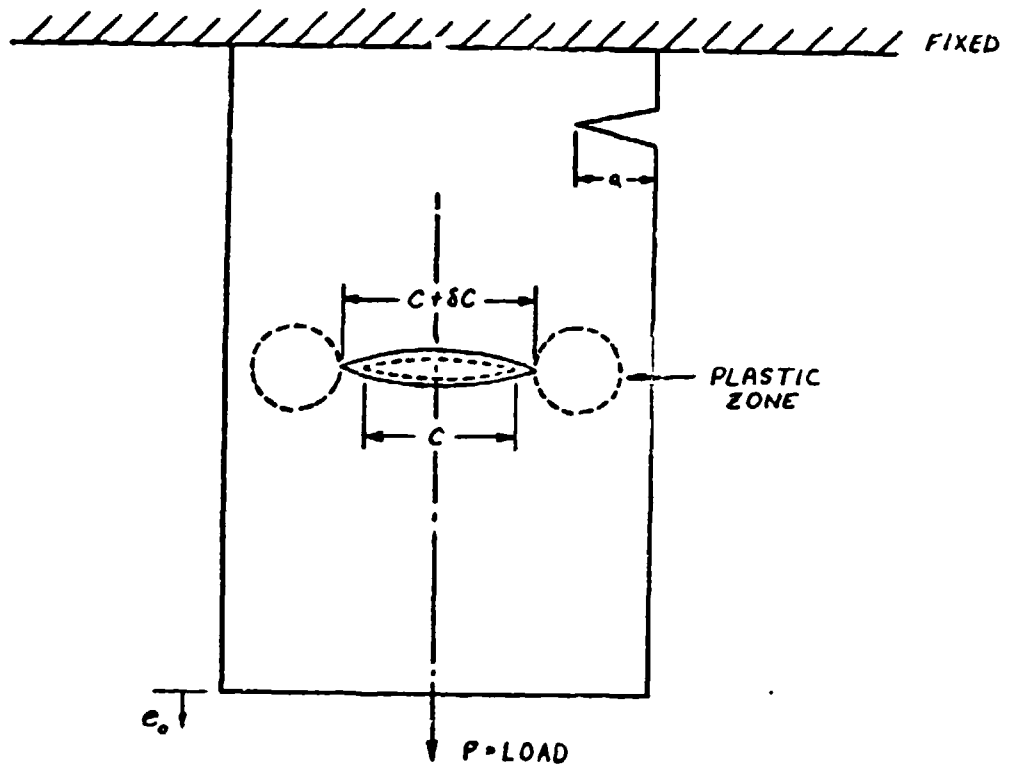
$$P = Me_0 \tag{12}$$

$$P/M = e_0 \quad \text{constant} \tag{13}$$

The compliance of a specimen is designated as 1/M in this approach.

Differentiating equations (11) and (13) with respect to (c) for a fixed (e) yields

$$\left(\frac{\delta u}{\delta c} \right)_e = 1/2 \left(\frac{\delta P}{\delta c} \right)_e e_0 \tag{14}$$

$$1/M \left(\frac{\delta P}{\delta c} \right)_{e_0} = -P \left(\frac{\delta}{\delta c} \frac{1}{M} \right)_{e_0} \tag{15}$$

$$\text{where } \frac{\delta P}{\delta M} = 0 \tag{16}$$

Substituting equation (13) into (14)

$$\left(\frac{\delta u}{\delta c} \right)_e = 1/2 \left(\frac{\delta P}{\delta c} \right)_{e_0} \frac{P}{M} \tag{17}$$

Recognizing the equivalence of terms in equation (17) to equation (15)

$$\left(\frac{\delta u}{\delta c} \right)_e = -\frac{P^2}{2} \left(\frac{\delta}{\delta c} \frac{1}{M} \right)_{e_0} \tag{18}$$

The parameters P and M are defined per unit thickness. A plot of specific loads and displacements is shown in Figure 15.

By using the compliance, $(1/M)$, and plotting it against the crack size (i.e. c_i, $i = 0,1,2,3$), the failure parameter, G_c for a flawed material can be graphically illustrated in Figure 16. Here, G is the crack extension or driving energy, where $G = -\frac{\delta u}{\delta c}$; $u =$ energy internal to body.

$$G = -\left(\frac{\delta u}{\delta c}\right)_{e_0} = \frac{P^2}{2}\left(\frac{\delta}{\delta c}\ \frac{1}{M}\right)_{e_0} \qquad (19)$$

Thus, the critical crack driving energy can be represented as follows,

$$G_c = \frac{P_c^2}{2}\left(\frac{\delta}{\delta c}\ \frac{1}{M}\right) \qquad (20)$$

5.2.2 Experimental Analysis in Weibull Parameterics

The future evaluation in crack extension energy, stress intensity, crack growth and fatigue life predictions has a critical focal point at compliance determination. Traditionally, the polynomial fit has been employed to a moderate degree of accuracy over a specific range of crack growth. An attempt to increase the precision of the curve fit and expand the range led to the following work. The rationale to pursue a Weibull type function stems from the empirically oriented concept of preference for best fit to date with a reduced or minimum number of fitting parameters. A purely mathematical advantage of the Weibull type function is observed as all data curves can be

Figure 15   Compliance Illustration of Increasing Crack Length (C_0 to C_3) Versus Load-Displacement Relationship.

Figure 16   Compliance, the Reciprocal of Stiffness, Fitted to a Traditional Polynomial over Increasing Crack Size.

57

Top figure: Plot of P (vertical axis) versus e (horizontal axis) showing lines labeled C_0, C_1, C_2, C_3 radiating from origin. Dashed lines mark P_0 at e_0 and P_3 at e_3. A line is annotated SLOPE : M.

Bottom figure: Plot of COMPLIANCE ($1/M$) versus CRACK SIZE (c) with points C_0, C_1, C_2, C_3, C_4, C_5, C_6 on horizontal axis. Curve annotated TRADITIONAL POLYNOMIAL FIT, and slope annotated $\frac{P_c^2}{2}\left(\frac{\partial}{\partial c}\frac{1}{M}\right)_c$.
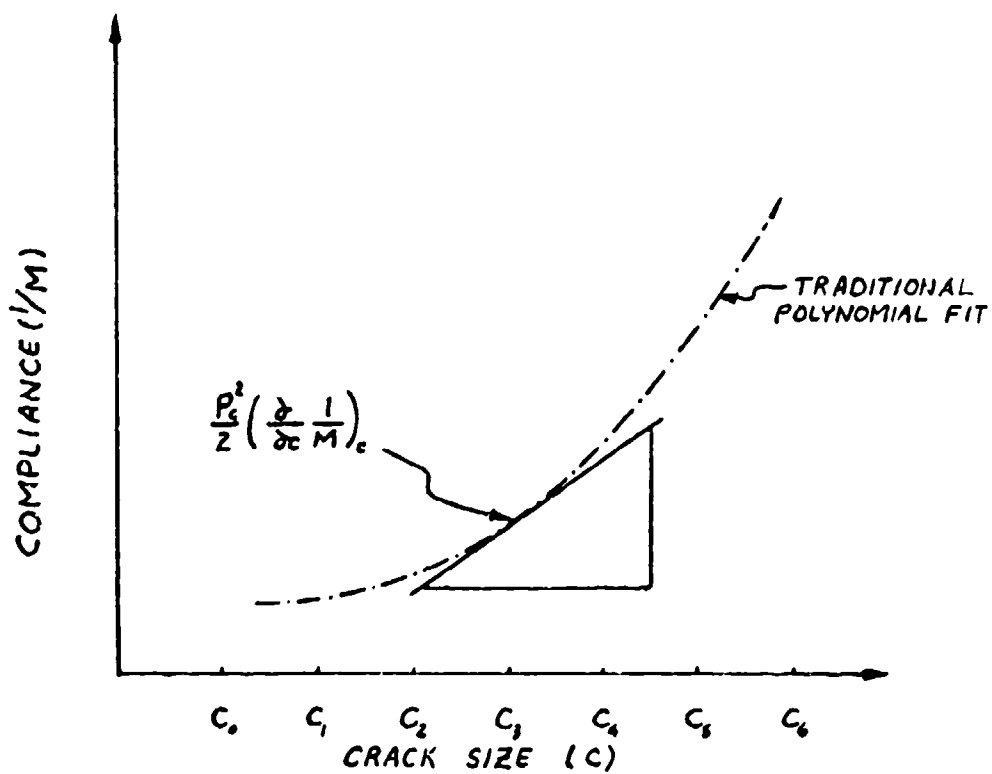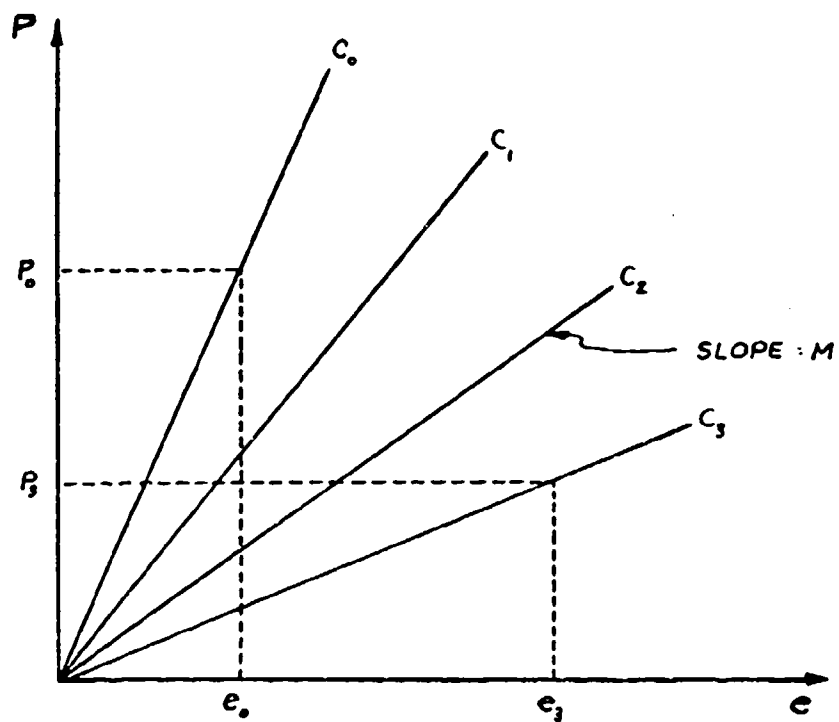
plotted through a common point permitting future relationships to be dependent on strictly one parameter, shape.

The algebraic mathematics appear rigorous compared to a series expansion of the polynomial type function, but is relatively elementary in the manipulations for compliance determination.

Base equation:
$$1 - a/W = \text{Exp}\left[-\left(\frac{\log_e\{\log_e(\frac{EB\delta}{P} + e)\}}{v}\right)^k\right] \quad (21)$$

The first order is to establish through linear regression analysis a coefficient of correlation, r, for sample of data. In this case the sample, N, was 26 data points measured by J.T. Ryder, Lockheed-California Rye Canyon Advanced Design and Research Laboratory.

The base equation (21) was modified to reflect the below form (22) with variables of the regression Y, YY indicated

$$\left|-\log_e(1 - a/W)\right|^{1/k} = 1/v \cdot \log_e\{\log_e(\frac{EB\delta}{P} + e)\} \quad (22)$$

$$Y = YY$$

$$Y = bX + a$$

The computations and data insert are carried out through a remote IBM-2741 terminal. The dialogue is in the Time Sharing Operation language, a TSO version of PL/I. The example of Weibull parameter estimation employs one stored subroutine.

As the program is called and entered, the number of sample points, N, are introduced. The option for center crack panel or wedge open loading specimen is presented, WOL is selected. After corresponding (a/W) versus (CEB) (i.e. EBδ/P) values are input to the system the iterative loop displays numerous values of w, which is 1/k, versus r. For structural alloys studied to date, the Weibull shape parameter k = 1/w shows $0<w<1$.

Upon reaching the best w and r, the cycle is terminated and the best w is supplied. At this point the regression variable forms are printed along with 26 values of Y and YY. The values are plotted in Figure 17 and show only one point outside the scatterband, 1.2 is permitted.

The following pages contain the slope of regression line, scatter in the vertical direction of observed points about the regression line linear equation and its measure of fit and WOL parameters k and v.

Through all remaining plots the k and v will be incorporated. The first demonstration of this comes when the measured CEB, a/W, and k and v terms are implemented to return a calculated a/W. The calculated values were incremented over an entire range of a/W, designated normalized crack length, and plotted in Figures 18 and 19 in conjunction with 22 of the data points from the measured sample. The correlation is impressively precise. Knowing that specimen compliance is the integral part of a stress intensity calculation, three compliance fitting equations are equalized and compared as follows.

Figure 17   Regression Variables Graphed with Corresponding 2σ Data
Points and a 2σ Scatter Band.

Figure showing regression plot with:

- Y-axis: REGRESSION VARIABLE $Y = [-\log_e(1 - a/W)]^{1/k}$
- X-axis: REGRESSION VARIABLE $(bX + a)$

Shape Parameter
$k = 2.99580574$

2σ

Sample Size N = 26

Sample Correlation
Coefficient, $r = 0.99953$

$a = 0.0000$
$b = 0.684190154$
$X = [B\delta/P$
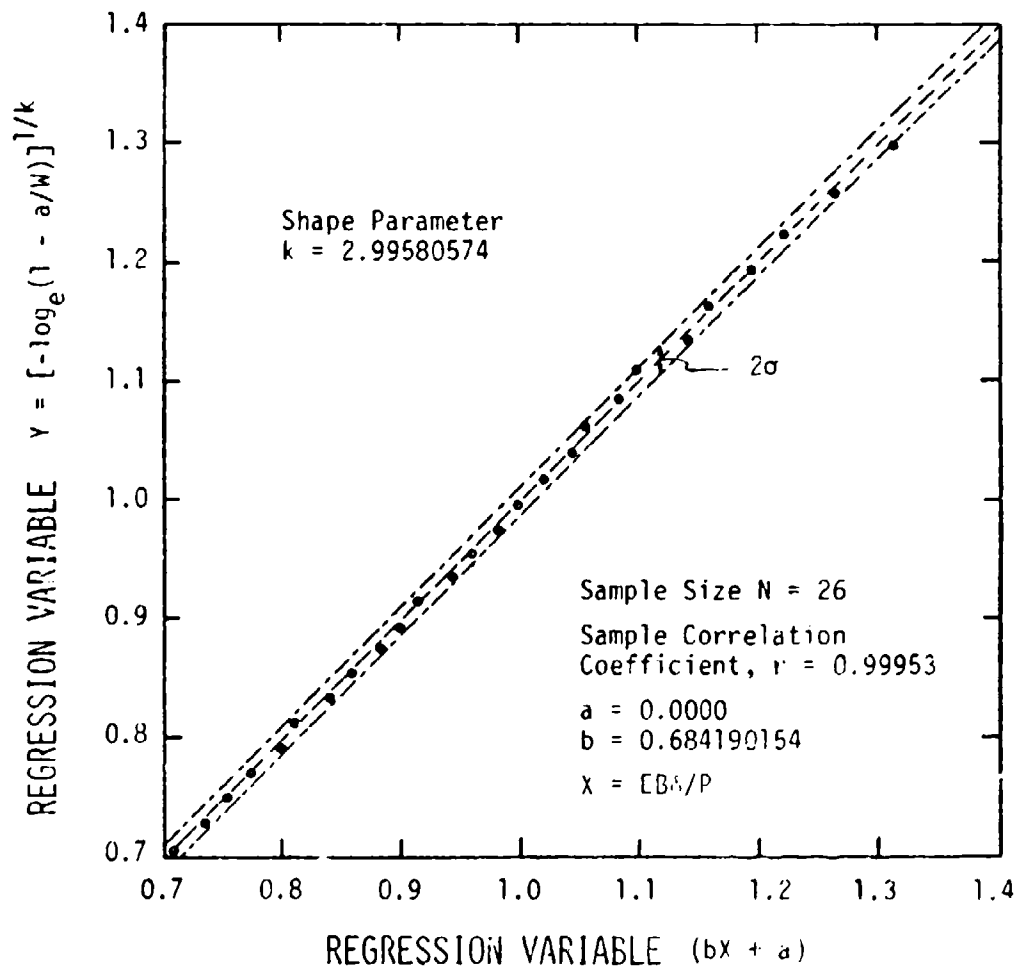
```
SUPPLY N, THE NUMBER OF POINTS
:
26
OPTION=0 IF CCP, =1 IF WOL
:
1
Z= 2C/W OR A/W VALUES
:
.297 .320 .344 .367 .392 .414 .438
+:.462 .486 .509 .533 .558 .580 .603
+:.627 .650 .674 .697 .721 .745 .768
+:.792 .816 .839 .862 .886
SUPPLY CEB VALUES
:
13.99 16.10 17.57 19.62 22.36 23.76
+:27.81 30.71 35.21 39.00 41.88 50.62
+:55.38 64.06 71.47 82.26 95.84 105.53
+:129.17 144.32 199.91 240.66 308.37 392.67
+:579.91 911.75
ENTER FLAG=1 IF BESTW FOUND, FLAG=0 IF NOT
:
1
SUPPLY BESTW
:
.3338
```

BESTW	R
0.33380	0.99953032

REGRESSION VARIABLE Y=(-LOG(1-A/W))**1/K
REGRESSION VARIABLE YY=B*LOG(LOG(CEB+EXP(1)))

Y	YY
7.0599E-01	7.0833E-01
7.2757E-01	7.3663E-01
7.4953E-01	7.5395E-01
7.7014E-01	7.7548E-01
7.9216E-01	8.0050E-01
8.1128E-01	8.1194E-01
8.3194E-01	8.4104E-01
8.5246E-01	8.5896E-01
8.7292E-01	8.8315E-01
8.9252E-01	9.0085E-01
9.1303E-01	9.1298E-01
9.3455E-01	9.4448E-01
9.5366E-01	9.5904E-01
9.7390E-01	9.8210E-01
9.9536E-01	9.9902E-01
1.0164E+00	1.0203E+00
1.0388E+00	1.0427E+00

Y	YY
1.0610E+00	1.0566E+00
1.0849E+00	1.0848E+00
1.1099E+00	1.0999E+00
1.1349E+00	1.1425E+00
1.1625E+00	1.1657E+00
1.1921E+00	1.1956E+00
1.2227E+00	1.2236E+00
1.2562E+00	1.2666E+00
1.2954E+00	1.3134E+00

THE SLOPE B OF THE REGRESSION LINE= 6.84190154E-01
THE Y INTERCEPT= 0.00000000E+00
THE SAMPLE CORRELATION COEFFICIENT = 0.99949735
THE SCATTER, IN THE VERTICAL (Y) DIRECTION
OF THE OBSERVED POINTS ABOUT THE REGRESSION
LINE IS FOUND TO BE 0.00556729
AT THIS VERTICAL DISTANCE ABOVE AND BELOW
THE REGRESSION LINE, TWO PARALLEL LINES
WILL INCLUDE 68.3% OF THE POINTS. AT TWICE
THIS DISTANCE, 95.4% OF THE POINTS ARE INCLUDED
THE LINEAR EQUATION Y= 0.68419015X
+ 0.00000000
HAS A MEASURE OF FIT = 0.00137254
THIS MEASURE IS THE SUM OF SQUARES OF VERTICAL
DEVIATIONS FROM REGRESSION LINE
THE WOL PARAMETERS K AND V ARE

K	V
2.99580574E+00	1.46158123E+00

	MEASURED	CALCULATED
CEB	A/W	A/W
13.9900	0.29700	0.29946
16.1000	0.32000	0.32983
17.5699	0.34400	0.34889
19.6199	0.36700	0.37303
22.3599	0.39200	0.40157
23.7599	0.41400	0.41477
27.8099	0.43800	0.44862
30.7100	0.46200	0.46962
35.2099	0.48600	0.49801
39.0000	0.50900	0.51875
41.8800	0.53300	0.53294
50.6200	0.55800	0.56947
55.3799	0.58000	0.58614
64.0599	0.60300	0.61222
71.4698	0.62700	0.63104
82.2599	0.65000	0.65421
95.8400	0.67400	0.67810

CEB	MEASURED A/W	CALCULATED A/W
105.5296	0.69700	0.69247
129.1699	0.72100	0.72090
144.3197	0.74500	0.73554
199.9099	0.76800	0.77473
240.6599	0.79200	0.79464
308.3684	0.81600	0.81874
392.6682	0.83900	0.83966
579.9089	0.86200	0.86865
911.7458	0.88600	0.89596

Figure 18   Normalized Plot of Compliance Versus Crack Length.   The
             circled 11 points characterize 11 measurements performed
             by J.T. Ryder (Personal Communication).

The Empirical Equation of the

Curve Is Given By:

$$\frac{EB\delta}{P} = Exp[Exp(v[-log_e(1 - a/W)]^{1/k})]-Exp(1.0)$$

$v = 1.46158123$
$k = 2.99580574$

Axis labels: NORMALIZED COMPLIANCE, $EB\delta/P$ (vertical), NORMALIZED CRACK LENGTH, a/W (horizontal)
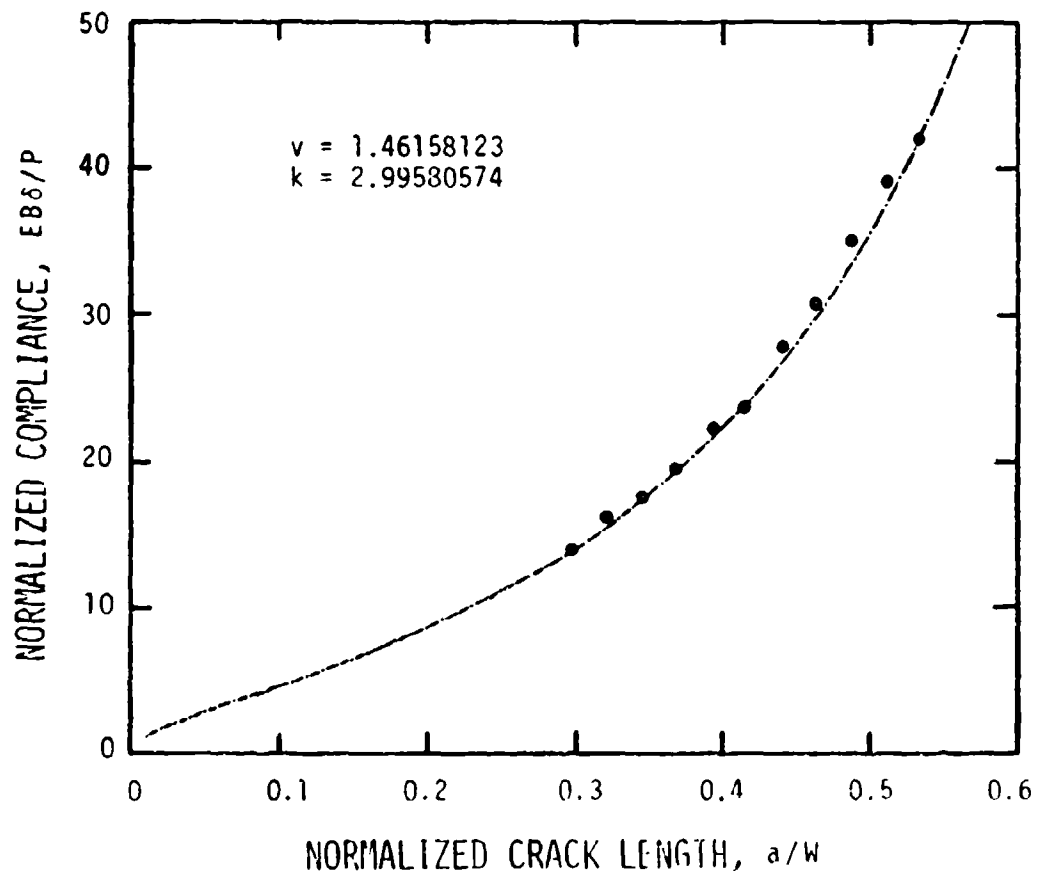
Figure 19   Normalized Plot of Compliance Versus Crack Length over an
Extended Range.   The circled 11 points were performed by
J.T. Ryder (Personal Communication).

The Empirical Equation of the

Curve Is Given By:

$$\frac{EB\delta}{P} = \text{Exp}[\text{Exp}(v[-\log_e(1 - a/W)]^{1/k})]-\text{Exp}(1.0)$$

NORMALIZED COMPLIANCE, EBδ/P

NORMALIZED CRACK LENGTH, a/W

v = 1.40158123
k = 2.99580574
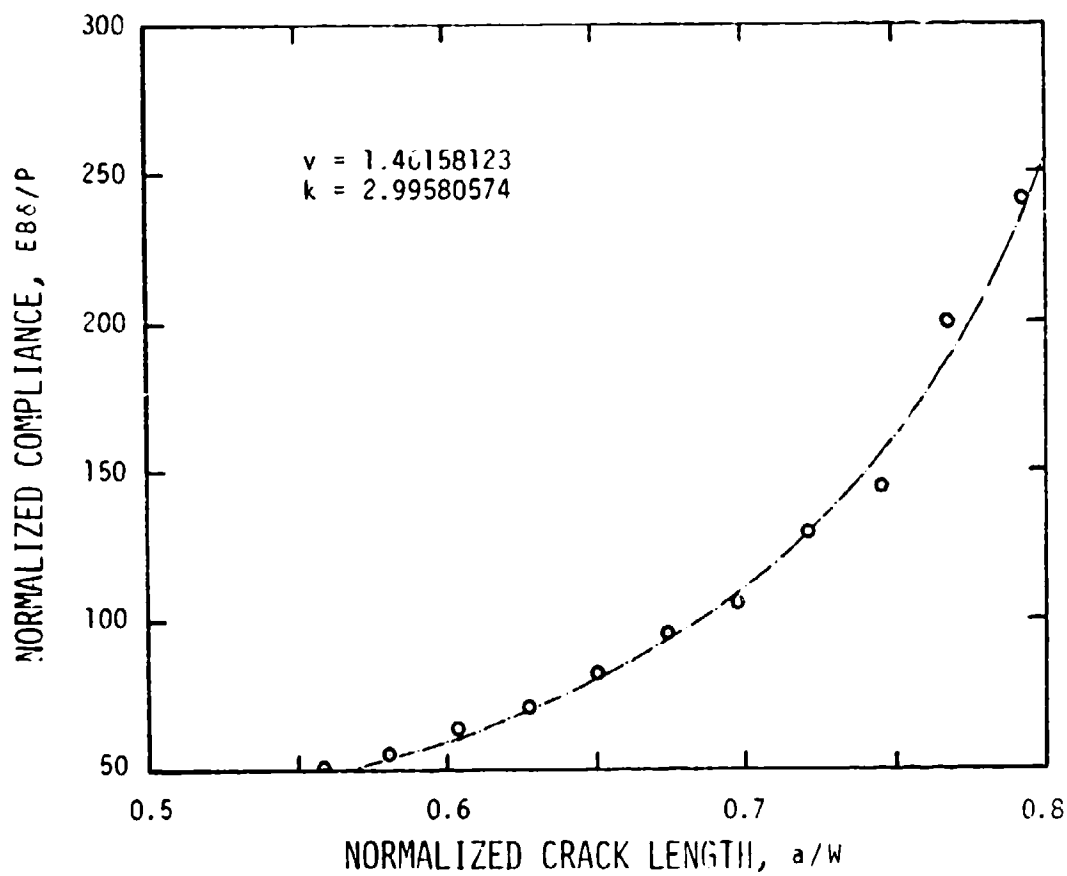
5.2.3 Summary on Stress Intensity Calibration Factor

In showing the entire range of data in Figure 20 and to demonstrate the mathematical advantages, the regression variable YY is plotted against the normalized crack length, a/W. Because at a/W, 1-1/e = 0.6321 where e, here is the naperian base equal to 2.71 while YY is equal to 1.0, all curves must pass through this common point leaving k, the Weibull shape parameter variable. Additionally, the exponential approach shows a higher degree of correlation to data fit.

Expanding on this final item, it was determined that a comparison should be developed between the values designated C_3 for two heavily used polynomials and the exponential expression of Weibull. The two expressions are #2 and #3 of Figures 21 and 22. The later will be the polynomial for the WOL specimen used in this study. The numerical relations of the curves are:

#1) $\quad C_3 = \left[.5 \ \frac{a}{W} \ \frac{dCEB}{d\ a/W} \right]^{1/2}$

$\qquad CEB = EB\delta/P$

$\qquad\qquad = Exp \ \{Exp(v[-\log_e(1-a/W)]^{1/k}); - Exp(1)$

$\qquad\qquad\qquad where \quad v = 1.46158123$

$\qquad\qquad\qquad\qquad k = 2.99580574$

#2) $\quad C_3 = \frac{a}{W} \cdot Y$

$\qquad\qquad where \ Y \quad 29.6 - 185.5 \ (\frac{a}{W}) + 655.7 \ (\frac{a}{W})^2 - 1017 \ (\frac{a}{W})^3$

$\qquad\qquad\qquad + 638.9 \ (\frac{a}{W})^4$

Figure 20 Regression Variable Versus Crack Length Plots all 26 Points
Over the Entire Range of a/W.

$$\frac{EB\delta}{P} = Exp[Exp(v[-log_e(1 - a/W)]^{1/k})]-Exp(1.0)$$

$$v = 1.46158123$$
$$k = 2.99580574$$

REGRESSION VARIABLE $YY = [log_e(log_e(\frac{EB\delta}{P} + Exp(1.0)))]/v$

0.63212

NORMALIZED CRACK LENGTH, a/W
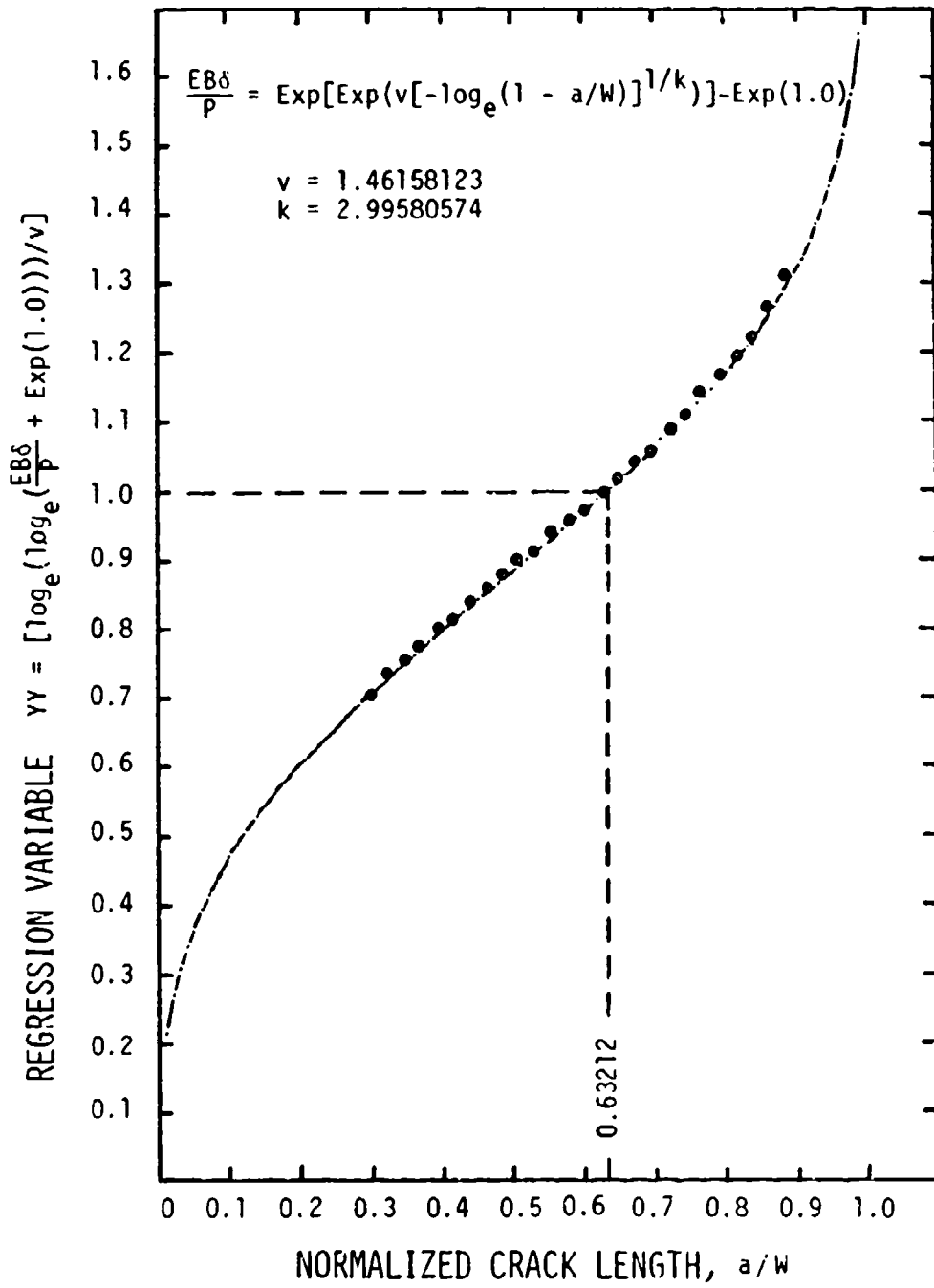
Figure 21   Comparison of Mathematical Compliance through Numerical
Relations of C_3 Curves Plotted over a Normalized Crack
Length Range 0.1 to 0.6.
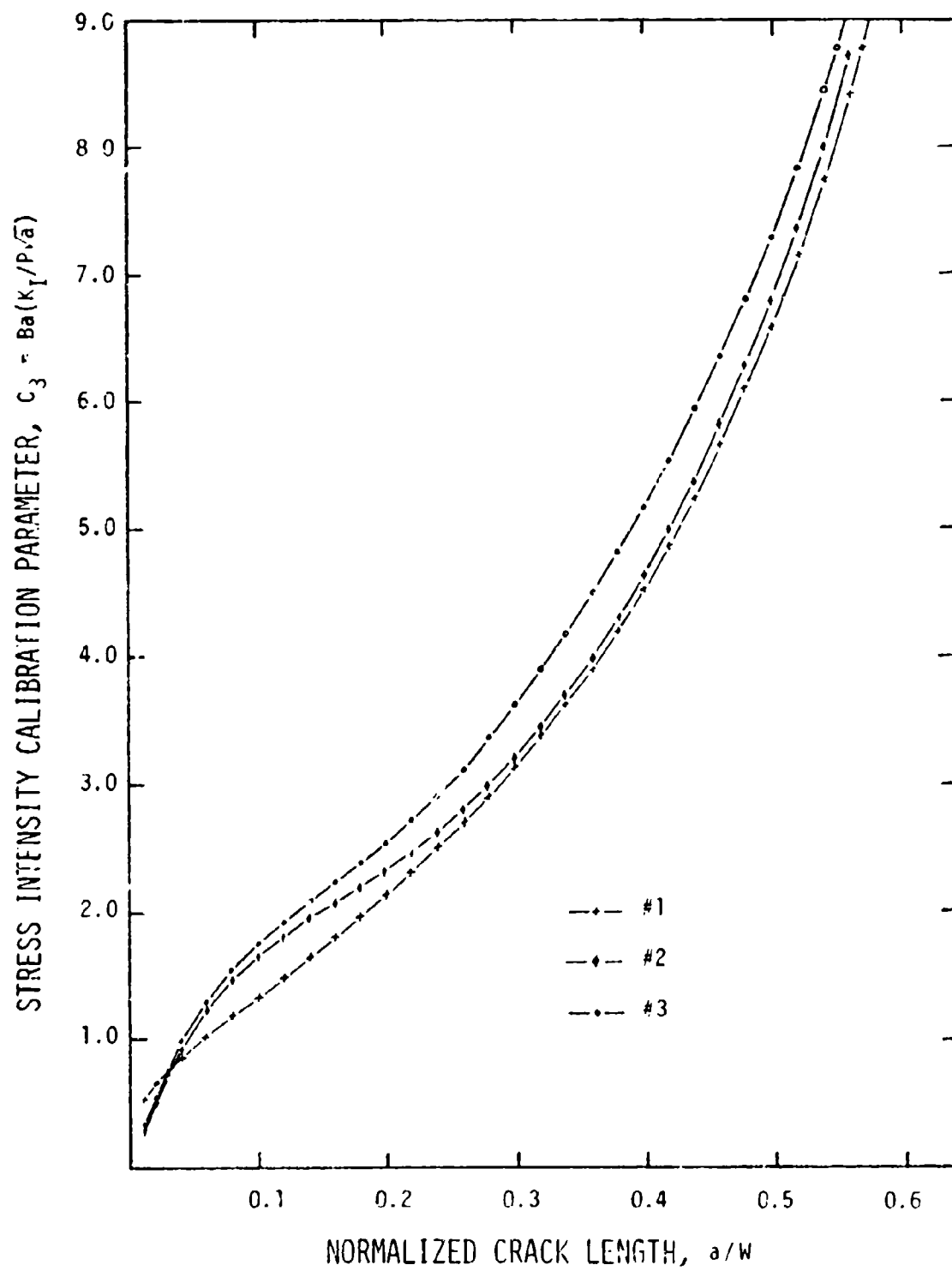
Figure 22   Comparison of Mathematical Compliance through Numerical
Relations of C_3 Curves Plotted over a Normalized Crack
Length Range 0.5 to 1.0.

Figure: Stress intensity calibration parameter $c_3 = Ba(K_I/P\sqrt{a})$ versus normalized crack length a/W.

Axes: STRESS INTENSITY CALIBRATION PARAMETER, $c_3 = Ba(K_I/P\sqrt{a})$ (vertical, 10 to 100); NORMALIZED CRACK LENGTH, a/W (horizontal, 0.5 to 1.0).

Legend: #1, #2, #3
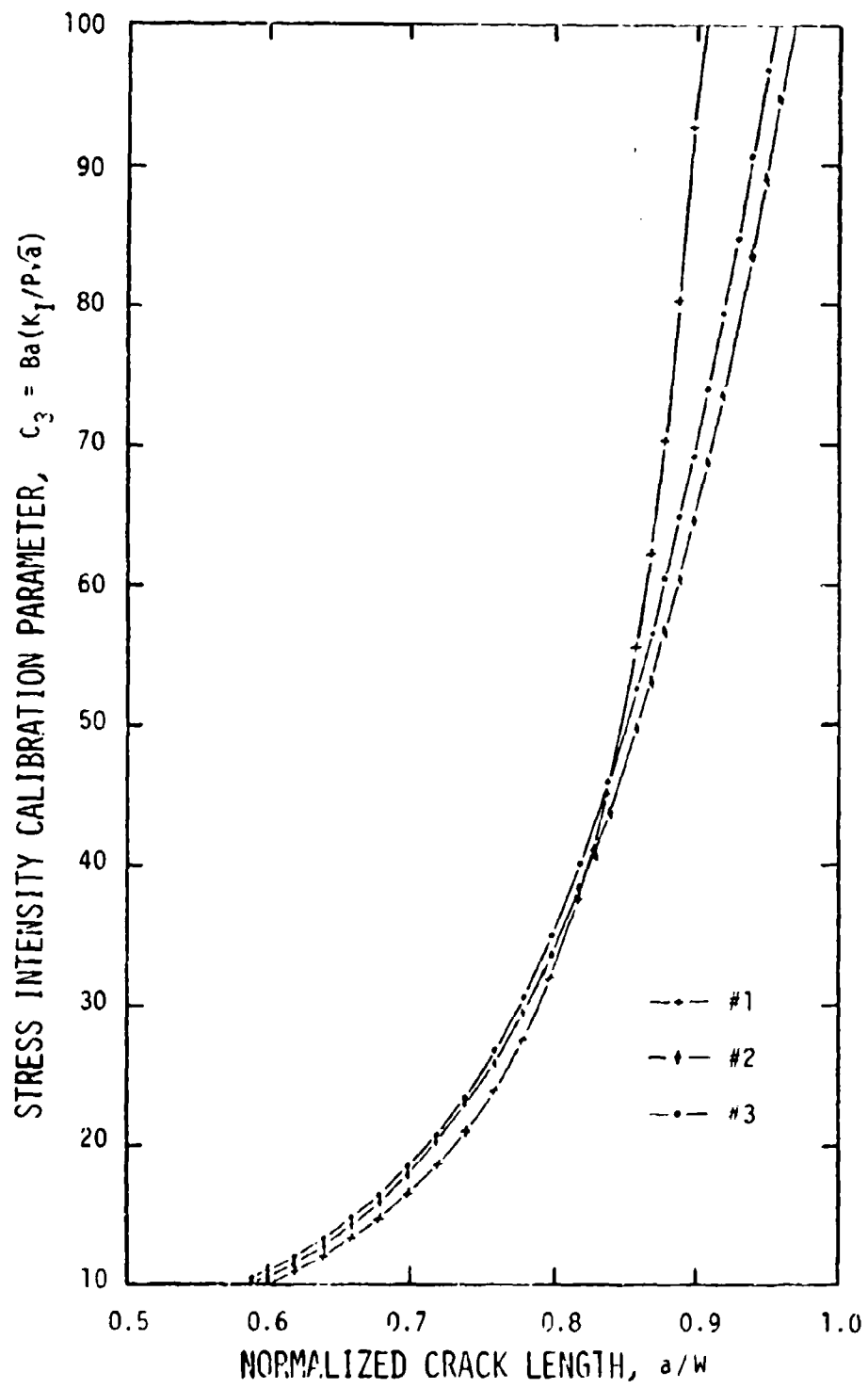
#3) $C_3 = \frac{a}{W} \cdot Y$ (Wilson Polynomial)

where $Y = 30.96 - 195.8 \left(\frac{a}{W}\right) + 730.6 \left(\frac{a}{W}\right)^2 - 1186.3 \left(\frac{a}{W}\right)^3$
$+ 754.6 \left(\frac{a}{W}\right)^4$

These polynomials (#2 and #3) are empirical best fits to data representing different specimen dimensions.

The rationale for multiplication of the polynomial values Y and a/W is as follows from Irwin and Kies, 1954

$$K_I = \frac{P}{B}\left[.5 \ \frac{1}{W} \ \frac{d(CEB)}{d(a/W)}\right]^{1/2} = \frac{P\sqrt{a}}{B \ a}\left[.5\left(\frac{a}{W}\right) \frac{d(CEB)}{d(a/W)}\right]^{1/2}$$

(23)

This is often e essed as:

$$Y = K_I \frac{BW}{P\sqrt{a}} \quad \text{or} \quad K_I = \frac{P}{B}\left[\frac{\sqrt{a}}{W} Y\right]$$

(24)

Thus, it is possible to write

$$Y \frac{\sqrt{a}}{W} = \left[.5 \left(\frac{1}{W}\right) \frac{d(CEB)}{d(a/W)}\right]^{1/2}$$

$$Y = \frac{W}{\sqrt{a}} \left[.5 \left(\frac{1}{W}\right) \frac{d(CEB)}{d(a/W)}\right]^{1/2}$$

(25)

$$Y = \left[.5 \left(\frac{1}{a/W}\right) \frac{d(CEB)}{d(a/W)}\right]^{1/2}$$

Thus, if $a \to 0$ then $Y \to \infty$. Knowing this and wanting to erradicate singularity, C_3 was used for comparison. (Note: Analytic functions may have different types of singularities. A singular point of an ana-

lytic function $f(x)$ is a point where $f(x)$ ceases to be analytic such as non-differentiable. Also, $f(x)$ is singular or has singularity at that point. The function $f(x)$ is termed singular at infinity if $f(\frac{1}{x})$ is singular at $x = 0$). Taking advantage of Wessel's work with the Wilson polynomial and combining with the modification in equation (23) an expression for C_3 can be written as

$$C_3 = \left(.5 \; (\frac{a}{W}) \; \frac{d(C[B)}{d(a/W)} \right)^{1/2}$$

$$= \left[.5 \; \frac{(\frac{a}{W})(\frac{a}{W})}{(\frac{a}{W})} \; \frac{d(C[B)}{d(a/W)} \right]^{1/2} \tag{26}$$

$$= \frac{a}{W} \left(.5 \; (\frac{1}{a/W}) \; \frac{d(C[B)}{d(a/W)} \right)^{1/2}$$

$$C_3 = (a/W) \cdot Y \tag{27}$$

The polynomial equations were modified as stated to provide equivalence for comparison and plotted in Figures 21 and 22. The stress intensity calibration parameter C_3 is expressed as

$$K_I \; \frac{B}{P} = \frac{\sqrt{a} \; Y}{W} = \left(.5(\frac{1}{W}) \; \frac{d(C[B)}{d(a/W)} \right)^{1/2} \tag{28}$$

$$Y = C_3 \; /(a/W) \tag{29}$$

$$K_I \; \frac{B}{P} = \frac{\sqrt{a}}{W} \; \frac{C_3}{(a/W)} = \frac{C_3}{\sqrt{a}} = \frac{C_3\sqrt{a}}{\sqrt{a}\sqrt{a}} = \frac{C_3\sqrt{a}}{a} \tag{30}$$

$$C_3 = Ba\left(\frac{K_I}{P\sqrt{a}} \right) \tag{31}$$

The error or difference plot in Figure 23 shows the most exten-
sive deviation of the polynomials outside a/W range of 0.3 to 0.7
where polynomials cannot account for the response. A large difference
is noted between curves 1 and 3 where 3 is the new polynomial ex-
pression moving toward adoption.

5.3 LIFE PREDICTION: REFINING NUMERICAL ANALYSIS

5.3.1 Convergence on Fitting Quality

5.3.1.1 Introduction

This section provides a review of some numerical interactions
regarding fitting relations and their quality. By standardizing the
discrimination power through precise data reduction and evaluation
techniques and increasing measurement efficiency, it is considered
possible to provide a methodology to reliably probe the macro-micro
interface of materials properties with respect to their fatigue-crack
growth behavior.

5.3.1.2 Candidate Exponential Curve Fitting Relations

It is usual to plot fatigue-crack propagation test results in the
form

$$Da/DN = f\ (\Delta K) \tag{32}$$

where Da/DN = crack propagation rate and ΔK = stress intensity
range. A suitable curve fitting relation for this type application
is one with a mathematical fit to the total physical behavior of fa-

Figure 23   Percent Differences Between the Empirical Calibration Parameters for Stress Intensity over a Normalized Crack Length Range.

The figure illustrates percent difference in stress intensity parameters C_3 (%) on the vertical axis versus normalized crack length, a/W, on the horizontal axis.

1 – Difference between curves #1 and #2 of previous graph.

2 – Difference between curves #1 and #3 of previous graph.

The curves illustrate differences in the calculated values of the form

$$\frac{[(C_3)_{new} - (C_3)_{old}]}{(C_3)_{new}} \times 100$$
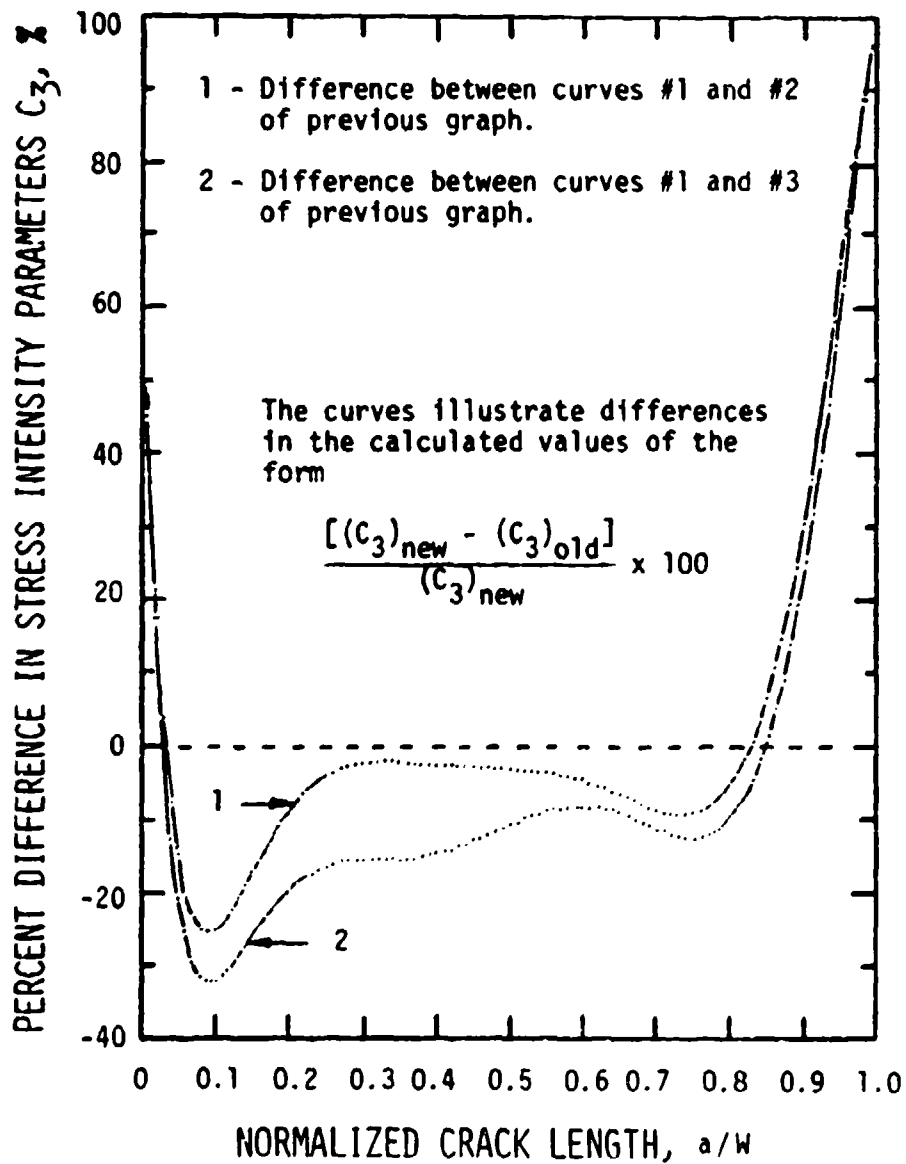
tigue-crack growth. This relation must have the following properties:

(1) The relation should lend itself to distinction be-
tween slow and fast crack growth rate segments.

(2) As ΔK approaches an upper limit, K_b, the crack growth
rate should increase indefinitely.

$$\lim_{\frac{\Delta K}{K_b} \to 1} \left| \frac{Da}{DN} \right| = \infty \tag{33}$$

(3) As ΔK approaches a lower threshold limit, K_{th}, the
crack growth rate should diminish to zero

$$\lim_{\Delta K \to K_{th}} \left| \frac{Da}{DN} \right| = 0 \tag{34}$$

A new class of exponential curve fitting relations with mathe-
matical form in the fatigue data reduction Weibull distribution
function were explored (Bowie, 1974-1976). This form is the same form
similar to that discussed for compliance considerations. Three mem-
bers of the class are:

Type   Relations

A) $1 - F = \text{Exp}\left(- \left(\frac{H - e}{v - e} \right) \right)^k$, $\tag{35}$

or $H = e + (v - e) \left| (- \log_e(1 - F)) \right|^{1/k}$;

B) $1-F = \text{Exp}\left[- \left(\dfrac{\log_e(H + 1) - e}{v - e} \right)^k \right]$,

or $H = -1 + \text{Exp}\ (e + (v - e)\left|(- \log_e(1 - F))\ \right|^{1/k})$ (36)

C) $1-F = \text{Exp}\left[- \left(\dfrac{\log_e \log_e(H + \exp(1)) - e}{v - e} \right)^k \right]$ (37)

or $H = -\text{Exp}(1) + \text{ExpExp}\ (e + (v - e)\ (- \log_e(1 - F))^{1/k})$

These relations meet the three criteria of acceptability previously stated. Computations are performed at an IBM Type 2741 remote computer terminal in PL/I language. The fitting routine contains logic for estimating the curve fitting parameters k, e, and v by a combination of linear regression and correlation coefficient optimization. In practice, Da/DN and ΔK values of a data set are stored as one dimensional arrays DaDN and dK. The regression analysis is performed on variables X and Y, in terms of the equation of regression

$$(- \log_e Y)^W = bX + a,$$ (38)

which has alternative form

$$Y = \text{Exp}\ (- (\tfrac{X - e}{v - e})^k)$$ (39)

where $k = 1/w$,

                $e = -a/b$,

and $v = (1 + be)/b$

The following operations are performed, for example, when applying candidate Type-B curve fitting:

```
DO i = 1 TO N

    X = log_e(DaDN(i) + 1)

    Y = (- log_e(1 - dK(i)/K_b))^W

    .          .

    .          .

    Regression and Correlation Coefficient Logic

    .          .

  END
```

In this case, the routine yields the Type-B relation

$$1 - \Delta K/K_b = \text{Exp}\left[-\left(\frac{\log_e(Da/DN + 1) - e}{v - e} \right)^k \right], \qquad (40)$$

where $\Delta K/K_b = F$, and $Da/DN = H$

Parameter K_b is the stress intensity range where Da/DN is indefinitely large. Estimation of K_b requires exercise of judgement in addition to interactive computing effort. At the outset of data set analysis, all three types of exponential curve fitting relations are tested, with $F = \Delta K/K_b$ and $H = Da/DN$ for each type. Measures of goodness of fit are used in deciding which, if any, type is suitable. For all three types, the particular stress intensity range where $Da/DN = 0$ is called the threshold stress intensity, K_{th}, where

$$K_{th} = K_b \left(1 - \text{Exp}\left(-\left(\frac{-e}{v - e} \right) \right)^k \right) \qquad (41)$$

Physical significance is attached to threshold K_{th} for cases where threshold parameter $e \leq 0$.

$$\text{a.} \quad \text{For } e = 0, \ K_{th} = 0 \tag{42a}$$

$$\text{b.} \quad \text{For } e < 0, \ K_{th} > 0 \tag{42b}$$

c. For $e > 0$, the suggestion is that (42c) crack growth begins at some $Da/DN > 0$ for arbitrarily small $\Delta K > 0$.

5.3.1.3 Measures of Goodness of Fit

For a data set of sample size N_p, linear regression is performed with systematic iteration on parameter w, ($w = 1/k$), until a sample correlation coefficient, r is maximized. In the routine

$$r = \frac{N_p \sum_{i=1}^{N_p} X_i Y_i - \sum_{i=1}^{N_p} X_i \sum_{i=1}^{N_p} Y_i}{\left\{ \left[N_p \sum_{i=1}^{N_p} X_i^2 - (\sum_{i=1}^{N_p} X_i)^2 \right] \left[N_p \sum_{i=1}^{N_p} Y_i^2 - (\sum_{i=1}^{N_p} Y_i)^2 \right] \right\}^{1/2}} \tag{43}$$

To the extend that it might be reasonable to assume that $Y = [- \log_e (1 - \Delta K/K_b)]^{1/k}$ for optimum k is randomly distributed, it may be inferred that regression of Y on X accounts for 100 r^2 percent of the variance of Y. The scatter of Y_i, $i = 1,2 \ldots N_p$, about regression line

$$Y = bX + a$$

is measured by computing the variance term

$$\sigma^2 = \frac{N_p - 1}{N_p - 2} (1 - r^2) \left\{ \left(N_p \sum_{i=1}^{N_p} Y_i^2 - (\sum_{i=1}^{N_p} Y_i)^2 \right) \div N_p(N_p-1) \right\}$$

(44)

It is a good idea to count the number of points (X_i, Y_i) which fall between the lines

$$Y' = bX + a + 2\sigma$$

and $\qquad\qquad Y'' = bX + a - 2\sigma$

When approximately, 95% of the points do fall between lines Y' and Y'', it is reasonable to plot 2σ bands in plots of Da/DN versus ΔK. For example, Type-B curve fitting yields 2σ bands defined by the relations

$$(Da/DN)' = -1 + Exp\ (e' + (v' - e')\ (-log_e(1 - \Delta K/K_b))^{1/k})$$

and $\quad (Da/DN)'' = -1 + Exp\ (e'' + (v'' - e'')\ (-log_e(1 - \Delta K/K_b))^{1/k})$,

(45)

where $\qquad e' = -(a + 2\sigma)/b$

$\qquad\qquad\quad v' = (1 + b\ e')/b$

and $\qquad\quad e'' = -(a - 2\sigma)/b$

$\qquad\qquad\quad v'' = (1 + b\ e'')/b$

A third measure of goodness of fit is monitored with the aid of the routine. It is the sum of squares of the deviations $(Y_i - (b\ X_i + a))$, and is called D^2

$$i.e., \quad D^2 = \sum_{i=1}^{N_p} (Y_i - (b\ X_i + a))^2$$

(46)

For Type-B curve fitting,

$$D^2 = \sum_{i=1}^{N_p} \left\{ (- \log_e(1 - \Delta K_i/K_b))^{1/k} - \frac{(\log_e(Da/DN_i + 1) - e)}{(v - e)} \right\}^2$$

(47)

Other investigators may choose to adopt an alternative computational procedure designed for selection of best values of parameters K_b, k, e, and v by minimizing D^2.

5.3.1.4 Distinction Between Slow and Fast Crack Growth

In current damage tolerant design practice, the terms "slow crack growth" and "fast crack growth" often are used in an entirely descriptive way. The following quantitative procedure represents a significant analysis development for distinguishing between slow and fast growth. The procedure must be applied with caution, because results are highly dependent on definition of the parameter K_b, the stress intensity range where Da/DN increases without bound. A given data set may or may not contain sufficient information to warrant selection of plausibly physical value K_b. In the event that acceptable K_b does not appear to be intrinsic to a data set, it is necessary to select K_b arbitrarily. It is believed that possible difficulty in estimating an unbiased value K_b has a parallel in ASTM E399, where it is necessary at times to specify that a fracture mechanics test has yielded an invalid estimate of fracture toughness K_{Ic}. The way in which a value K_b is selected when applying the routine to a data set

$(DaDN_i, dK_i)$ is as follows: The largest value of ΔK in the set is noted and an initial estimate for K_b is chosen to be

$$K_b = \Delta K_{max} + \varepsilon, \quad 0.01 \leq \varepsilon \leq 1.0 \tag{48}$$

An initial curve fitting relation is found, and the initial correlation coefficient, r_0, is noted. The computational process is repeated with successively larger K_b estimates, usually in increments of 10 ksi $\sqrt{in}$ (11 MPa $\sqrt{m}$). Two possibilities exist:

- Either r can be maximized at a particular K_b
- r increases relatively slowly in a monotonic way, even for values $K_b >> \Delta K_{max}$

In the first instance, K_b is optimized to ± 0.5 ksi $\sqrt{in}$ (± 0.55 MPa $\sqrt{m}$) approximately. In the second, appeal is made to similar data set examinations, to the approximation

$$K_b \cong (1 - \text{Load Ratio, R}) K, \tag{49}$$

where K might be a fracture toughness value (e.g. K_{Ic} or K_Q) determined in some other test, or K_b is selected arbitrarily, sometimes with a yield stress value in mind.

5.3.1.5 Risk Analysis

The ratio of highest to lowest Da/DN value in a data set can be of the order of 10^6. It is no wonder that fracture mechanics' investigators plot Da/DN to a logarithmic scale. Whether a linear or

logarithmic ΔK scale is used is a matter of custom. The log-log format can be helpful when the data seem to be reduced to a straight line over a control ΔK region. The log-linear format is recommended when exponential curve fitting is appropriate.

The trend of the natural logarithm of Da/DN with increasing ΔK is used as a guide in defining the transition between slow and fast growth. The trend is called a risk function, r^*, given by

$$r^* = \frac{\partial \log_e Da/DN}{\partial(\Delta K/K_b)} = \frac{1}{(Da/DN)} \cdot \frac{\partial(Da/DN)}{\partial(\Delta K/K_b)} \tag{50}$$

For Type-B curve fitting,

$$r^* = \frac{(v-e)}{k} \cdot \frac{(Da/DN + 1)}{Da/DN} \cdot \left[\frac{-\log_e(1 - \Delta K/K_b)}{(1 - \Delta K/K_b)} \right]^{-1 + 1/k} \tag{51}$$

When plotted as a function of $\Delta K/K_b$ or ΔK, risk function, r^*, is U-shaped. The value of ΔK where $r^*(\Delta K)$ is minimal, is proposed as a quantitative location of the transition from slow to fast growth, with symbol ΔK_{sf}.

$$\text{i.e., for } \Delta K = \Delta K_{sf}, \quad \frac{\partial r^*(\Delta K)}{\partial \Delta K} = 0. \tag{52}$$

To demonstrate the operation of the previous section's analysis an example is considered using Ti-6A1-6V-2Sn fatigue-crack growth data.

This data was generated and reduced at University of Missouri-Columbia, during Winter Semester 1975.

5.3.2 Numerical Analysis of Crack Propagation Measurements

5.3.2.1 Purpose of Improved Curve Fitting

Numerical procedures can be employed for predicting the number of load cycles for crack growth from an initial crack length to a final length corresponding to a design life or an inspection interval. These procedures can be evaluated using compact tension (CT) or wedge open loading (WOL) specimen compliance calibration and crack growth rate test results. As in section 5.2.3 the WOL specimen stress intensity factor K can be expressed by rearranging Eq. 31 as:

$$K = \frac{P\sqrt{a}}{Ba} \left[.5 \left(\frac{a}{W}\right) \frac{d(CCB)}{d(a/W)}\right]^{1/2} = \left[\frac{P\sqrt{a}}{Ba}\right]C_3 \qquad (53)$$

where $C_3 = \left[.5 \left(\frac{a}{W}\right) \frac{d(CCB)}{d(a/W)}\right]^{1/2}$ and $CCB = \frac{CB}{P}$ is the

compliance calibration parameter. Calculation of K requires a differentiable fitting relation for CCB as a function of a/W. One approach used widely in the past by fracture mechanicians, is to apply a compliance calibration expression of the following form:

$$CEB = Exp[\sum_{i=1}^{6} k_i \ (a/W)^{i-1}] \tag{54}$$

usually considered valid for $0.3 \leq a/W \leq 0.8$. The polynomial co-efficients k_i can be determined with the aid of an interactive pro-gramming system (PL/I) curvilinear regression routine, POLFIT.

The results of the polynomial regression analysis for the calibration data can be used in conjunction with the curve fitting relation to express the polynomial compliance calibration. This curve segment has been seen to fit adequately for a range in a/W between 0.3 to 0.8. Using WOL crack propagation results as a test case life or inspection interval prediction exercises can be per-formed.

It is desirable to expand the boundary conditions so that the stress intensity range ΔK, given by

$$\Delta K = (1 - \text{load ratio, } R) \frac{P\sqrt{a}}{Ba} C_3, \tag{55}$$

could be calculated for values of C_3 outside the range 0.3 to 0.8 of a valid compliance calibration fitting relation.

Consider a more useful fitting relation that would extend the allowed range of a/W to $0 \leq a/W \leq 1.0$. To explore the possibility, the Weibull distribution was determined to display better physical relation to the required boundary conditions. As previously mentioned an interactive (PL/I) routine called WYBULL was developed (Bowie et al, 1974) for estimating the three parameters k, e, v of

the Weibull distribution function:

$$P(x) = \text{Exp} \left[- \left(\frac{x - e}{v - e} \right)^k \right] \tag{56}$$

Minor modifications of the routine yielded a new program, called
WOLFIT that is used to obtain the three parameters k, e, and v, for
the new WOL specimen compliance calibration fitting relations in
section 5.3.1.2

$$CEB = H \quad \text{and} \quad a/W = 1 - F$$

The boundary condition of $a/W = 1$

requires $1 - F = 0$, is satisfied when $\lim_{a/W \to 1} (CEB) = \infty$.

The boundary condition of $a/W = 0$

requires $1 - F = 1$, implies $\log_e \log_e (CEB + \text{Exp}(1)) - e = 0$

or $CEB(a/W = 0) = \text{ExpExp}(e) - \text{Exp}(1)$.

For example, if $\text{Exp}(e) = 1$, that is $e = 0$, then $CEB = 0$ when $a/W = 0$.
When comparing the polynomial form of C_3 and that of the Weibull
distribution form, it was seen that the difference of Weibull C_3 was
negligible for the range 0.3 to 0.6 of a/W, but was 20% lower at
$a/W = 0.1$ and at $a/W = 0.8$ was 10% lower than the polynomial C_3
(Figure 23).

5.3.2.2   Initial Test Data Reduction

The compact tension specimen test results studied to date con-
sist of sets of crack length and load cycle values obtained in ex-

periments performed at a set of loads with sine form, where load ratio, R = 0.05. Crack length measurements were made on both sides of the specimen. A typical raw data set studied was for the case of specimen thickness B = 0.996 in. (2.53 cm), and width W = 3.0 in. (7.62 cm). Load cycles were applied to a frequency of 10 Hz, and the test was performed at room temperature in laboratory air environment. Note that Table IV contains 48 pairs of crack length measurements and 48 numbers of load cycles at which the crack length measurements were performed. Experimental values of crack propagation rate are given by

$$Da/DN(i) = 10^{-6} \frac{\Delta a(i)}{\Delta N(i)} \qquad (57)$$

$$= 10^{-6} \frac{A(i + 1,1) + A(i + 1,2) - A(i,1) - A(i,2))/2}{N(i+1) - N(i)}$$

$$i = 1,2,3 \dots \qquad (58)$$

where $A(j,1)$, $A(j,2)$ are crack lengths measured on sides 1 and 2 of the specimen and $N(j)$ is the cumulative number of load cycles. Experimental values of stress intensity range are given by

$$\Delta K(i) = (1-R) \frac{P(i)\sqrt{a(i)}}{(B \ a(i))} C_3(i), \ ksi \ \sqrt{in} \ (MPa \ \sqrt{m}), \ i=1,2,3..(59)$$

Derivations of numerical expressions for function C_3 were discussed in section 5.2.3. The value of K_b was chosen to be 50 ksi $\sqrt{in}$ (54.9 MPa $\sqrt{m}$).

A summary of initial test data reduction for specimen T-92B-1 run at the University of Missouri, Winter 1975, is given in Table V.

TABLE IV

FATIGUE-CRACK GROWTH RAW DATA

	Crack Length Side 1 inch	Side 2 inch	Cycles, N	Max. Load kips.
1	1.0520	1.0540	0	4.0
2	1.0581	1.0589	2000	4.0
3	1.0622	1.0666	4000	4.0
4	1.0694	1.0720	6000	4.0
5	1.0745	1.0815	8000	4.0
6	1.0830	1.0870	10000	4.0
7	1.0886	1.0906	12000	4.0
8	1.0905	1.0925	14000	4.0
9	1.0980	1.1004	16000	4.0
10	1.1025	1.1055	18000	4.0
11	1.1153	1.1193	20000	4.0
12	1.1250	1.1350	22000	4.0
13	1.1395	1.1415	24000	4.0
14	1.1360	1.1560	26000	4.0
15	1.1420	1.1560	28000	4.0
16	1.1670	1.1710	30000	4.0
17	1.1690	1.1810	32000	4.0
18	1.1865	1.1895	34000	4.0
19	1.1960	1.1980	36000	4.0
20	1.2055	1.2105	38000	4.0
21	1.2140	1.2160	40000	4.0
22	1.2239	1.2311	42000	4.0
23	1.2345	1.2385	44000	4.0
24	1.2462	1.2526	46000	4.0
25	1.2608	1.2632	48000	4.0
26	1.2720	1.2750	50000	4.0
27	1.2829	1.2871	52000	4.0
28	1.2995	1.2995	54000	4.0
29	1.3120	1.3096	56000	4.0
30	1.3261	1.3241	58000	4.0
31	1.3390	1.3374	60000	4.0
32	1.3593	1.3573	62000	4.0
33	1.3665	1.3625	64000	4.0
34	1.3780	1.3764	66000	4.0
35	1.3950	1.3936	68000	4.0
36	1.4145	1.4139	70000	4.0

TABLE IV (cont.)

	Crack Length			
	Side 1 inch	Side 2 inch	Cycles, N	Max. Load kips.
37	1.4280	1.4276	72000	4.0
38	1.4645	1.4635	74000	4.0
39	1.4798	1.4788	76000	4.0
40	1.5831	1.5823	90000	4.0
41	1.6229	1.6209	92000	4.0
42	1.6598	1.6588	94000	4.0
43	1.6964	1.6954	96000	4.0
44	1.7323	1.7303	98000	4.0
45	1.7761	1.7741	100000	4.0
46	1.8295	1.8285	102000	4.0
47	1.9011	1.9011	104000	4.0
48	2.0192	2.0172	106000	4.0

TABLE V

FATIGUE-CRACK GROWTH REDUCED DATA

	Δa	ΔN	Da/DN	ΔK	Max. Load
1	0.0045	2000	2.25	12.843	4.0
2	0.0059	2000	2.95	12.890	4.0
3	0.0063	2000	3.15	12.941	4.00
4	0.0073	2000	3.65	13.002	4.00
5	0.0070	2000	3.50	13.061	4.00
6	0.0046	2000	2.30	13.100	4.00
7	0.0019	2000	0.95	13.116	4.00
8	0.0077	2000	3.85	13.183	4.00
9	0.0048	2000	2.40	13.225	4.00
10	0.0133	2000	6.65	13.344	4.00
11	0.0127	2000	6.35	13.461	4.00
12	0.0105	2000	5.25	13.560	4.00
13	0.0055	2000	2.75	13.612	4.00
14	0.0030	2000	1.50	13.641	4.00
15	0.0200	2000	10.00	13.838	4.00
16	0.0060	2000	3.00	13.898	4.00
17	0.0130	2000	6.50	14.031	4.00
18	0.0090	2000	4.50	14.124	4.00
19	0.0110	2000	5.50	14.240	4.00
20	0.0070	2000	3.50	14.315	4.00
21	0.0125	2000	6.25	14.451	4.00
22	0.0090	2000	4.50	14.551	4.00
23	0.0129	2000	6.45	14.696	4.00
24	0.0126	2000	6.30	14.840	4.00
25	0.0115	2000	5.75	14.974	4.00
26	0.0115	2000	5.75	15.111	4.00
27	0.0145	2000	7.25	15.286	4.00
28	0.0108	2000	5.40	15.418	4.00
29	0.0148	2000	7.40	15.603	4.00
30	0.0133	2000	6.65	15.772	4.00
31	0.0199	2000	9.95	16.031	4.00
32	0.0062	2000	3.10	16.113	4.00
33	0.0127	2000	6.35	16.283	4.00
34	0.0171	2000	8.55	16.517	4.00
35	0.0199	2000	9.95	16.796	4.00
36	0.0136	2000	6.80	16.991	4.00
37	0.0362	2000	18.10	17.528	4.00

TABLE V (cont.)

38	0.0153	2000	7.65	17.763	4.00
39	0.1034	14000	7.39	19.501	4.00
40	0.0392	2000	19.60	20.237	4.00
41	0.0374	2000	18.70	20.988	4.00
42	0.0366	2000	18 30	21.774	4.00
43	0.0354	2000	17.70	22.589	4.00
44	0.0438	2000	21.90	23.680	4.00
45	0.0539	2000	26.95	25.168	4.00
46	0.0721	2000	36.05	27.456	4.00
47	0.1171	2000	58.55	32.097	4.00

The object of crack propagation rate curve fitting is to select a relation to represent the experimental results in the Da/DN and $\Delta K/K_b$ columns of Table V.

The Type-A exponential crack propagation curve fitting relations defined in section 5.3.1.2 were applied to the measurements of Da/DN and $\Delta K/K_b$ listed in Table VI. The PL/I routine was used to estimate the Weibull parameters k, e, and v. The regression analysis results are summarized in Figure 24, where the circled points have regression variable coordinates

$$Y = [- \log_e(1 - \Delta K/K_b)]^{1/k} \tag{60}$$

and

$$X = b \, Da/DN + a$$

5.3.2.3 Type-A Curve Fitting Relations for Ti-6Al-6V-2Sn, Specimen T-92B-1, Tested in 45.9% R.H. Lab Air at R = 0.05

Application of Type-A crack propagation curve fitting relation was made for the case of a set of 47 Da/DN and ΔK measurements for a Ti-6Al-6V-2Sn WOL specimen tested under a 10 Hz sine wave, with R = 0.05 in ambient laboratory air (R.H. = 45°, 80 F (26.7 C)). The specimen T-92B-1 dimensions were as follows: specimen thickness, b = 0.996 in (2.53 cm) width, W = 3.0 in (7.62 cm) and initial flaw (machined), a_i = 0.90 in (2.29 cm).

TABLE VI

MEASURED AND CALCULATED ΔK

THE CRACK GROWTH PARAMETERS K, E, V ARE

K	E	V
0.55710334	-3.97261906	57.96824646

MEASURED		CALCULATED
DADN	DELTAK	DELTAK
2.25000	12.84300	12.13429
2.95000	12.89000	12.77290
3.15000	12.94100	12.94811
3.65000	13.00200	13.37341
3.50000	13.06100	13.24767
2.30000	13.10000	12.18129
0.95000	13.11600	10.82383
3.85000	13.18300	13.53870
2.40000	13.22500	12.27463
6.65000	13.34400	15.61683
6.35000	13.46100	15.41237
5.25000	13.56000	14.62808
2.75000	13.61200	12.59458
1.50000	13.64100	11.40045
10.00000	13.83800	17.67674
3.00000	13.89800	12.81698
6.50000	14.03100	15.51508
4.50000	14.12400	14.05850
5.50000	14.24000	14.81138
3.50000	14.31500	13.24767
6.25000	14.45100	15.34337
4.50000	14.55100	14.05850
6.45000	14.69600	15.48095
6.30000	14.84000	15.37793
5.75000	14.97400	14.99162
5.75000	15.11100	14.99162
7.25000	15.28600	16.01471
5.40000	15.41800	14.73843
7.40000	15.60300	16.11198
6.65000	15.77200	15.61683
9.95000	16.03098	17.64859
3.10000	16.11298	12.90460
6.35000	16.28297	15.41237

TABLE VI (cont.)

8.55000	16.51698	16.83093
9.95000	16.79597	17.64859
6.80000	16.99098	15.71765
18.09999	17.52798	21.51921
7.65000	17.76297	16.27225
7.39000	19.50098	16.10553
19.59999	20.23698	22.11096
18.70000	20.98798	21.75949
18.29999	21.77397	21.59984
17.70000	22.58897	21.35626
21.89999	23.67998	22.96436
26.95000	25.16798	24.64584
36.04999	27.45598	27.17189
58.54999	32.09697	31.70181

Figure 24   Regression Analysis for Ti-6Al-6V-2Sn Fatigue-Crack
Growth Data for a Mill Annealed High Oxygen Alloy (Speci-
men T-92B-1).

The figure shows a regression plot with axes:

- Y-axis: REGRESSION VARIABLE $Y = \left[-\log_e (1 - \Delta K/K_b) \right]^{1/k}$
- X-axis: REGRESSION VARIABLE $X = b \, Da/DN + a$

Annotations on the plot:

K_b = 50 ksi$\sqrt{\text{in}}$ (54.9 MPa$\sqrt{\text{m}}$)
k = 0.55710
a = 0.06413n
b = 0.016144

2σ band

Sample Size N = 47
Sample Correlation
Coefficient, r = 0.9724
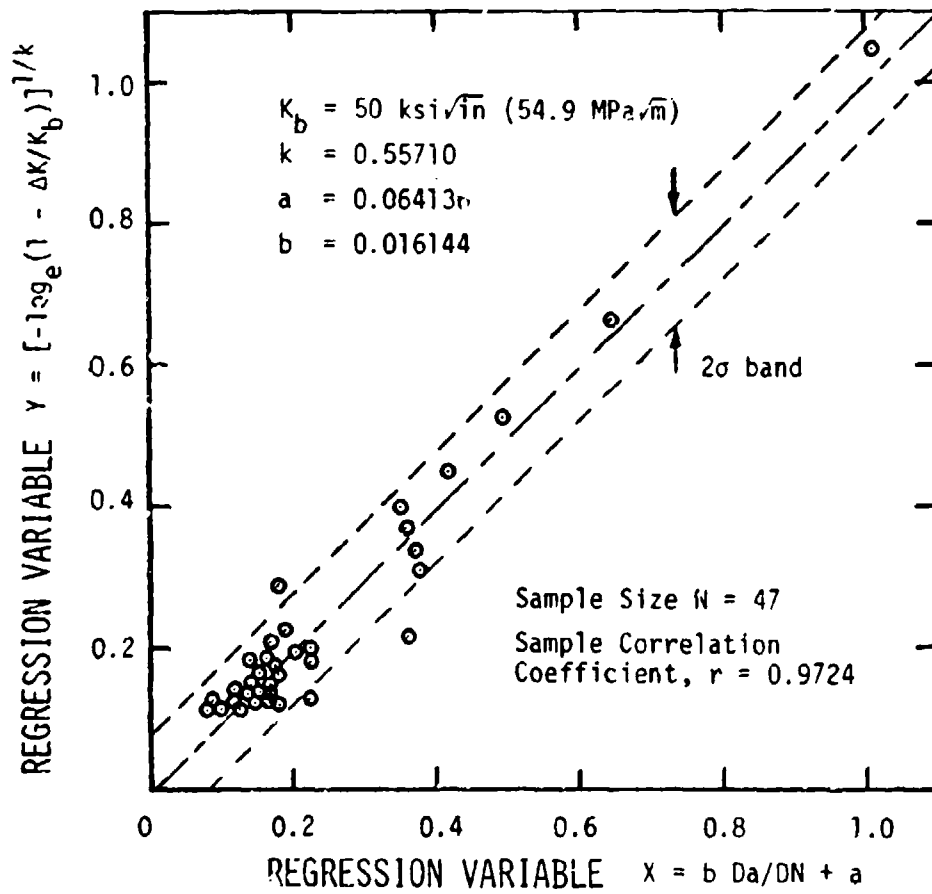
For the example, the value of K_b was estimated to be 50 ksi $\sqrt{in}$ (54.9 MPa $\sqrt{m}$). The results of the curve fitting exercise are shown in Figure 25, where the ordinate is Da/DN to a logarithmic scale and the abscissa is $\Delta K/K_b$ to a linear scale. The dash-dot curve represents the median fitting relation

$$Da/DN = e + (v-e)(-\log_e(1 - \Delta K/K_b))^{1/k} \qquad (61)$$

where

$$
\begin{aligned}
e &= -3.9726 \\
v &= 57.9682 \\
k &= 0.5571 \\
K_b &= 50 \text{ ksi } \sqrt{in} \ (54.9 \text{ MPa } \sqrt{m})
\end{aligned}
$$

The threshold stress intensity, K_{th}, was calculated to be equal to 9.733 ksi $\sqrt{in}$ (10.71 MPa $\sqrt{m}$). Measured and calculated values of ΔK are compared in Table VI at the 47 values of measured Da/DN. The values are plotted in Figure 25 with the ΔK being normalized.

5.3.2.4 Use of Risk Analysis to Distinguiᶜ   w and Fast Crack Growth

For the Weibull distribution function, used in fatigue data analysis, i.e.

$$P(x) = \text{Exp} \left[- \left(\frac{x - e}{v - e} \right) \right]^k , \qquad (62)$$

it is usual to define a risk function, $r^*(x)$, as

$$
\begin{aligned}
r^*(x) &= - \frac{1}{P(x)} \frac{d\, P(x)}{dx} \\
&= \frac{k}{(v - e)} \left(\frac{x - e}{v - e} \right)^{k-1} \qquad (63)
\end{aligned}
$$

Figure 25   Type-A Curve Fit for Ti-6Al-6V-2Sn Fatigue-Crack Propaga-
tion Data (Specimen T-92B-1).
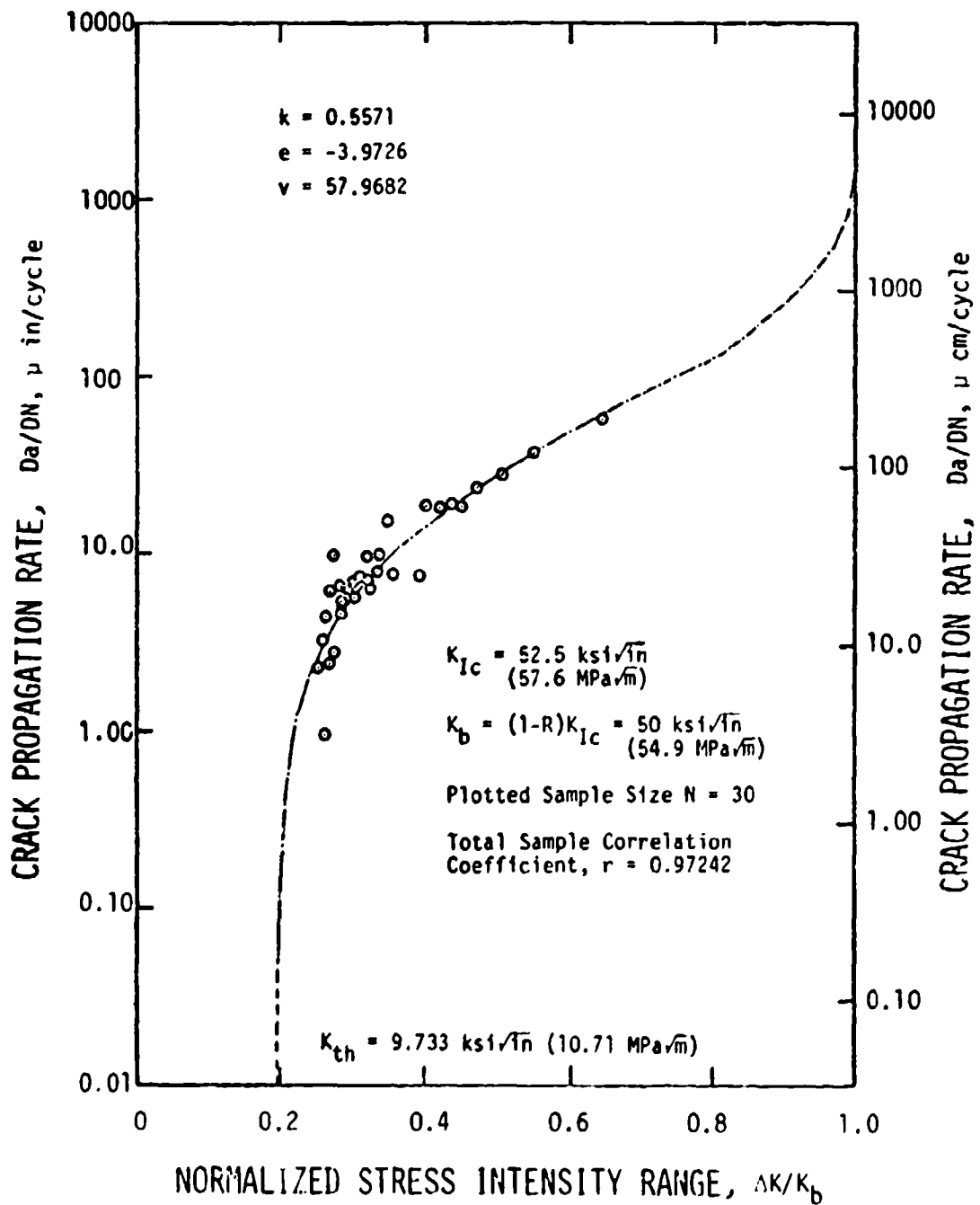
For the purposes of this work, a new definition of risk function was developed which holds promise of being useful for distinguishing between slow and fast growth segments of curve fitting relations A, B and C. The new risk function is defined as

$$r^* = \frac{1}{Da/DN} \frac{\delta(Da/DN)}{\delta(\Delta K/K_b)}$$ (64)

For example, when the risk function and slope

$$\frac{\delta(Da/DN)}{\delta(\Delta K/K_b)}$$ (65)

are known at some $\Delta K/K_b$, then

$$Da/DN = \frac{1}{r^*} \frac{\delta(Da/DN)}{\delta(\Delta K/K_b)}$$ (66)

The crack propagation curve fitting relation, of Type-A was used to calculate a numerical risk function, summarized in Figure 26. Note that the curve is U-shaped. It is proposed that the value of $\Delta K/K_b$ at the minimal values of r^* is a suitable point for distinguishing between slow and fast crack growth on the median Da/DN versus $\Delta K/K_b$ curve.

5.3.3 Numerical Integration of Crack Propagation Relations

5.3.3.1 The Crack Propagation Integral

The main reason why crack propagation test results are expressed by relations of the form

$$Da/DN \quad f(\Delta K)$$ (67)

Figure 26   Risk Analysis Plct to Determine Slow to Fast Transition
in Crack Growth Rate Data.

For a Specified Increment $(\Delta K/K_b)$,

the Fraction $\frac{\delta(Da/Dn)}{Da/DN}$ is given by

$$\frac{\delta(Da/DN)}{Da/DN} = r \ \delta(\Delta K/K_b)$$

Minimum r*= 5.1823

$\Delta K_{sf}/K_b = 0.668$

NORMALIZED STRESS INTENSITY RANGE, $\Delta K/K_b$

(y-axis) RISK FUNCTION $r^* = \delta(Da/DN)/(\Delta K/K_b)/(Da/DN)$
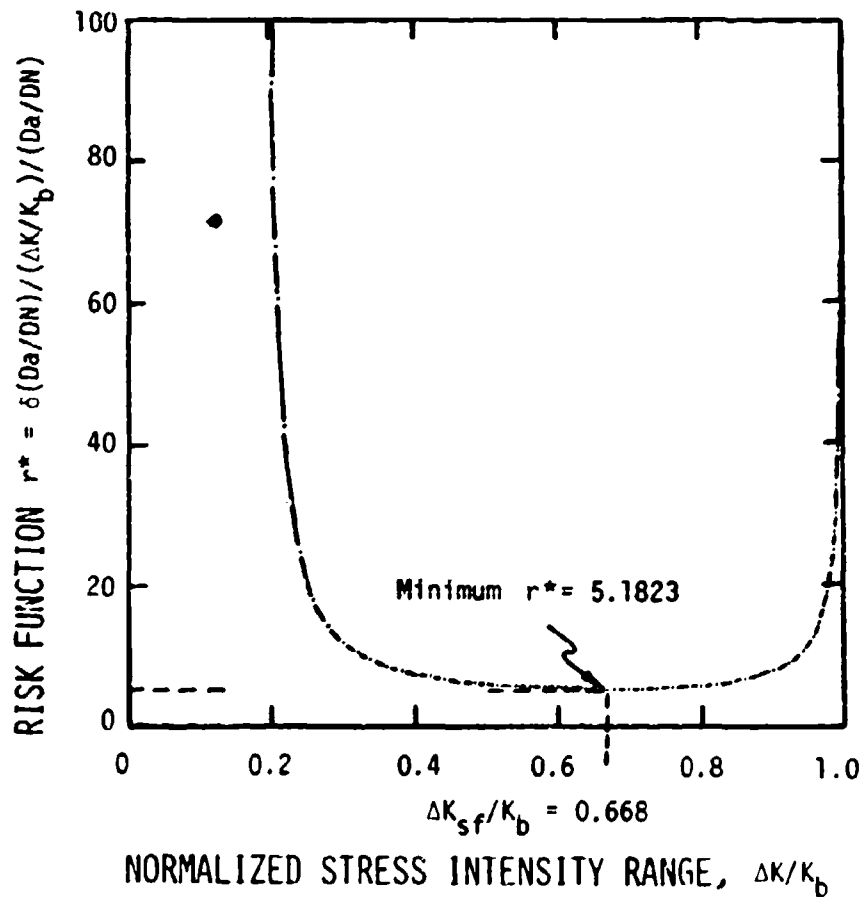
is to permit prediction of the number of cycles for growth from an initial crack length a_i to a final length a_f consistent with a cyclic load history that is usually different than the load history for which experimental crack propagation test results were obtained. The increment in the number of load cycles for crack growth from length a_i to length a_f is defined by the integral

$$N_f - N_i = \int_{a_i}^{a_f} \frac{10^6}{Da/DN(\Delta K)} \, da, \text{ cycles}, \qquad (68)$$

The usefulness of a crack propagation rate curve fitting relation can be judged by successive integration using the sequences of compact tension specimen crack lengths as limits of integration, while taking due account of the test load history. The results can be plotted in the form

$$a = a(N)$$

and can be compared with experimental pairs (a,N).

5.3.3.2 Numerical Integration Routine

The numerical form of the crack propagation integral can be calculated with the aid of a PL/I routine. The routine employs a variable mesh Simpson's rule integration scheme (Bowie et al, 1974). The argument of the integral is first computed at the 11 crack lengths,

$$a(j) = a_1 + (j - 1) h, \text{ in (cm)}, \quad j = 1,2,\ldots,11, \tag{69}$$

where

$h = (a_u - a_1)/10,$
a_1 = lower limit crack length, in (cm)
a_u = upper limit crack length, in (cm).

At each crack length $a(j)$, the normalized stress intensity range, $\Delta K/K_b$ is calculated as follows:

$$\frac{\Delta K(j)}{K_b} = (1-P) \frac{C(j)\sqrt{a(j)}}{b a(j)} C_3(j), \quad j=1,2,\ldots 11 \tag{70}$$

The values of $Da/DN(j)$ at the 11 crack lengths, are determined using one of the Type-A, B, or C curve fitting relations defined in paragraph 5.3.1.2. The numerical form of the crack propagation integral is given by

$$\Delta N = 10^6 \left[\frac{h}{3} \left(\frac{1}{Da/DN(1)} + \frac{1}{Da/DN(u)} \right) + \sum_{j=2,4,8} \frac{4h}{3} \frac{1}{Da/DN(j)} \right.$$

$$\left. + \sum_{j=3,5,\ldots 9} \frac{2h}{3} \frac{1}{Da/DN(j)} \right], \text{ cycles.} \tag{71}$$

The mesh size is increased from 10 to 12 and the process is repeated at 13 crack lengths

$$a(j) = a_1 + h(j-1), \text{ in (cm)}, \quad j = 1,2,3, \ldots 13 \tag{72}$$

where

$h = (a_u - a_1)/12$

and the absolute difference between ΔN values for the two mesh sizes is compared with a specified error increment, usually taken to be 1.0 cycle. Iteration of the numerical procedure is performed with the mesh size increased by two until the specified precision is achieved.

5.3.3.3 Recovery of (a,N) Data by Integration of Compact Tension Specimen Crack Propagation Curve Fitting Relation

The object of integrating crack propagation relations of the form

$$Da/DN = f(\Delta K)$$

is to find the relation between crack length, a, and load cycles, N, for a particular load history to predict inspection intervals and establish operating ranges. The condition for failure is simply

$$\Delta K = K_b \qquad \text{ksi } \sqrt{\text{in}} \text{ (MPa } \sqrt{m}) \tag{73}$$

For the exponential crack propagation curve fitting relations, the term

$$[- \log_e (1 - \Delta K/K_b)]^{1/k} \tag{74}$$

is singular for the failure condition. In practice, when applying the numerical integration routine, the failure, or unstable crack growth, condition is defined as

$$0.99 \, K_b \leq \Delta K < K_b \qquad \text{ksi } \sqrt{\text{in}} \text{ (MPa } \sqrt{m})$$

It would seem, in theory, possible to integrate the exponential Da/DN relations at increasing ΔK beginning at

$$\Delta K = K_{th} + \varepsilon = K_b(1 - \text{Exp} [- (\frac{-e}{v-e})]^k) + \varepsilon, \quad \text{ksi} \sqrt{1n} \text{ (MPa} \sqrt{m}) \quad (75)$$

where ε is arbitrarily small. When this approach is followed at selected ε, numerical difficulties are often encountered when attempting to reproduce measured crack length and load cycle data sets. The difficulties relate to the following factors:

1. Resolution of crack length increments at ΔK values near K_{th} is inferior with respect to resolution at relatively high ΔK values.

2. Crack propagation rate experiments at low ΔK are relatively time consuming, with the result that median crack propagation curve fitting relations are commonly weighted to a minor degree by the low ΔK measurements.

3. Measurements at low ΔK are apt to reflect local differences in test specimen microstructure, with the result that scatter in Da/DN and ΔK measurements is relatively severe and is not well represented by median curve fitting relations determined by analysis of the entire data set for a specimen.

At present, judgement must be exercised to select the lowest ΔK at which integration of an exponential curve fitting relation should

be attempted.

The results of applying a PL/I routine, LIFE, to integration
of the exponential Da/DN relation for specimen T-92B-1 with two
beginning points of integration from a_o = 0.9 in (2.29 cm) and
a_o = 1.0 in (2.54 cm) are plotted in Figure 27. The ordinate re-
presents load cycles, N, to a logarithmic scale and the abscissa
indicates the crack length, a. The circled points are experimental
measured values. The two curves are numerical integration results;
Curve 1 assumes a K associated with the last measureable a_f = 2.0182
in (5.126 cm) with an initial crack length a_o = 0.9 in (2.29 cm) and
Curve 2 assumes a K_b equal to 50 ksi $\sqrt{in}$ (54.9 MPa $\sqrt{m}$) with an initial
crack length a_o = 1.0 in (2.54 cm) and a predicted final crack length
a_f = 2.1404 in (5.437 cm). The choice of the first curve and close
scrutiny in the measurement of the WOL specimen yield the most accu-
rate correlation. The measured and calculated values are given in
Table VII.

5.3.3.4 Examples of Practical Graph Formats for Life or Crack
        Growth Internal Prediction

For all of the example curves, the initial assumption was made
that load cycle counting began when the crack length was equal to
1.0 inch (2.54 cm).

Constant Load a-N-P Curves - Figure 28 includes 8 curves, for
constant load amplitudes from P = 3 kips (13.344 nt) to P = 10 kips

Figure 27   Curve Fit for Ti-6Al-6V-2Sn Fatigue-Crack Length Versus
            Load Cycles Data (Specimen T-92B-1). Curve 1
            illustrates comparison of an integration scheme using
            Simpson's mesh with Weibull parameters and measured data
            for a_o = 0.9 inch. Curve 2 plots the measured data
            against a predictive technique using the Weibull para-
   meters, k, e, v, and K_b = 50 with an initial crack
            length of a_o = 1.0 inch.

CRACK LENGTH, a, cm

LOAD CYCLES, N

○ Measured Data

—·—·— Integration scheme and Prediction Method

Specimen Failure

Predicted Unstable Crack Growth Failure for P = 4 kip (17,792 nt)
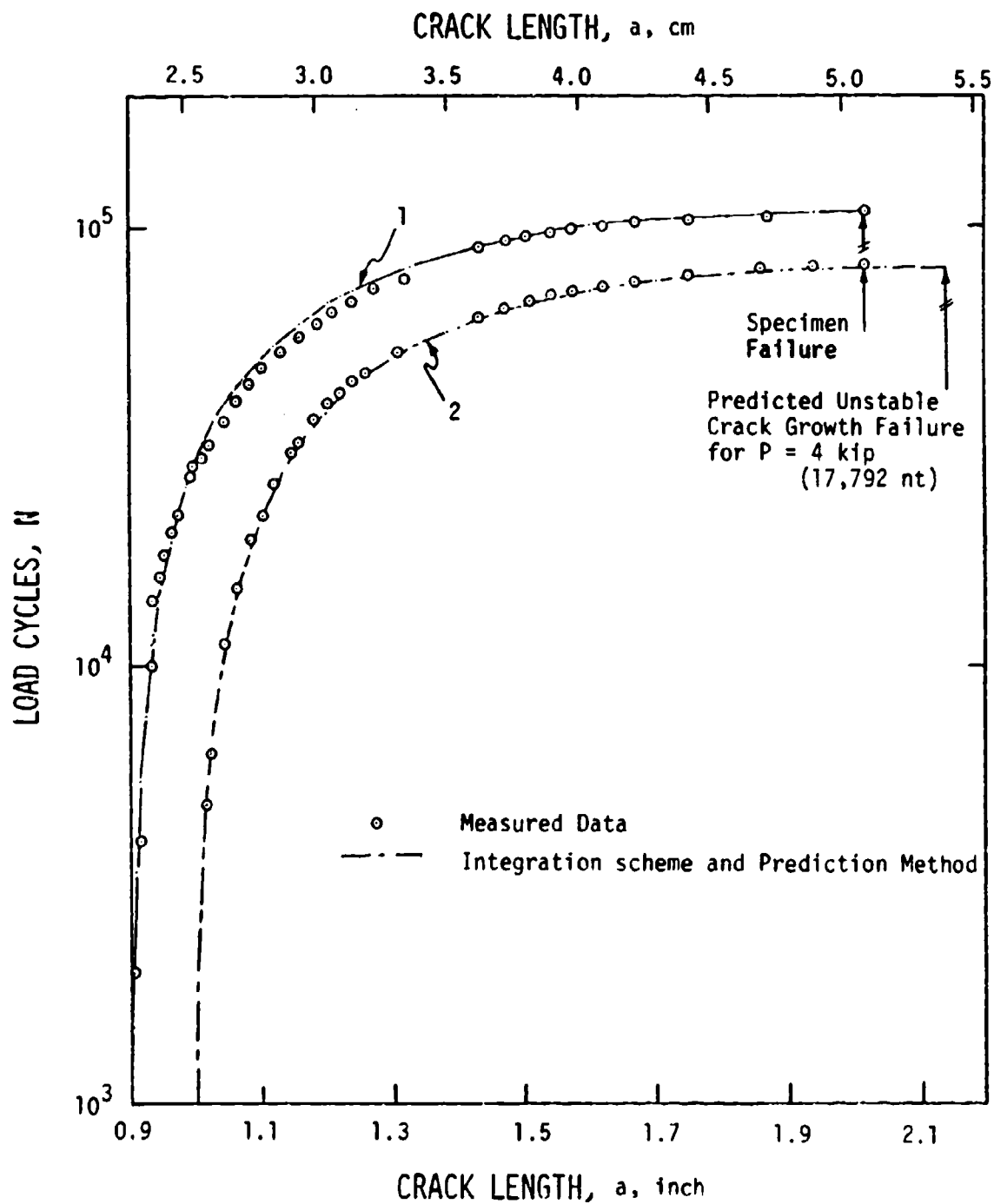
CRACK LENGTH, a, inch

TABLE VII

MEASURED AND CALCULATED FATIGUE CYCLES

	Measured Quantities		Calculated
	Crack Length, in	Cycles	Cycles
1	.900	0	0
2	.904	2000	1495
3	.910	4000	3426
4	.917	6000	5450
5	.924	8000	7748
6	.931	10000	9904
7	.936	12000	11297
8	.937	14000	11867
9	.945	16000	14142
10	.950	18000	15534
11	.963	20000	19288
12	.976	22000	22735
13	.986	24000	25487
14	.992	26000	26895
15	.995	28000	27652
16	1.015	30000	32536
17	1.021	32000	33946
18	1.034	36000	36914
19	1.043	36000	38904
20	1.054	38000	41265
21	1.061	40000	42728
22	1.073	42000	45268
23	1.082	44000	47040
24	1.095	46000	49500
25	1.108	48000	51817
26	1.119	50000	53859
27	1.131	52000	55834
28	1.145	54000	58235
29	1.156	56000	59960
30	1.171	58000	62239
31	1.184	60000	54208
32	1.204	62000	67021
33	1.210	64000	67866
34	1.233	66000	69552
35	1.240	68000	71730
36	1.260	70000	74139
37	1.274	72000	75711
38	1.310	74000	79619

TABLE VII (cont.)

39	1.325	76000	81158
40	1.429	90000	90018
41	1.468	92000	92765
42	1.505	94000	95114
43	1.542	96000	97176
44	1.577	98000	98968
45	1.621	100000	100929
46	1.675	102000	102990
47	1.747	104000	105209
48	1.864	106000	107714

	Measured Quantities		Calculated
	Crack Length, in	Cycles	Cycles
1	1.0	0	0
2	1.015	4884	
3	1.021	6294	
4	1.043	11252	
5	1.050		11514
6	1.061	15076	
7	1.082	19388	
8	1.100		21434
9	1.108	24164	
10	1.119	26204	
11	1.145	30583	
12	1.156	32308	
13	1.184	36556	
14	1.200		37525
15	1.204	39369	
16	1.210	40214	
17	1.240	44078	
18	1.260	46487	
19	1.300		.49675
20	1.310	51967	
21	1.400		58904
22	1.429	62367	
23	1.468	65113	
24	1.500		65892
25	1.505	67462	
26	1.542	69525	

TABLE VII (cont.)

27	1.577	71316	
28	1.600		
29	1.621	73277	
30	1.575	75338	
31	1.700		74923
32	1.747	77557	
33	1.800		77590
34	1.864	80061	
35	1.891		79223
37	1.950		79952
38	2.018	81779	
39	2.050		80713
40	2.100		80909
41	2.120		80956
42	2.140		80981
43	2.1404		80982

Figure 28   Constant Load a-N-P Curves for Ti-6Al-6V-2Sn Crack Growth
Data (Specimen T-92B-1).

CRACK LENGTH, a, cm

NUMBER OF LOAD CYCLES, N

CRACK LENGTH, a, inch

SLOW GROWTH

FAST GROWTH

UNSTABLE CRACK GROWTH

P = 3 kips

4 kips

5 kips

6 kips

7 kips

8 kips

9 kips

10 kips

Da/DN = 69.8 μ in/cycle

A

Aa

Curve "A" represents
an example load
shedding case:

Crack from	Growth to	Load kips
1.0 in	1.1 in	10
1.1	1.2	9
1.2	1.3	8
1.3	1.4	7
1.4	1.5	6
1.5	1.6	5
1.6	1.7	4
1.7	2.296	3

Initial Crack Length a_i = 1.0 in
(2.54 cm)

Stress Ratio R = 0.05
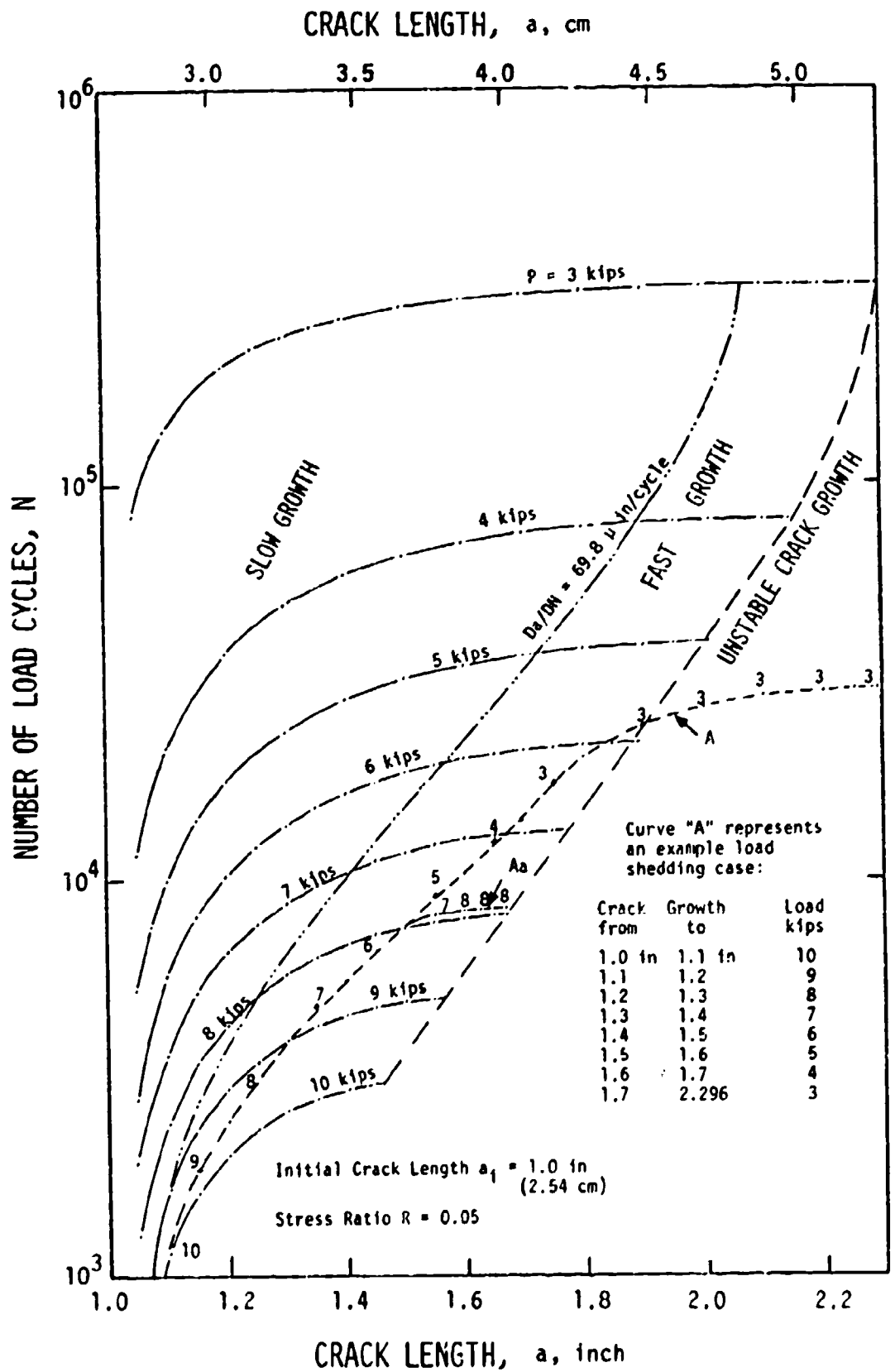
(44,480 nt) at 1.0 kip (4,448 nt) interval. The locus labelled Da/DN = 69.8 µ in/cycle (1772.9 µ mm/cycle) separates slow and fast growth regimes, determined by the risk function analysis method of section 5.3.1.5.

Constant Crack Length N-P-a Curves - Figure 29 includes 4 curves, for constant crack length from a = 1.1 in (2.79 cm) to a = 1.4 in (3.56 cm) at 0.1 in (0.254 cm) intervals. The unstable crack growth locus is reminiscent of a conventional low cycle fatigue S-N curve. The curve separating slow and fast growth regimes was determined by the risk analysis method.

Load Shedding Curves - The staircase function plotted in Figure 29 represents a load shedding example in which load cycle counting began at crack length a = 1.0 inch (2.54 cm) with load P = 10 kips (44,480 nt). The load was reduced by 1.0 kip (4,448 nt) increment for each 0.1 inch (0.254 cm) increment in crack growth until a representative lower load limit P = 3 kips (13,344 nt) was attained. This lower load limit was maintained in the numerical analysis until predicted unstable crack growth was attained. The same example is represented in Figure 28 by the curve labelled "A".

The curve segment labelled "Aa" in Figure 28 was generated to illustrate an important principle for in-service structural component life prediction when load shedding is practiced. The numerical analysis for the above load shedding example was repeated until crack length a = 1.5 inch (3.81 cm) was attained at load P = 6 kips (26,688

Figure 29 Constant Crack Length N-P-a Curves for Ti-6Al-6V-2Sn
Crack Growth Data (Specimen T-92B-1).

APPLIED LOAD, P, Nt.

APPLIED LOAD, P, KIPS

NUMBER OF LOAD CYCLES, N

Initial Crack Length a_i = 1.0 in (2.54 cm)

Stress Ratio R = 0.05

Unstable Crack Growth

a = 1.4 in
a = 1.3 in
a = 1.2 in
a = 1.1 in

Unstable at a = 2.296 in

Fast
Slow

The Staircase represents a load shedding example
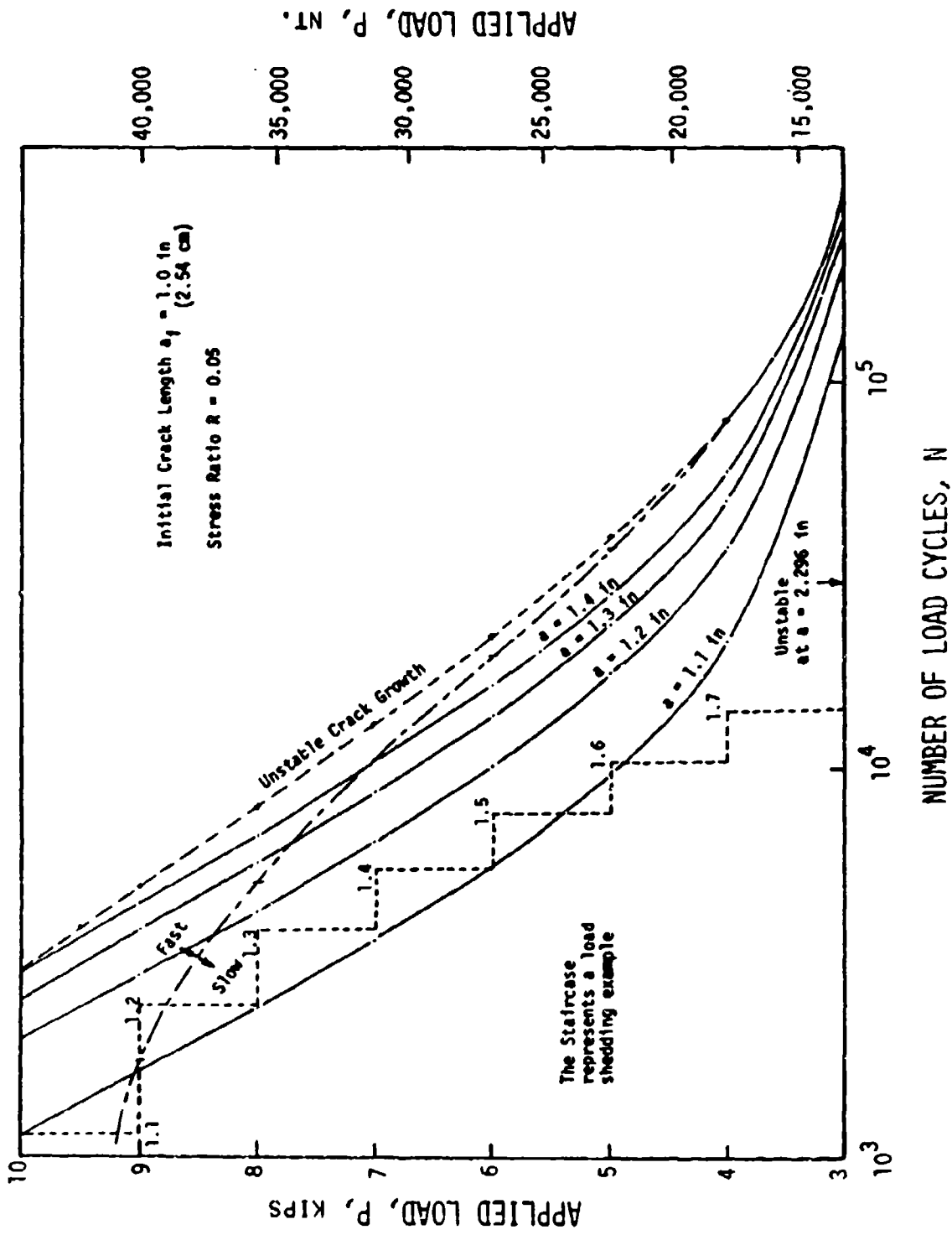
nt). The load was then increased to P = 7 kips (31,136 nt) for growth from a = 1.5 inch (3.81 cm) to a = 1.55 inch (3.94 cm). The load was then further increased to P = 8 kips (35,584 nt) and was maintained until predicted unstable growth was attained. This exercise illustrates the principle that when load shedding is practiced for an in-service structural component, a decision to interrupt a load shedding schedule in favor of brief application of higher than scheduled loads can result in drastic reduction in component life.

Two additional load shedding examples are summarized in Figure 30. Comparison of curves B and C reveals the effects of delaying load shedding on crack growth and life prediction. Let curve B represent an in-service structural component nominal load shedding example, and curve C a possible deviation. If the two components were to be inspected after 7000 load cycles had been applied, predicted crack growth for curve B would be from 0.9 inch (2.29 cm) to 1.252 inch (3.18 cm) and from 0.9 inch (2.29 cm) to 1.500 inch (3.81 cm) for curve C. If the next inspection were to be delayed until 10,000 load cycles had been applied, the crack length for curve B would be 1.404 inch (3.57 cm), and 1.72 inch (4.37 cm) for curve C. At this stage, component B would have a remaining life of approximately 15,000 load cycles, and component C approximately 6,000 cycles.

Figure 30   Loading Example to Demonstrate Component Shedding Regimes
             as Applied to Specimen T-92B-1. Curve "B" illustrates
             a load P = 10 kips for 973.7 cycles, with slow growth
             from 10 kips to 3 kips determined by a scheme that pro-
             hibits fast growth rates. From N = 973 to 23821 cycles
             the risk function, r^*, has a minimum value, r^* =
             5.1823. For 23821<N<25375 cycles, fast growth occurs
             at load P = 3 kips. For curve "C", the initial load
             P = 10 kips is maintained until a = 1.163 inches,
             at N = 3205 cycles. Load shedding then takes place,
             from P = 10 kips to P = 3 kips with an average
             minimum risk value, r^* = 5.552.

CRACK LENGTH, a, cm

NUMBER OF LOAD CYCLES, N

CRACK LENGTH, a, inch

Initial Crack Length a_i = 0.9 inch
(2.29 cm)

Stress Ratio, R = 0.05
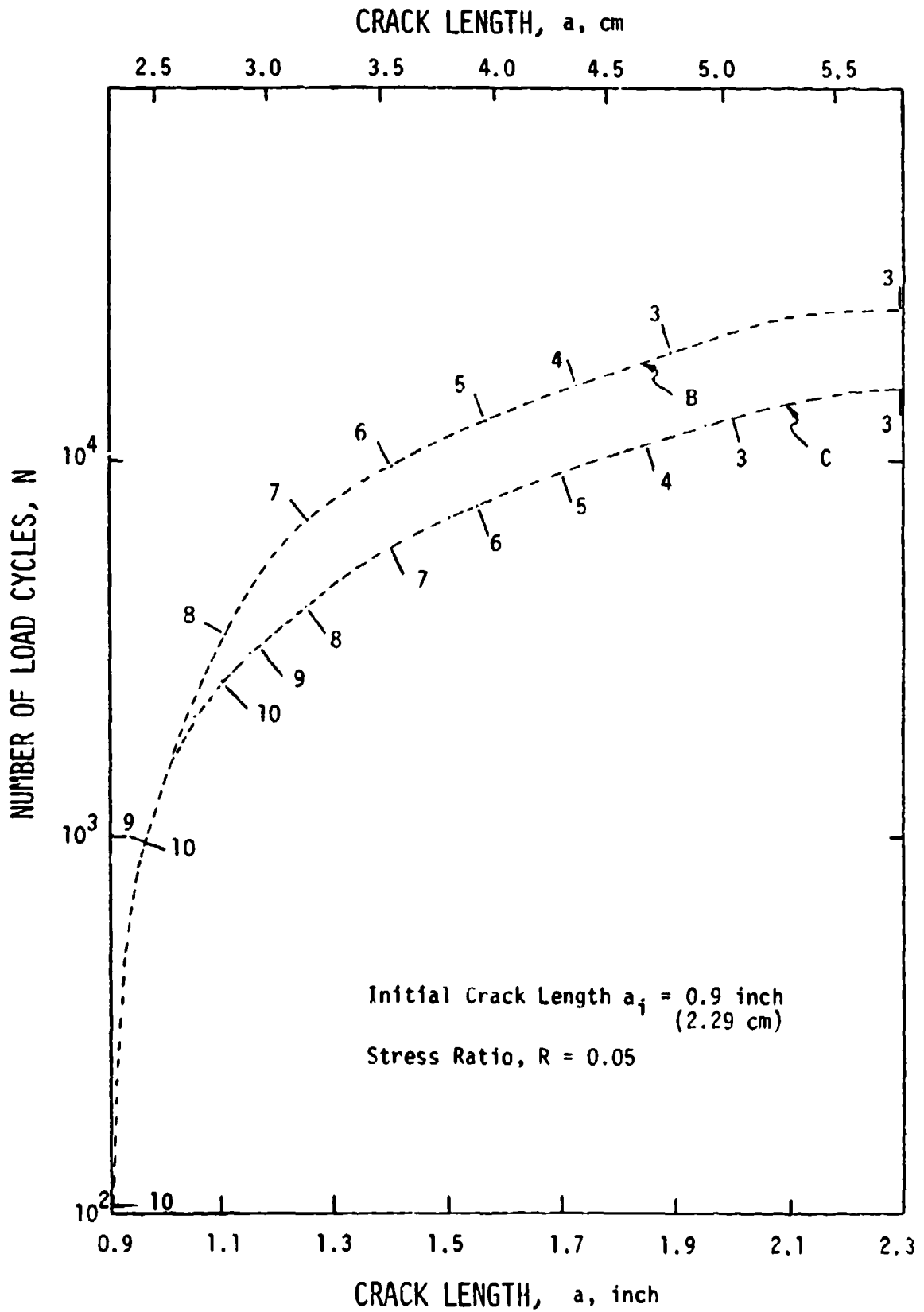
CHAPTER 6

TECHNICAL DISCUSSION ON STUDY RESULTS

A graphical sequence of analysis in fracture and fatigue life mechanics was explored with respect to a single alloy test in chapter 5.0. Recognizing the discrimination potential, this study's major thrust was to evaluate differences in materials' microstructure through their response to various combinations of parameters as applied through fatigue-crack propagation. The approach was to perform fatigue-crack propagation testing on standard WOL specimens, at three different laboratories, and use a "best-fit" approach to data as determined by the definition of mathematical boundary conditions to the physics of fatigue-crack propagation (section 5.3.1.2). It appears that this idea coupled with substantial and precise data collection for quantizing factors such as compliance, crack length and K, matched with this data reduction technique, resulted in distinguishable data trends for heat treatments, stress ratios, wave forms and environments applied to the test materials. The results are represented by two fatigue-crack growth rate (DaDN) versus stress intensity (ΔK) plots, one log-linear, the other log-log. Both plots reflect the Weibull characteristic value v, intersecting the log ordinate axis (DaDN) and a value equivalent to 0.63212 times the final K_b, intersecting the linear abscissa. All comparative analyses were performed with log-

linear representations. The latter curves (Appendix 1) were included for traditional benefit and to provide a bridge from straight line expressions to a suitable curve fitting formulations that attempt to establish boundary conditions in accordance with the mathematical physics of the event. It can be noted that all graphs have curves which asymptotically approach a final value K_b. Conversely, a threshold K_{th} can be considered as a point where the fatigue-crack growth rate DaDN is low enough to be considered virtually unidentifiable at the present. Equation 41 should not be misconstrued as DaDN = 0 even though it uses this method to arrive at a limiting K_{th}. Alternatively, it is best to be considered as a value for DaDN approaching zero.

Another graphical format similar to Figure 25 plots the Weibull analysis reduced to one shaping parameter, k. Here the log ordinate is the Z variate, (X-e)/(v-e) and the linear abscissa is the normalized stress intensity range, $\Delta K/K_b$.

6.1 COMPLIANCE EVALUATION

The Wilson polynomial (section 5.2.3) was used in the calibration of K permitting comparison with future data. Albeit this expression does not attempt to approximate an ever changing Modulus of Elasticity, nor plastic zone size, but at the present it does endeavor to provide continuity to a specimen's stress intensity factor, K. All base-line specimens were subject to compliance testing. Calculations using an optically judged crack length (section 4.4) (i.e.

natural fatigue crack versus a machined notch) were made and plotted in Figure 31. The data aligned between test specimens and was further compared with data available from Sullivan (1975). This latter comparison presented in Table VIII of Figure 31 uses machined cut notches. Agreement is seen at the lower a/W ratio and deviated slightly at higher a/W ratios. This may be due to subtle crack front eccentricity or the use of natural fatigue crack.

6.2 WEIBULL PARAMETER

The logic for estimating the three parameters (k,e,v) is with an interactive program (section 5.3.1.2). The parameters are derived from the linearization of the Weibull equation (equation 38) hv deducing the appropriate values of W, a, and b. Optimization data fit by linear regression analysis results by a numerical analysis "best-fit" when a maximum sample correlation coefficient is reached. The rationale for implementing a Weibull type fitting technique lies in the Weibull's power to segregate subtle changes in data sets. This capacity to describe behavior by only three and possibly a single parameter makes it attractive. Depending on an alloy's microstructure, what is considered a discreet selection or change in operational variables, based on existing data basis can induce substantial unsuspected limitations or lead to total deterioration of the structure. Figures 29 and 30 are indicative of a typical scenario that would ignore a load shedding regime. Identi-

Figure 31 Compliance Evaluation Curve. The compliance response used
for this study is plotted with the data. Comparison is
shown in the incorporated Table VIII that presents CEB
data for the University of Missouri and Naval Research
Laboratory at the indicated a/W levels.

TABLE VIII   COMPLIANCE EVALUATION DATA

a/W	CEB					
	0.20	0.30	0.35	0.40	0.50	0.60
UMC	20.9	32.3	39.1	50.4	74.2	110.7
NRL	20.8	32.0	39.0	47.4	72.9	113.7

CEB (y-axis)

a/W (x-axis)
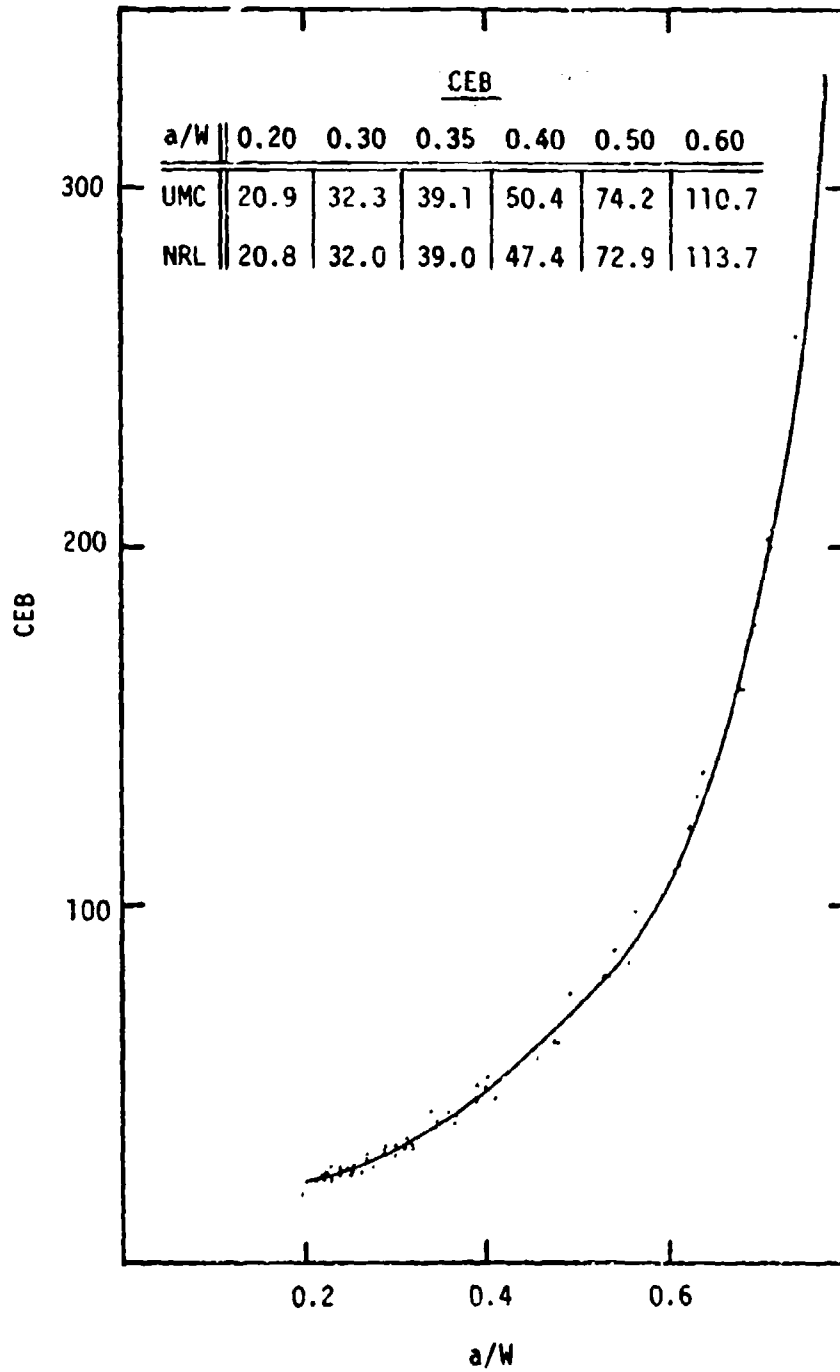
fication of the responses to adjustments in operation variables may be recognized, but the differences or deviations may appear muted in rapid or limited laboratory tests and totally non-existent when results are plotted in a log-log regime. Thus, a needed capability has been recognized not only in an academic sense but has gained visibility by the continuing limitations placed on field operation of high performance structures.

6.2.1 Fitting Data for Test Matrix

A fractional factorial test matrix was pursued for both materials per Table IX. The resulting fitting data associated with these data sets are shown in the bottom portion of Table IX. As will be seen the fatigue-crack growth rate curves are plotted with a characteristic value, v, against a normalized abscissa $\Delta K/K_b$. This can be interpreted as the transition point between slow and fast crack growth. Further, the characteristic can be used as a standardized point or fulcrum in the following plots which look at the shaping factor.

By defining $Z = (X-e)/(v-e)$ as a reduced variate, where $X = DaDN$, the survivorship function, $P(Z) = Exp[-Z^k]$, can be related to the probability of failure by Equation 35. Thus, $1-P(Z)$ is identified as $1-F$ or $1-\Delta K/K_b$; hence, $P(Z) = 1-Exp[-Z^k]$. It can be noted if $Z = 1$, $\Delta K/K_b = 1-Exp(-1) = 0.63212$ and when $Z = 0$, then $\Delta K/K_b = 0$ for all k. Using Z and $\Delta K/K_b$ as axes the "Spider" plots in Figures 32 and 33 were produced to illustrate the generic be-

TABLE IX   WEIBULL TYPE-A FITTING PARAMETERS

	Sine Wave, 10 Hz Ambient Air		1 min Hold-Time Ambient Air		1 min Hold-Time Sea Water	
R	0.05	0.67	0.05	0.67	0.05	0.67
H 1050	1, T*	5	2	6, E*		
H 1100	8, H*	11	12, N*	K*	10, B*	L*

17-4 PH	k	e	v	Sverv	r	K_{th}	K_b
1	1.8518	-23.3152	51.0053	0.0375	0.9780	16.5	150
2	1.4285	-194.8995	218.3016	0.1873	0.7710	49.5	170
5	0.5000	-1.4917	16.4075	0.1310	0.9118	12.5	50
6	0.5310	-2.8944	15.7506	0.9292	0.8004	18.9	61
8	1.2853	-17.2463	57.8724	0.0195	0.9948	21.0	150
10	0.4273	-0.1453	177.0029	0.1440	0.9540	7.5	160
11	0.5000	-0.8699	15.8099	0.1108	0.9711	12.3	60
12	0.9352	-21.9354	100.1449	0.0736	0.9865	30.9	170

15-5 PH*

	k	e	v	Sverv	r	K_{th}	K_b
B	0.8368	-24.4371	221.8436	0.0743	0.9821	25.0	186
E	0.7813	-16.2135	15.9459	0.5571	0.7828	27.9	63
H	0.6083	-6.5903	151.6395	0.2011	0.9695	24.1	179
K	0.7000	-65.4556	18.5453	0.2630	0.5633	34.1	60
L	0.6968	-0.4855	43.2530	0.3461	0.9319	2.5	58
N	0.5347	-11.2067	163.9067	0.2386	0.9137	33.9	165
T	1.9230	-28.6542	46.2079	0.0059	0.9995	21.9	150

*15-5 PH

Figure 32 A "Spider" Diagram of 17-4 PH for all Test Conditions in this Study is Graphed. The reduced variate, $Z = (DaDN-e)/(v-e)$ is plotted against the normalized stress intensity $\Delta K/K_b$ to observe the shaping factor (K) effect.
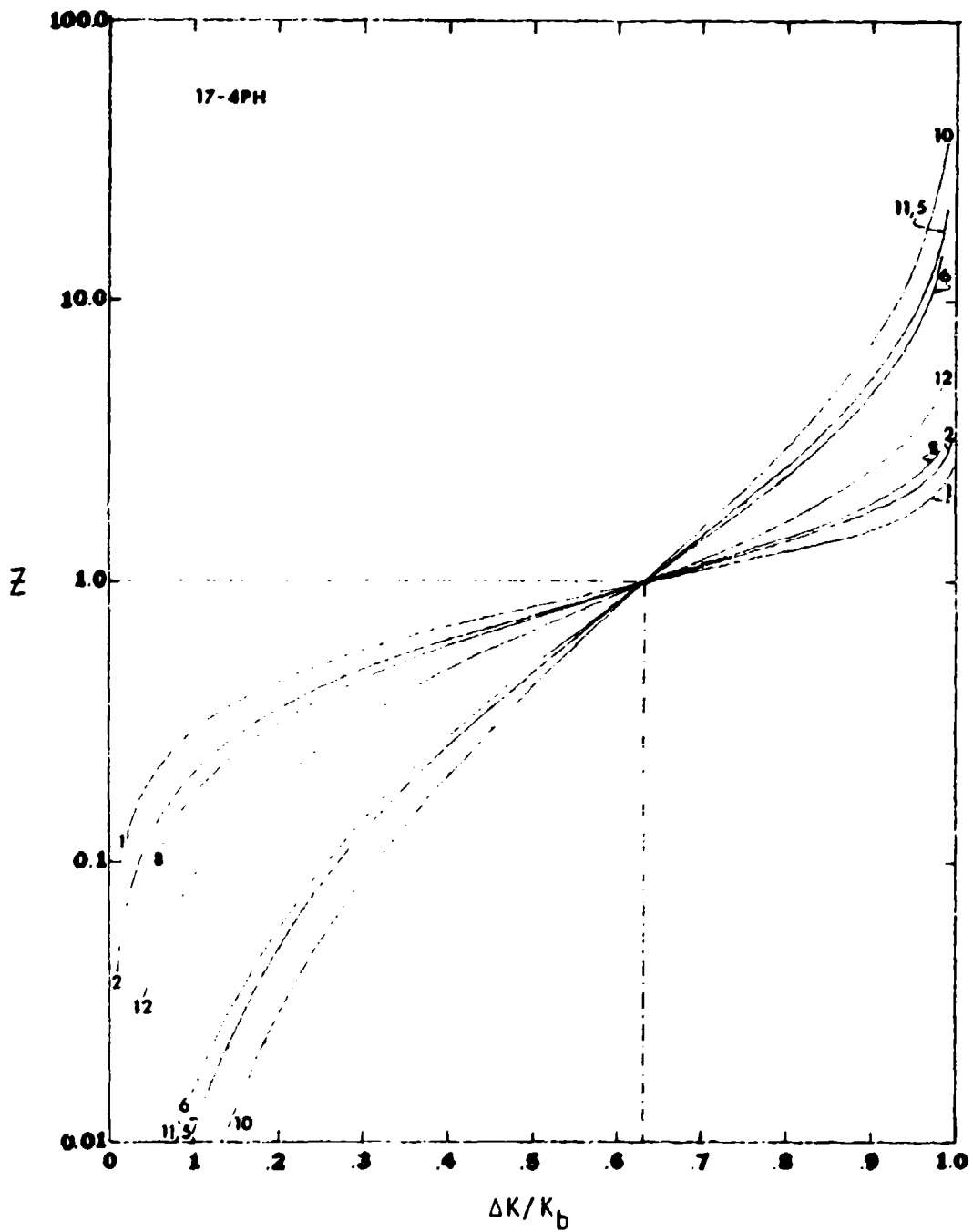
Figure 33 A "Spider" Diagram of 15-5 PH for all Test Conditions in this Study is Graphed. The reduced variate, $Z = (DaDN-e)/(v-e)$ is plotted against the normalized stress intensity $\Delta K/K_b$ to observe the shaping factor (K) effect.
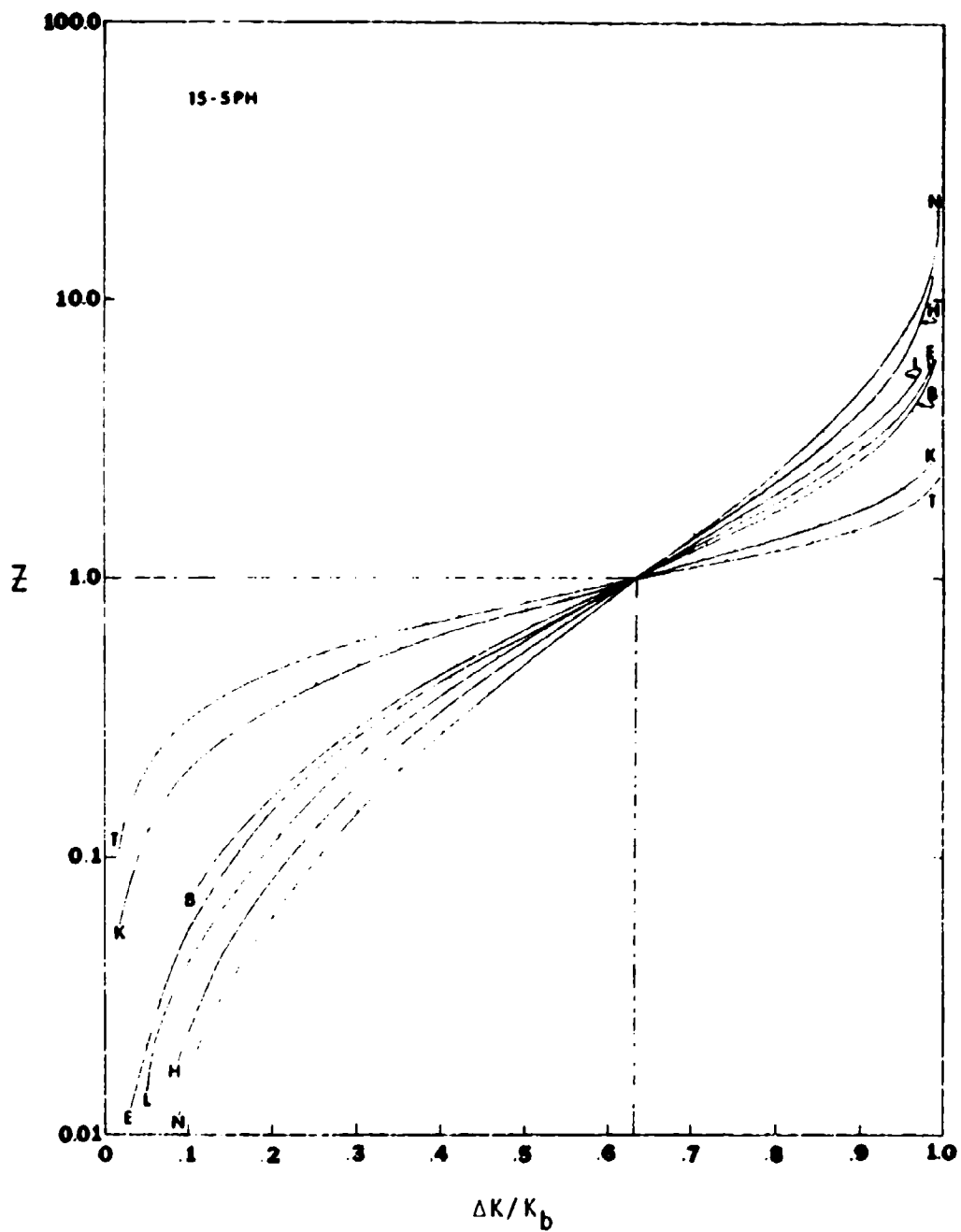
havior of k.

6.2.2 Behavior Evaluation by Shaping Factor

In considering the influence of curve shaping, the differences between test data sets must be identified and partitioned with respect to the conditions of interest. In deriving a rational explanation for overall data response as associated with a fitting parameter k, and in the attempt to align a hypothesis for optimized fatigue-crack growth behavior, five distinct sets were reviewed. These data sets that are illustrated and compared on Figures 32 and 33 are 7 and 8, 2 and 12, 5 and 11, E and K, and T and H. By observation it was determined that to optimize (i.e. achieve maximum life) an alloy's fatigue crack behavior two items are required. First, k must tend to increase positively, secondly, e must tend to increase negatively.

The assumptions considered are: that initial manufacturing or service flaws can be identified for the materials' forms of interest; and the test conditions reflect the actual design's operational performance. With these boundary conditions it becomes essential in a lifing analysis to insure that entry into the crack growth rate curves does not occur by selective internal microstructural bursting. This last factor has the ability to erradicate all safety margins along with some equipment and structures.

As k increases it appears to indicate a higher resistance to fatigue damage by extending the curve to a reduced crack growth rate

over a larger stress intensity range. This can be seen in Figures
32 and 33 for Specimens 1 and T, respectively. However, e, the
threshold value, must tend to be more negative in order to increase
K_{th}. This combination is a first step in material optimization by
data set scanning. The obvious limitation is in the ability to define
all conditions of interest and compare these conditions to the avail-
able collected data set of interest. This study indicates the sub-
stantial impact a set of applied variables have on alloys' perfor-
mance.

Lastly, the characteristic, v, is normalized in the "Spider"
diagrams (Figures 32 and 33) and tends to act as the pivot point
discriminating between slow and fast crack growth rates. Without
definition of k, e and the final K_b, the interpretation of v is
nebulus, at best. However, if the set was defined, v has the poten-
tial to link directly with design methodology safety margins for
finite life designs.

6.2.3 Collected Data with Curve-Fit

It is believed worthy to illustrate in log-linear format all
the fatigue-crack growth curves of the data set with their data.
The intercept of the curve indicates a characteristic value, v,
selected to be the slow to fast transition point partitioning the
curve into two distinct parts. The curves are presented in numeric
order for 17-4 PH and alphabetic order for 15-5 PH in the same man-
ner as Table IX (Figures 34 to 48). Identical data plots made

Figure 34   Log-Linear Graph of Specimen 1 Fatigue-Crack Growth Rate
Test Fitted with a Type-A Weibull Curve. The slow to fast
transition intercept on the curve indicates a DaDN
characteristic value (51.0 in/cycle) and 63.21% of the
final stress intensity, K_b (150 ksi $\sqrt{in}$).

DELTA K, MPa√m

da/dN, in./cycle

da/dN, mm/cycle

DELTA K, ksi√in.

17-4PH
H1050
R = 0.05
f = 10 Hz.
Sine Wave
Ambient Air
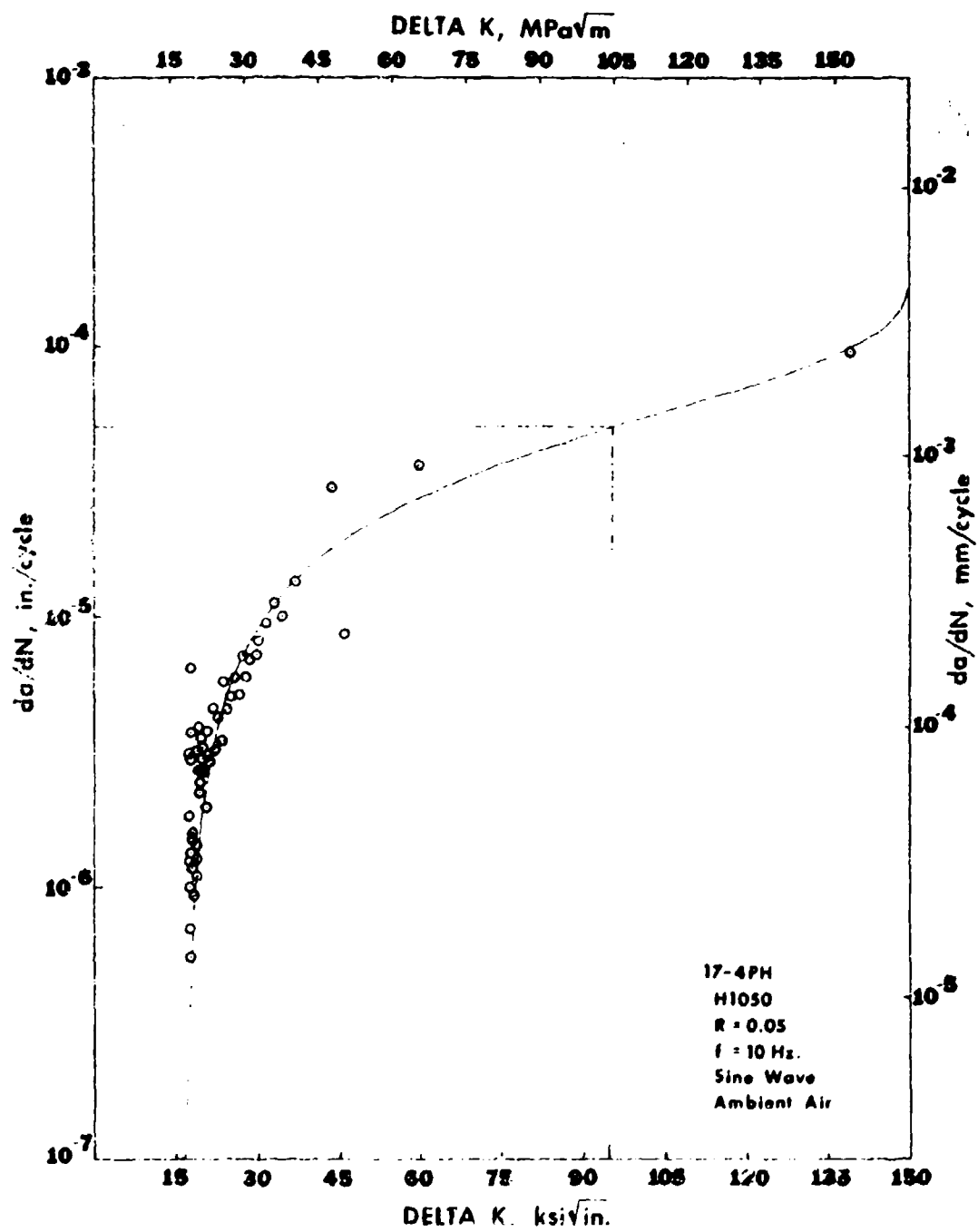
Figure 35   Log-Linear Graph of Specimen 2 Fatigue-Crack Growth Rate
Test Fitted with a Type-A Weibull Curve. The slow to
fast transition intercept on the curve indicates a DaDN
characteristic value (218.3 in/cycle) and 63.21% of the
final stress intensity, K_b (170 ksi $\sqrt{in}$).

DELTA K, MPa√m

DELTA K, ksi√in.

da/dN, in./cycle

da/dN, mm/cycle

17-4PH
H1050
R=0.05
One Minute Hold
Ambient Air
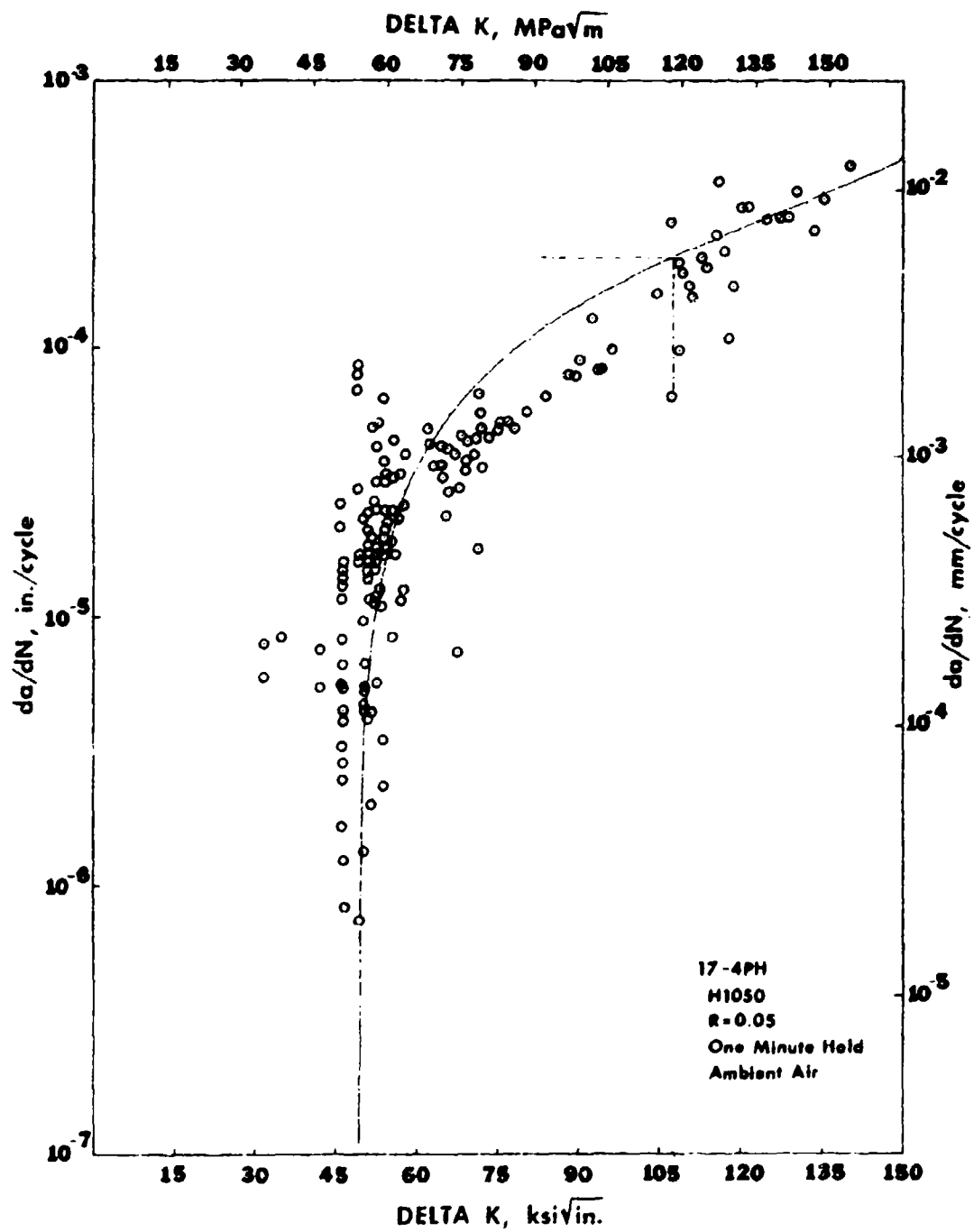
Figure 36 Log-Linear Graph of Specimen 5 Fatigue-Crack Growth Rate
Test Fitted with a Type-A Weibull Curve. The slow to
fast transition intercept on the curve indicates a DaDN
characteristic value (16.4 in/cycle) and 63.2)% of the
final stress intensity, K_b (50 ksi $\sqrt{in}$).

DELTA K, MPa√m

17-4PH
H1050
R = 0.67
f = 10 Hz.
Sine Wave
Ambient Air
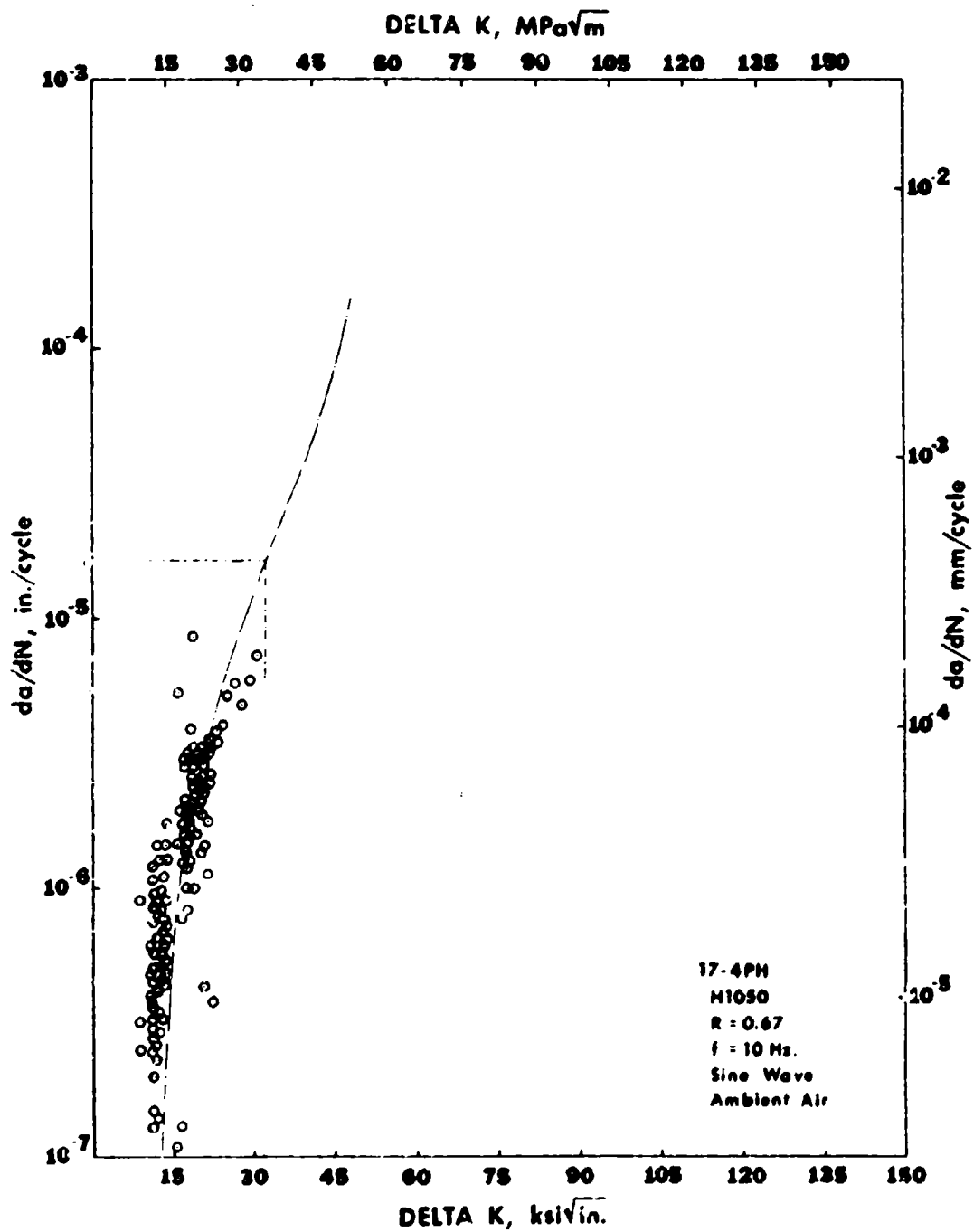
Figure 37   Log-Linear Graph of Specimen 6 Fatigue-Crack Growth Rate
Test Fitted with a Type-A Weibull Curve. The slow to
fast transition intercept on the curve indicates a DaDN
characteristic value (15.7 in/cycle) and 63.21% of the
final stress intensity, K_b (61 ksi $\sqrt{in}$).

DELTA K, MPa√m

DELTA K, ksi√in.

da/dN, in./cycle

da/dN, mm/cycle

17-4 PH
H1050
R·0.67
One Minute Hold
Ambient Air
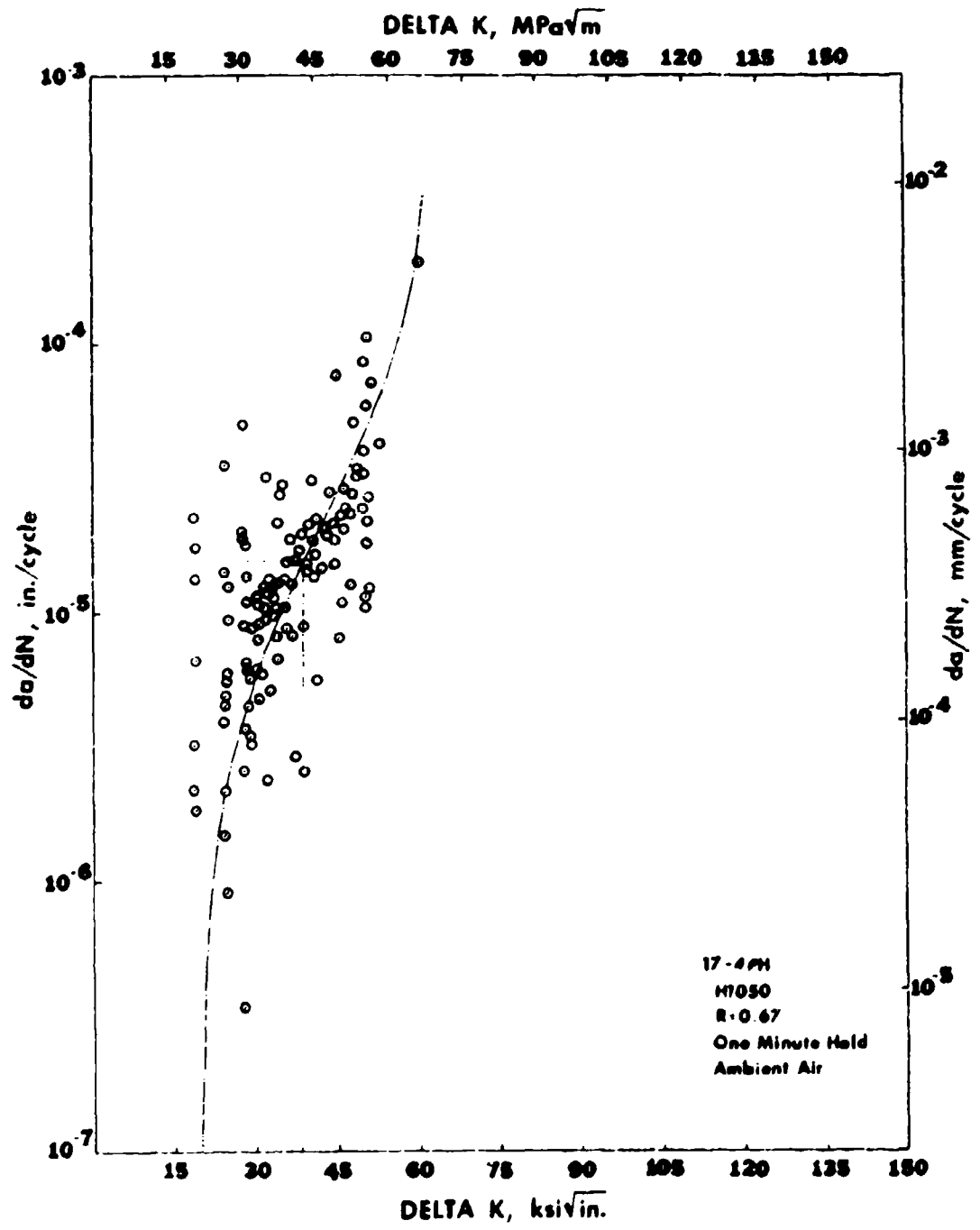
Figure 38 Log-Linear Graph of Specimen 8 Fatigue-Crack Growth Rate
Test Fitted with a Type-A Weibull Curve. The slow to
fast transition intercept on the curve indicates a DaDN
characteristic value (57.8 in/cycle) and 63.21% of the
final stress intensity, K_b (150 ksi $\sqrt{in}$).

DELTA K, MPa√m

da/dN, in./cycle

da/dN, mm/cycle

17-4PH
M1100
R = 0.05
f = 10 Hz.
Sine Wave
Ambient Air

DELTA K, ksi√in.
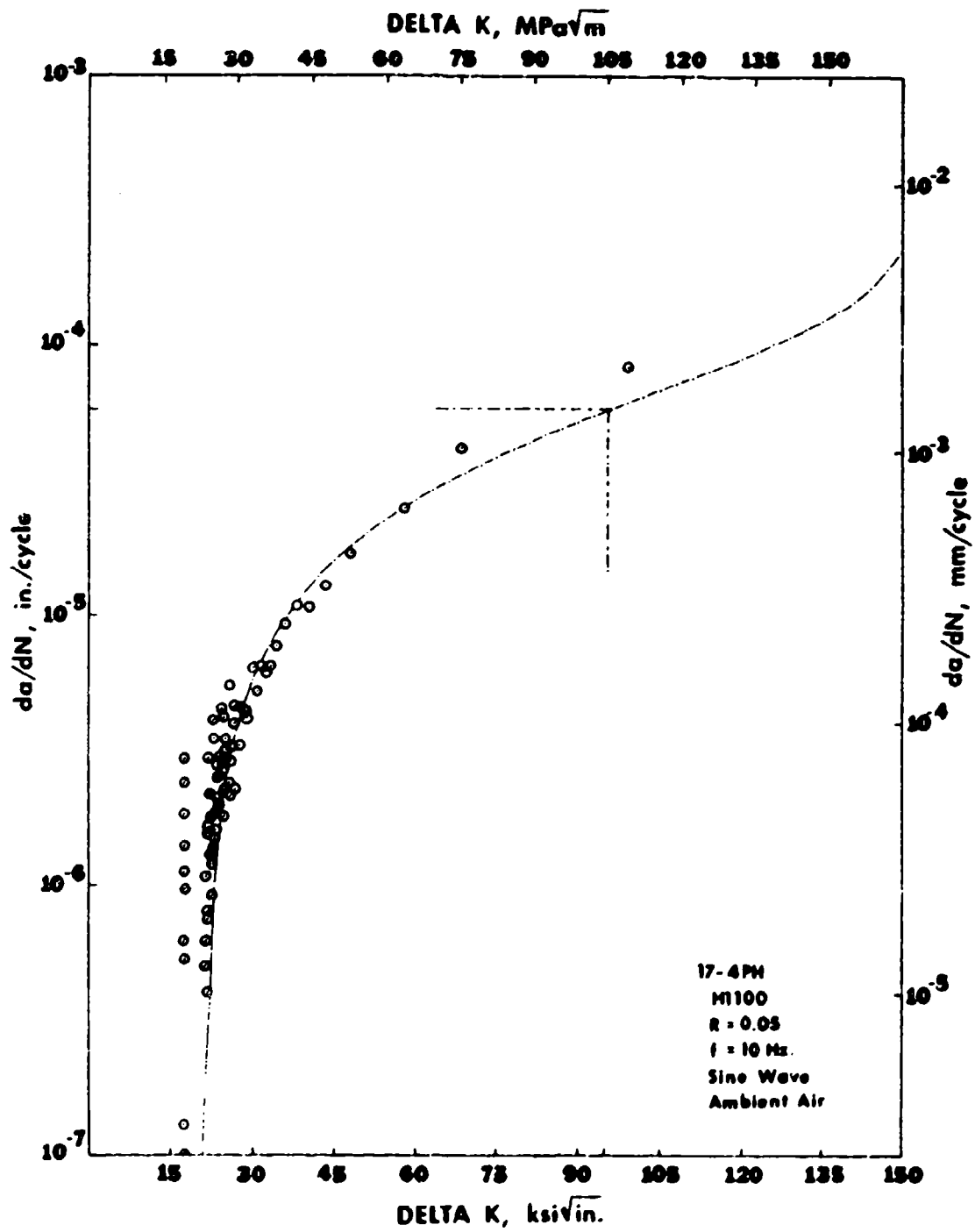
Figure 39   Log-Linear Graph of Specimen 10 Fatigue-Crack Growth Rate
Test Fitted with a Type-A Weibull Curve. The slow to
fast transition intercept on the curve indicates a DaDN
characteristic value (177.0 in/cycle) and 63.21% of the
final stress intensity, K_b (160 ksi $\sqrt{in}$).

DELTA K, MPa√m

DELTA K, ksi√in.

da/dN, in./cycle

da/dN, mm/cycle

17 - 4PH
H1100
R · 0.05
One Minute Hold
Salt Water
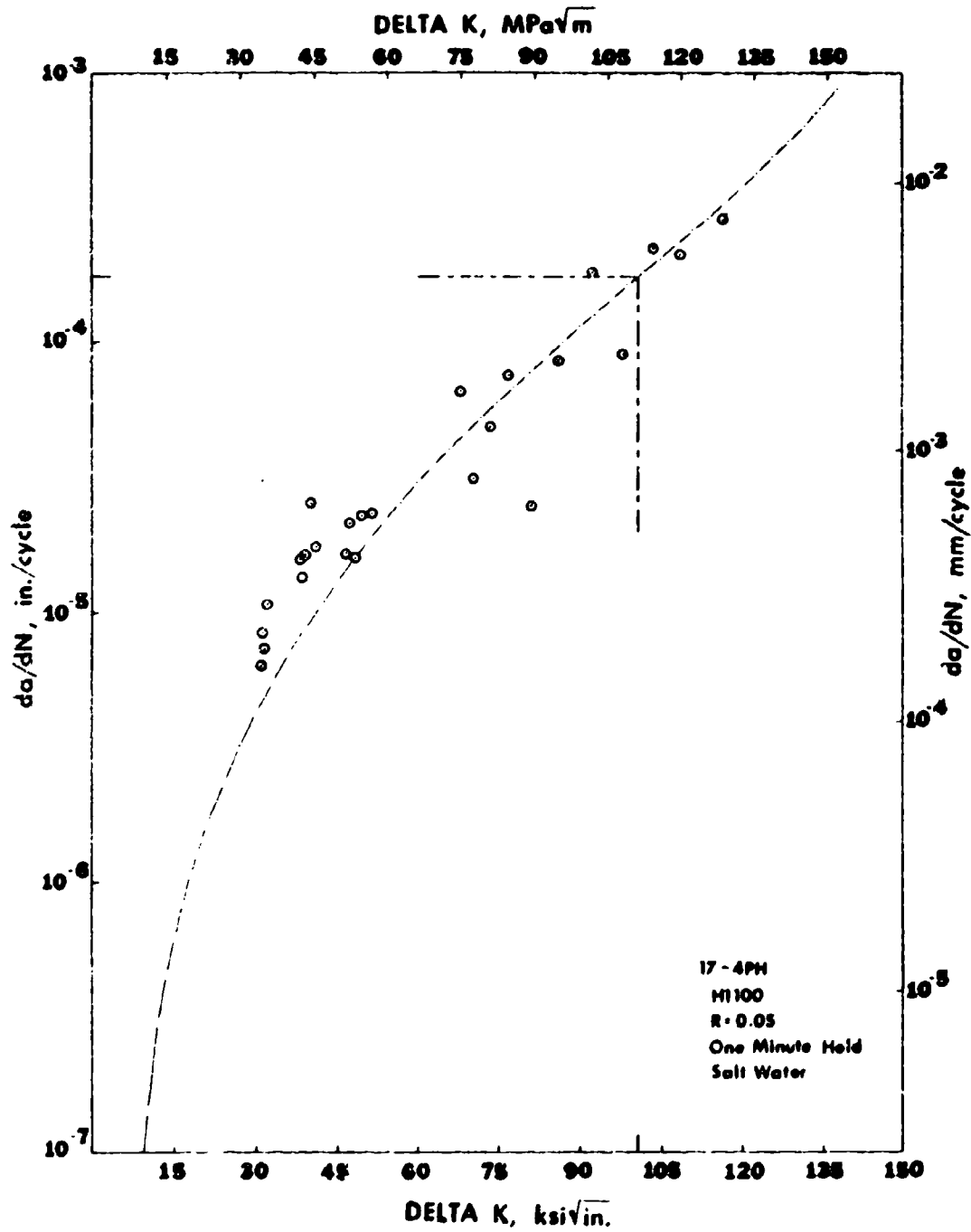
Figure 40 Log-Linear Graph of Specimen 11 Fatigue-Crack Growth Rate Test Fitted with a Type-A Weibull Curve. The slow to fast transition intercept on the curve indicates a DaDN characteristic value (15.8 in/cycle) and 63.21% of the final stress intensity, K_b (60 ksi $\sqrt{in}$).

DELTA K, MPa√m

17-4 PH
H1100
R = 0.67
f = 10 Hz.
Sine Wave
Ambient Air

DELTA K, ksi√in.
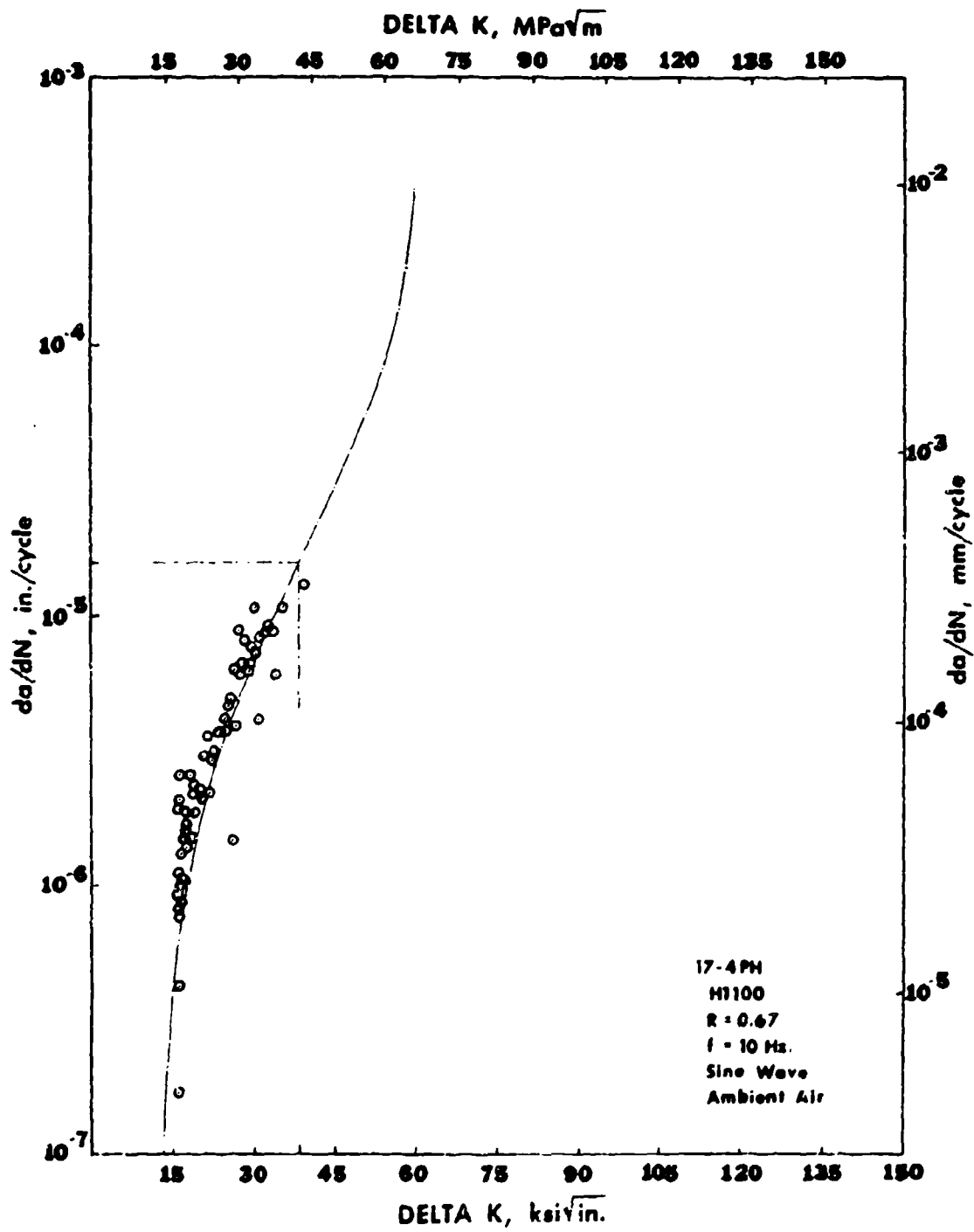
Figure 41   Log-Linear Graph of Specimen 12 Fatigue-Crack Growth Rate
Test Fitted with a Type-A Weibull Curve. The slow to
fast transition intercept on the curve indicates a DaDN
characteristic value (100.1 in/cycle) and 63.21% of the
final stress intensity, K_b (170 ksi $\sqrt{in}$).

DELTA K, MPa√m

DELTA K, ksi√in.

da/dN, in./cycle

da/dN, mm/cycle

17 - 4PH
H1100
R = 0.05
One Minute Hold
Ambient Air
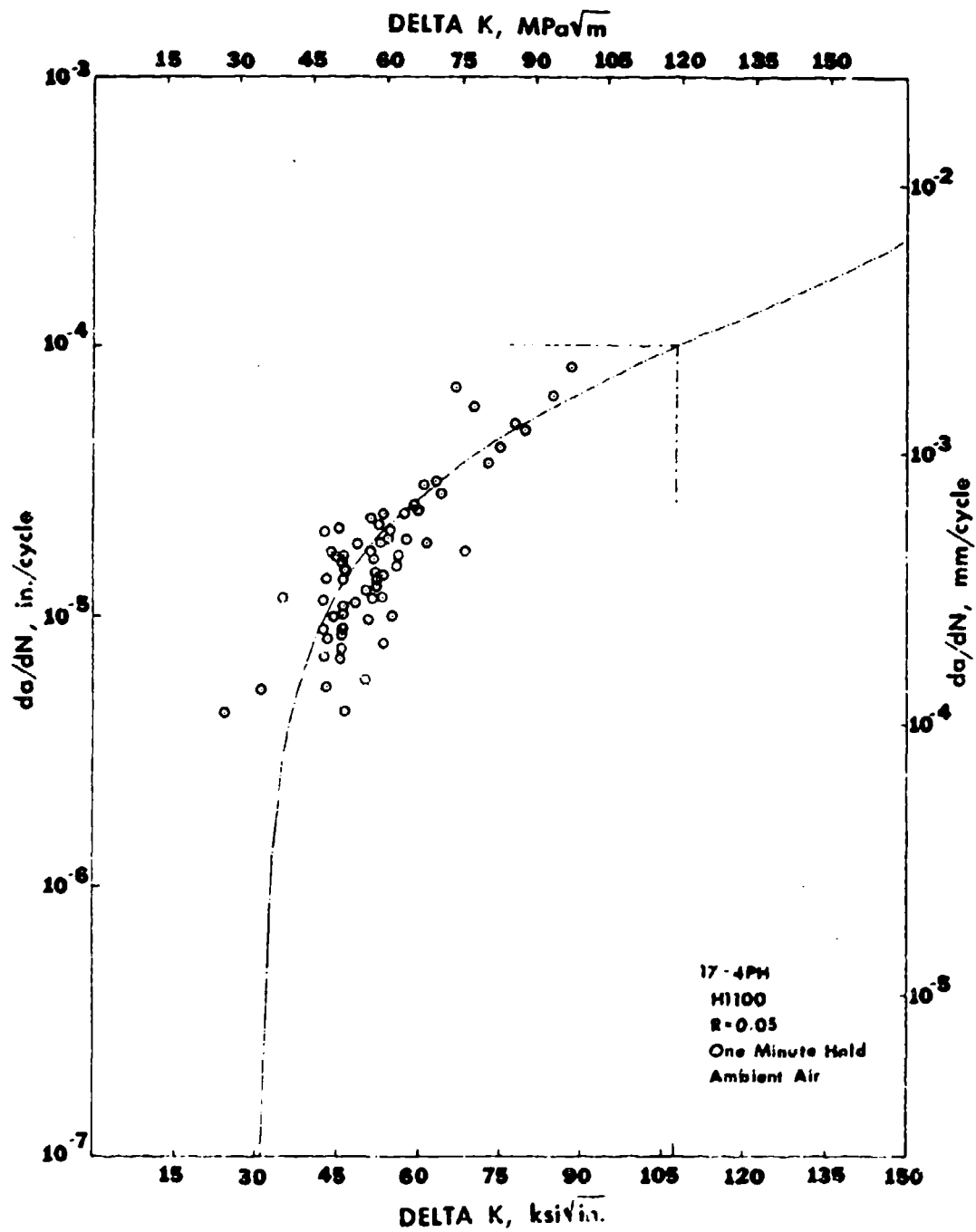
Figure 42 Log-Linear Graph of Specimen B Fatigue-Crack Growth Rate
Test Fitted with a Type-A Weibull Curve. The slow to
fast transition intercept on the curve indicates a DaDN
characteristic value (221.8 in/cycle) and 63.21% of the
final stress intensity, K_b (186 ksi $\sqrt{in}$).

DELTA K, MPa√m

DELTA K, ksi√in.

15 - 5PH
H1100
R = 0.05
One Minute Hold
Salt Water
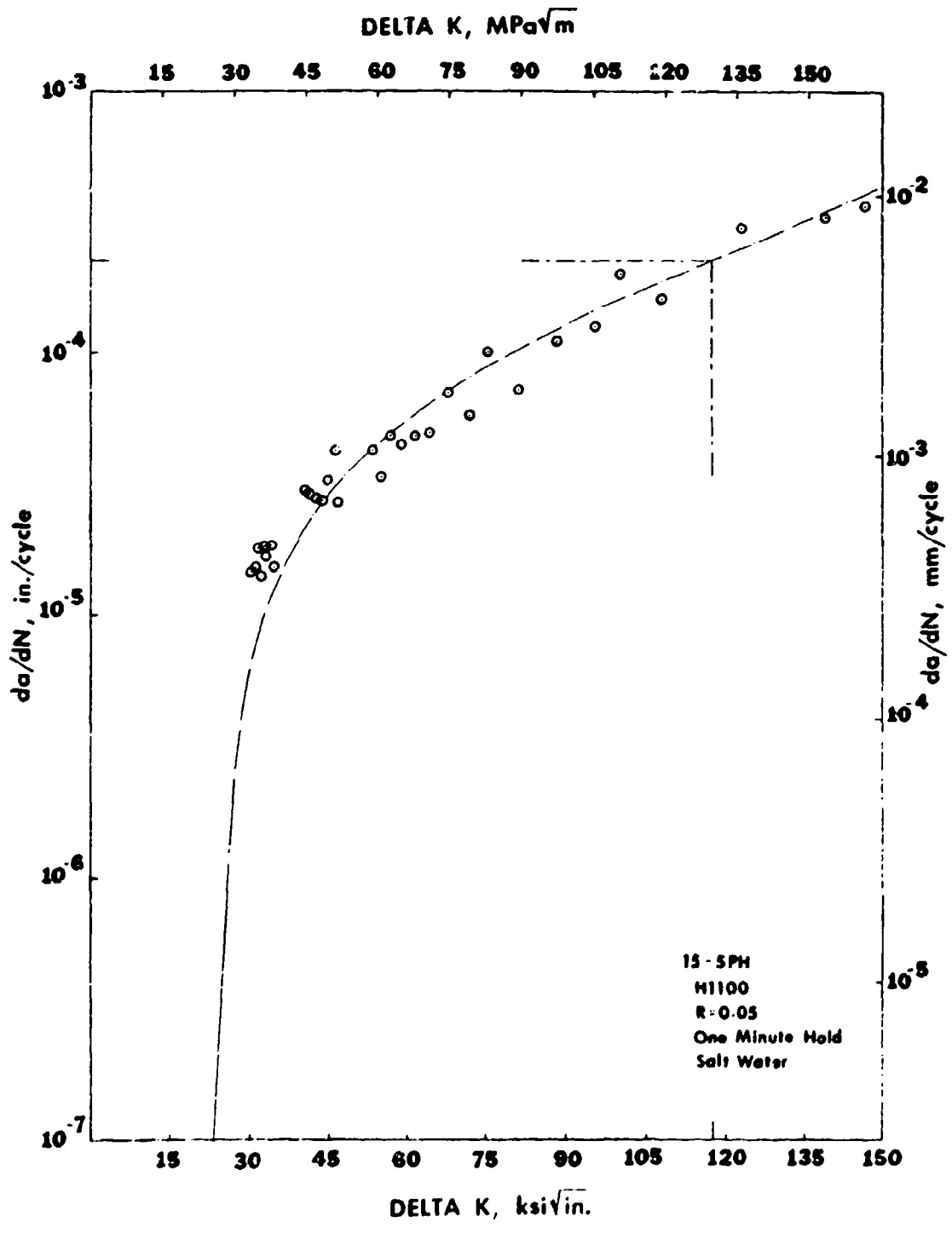
Figure 43 Log-Linear Graph of Specimen E Fatigue-Crack Growth Rate
Test Fitted with a Type-A Weibull Curve. The slow to
fast transition intercept on the curve indicates a DaDN
characteristic value (15.9 in/cycle) and 63.21% of the
final stress intensity, K_b (63 ksi $\sqrt{in}$).

DELTA K, MPa√m

da/dN, in./cycle

da/dN, mm/cycle

DELTA K, ksi√in.

15-5PH
H1050
R-0.67
One Minute Hold
Ambient Air
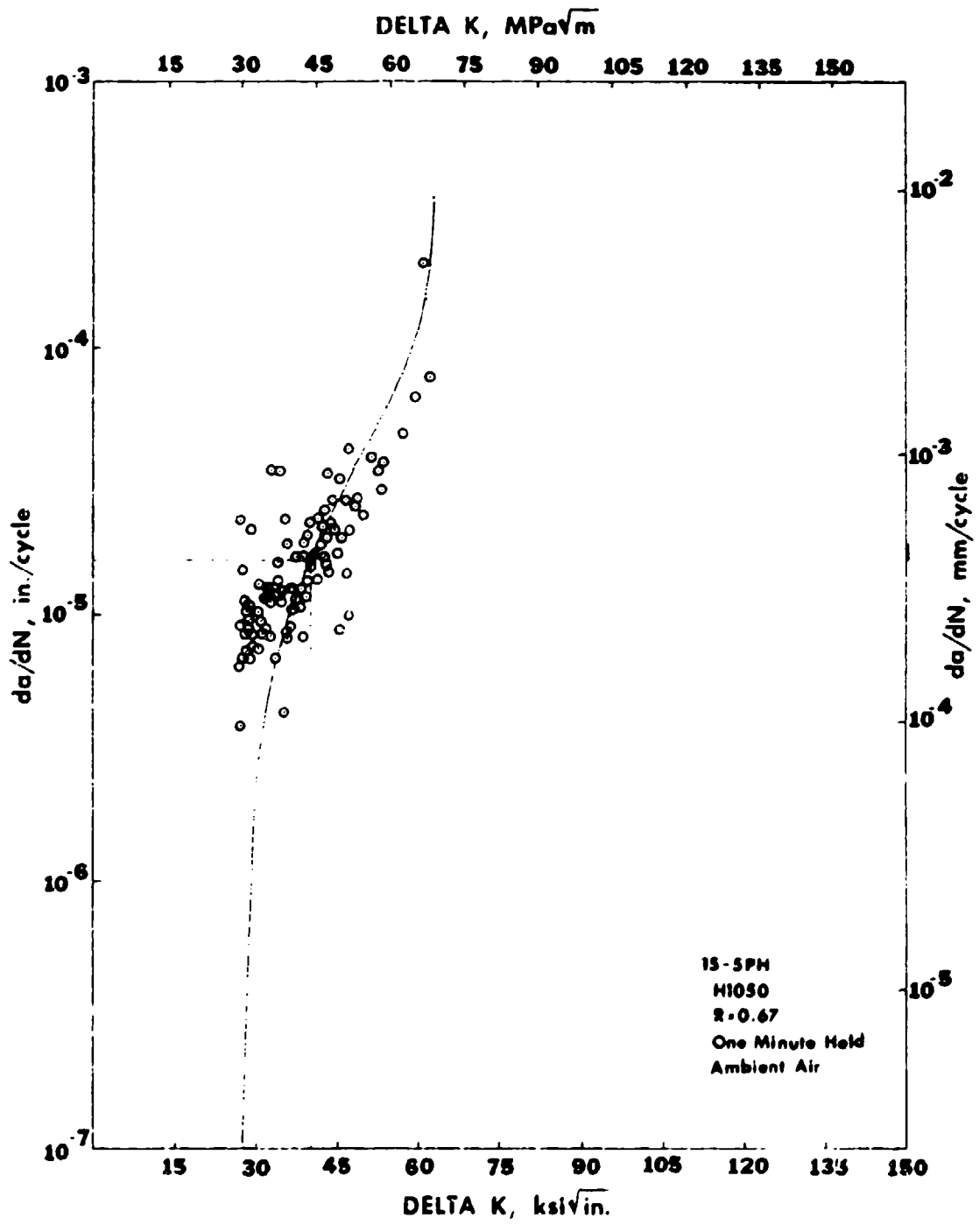
Figure 44   Log-Linear Graph of Specimen H Fatigue-Crack Growth Rate Test Fitted with a Type-A Weibull Curve. The slow to fast transition intercept on the curve indicates a DaDN characteristic value (151.6 in/cycle) and 63.21% of the final stress intensity, K_b (179 ksi $\sqrt{in}$).

DELTA K, MPa√m

15   30   45   60   75   90   105   120   135   150

10^{-3}

10^{-2}

10^{-4}

10^{-3}

da/dN, in./cycle

10^{-5}

da/dN, mm/cycle

10^{-4}

10^{-6}

10^{-5}

15-5PH
H1100
R = 0.05
f = 10 Hz.
Sine Wave
Ambient Air
*NRL Data

10^{-7}

15   30   45   60   75   90   105   120   135   150

DELTA K, ksi√in.
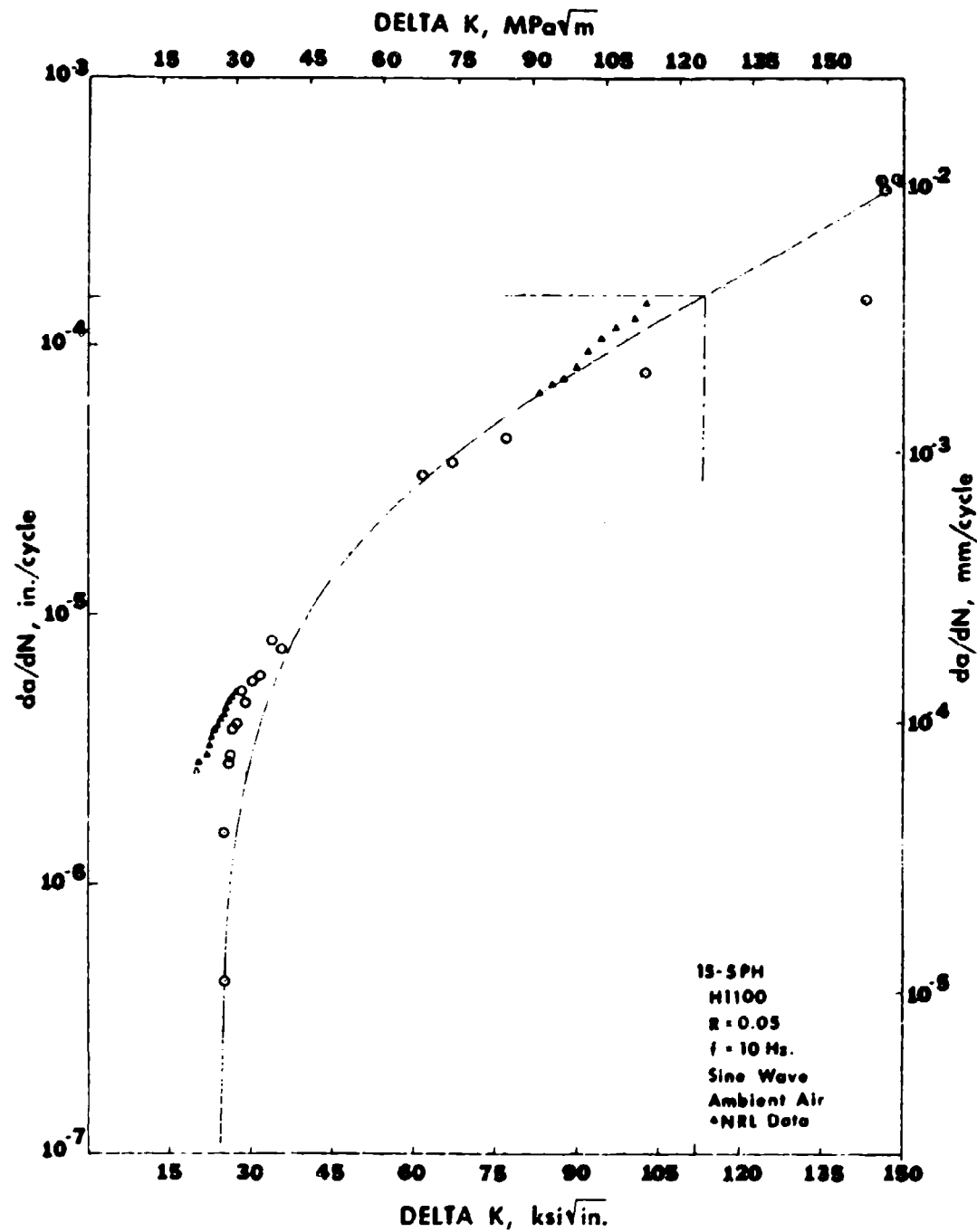
Figure 45   Log-Linear Graph of Specimen K Fatigue-Crack Growth Rate
Test Fitted with a Type-A Weibull Curve. The slow to
fast transition intercept on the curve indicates a DaDN
characteristic value (18.5 in/cycle) and 63.21% of the
final stress intensity, K_b (60 ksi $\sqrt{in}$).

DELTA K, MPa√m

da/dN, in./cycle

da/dN, mm/cycle

15 - 5PH
H1100
R - 0.67
One Minute Held
Ambient Air

DELTA K, ksi√in.
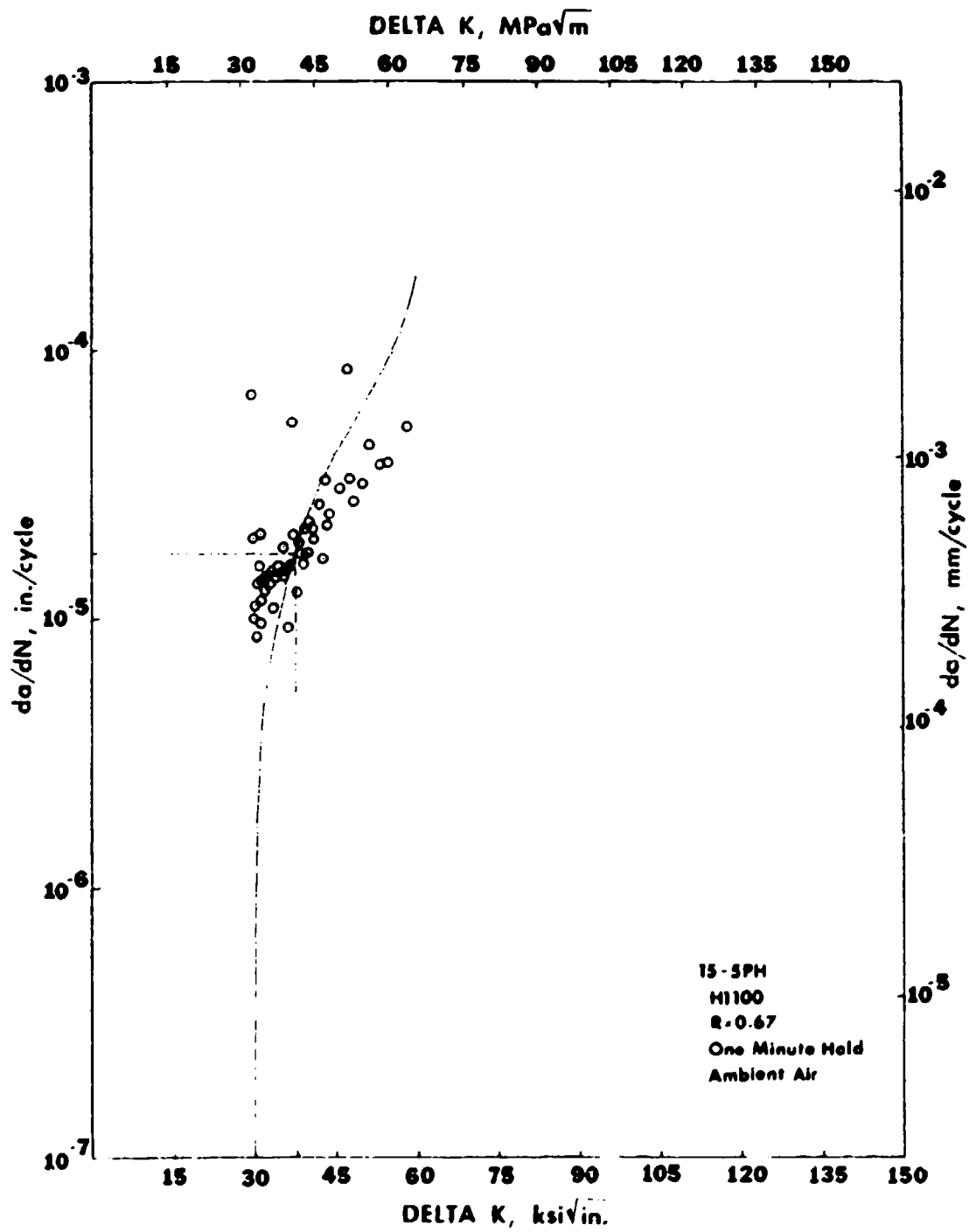
Figure 46   Log-Linear Graph of Specimen L Fatigue-Crack Growth Rate
             Test Fitted with a Type-A Weibull Curve. The slow to
             fast transition intercept on the curve indicates a DaDN
             characteristic value (43.2 in/cycle) and 63.21% of the
             final stress intensity, K_b (58 ksi $\sqrt{in}$).

DELTA K, MPa√m

da/dN, in./cycle

da/dN, mm/cycle

IS - SPH
H1100
R=0.67
One Minute Hold
Salt Water

DELTA K, ksi√in.
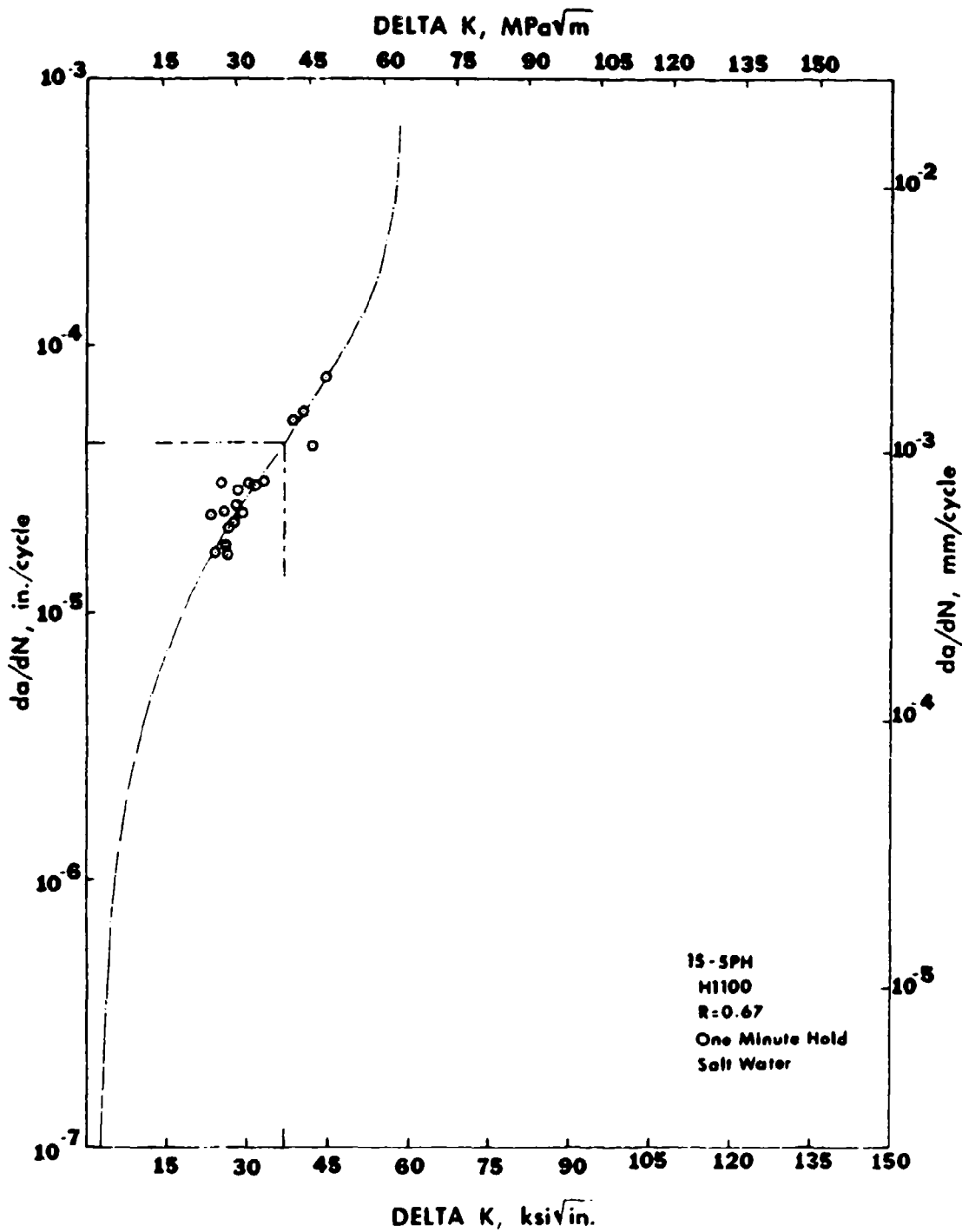
Figure 47 Log-Linear Graph of Specimen N Fatigue-Crack Growth Rate
          Test Fitted with a Type-A Weibull Curve. The slow to
          fast transition intercept on the curve indicates a DaDN
          characteristic value (163.9 in/cycle) and 63.21% of the
          final stress intensity, K_b (165 ksi $\sqrt{in}$).
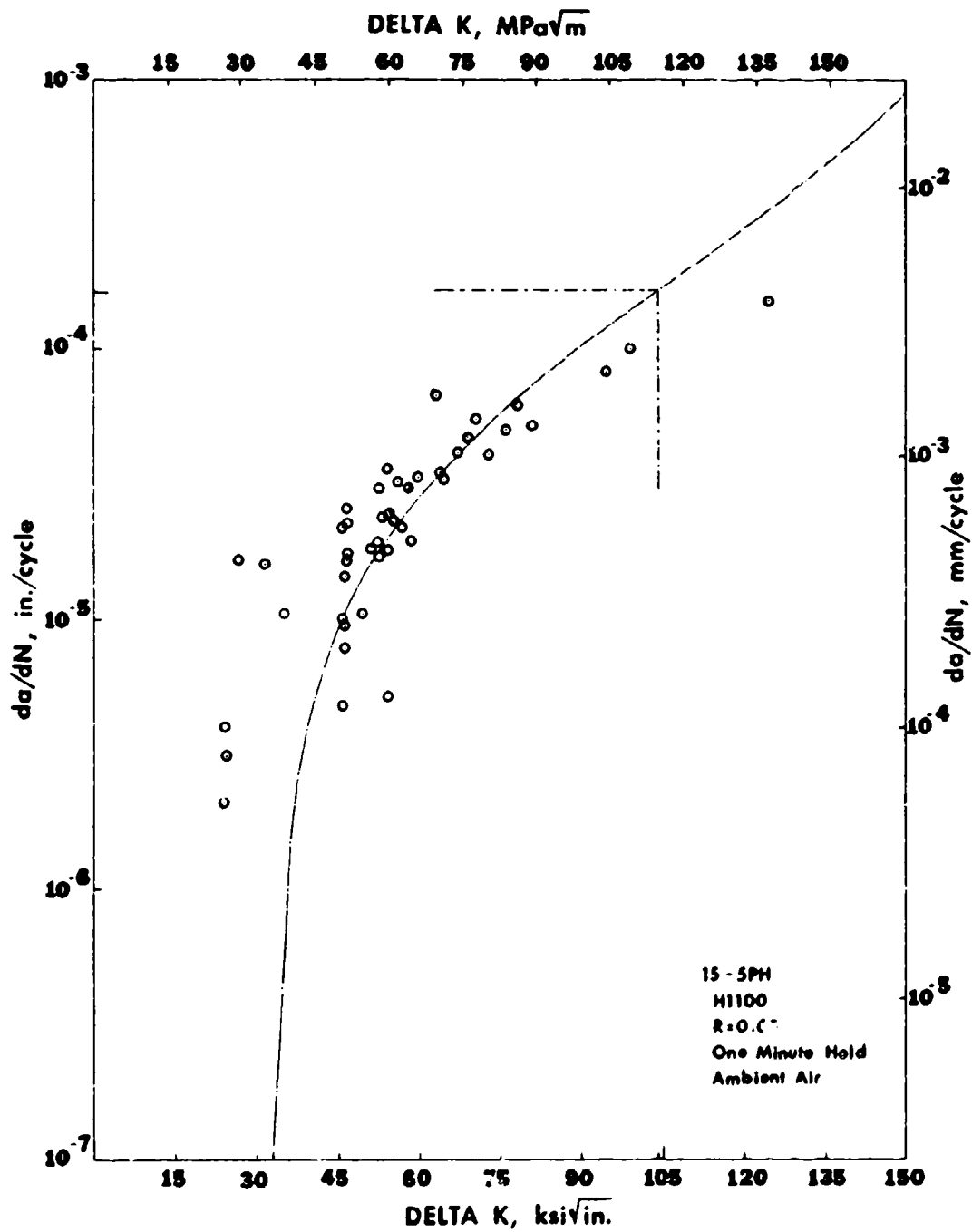
Figure 48 Log-Linear Graph of Specimen T Fatigue-Crack Growth Rate
Test Fitted with a Type-A Weibull Curve. The slow to
fast transition intercept on the curve indicates a DaDN
characteristic value (46.2 in/cycle) and 63.21% of the
final stress intensity, K_b (150 ksi $\sqrt{in}$).

DELTA K, MPa√m

da/dN, in./cycle

da/dN, mm/cycle

15-5PH
H1050
R = 0.05
f = 10 Hz.
Sine Wave
Ambient Air

DELTA K, ksi√in.
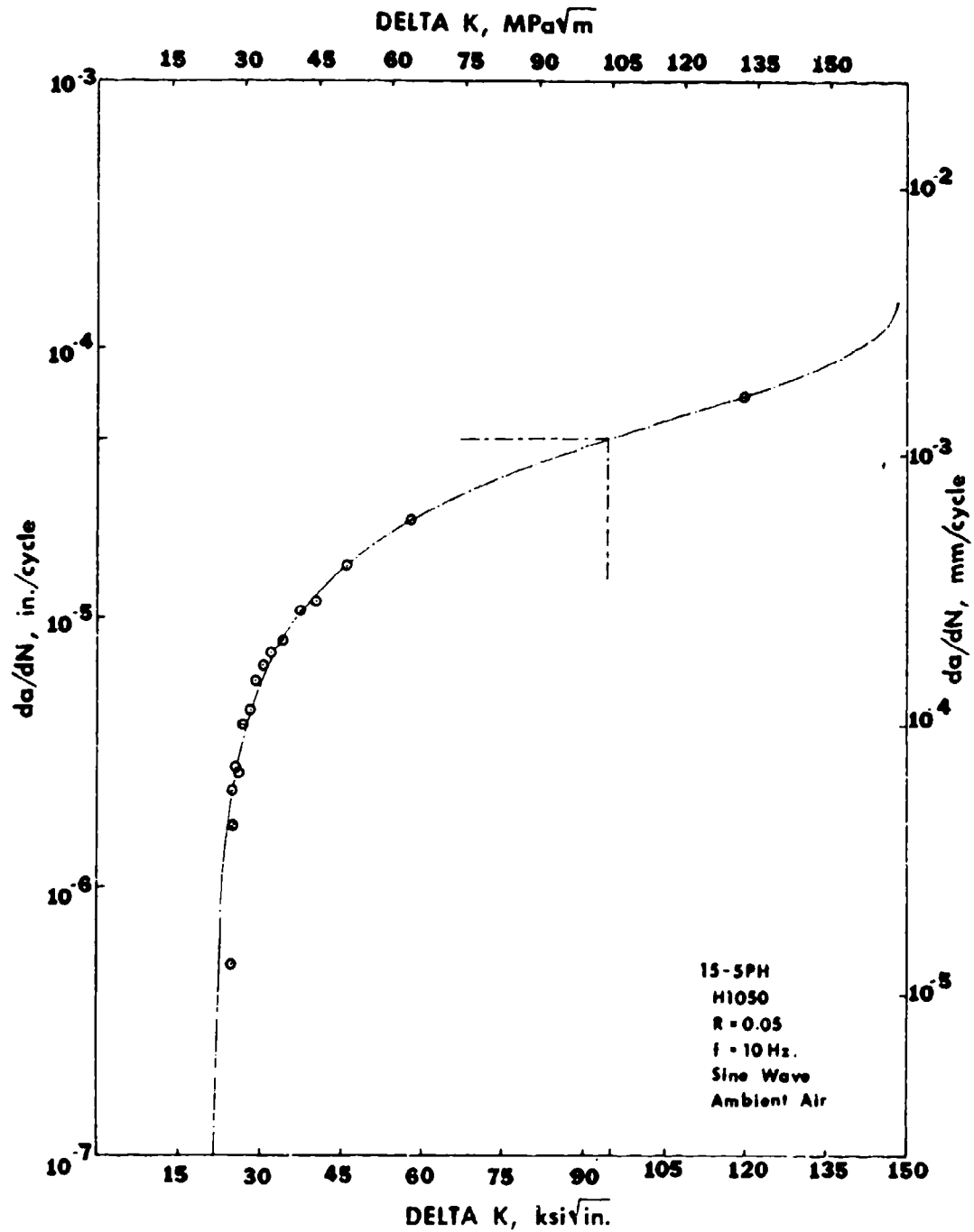
straight are found in log-log form, Appendix 1.

6.3 COMPARATIVE ANALYSIS OF FATIGUE-CRACK GROWTH RATES

The major point to be derived in this study is to show that microstructure does effect fatigue-crack growth and that the effect can be over entire rate and stress intensity ranges. The primary thrust is to examine a result that may have its explanation and final control in understanding a combination of metal physics, micromechanics, continuum and fracture mechanics. Microstructural morphology, tessellated residual strains, secondary particle compatibility and activation mechanisms which are slightly understood, do direct the rate at which materials shall be reclaimed to a lower energy state in nature.

To appreciate the differences between the following test set parameters and facilitate viewing, composite graphs were constructed.

6.3.1 Heat Treatment Effect

The alloys' microstructures were alterred by the final tempering or aging portion of the heat treat process. Both alloys had their microstructures put in the H 1050 and H 1100 heat treated condition. The basic chemical differences (Table III) left 17-4 PH with some delta ferrite that formed into extended pools and stringers, whereas 15-5 PH is virtually delta ferrite free. The retained austenite was too fine for identification in either alloy or heat treated condition.

Initially for a 17-4 PH base-line, both heat treats were tested under a 10 Hz sine wave for two R-ratios, R = 0.05 and R = 0.67. Table IX will identify the location of all test specimens with respect to the test conditions and curves. In Figure 49, the test material with R = 0.05 and H 1050 (curve 1) has a lower threshold than curve 8 at H 1100. But as curve 1 moves toward its characteristic, v its crack growth rate decreases. For R = 0.67 (curves 5 and 11), the differences were negligible for threshold, but the H 1100 (curve 11) tended to require more stress intensity for fatigue cracking. This probably is not surprising in that the H 1100 is more tempered with a lower yield strength and a higher resistance to fracture. However, the opposite response occurs for curves 1 and 8. In Figure 50, the 15-5 H 1050 and H 1100 curves T and H align similarly to the corresponding 17-4 curves 1 and 8 whereas for R = 0.67, the 15-5 H 1050 and H 1100 curves E and K are opposite to the 17-4 curves 5 and 11, and the 15-5 curves T and H. Further testing at R = 0.05 under a one minute hold-time trapezoidal wave showed distinct microstructural response differences from the above mentioned base-line. At H 1050 (curve 2), the threshold in conjunction with overall fatigue-crack growth rates increased substantially. For the H 1100 (curve 12) material under the same regime neither threshold or rate increased as much as curve 2. However, curve 12, still exceeded the equivalent 10 Hz base-line of curve 8. It can be concluded that the effect of heat treatment shown by the microstructure can vary with mean stress. Note that on comparing only those

Figure 49   Composite Log-Linear Plot of Fatigue-Crack Growth Rates
of 17-4 PH Used to Compare Heat Treatment (1 vs. 8, 2
vs. 12, 5 vs. 11), R-ratio (1 vs. 5, 8 vs. 11, 2 vs.
6) and Wave Form (1 vs. 2, 5 vs. 6, ᴄ vs. 12).
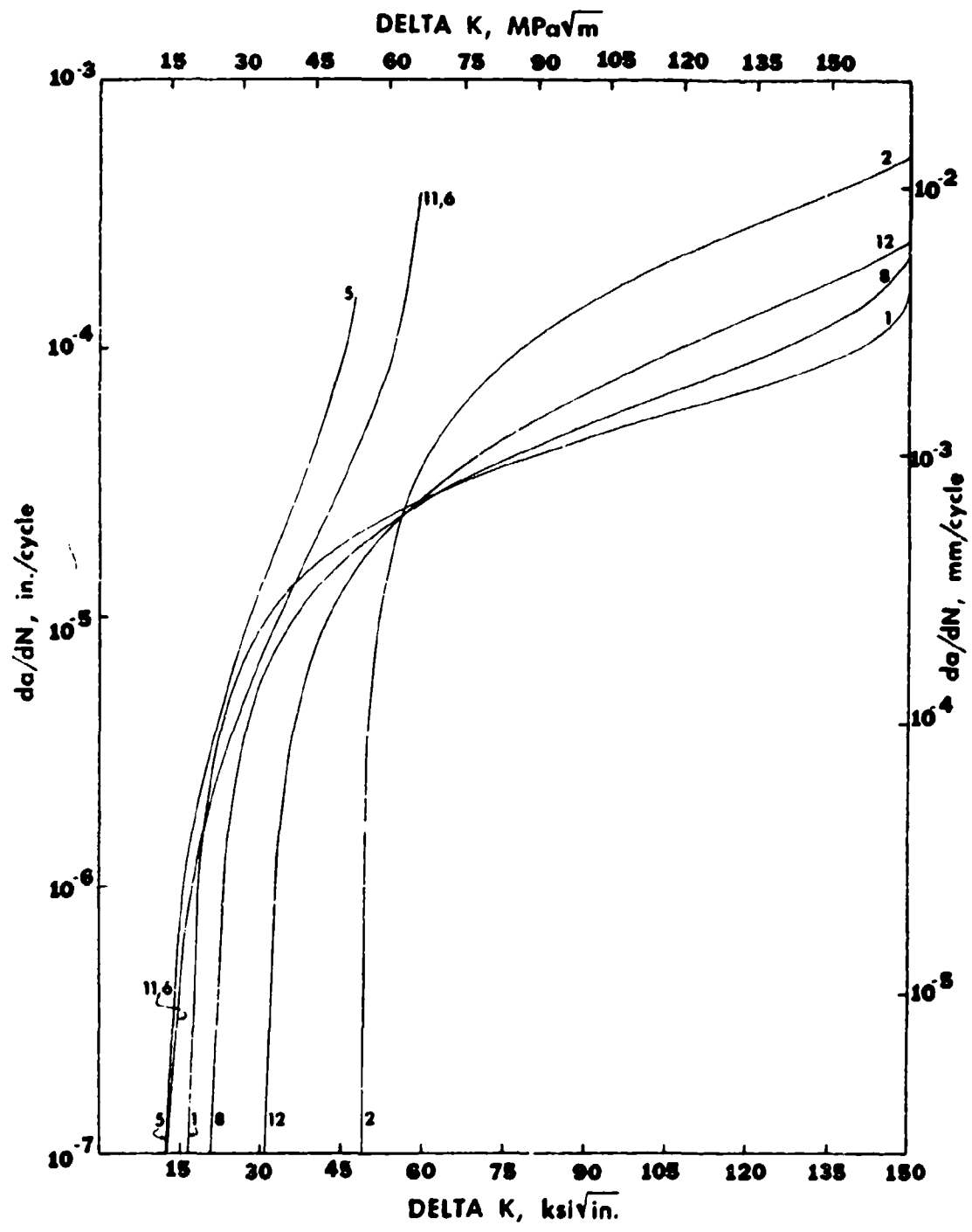
Figure 50   Composite Log-Linear Plot of Fatigue-Crack Growth Rates of
15-5 PH Used to Relate Heat Treatment (H vs. T, K vs. E).
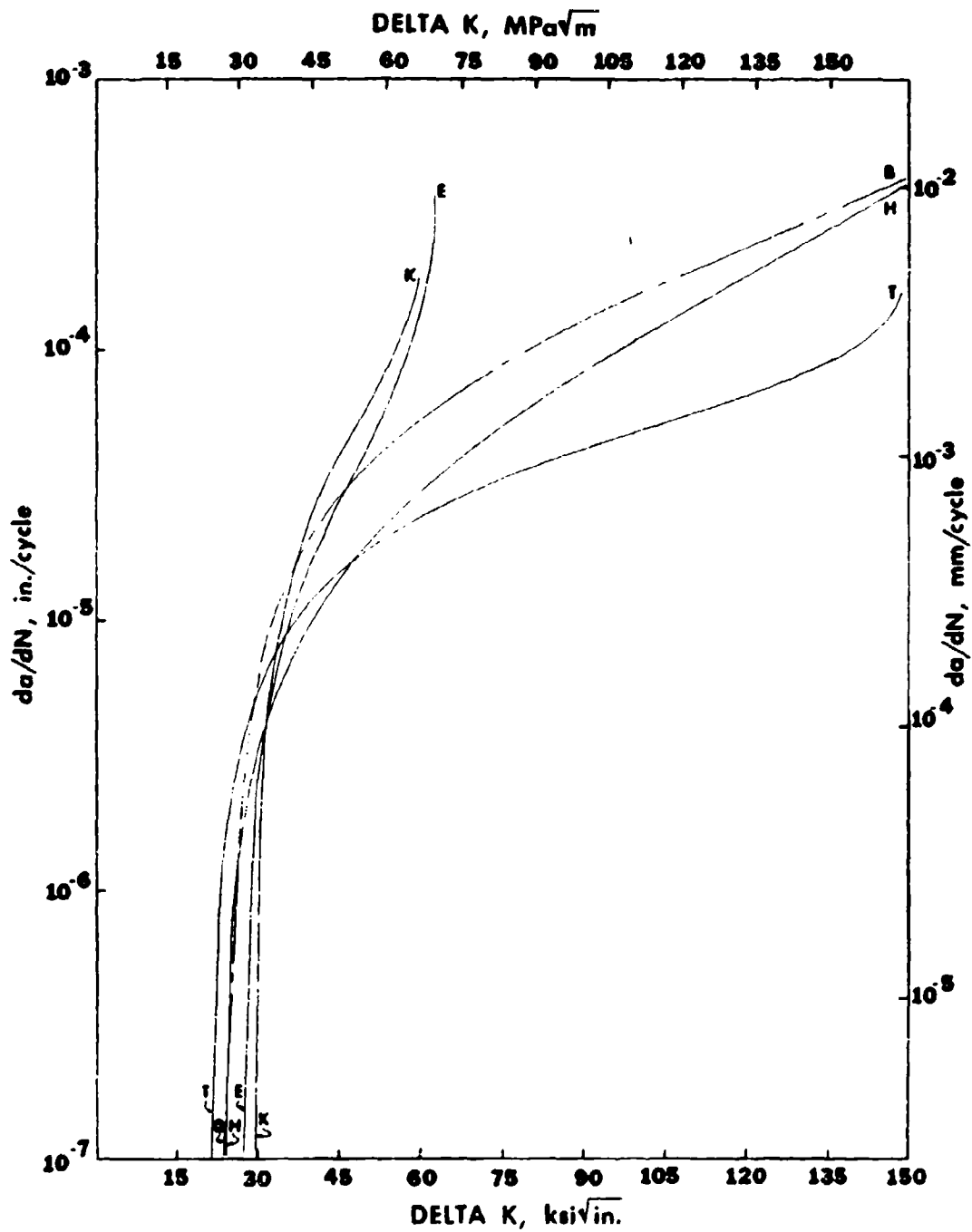
test variables under 10 Hz sine wave, the 15-5 PH alloy does indicate slower fatigue-crack growth rates than the 17-4 PH alloy.

6.3.2 R-Ratio Effect

As the mean stress increases the fatigue-crack growth rates increase. The extent of the increase, is largely determined on the applied stress the microstructure experiences (i.e. including its internal residual stress). A possible explanation for 17-4 PH H 1050 (curve 5) requiring less stress intensity to fracture may be found in the metal's microscopy and fractography. A more precipitated matrix with larger delta ferrite stringers are indicated in H 1100 versus H 1050. This combination appears to be an active retardant to fatigue-crack growth over a limited ΔK range in 17-4 PH. This is seen in the upper portion of (curve 11), and in the increased thresholds of curves 2 and 12 as compared to curve 8 (Figure 49).

In 17-4 PH H 1050 a large difference (30 ksi $\sqrt{in}$, 33 MPa $\sqrt{m}$) threshold of curves 2 and 6 is seen if wave form is considered constant and R-ratio (0.05 versus 0.67) is compared (Figure 49). The counterpart in 15-5 PH but under a H 1100 heat treat shows a smaller threshold separation (6 ksi $\sqrt{in}$, 6.6 MPa $\sqrt{m}$) for curves N and K. The N and K curves do tend to diverge to fast crack growth rates more rapid than comparable 17-4 PH curves 2 and 6.

6.3.3 Wave Form Effect

This portion of the work evaluates the impact of load wave form on microstructure by considering alloy performance over an entire

stress intensity and fatigue-crack growth range. Figure 49 can be used to compare 10 Hz sine wave to one minute hold-time trapezoidal wave for curves 1 and 2, 5 and 6, 8 and 12. Figure 51 can be used to compare H and N. All comparisons are under the same heat treat, R-ratio and environment. Observations are that due to substantial curve shifts in 2 and 12, 17-4 PH under this wave form is responding to what is hypothesized to be strain-induced stress relaxation assisted by the microstructural feature, delta ferrite. The premise is that under a one minute hold-time at load, an increasing number of slip systems are activated, elastically spreading applied strain. In conjunction with this a possibility exists that delta ferrite is acting like a strain absorber by producing a ductile rupture in lieu of cleaving in the microstructure. Both alloys 17-4 PH and 15-5 PH are basically similar, except for the delta ferrite present in the 17-4 microstructure. It is suspected that delta ferrite is contributing to the variance in fatigue-crack growth rate response over the entire ΔK range (Figure 49).

6.3.4 Environmental Effect

This study culminates its purpose by exploring the wave form hold-time effect in a 3.5% ASTM salt water environment. The objective was to relate laboratory environment and testing of a specimen with a comparable field environment and use a discrete wave form element, relative to a structure's actual load spectrum. Figure 52 illustrates a composite plot for the conditions of H 1100, R = 0.05

Figure 51   Composite Log-Linear Plot of Fatigue-Crack Growth Rates of
15-5 PH Used to Relate Wave Form (H vs. N), R-ratio (N
vs. K, B vs. L) and Environment (N vs. B, K vs. L).

DELTA K, MPa√m
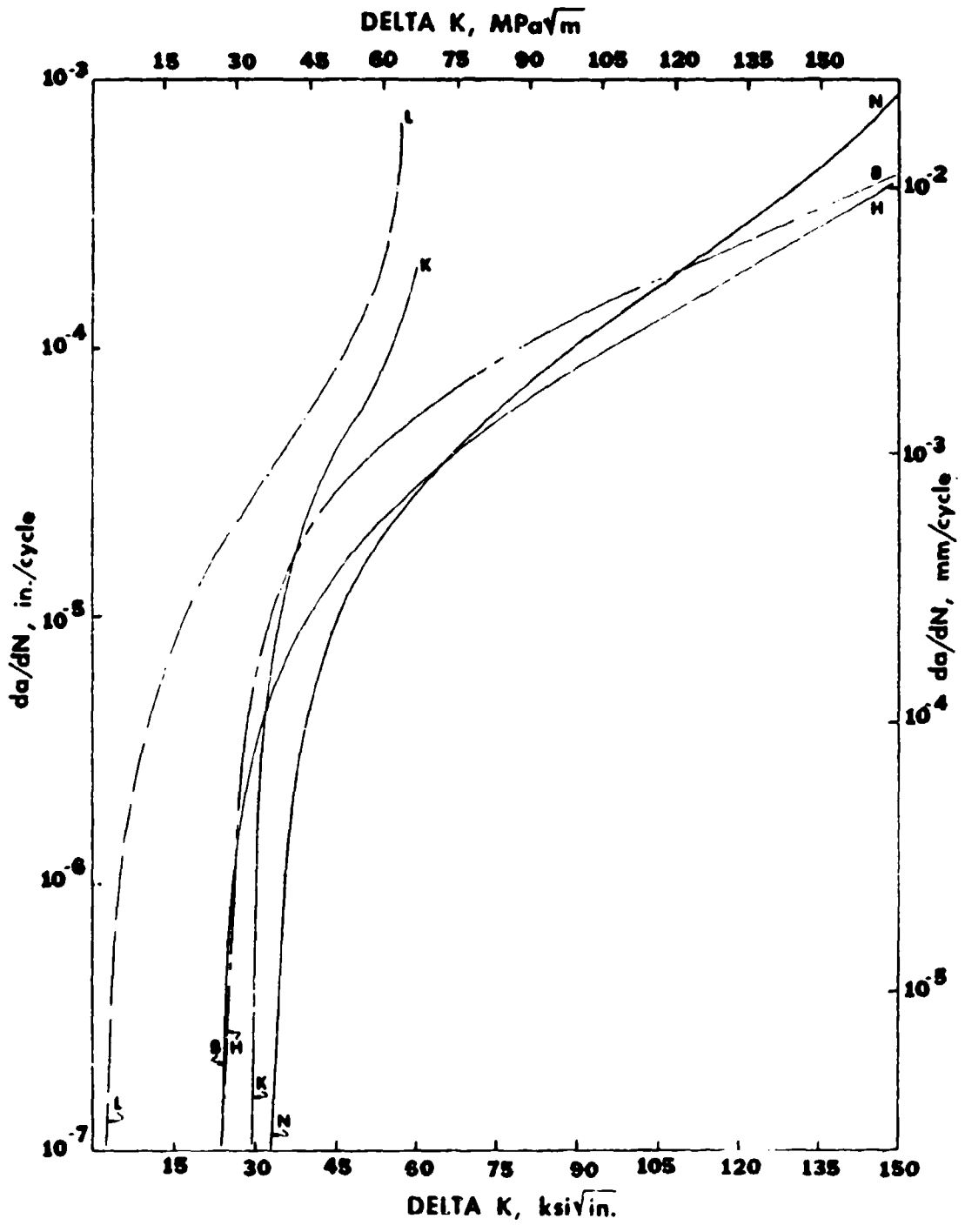
Figure 52 Composite Log-Linear Plot of Fatigue-Crack Growth Rates of
17-4 PH and 15-5 PH Used in the Evaluation of Environment
Under Similar Heat Treat Condition, R-ratio and Wave Form
(12 vs. 10 vs. N, N vs. B, 10 vs. B, K vs. L) Between
Materials.

144
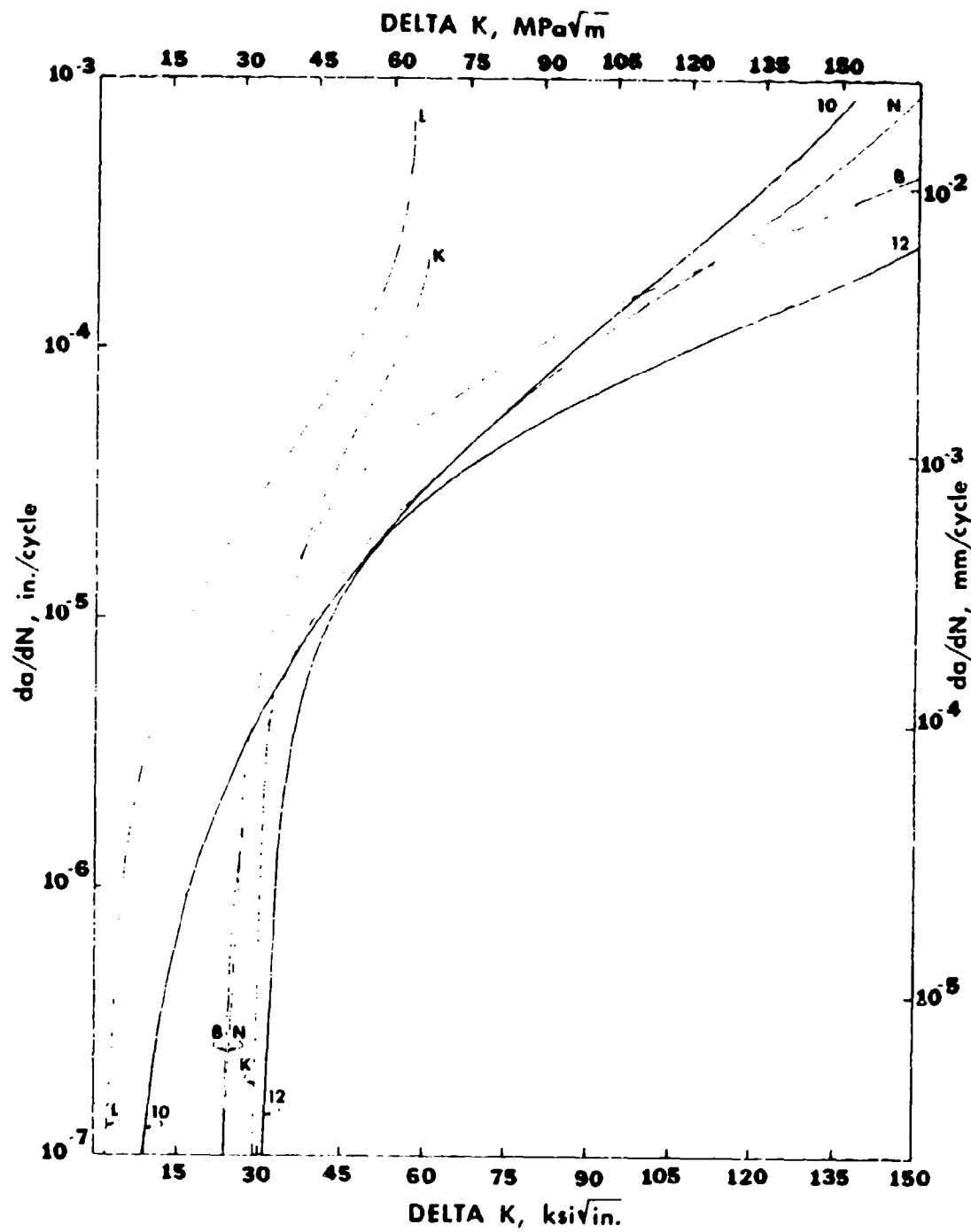
and trapezoidal one minute hold-time for 17-4 PH in ambient air and salt water (curves 12 versus 10) and 15-5 PH (curves N versus B). Here for rational interpretation, considerations must be three fold: where are the curves entered due to manufacturing defects; what are the magnitudes of deviation from a 10 Hz design and decision baseline; and what are stress ratio effects (i.e. R-ratio, residual stress). A 15-5 PH curve for H 1100 and R = 0.67 was generated. The deviation from curve B (H 1100 and R = 0.05) was substantial (Figure 52).

With the above factors in mind, it is believed from the shifting of these curves for the different test conditions that there is no doubt microstructure dictates the alloy performance under fatigue-crack propagation. Further, the slower growth rates of 17-4 PH (curve 10) between the stress intensity of 24 ksi $\sqrt{in}$ (26.4 MPa $\sqrt{m}$) and 90 ksi $\sqrt{in}$ (98.9 MPa $\sqrt{m}$) versus 15-5 PH (curve B) is believed to be attributed to the microstructure being strain-induced to relax the stress into the matrix.

CHAPTER 7

MICROSTRUCTURAL METALLOGRAPHY AND FRACTOGRAPHY

By collectively considering alloy chemistry, thermo-mechanical history, metallography and fractography an explanation may be developed for alloy performance. The rudimentary factors requisite for understanding microstructural control to precisely predict component material life rest in comprehending the relation of energy balance, molecular arrangement and strain compatibility to the material fracturing process. Proceeding with the supposition that these factors are e⬤ :.al, coupled with verification of the hypothesis of this work (i.e. microstructure does dictate alloy performance, chapter 6) attempts are made to discriminate and relate "why" and "how" observed differences between microstructures and between fracture surface determine alloy performance. Here, a foundation exists for bridging material performance to design requirements by way of the presented fracture and fatigue mechanics methodology (chapter 5). This technique can comprehend and decipher the effect of operational performance elements.

7.1 METALLOGRAPHIC OBSERVATION

The 17-4 and 15-5 alloys were examined in both heat treats, H 1050 and H 1100 for all three directions (T, S, L). At H 1050 the finely dispersed copper-rich particles are becoming observable at 500x.

The effect of these dispersed particles is in preventing dislocation motion which depends in a complex way on the particle size and shape, conformity of the particle's crystal structure to the matrix, and the elastic properties of the particle.

A crystallographic alignment between particles and matrix at the atomic bonding level can lead to complete coherency. In a coherent structure the particles produce elastic strains in the matrix developing strain fields that resist free dislocation movement and are a major source of hardening in the alloy. In fatigue, the copper-rich precipitates or particles in 17-4 and 15-5 alloys limit the free dislocation slip-path, (i.e. across the grain) restricting dislocation movement over small distances. Thus, the presence of these particles tend to develop a finer overall slip behavior requiring more energy and increased number of repetitive load cycles to fracture the material. For the H 1100 heat treat condition particle size and shape change minutely with respect to particles surface area. The major difference between heat treat conditions is recognized in the temper state of the martensite. The H 1100 condition tends to precipitate more carbon in the matrix, relaxing internal crystal lattice strains. An optical comparison can be made between Figures 53, 54 and Figures 59, 60 to see the additional precipitated carbon darkening the latter micrographs and increasing the definition of grain boundaries. All micrographs lend themselves to a comparison between the heat treat condition as follows; H 1050 Figures 53 through and including 58 versus H 1100 Figures 59 through and including 64. Any retained austenite appears to be submicro-

Figure 53 Microstructure of 17-4 PH, H 1050 Heat Treat Condition.
          View is into the plane parallel to T in specimen T-L,
          Figure 10. Tempered martensitic matrix with elongated
          pools of delta ferrite, and finely dispersed copper-rich
          precipitate particles. (Magnification: 500x, Etch: Mixed
          Acids).

Figure 54 Microstructure of 15-5 PH, H 1050 Heat Treat Condition. View
          is into the plane parallel to T in specimen T-L, Figure 10.
          Tempered martensitic matrix, similar carbon presence as in
          Figure 53 but virtually no delta ferrite. (Magnification:
          500x, Etch: Mixed Acids).

Figure 55 Microstructure of 17-4 PH, H 1050 Heat Treat Condition. View is into the plane parallel to L in specimen T-L, Figure 10. The delta ferrite pools are substantially increased over those in Figure 53 within a martensitic matrix. (Magnification: 500x, Etch: Mixed Acids).

Figure 56 Microstructure of 15-5 PH, H 1050 Heat Treat Condition. View is into the plane parallel to L in specimen T-L, Figure 10. Delta ferrite appears to be small oblated spheriods throughout the martensitic matrix. (Magnification: 500x, Etch: Mixed Acids).
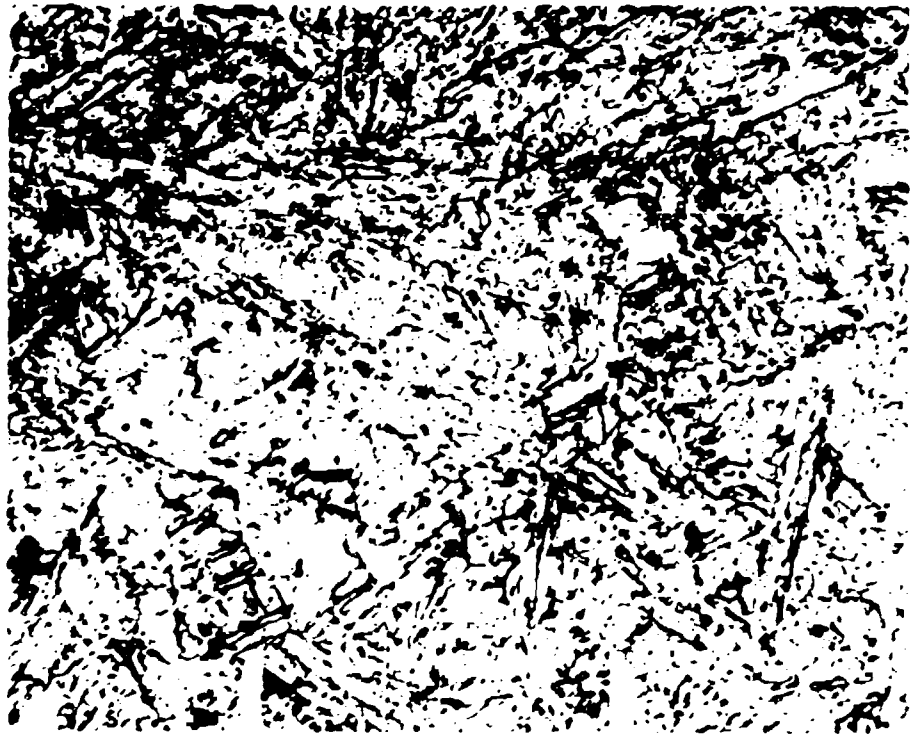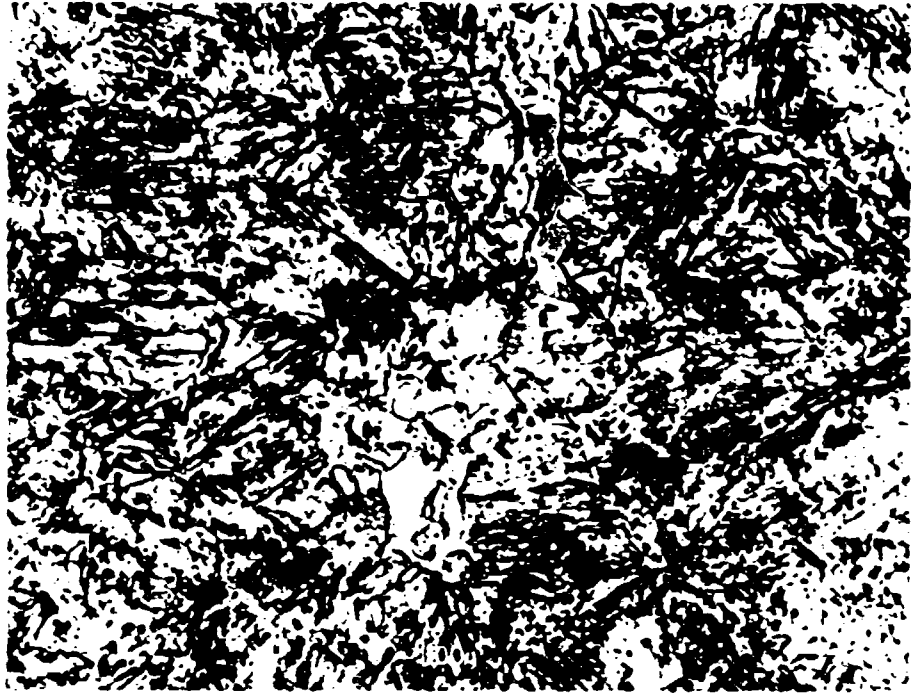
Figure 57   Microstructure of 17-4 PH, H 1050 Heat Treat Condition. View
is into the plane parallel to S in specimen T-L, Figure 10.
The delta ferrite forms in well defined stringers in a marten-
sitic matrix. (Magnification: 500x, Etch: Mixed Acids).

Figure 58   Microstructure of 15-5 PH, H 1050 Heat Treat Condition. View
is into the plane parallel to S in specimen T-L, Figure 10.
The matrix reflects a primarily martensitic structure.
(Magnification: 500x, Etch: Mixed Acids).

150

Figure 59   Microstructure of 17-4 PH, H 1100 Heat Treat Condition. View
is into the plane parallel to T in specimen T-L, Figure 10.
The delta ferrite stringers are prevalent throughout the
martensitic matrix. In this heat treat condition the copper-
rich finely dispersed precipitates tend to increase in size.
(Magnification: 500x, Etch: Mixed Acids).

Figure 60   Microstructure of 15-5 PH, H 1100 Heat Treat Condition. View
is into the plane parallel to T in specimen T-L, Figure 10.
The matrix tends to increase its carbon presence in the
martensitic form as the grain boundary definition is enhanced.
Delta ferrite is virtually absent. (Magnification: 500x,
Etch: Mixed Acids).

Figure 61   Microstructure of 17-4 PH, H 1100 Heat Treat Condition. View
is into the plane parallel to L in specimen T-L, Figure 10.
The delta ferrite, similar to Figure 55, tends to agglomerate
into extended pools within the martensitic matrix. (Magnifi-
cation: 500x, Etch: Mixed Acids).

Figure 62   Microstructure of 15-5 PH, H 1100 Heat Treat Condition. View
is into the plane parallel to L in specimen T-L, Figure 10.
The matrix has increased carbon within the martensitic struc-
ture. Grain boundaries are more defined. (Magnification: 500x,
Etch: Mixed Acids).

152
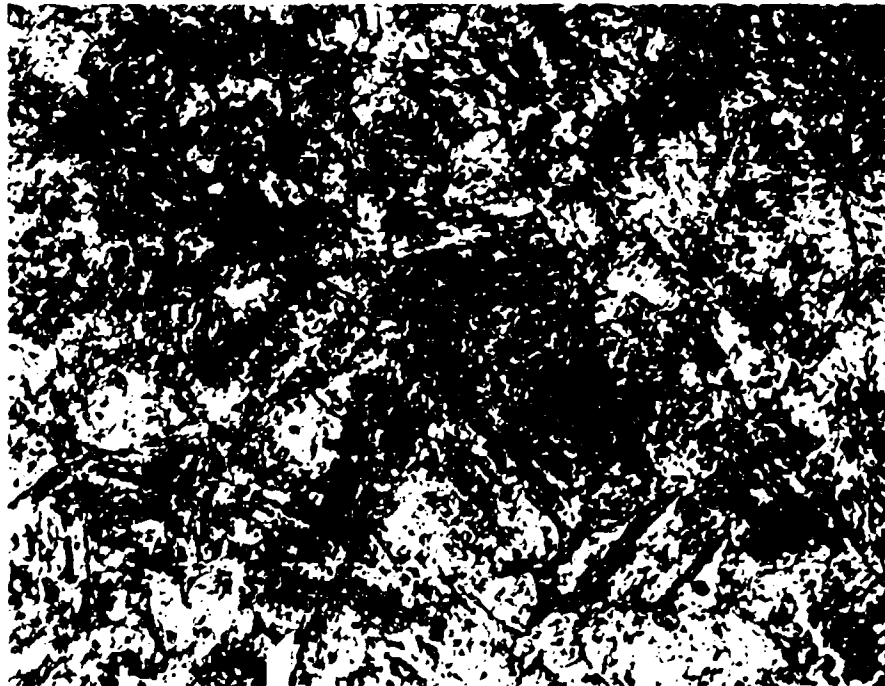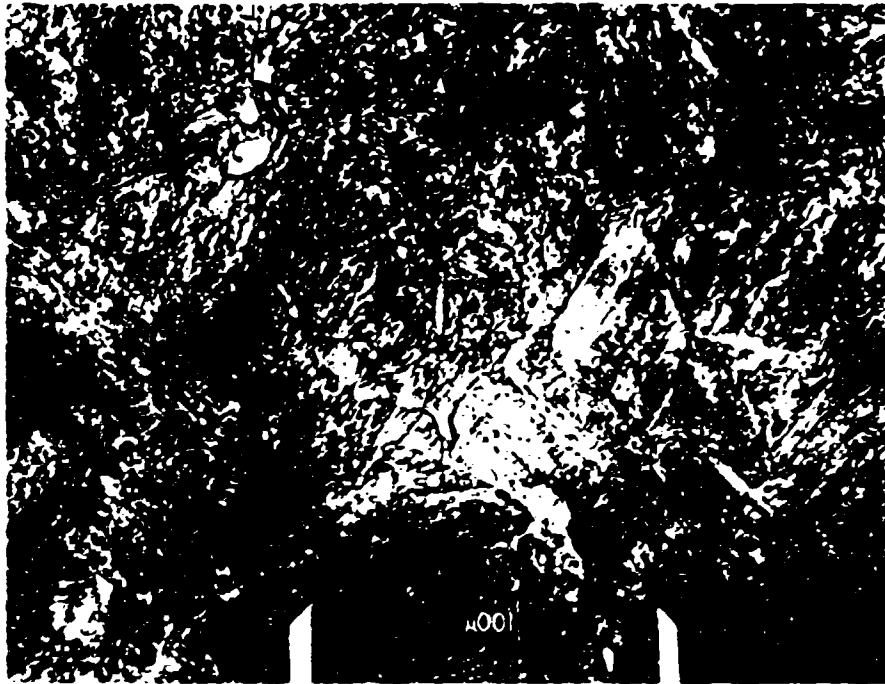
Figure 63 Microstructure of 17-4 PH, H 1100 Heat Treat Condition. View
is into the plane parallel to S in specimen T-L, Figure 10.
The structure has well defined grain boundaries due to in-
creased carbon precipitation in H 1100 versus H 1050. The
martensitic matrix is a complex lamellar structure with copper-
rich particles appearing throughout. The delta ferrite
stringers are in the rolling direction. (Magnification: 500x,
Etch: Mixed Acids).

Figure 64 Microstructure of 15-5 PH, H 1100 Heat Treat Condition. View
is into the plane parallel to S in specimen T-L, Figure 10.
The structure has well defined grain boundaries due to in-
creased carbon precipitation in H 1100 versus H 1050. The
matrix tends to elongate the copper-rich particles. Delta
ferrite is virtually non-existent. (Magnification: 500x,
Etch: Mixed Acids).

153

scopic and not influencing the measurable hardness of the alloys.

The most observable variance between 17-4 PH and 15-5 PH micro-structures for both heat treat conditions in all directions is the presence of delta ferrite stringers in 17-4 PH and not in 15-5 PH. Depending on the thickness, the stringers appear as either a white or light gray extended pool in micrographs of Figures 53, 55, 57, 59, 61 and 63.

At first glance, most inclusions are thought to be incoherent with the matrix, having mismatch in elastic modulus and becoming active stress raisers. In general terms, inclusions do not have to be detri-mental. For example, inclusions, such as those in free-cutting steels containing sulphur and phosphorus for increased machinability, do not deteriorate fatigue properties (Forsyth, 1969). However, silicate, nitride, hydride, and lead inclusions can be detrimental to fatigue-crack growth.

As previously mentioned in section 6.3.4, the effect of the delta ferrite inclusions in 17-4 PH appears to be beneficial over a limited stress intensity range. Their coherency with the matrix may be adequate enough to produce a retardation in fatigue-crack growth rates as the crack moves through the microstructure. Additionally, the delta ferrite is coherent within itself and may transfer strains to more matrix by virtue of its surface area, consequently inducing a stress relaxation by increased strain spreading.

In Figure 52 the 15-5 (curve B) shows an initial resistance over 17-4, (curve 10) by indicating a higher threshold value. Compared to curve 10, curve B accelerates more rapidly to 90 ksi $\sqrt{in}$ (98.9 MPa $\sqrt{m}$) then slows to lower crack growth rate than curve 10 until final fracture. A possible explanation for 17-4 (curve 10) performance may be in the presence of delta ferrite.

Monotonic hydrogen and/or chlorine may diffuse into a material under mechanical cycling (e.g. fatigue) along grain or stringer boundaries. The delta ferrite stringers having surface exposures typical of Figures 54 and 57 in a manufactured structure and Figures 55 and 58 for this through cracked specimen may perform in one of several ways. A possibility is the stringer boundaries may act to a limited extent as extra paths for atomic hydrogen entering the matrix. This may result in an earlier cracking stage, fracturing small volumes of metal quickly. However, when the applied strains increase, strain spreading through the ferrite stringers may become more effective, perhaps due to the entire volume and surface area of the stringer now being affected. In return the delta ferrite stringer tends to effect more of the matrix surpassing the hydrogen effect. The initial effect of diffusing atomic hydrogen may not be as intense along the large surface area of the ferrite stringers. Either one or a combination of both mechanisms would permit the stringer phase to fracture in a manner of microvoid coalescence or ductile rupturing. When the stress intensity increases to a high enough point (e.g. 100 ksi $\sqrt{in}$, 110 MPa $\sqrt{m}$) the martensitic matrix influences the remaining life in fatigue-crack

growth behavior.

7.2 FRACTOGRAPHIC EVALUATION

The study of fracture surfaces provides a diagnostic tool for failure investigators and those working in fracture mechanics. The haphazard appearance can provide a discernible history of the fracture plus reveal something of the basic mechanism of fatigue-crack growth.

Fine precipitates, and undissolved carbides, silicates, oxides, nitrides or other particles with a propensity toward cleavage are frequently present in large numbers in all but the purest of metals. When the matrix around these particles plastically deforms, the particles often cleave or pullout of the matrix generating new surfaces. These surfaces nucleate microvoids that can grow. The spherical shape of the voids prohibits simple glide and forces complex slip to occur through these plastically worked surfaces of the void. As oids grow and finally impinge on each other the last material separates leaving the typical cup-cone equiaxed dimple. If these dimples coalesce in a shearing direction they are elongated in that direction and called "shear dimples". This briefly describes "microvoid coalescence" or "dimpled rupture".

In Figure 65 and Table X a graphic representation is presented for the measured positions from which the fracture surfaces were sampled. The average crack growth rates and stress intensities are shown with respect to these positions. All fracture specimens compared were tested

Figure 65 Fractographic Layout. The average crack growth rate and
average stress intensity are indicated for the locations.
Fracture sections were removed and photographed.
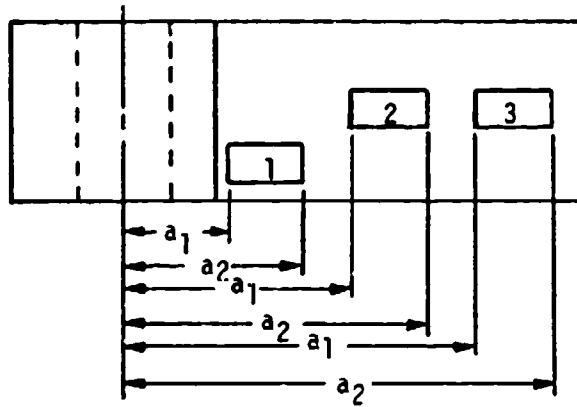
TABLE X   FRACTOGRAPHIC LAYOUT

Specimen	Section	a_1	a_2	Average Da/DN ($\times 10^{-6}$)	Average ΔK
8	1	0.516	0.922	1.4	23.0
	2	1.267	1.455	9.0	34.4
	3	1.861	2.144	Unstable	
12	1	0.571	0.892	19.0	53.4
	2	1.240	1.524	60.0	86.2
	3	1.595	1.894	Unstable	
10	1	0.570	0.675	1.4	26.4
	2	0.748	1.093	8.9	39.2
	3	1.166	1.565	68.0	78.6
H	1	0.750	0.988	13.5	35.4
	2	1.301	1.626	107.0	84.0
	3	1.900	2.175	Unstable	
N	1	0.513	0.825	15.5	51.5
	2	1.086	1.300	78.0	83.6
	3	1.456	1.746	430.0	133.2
B	1	0.523	0.931	3.6	28.8
	2	1.328	1.548	84.7	72.7
	3	1.867	2.107	Unstable	

at R = 0.05 under a 10 Hz sine wave in the H 1100 condition. Looking at Specimens 8 and H (Figures 66 and 67), a fine slip is prevalent throughout the first two fracture sections with both exhibiting river patterns or ledges thought to be signs of local ductile fracture. The ledges appear to be at an intermediate stage of growth when the fatigue crack is progressing in the "slow growth" regime. The crack appears to follow a jogged path influenced by the local microstructure while break- ing in a ductile manner (i.e. slip) between these various levels. In the fast growth regime of 15-5 PH (Figure 67, H-3) the dimples are finer and ledges tend to be subdued, indicating that in unstable frac- ture the sensitivity to microstructure is reduced. Even though micro- void coalescence or dimpled rupture does occur in both alloys the 17-4 PH (Figure 66, 8-3) does have unstable dimples on several plateaux that are divided by steps, ridges or channels indicating microstructural sensitivity under fast fracture. An explanation of 15-5 PH having a higher fatigue-crack growth rate than 17-4 PH under these conditions is believed found in the above microstructural effects on fracture.

The fracture surfaces of the alloys tested under a one minute hold-time, Specimens 12 and N (Figure 68 and 69), shows distinct ledges, rivers and troughs. Both alloys have extensive secondary cracking in the longitudinal and transverse depth directions. In Figure 68, sec- tion 12-2, intricate slip design occurs throughout the area, as the main crack path follows the microstructure intergranularly. Through the center of the picture a longitudinal sequence of dimpled rupture occurs

Figure 66   Fracture Surface of Specimen 8, 17-4 PH, H 1100 Heat Treat
             Condition, Tested under 10 Hz Sine Wave, R = 0.05 in
             Ambient Air. Location of fractographs to original fracture
             surface with corresponding DaDN and ΔK are in Table X. The
             arrow on micron marker indicates crack growth direction.

             8-1) This view shows a slip design moving intergranularly
                  with modest cracking in the longitudinal depth direc-
                  tion. (Magnification: 1000x).

             8-2) Slip formation is recognizable with some mixed modes
                  of quasi-cleavage appearing. The long cracks in the
                  direction of cracking appear to occur at the bottom
                  of trenches. (Magnification: 750x).

             8-3) Dimpled rupture in unstable fracture regions with in-
                  tense pullouts around what appear to be secondary
                  particles. Well defined terraces or planes are seen
                  as the crack moves through the microstructure.
                  (Magnification: 750x).
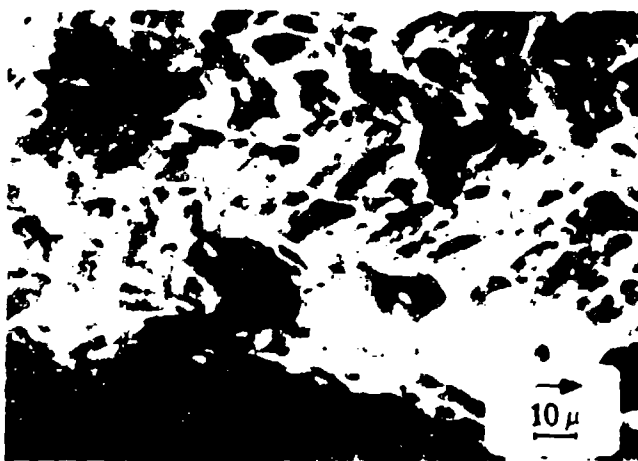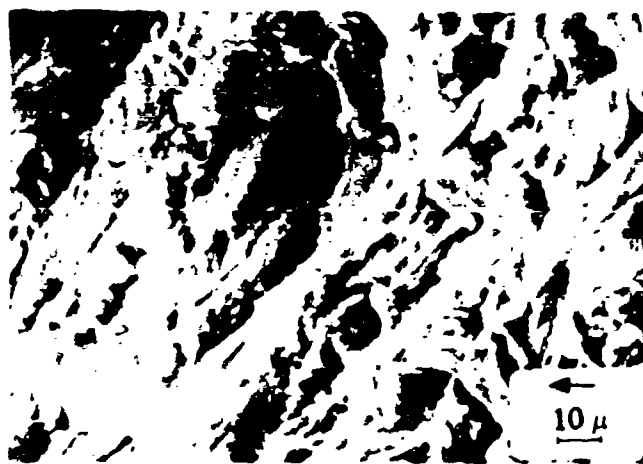
Figure 67 Fracture Surface of Specimen H, 15-5 PH, H 1100 Heat Treat
Condition, Tested under 10 Hz Sine Wave, R = 0.05 in
Ambient Air. Location of fractographs to original fracture
surface with corresponding DaDN and ΔK are in Table X. The
arrow on micron maker indicates crack growth direction.

H-1) The view represents the typical intergranular slipped
surfaces with extensive longitudinal and transverse
depth cracks, more than in Specimen 8. (Magnifi-
cation: 750x).

H-2) Looking into the depth of suspect intergranular
cracking, slip ridges can be observed at many levels
with these transverse depth cracks. (Magnification:
750x).

H-3) Final unstable fracture exhibits more dimpled rupture
with noticeable pullouts in conjunction with more
secondary depth cracking than in Specimen 8. (Magni-
fication: 750x).
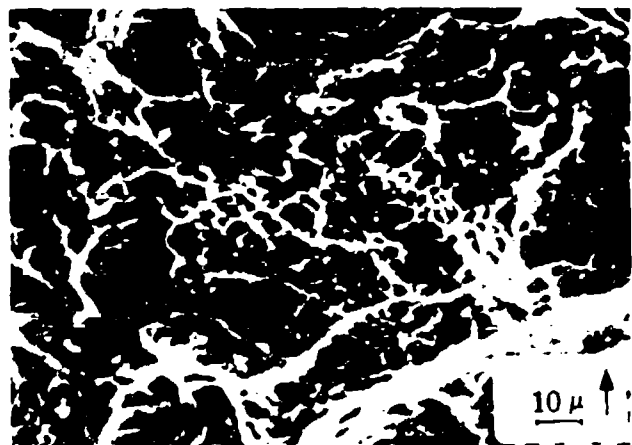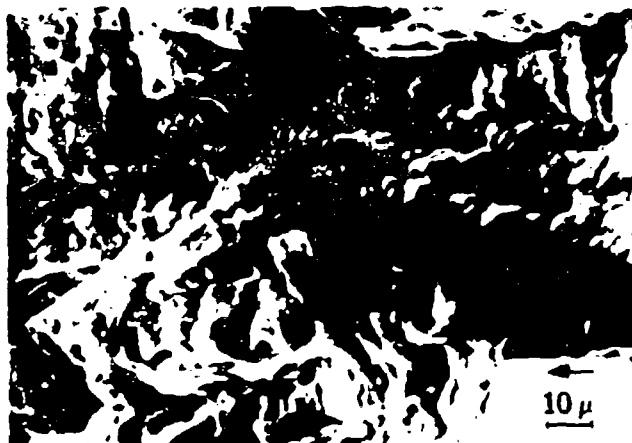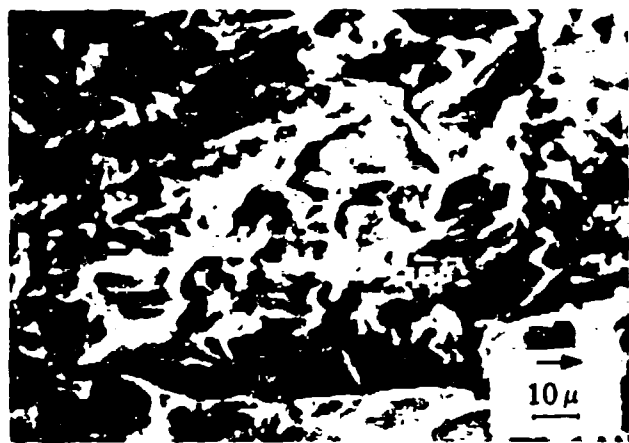
Figure 68   Fracture Surface of Specimen 12, 17-4 PH, H 1100 Heat Treat
             Condition, Tested under a One Minute Hold-Time Trapezoidal
             Wave, R = 0.05 in Ambient Air. Location of fractographs
             to original fracture surface with corresponding DaDN and ΔK
             are in Table X. The arrow on micron marker indicates crack
             growth direction.

        12-1) Cracking appears to be more transgranular slipping
              with extensive secondary cracking in longitudinal
              and transverse depth direction. (Magnification: 750x).

        12-2) The retardation or suck-back of slip striations can be
              seen as they encounter a cluster of voids or pulled
              out stringers, believed to be delta ferrite.
              (Magnification: 750x).

        12-3) Glide planes or wavy surfaces, possibly serpentine
              glide, are visible at the center right. In the
              direction of crack growth, river patterns prevail
   with slip. (Magnification: 750x).
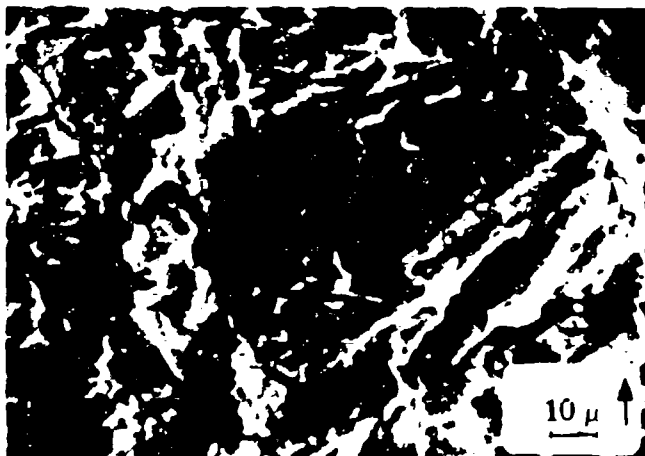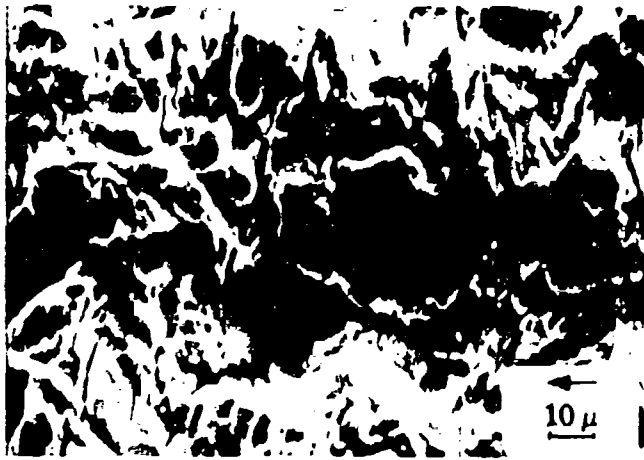
Figure 69 Fracture Surface of Specimen N, 15-5 PH, H 1100 Heat Treat
Condition, Tested under a One Minute Hold-Time Trapezoidal
Wave, R = 0.05 in Ambient Air. Location of fractographs
to original fracture surface with corresponding DaDN and ΔK
are in Table X. The arrow on micron marker indicates crack
growth direction.

N-1) Intergranular cracking, predominantly slip, with
secondary cracking and scattered pullout exists.
(Magnification: 750x).

N-2) Slipping through a region with obvious mixed mode
where cleavage is a vertical plane, concentration
of voids or pullouts is low, perhaps due to limited
delta ferrite. (Magnification: 750x).

N-3) Ductile rupture or microvoid coalescence prevail as
dimples indicative of unstable ductile fracture form
on this area of the specimen. (Magnification: 750x).

10 µ ↑

10 µ →

10 µ →
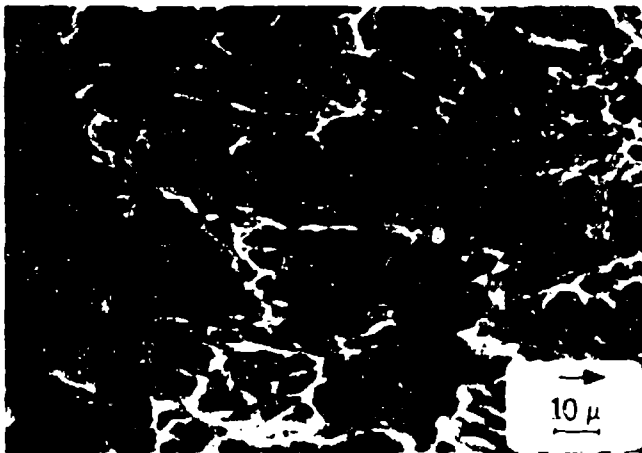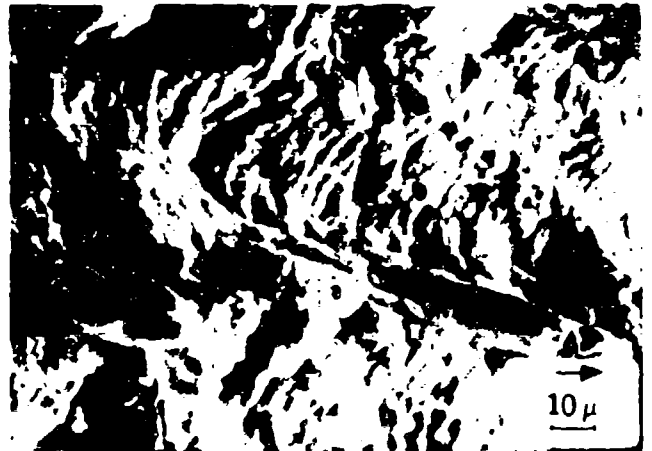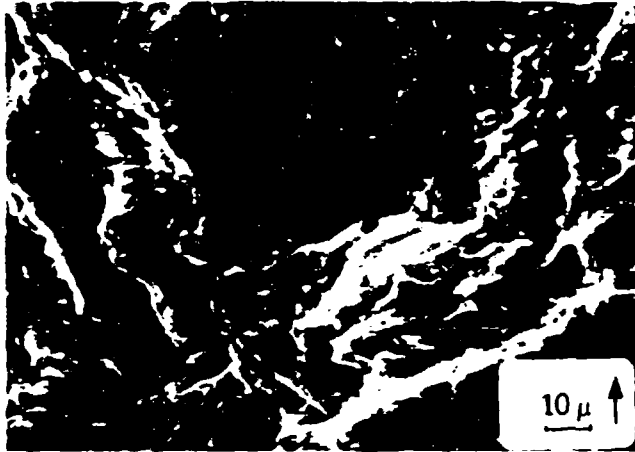
as the striations are sloped back or retarded with respect to the crack direction. This is believed to be a delta ferrite stringer rupturing. A combination of strain spreading in conjunction with the observed longitudinal dimpled rupture in 17-4 PH is believed responsible for the overall reduction of the fatigue-crack growth rate and increase in the defined threshold K_{th} as compared to 15-5 PH. Further 15-5 PH (Figure 69, N-2) exhibits mixed mode cleavage planes vertical to the slip design and crack direction.

The last sequence of fracture surfaces represent the two alloys: 17-4 PH and 15-5 PH, (Figures 70 and 71, respectively) tested under one minute hold-time in 3.5% salt water. The 17-4 PH showed an intense slip design throughout the sections. However, evident in 10-1 (Figure 70) are vertical planes or ridges rising out of the fracture surface which may be evidence of a mechanism called slip-plane initiation, persisting as part of the growth process. This mechanism labelled Stage I by Forsyth (1969) is quickly succeeded by normal or Stage II growth forming striations. Briefly stated the origin of fatigue cracks develop from slip bands extending along slip planes. The crack origin is associated with crystal slip or shear making planes oriented approximately 45° to the maximum tensile stress susceptible to a maximum shear stress. There are numerous exceptions to this idea but this mode of failure exists. Cracking of this type may be distinguished by virtually featureless fracture surfaces or surface ridges in the direction of crack growth (Forsyth, 1969). The remaining fracture sections

Fracture Surface of Specimen 10, 17-4 PH, H 1100 Heat Treat
Condition, Tested under a One Minute Hold-Time Trapezoidal
Wave, R = 0.05, in 3.5% Salt Water. Location of fractographs
to original fracture surfaces with corresponding DaDN and ΔK
are in Table X. The arrow on the micron marker indicates
crack growth direction.

10-1) Majority of surface has slipped with occasional mixed
      mode quasi-cleavage area. Depth crack runs longitudinal
      to crack growth direction. (Magnification: 750x).

10-2) High intensity of slip, very little mixed mode. Intense
      transverse depth cracks and pullouts are seen. Pullouts
      or voids tend to agglomerate in a cluster or stringer
      formation and suggest delta ferrite tearing apart in a
      ductile manner. (Magnification: 750x).

10-3) Moving to the edge of unstable fracture initiation,
      slip design if observed in the depth of a crater, most
      probably an intergranular, while accompanied by
      secondary cracking and some minor mixed mode. (Magnifi-
      cation: 750x).
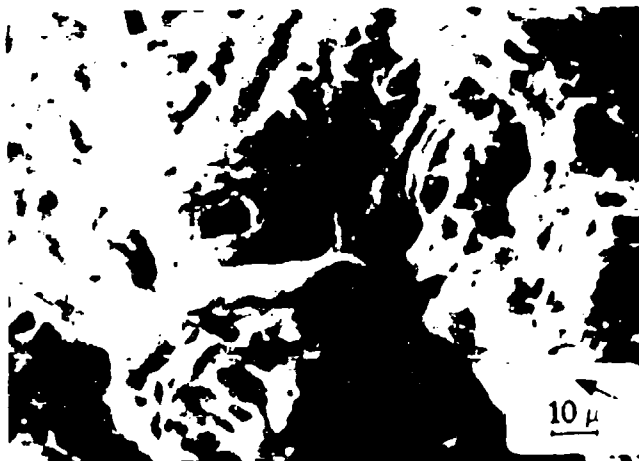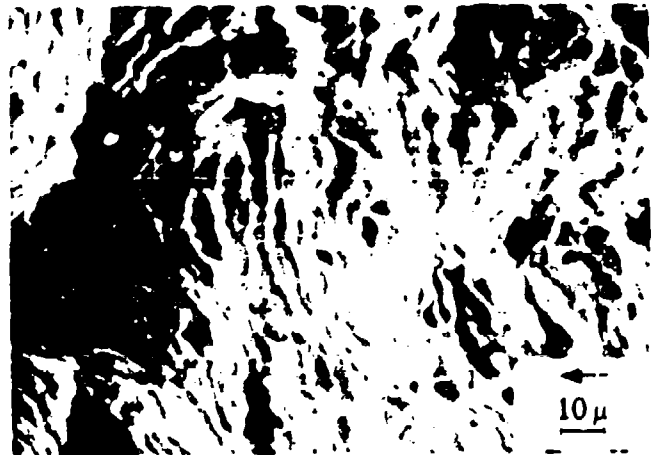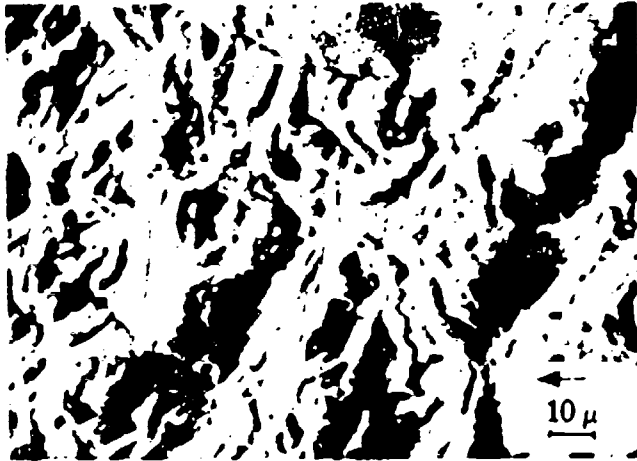
Figure 71   Fracture Surface of Specimen B, 15-5 PH, H 1100 Heat Treat
Condition, Tested under a One Minute Hold-Time Trapezoidal
Wave, R = 0.05, in 3.5% Salt Water. Location of fractographs
to original fracture surfaces with corresponding DaDN and ΔK
are in Table X. The arrow on the micron marker indicates
crack growth direction.

B-1) The cracking exhibits transgranular cleavage with
associate longitudinal and transverse depth crack
in a mixed field of slip. (Magnification: 750x).

B-2) A typical cleavage burst surrounded by quasi-
cleavage and slip design at various depth levels.
The center and the outside edges of the burst appear
to be pullouts or voided points from which the burst
may have occurred. (Magnification: 750x).

B-3) Mixed mode fracture is near-vertical cleaving of the
microstructure, then slipping and horizontal cleaving.
Notice pullouts or voids on the rounded slope in con-
junction with well defined striation design. (Magnifi-
cation: 750x).
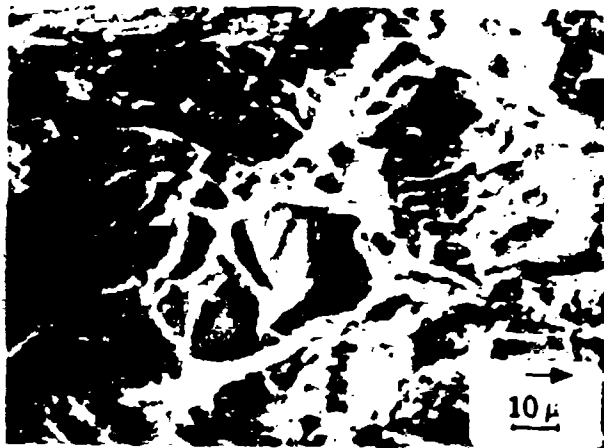
of Figure 70, 10-2 and 10-3, show slipping in conjunction with sequential longitudinal dimples rupture. Exploring an intergranular boundary in 10-3, slip striations can be observed with secondary cracking and noticeable pullout or void coalescence. Specimen B, the 15-5 PH counterpart to 17-4 PH, Specimen 10 clearly illustrates why its fatigue-crack growth mode may be treacherous to a design. The material with delta ferrite absent is affected by the 3.5% salt water environment. At an early stage transgranular cleavage fracture is evident as the applied stress intensity increases with crack extension, cleavage bursting occurs from a central nucleus. This nucleus or initiation site for this type of fracture can be due to a cleaved particle resulting in a void or any one of a number of void generators; even a "fish eye" characteristic of hydrogen embrittlement. In the last section B-3, vertical cleavage, a slipped or striated plateau and another cleaved wall is indicative of a mechanism that deteriorates grain boundary cohesion. By comparing the collection of fractures it is concluded that 15-5 PH is more affected by salt water and hold-time than 17-4 PH. Also, when the crack growth regimes enter a fast growth mode 15-5 PH relies on its inherent fracture toughness to elusively suggest a benefit. The transition point to final fracture being an area where a structures useful life is almost ended.

CHAPTER 8

CONCLUSIONS AND SUMMARY

8.1 CONCLUSIONS

As concluded from the results of this work and the data herein
the following observations are presented.

- From this study in accordance with the proposed
  hypothesis it is determined that microstructural
  control can be used to influence an alloy's re-
  sponse in fatigue-crack growth.

- The results determined that slight microstructural
  alterations developed through heat treatments
  responded differently for fatigue-crack growth
  testing conditions such as R-ratio, wave form
  and environment.

- A combination of salt water, hold-time and residual
  stress caused the microstructures to respond
  differently than a 10 Hz sine wave, ambient air
  fatigue-crack growth test.

- This study has accomplished the identification of
  a unique hold-time behavior in 17-4 PH not seen
  nor even suspect before in fatigue-crack growth
  response of a martensitic steel or stainless
  steel.

- A contemporary Weibull-type mathematical method
  has been demonstrated to be applicable to the
  quantification of microstructural effects on fa-
  tigue-crack growth.

167

. The data are representable through four para-
meters of a functional curve, not a straight
line, that precisely applies mathematical boundary
conditions to the physics of the fatigue-crack
growth process.

Detailed methods for application of mathematical physics to fatigue -

crack growth are:

. Exponential crack propagation relations have been
introduced that meet three key criteria of
acceptability.

1. As ΔK approaches an upper limit, K_b, the crack
growth rate increases asymptotically.

2. As ΔK approaches a lower threshold, K_{th}, the
crack growth rate diminishes to zero.

3. Slow and fast crack growth can be distinguished.

. Mathematical derived values of stress intensity
threshold, K_{th}, can be used to predict the size of
the largest flaw which will not grow for a given
loading condition.

. The threshold stress intensity, K_{th}, determined by e
and a calculated characteristic value, v, the upper
limit of slow crack growth, can be used as key
analytical initial conditions in planning in-service
inspection schedules.

. The included graphical representations of fatigue
and fracture mechanics diagrams provide a means to
consider load shedding, maintenance and finite
life design for field operational applications.

As a result of this work, it is believed from the range of variables

covered by the ten thousand data points generated herein, that

traditional fatigue-crack growth testing when combined with con-

temporary Weibull type fitting relations can be used to predict component life.

8.2 SUMMARY

The background work for the study included preparation of three interactive Conversational Programming System routines, as follows:

Routine	Application
POLFIT	Conventional compact specimen compliance calibration data reduction
WOLFIT and WYBULL	Derivation of Type-A, -B or -C exponential curve fitting relations for either ...iance calibration or fatigue-crack propagation data reduction
LIFE	Prediction of crack length as a function of number of load cycles for prescribed load history.

The utility of the routines has been demonstrated throughout chapter 5 with the aid of examples based on mill annealed Ti-6Al-6V-2Sn, high oxygen alloy fracture mechanics test results.

The study technique was developed at the Lockheed Fatigue and Fracture Mechanics Laboratory, Rye Canyon Advanced Design and Research Laboratories during the period 1969-1976 and has been expanded at the University of Missouri-Columbia from 1974 to the current data. This study is the most extensive use of the technique specifically with regard to discriminating microstructural effects through physically relevant curves in lieu of straight lines. The

combined support of metallography and fractography in fatigue-crack propagation testing has strengthened the analytical methods relevancy and interpretation. Steel producers and specification writers have empirically manipulated microstructural chemistries of these two alloys to increase weldability of 17-4 PH with the presence of delta ferrite, then to increase short transverse toughness of 15-5 PH by limiting delta ferrite. These present resultant alloys when tested for fatigue-crack growth rates under variables that relate to a vehicle's operation profile can distinctly alter fatigue-crack growth behavior. Increases in fatigue-crack growth rates were experienced with increasing R-ratio from R = 0.05 to R = 0.67. This trend prevailed throughout the wave forms and heat treatments considered.

The wave form influenced a crack growth response substantially by retarding the crack growth through a proposed microstructural mechanism of strain-induced stress relaxation. Adding the salt water environment to this wave form effect reduced the threshold on 17-4 PH but not on 15-5 PH. However, the fatigue-crack growth rates on 15-5 PH accelerated more rapidly than the 17-4 PH until a stress intensity of approximately 90 ksi $\sqrt{in}$ (98.9 MPa $\sqrt{m}$) was developed.

An additional factor worthy of note surfaced during metallographic and fractographic analysis. This is, in alloys (e.g. 17-4 PH and 15-5 PH) that derive strength from precipitated particles blocking dislocation motion during fatigue any application of heat after fatiguing will cause increased precipitation and diffusion in the fatigued material due to the stored energy from previous dislo-

cation motion (Forsyth, 1969). Due to these mechanisms, if a structure is cracked, it is believed to be difficult, if not impossible, to weld repair for satisfactory long term operation. The heat in repair welding will increase the size of the particles for a zone of material leading to an incoherent particle size permitting more voids to crack within the microstructure. If the structural component could be restrained for complete reheat treatment, satisfactory repair may be possible.

In summarizing, compliance calibration and fatigue-crack propagation variables are expressible in terms of fitting elements of a distinct class of exponential curve fitting relations.

Calculation of threshold stress intensity range values, distinction between slow and fast growth by means of risk function analysis, and life prediction by integration of crack propagation curve fitting relations have been demonstrated in chapter 5. Except for the last integration all considered analytic methods have been applied to the data per the test matrix in Table IX. Four parameters k, e, v and K_b have been used to describe the test data and microstructural responses.

The microstructure controls final operational material response. If a material does not experience a simulated or actual operational profile of a structure, the resulting test data can not be employed to describe the operational life of the structure.

Microstructural sensitivity exists in advanced high performance structural materials and varies in degree depending on the operational conditions of interest. This uncertainty of materials' re-

sponse in fatigue-crack growth behavior dictates a clear need for a reality that reflects simulated or operational profiles in testing and in data representation. Comprehending the need for actual or testing under the structure's conditions of interest will culminate in a worthwhile and satisfactory result of structural integrity. Ignorance of this need will end in devastation. There is a permanence to this type of consequence that ignored the responsibility in science and engineering. This can best be expressed by reflecting on Voltaire's words: "To the living, one owes consideration; to the dead, only the truth".

REFERENCES

1. Armco Research Center "Technical Bulletin on 17-4PH," Armco
    Steel Corporation, Middletown, Ohio, 1969.

2. ASTM. A Guide for Fatigue Testing and the Statistical Analysis
    of Fatigue Data. ASTM STP 91-A, Philadelphia: ASTM, 1963.

3. ASTM Task Group E24.04.01. Report on A Digest of a Tentative
    Standard Method of Test for Fatigue Crack Growth of Metallic
    Materials, Philadelphia: ASTM, July 1975.

4. ASTM E399-72. "Plane Strain Fracture Toughness Test of Metallic
    Materials," Part 31, ASTM Standards, 1972, pp. 955-971.

5. Bauman, W.D., Personal Communication, 1974.

6. Bowie, G.E., Personal Communication, 1974-1976.

7. _____, Class Notes, Jan. 1975.

8. _____, Class Notes, July 1975.

9. _____, Pettit, D.E., Ryder, J.T., and Krupp, W.E., "NDI Life
    Analysis Interface," Lockheed-California Co., Rye Canyon Re-
    search Laboratory, Report LR 27013, Sept. 1974.

10. Brown, W.F., Jr. Stress-Corrosion Cracking in High Strength
    Steels and in Titanium and Aluminum Alloys. Naval Research
    Laboratory, Washington, D.C., 1972.

11. Brown, W.F., Jr. and Srawley, J.E., Plane Strain Crack Toughness
    Testing of High Strength Metallic Materials, ASTM STP 410, ASTM
    1966.

12. Coffin, L.F., Jr., "Fatigue," Annual Review of Materials Science,
    Vol. 2, 1972, pp. 313-348.

13. _____, "The Deformation and Fracture of a Ductile Metal Under
    Superimposed Cyclic and Monotonic Strain," ASTM STP 467, ASTM,
    Philadelphia, Pa., 1970, pp. 53-76.

14. Crooker, T.W., "The Role of Fracture Toughness in Low-Cycle Fa-
    tigue Crack Propagation for High-Strength Alloys," Engineering
    Fracture Mechanics, Vol. 5, 1973, pp. 35-43.

15. _____, "Basic Concepts for Design Against Structural Failure by Fatigue Crack Propagation," Naval Research Lab., Washington, D.C., Report 7347, Jan. 1972.

16. Dieter, G.R., Jr., Mechanical Metallurgy, New York: McGraw-Hill Book Company, 1961.

17. Feltner, C.E. and Beardmore, P., "Strengthening Mechanisms in Fatigue," ASTM STP 467, ASTM, Philadelphia, Pa., 1970, pp. 77-108.

18. _____, and Landgraf, R.W., "Selecting Materials to Resist Low-Cycle Fatigue," Paper No. 69-DE-59, ASME, 1969.

19. Forman, R.G., Kearney, V.E. and Engle, R.M., "Numerical Analysis of Crack Propagation in Cyclic Loaded Structures," J. Basic Engineering, Vol. 89, 1967, pp. 459-464.

20. Forsyth, P.J.E., Physical Basis of Metal Fatigue, Blackie and Son Limited, London, 1969.

2. Fracture Toughness Testing and Its Applications, ASTM STP 381, ASTM, 1965.

22. Freudenthal, A.M., "Fatigue and Fracture Mechanics," Engineering Fracture Mechanics, Vol. 5, pp. 403-414, 1973.

23. _____, Class Notes, December 1973.

24. _____, "Safety, Reliability and Structural Design," Journal of Proceedings of American Society of Civil Engineers, March 1969.

25. _____, "Fatigue," Encyclopedia of Physics Vol. VI, Ed., S. Flugge, 1958, pp. 591-613.

26. _____, and Gumbel, E.J., "Physical and Statistical Aspects of Fatigue," Applied Mechanics Vol. IV. New York: Academic Press, 1956.

27. Griffith, A.A., "Phenomena of Rupture and Flow in Solids," Philosophical Transactions of the Royal Society (London), series A 221, 1921, pp. 163-198.

28. Grosskreutz, J.C., "Strengthening and Fracture in Fatigue," Metallurgical Transactions, Vol. 3, May 1972, pp. 1255-1261.

29. Gumbel, E.J., Statistics of Extremes, Columbia University Press, New York, 1958, pp. 272-279.

30. Harrigan, M., Personal Communication, Aug. 1973.

31. _____, Sommer, A. and Kaplan, M., "The Effects of Chemistry and Heat Treatment on the Fracture Mechanics Properties of Ti-6Al-4V Alloy," North American Rockwell, Report NA-72-235, March 1972.

32. Hoeppner, D.W., "Corrosion Fatigue Consideration in Materials Selections and Engineering Design," Corrosion Fatigue, NACE-2, 1972, p. 3.

33. _____, "Effect of Grain Size on Fatigue Crack Propagation in Copper," ASTM STP 415, ASTM, Philadelphia, Pa., 1967, pp. 486-504.

34. _____, Class Notes, Fall 1975.

35. _____, Personal Communication, 1973-1976.

36. _____, A Fractographic Analysis of Flaw Growth in A High High Strength Titanium Alloy, University of Missouri-Columbia, Aug. 1975.

37. _____, Proposed Program on the Effect of Cyclic Load Frequency Chemical Environment, Load Wave Form, and Nuclear Irradiation on the Fatigue Crack Growth Behavior of Pressure Vessel Steels, University of Missouri-Columbia, Jan. 1975.

38. _____, and Krupp, W.E., "Prediction of Component Life by Application of Fatigue Crack Growth Knowledge," Engineering Fracture Mechanics, Vol. 6, No. 1, March 1974, pp. 47-70.

39. _____, Pettit, D.E., Fedderson, C.E. and Hyle, W.S., "Determination of Flaw Growth Characteristics of Ti-6Al-4V Sheet in the Solution-Treated and Aged Condition," NASA, Contract NAS 9-6969, Battelle Memorial Institute, Columbus, Ohio, Jan. 1968.

40. Imoff, E.J. and Barsom, J.M., "Fatigue and Corrosion Fatigue of 4340 Steel at Various Yield Strengths," U.S. Steel, Monroeville Research Lab., Aug. 1972.

41. Inglis, C.E., Stresses in a Plate Due to the Presence of Cracks and Sharp Corners, Transactions of the Institution of Naval Architects (London) 60, 1913, pp. 219-230.

42. Irwin, G.R., Fracture Dynamics, Fracturing of Metals, American Society for Metals, Cleveland, Ohio, 1948, pp. 147-166.

43. ____, "Fracture", Encyclopedia of Physics Vol. VI, Ed., S. Flugge, 1958, pp. 551 590.

44. ____, "The Crack Extension Force for A Crack at A Free Surface Boundary " Report No. 5120, Naval Research Lab., 1958.

45. ____, Fracture Mode Transition for a Crack Traversing a Plate, Journal of Basic Engineering, Transactions ASME 82, 1960, pp. 417-423.

46. ____, Kies, J.A. and Smith, H.L., "Fracture Strengths Relative to Onset and Arrest of Crack Propagation," Proc. ASTM 58, 1958, pp. 640-660.

47. ____, and McCl ntock, F.A., "Plasticity Modifications to Crack Stress Analysis," ASTM STP 381, 1970.

48. Jaske, C.E., Fedderson, C.E., Davis, K.B. and Rice, R.C., Analysis of Fatigue, Fatigue Crack Propagation and Fracture Data, NASA CR-132332, Nov. 1973.

49. Judy, Jr., R.W., "Review of Principles for Assurance of Structural Integrity," Naval Research Laboratory, Washington, D.C., Report 2501, Sept. 1972.

50. Krempl, E. and Wundt, B.M., "Hold-Time Effects in High-Temperature Low-Cycle Fatigue," ASTM STP 489, 1971.

51. Kondas, K.R., Crooker, T.W. and Gilmore, C.M., "Cyclic Crack Growth and Fracture Resistance of Ti-6Al-6V-2Sn as Influenced by Recrystallization Anneal and Interstitial Oxygen Content," Engineering Fracture Mechanics, Vol. 7, 1975, pp. 641-647.

52. Krupp, W.E. and Hoeppner, D.W., "The Relationship Between Microstructure and Sustained Load Crack Growth," presented at 1973 ASM Westec Conference, Los Angeles, California, March 13, 1973 to be published.

53. Laird, C., "The Influence of Metallurgical Structure on the Mechanisms of Fatigue Crack Propagation," ASTM STP 415, ASTM, Philadelphia, Pa., 1967, pp. 131-165.

54. Landgraf, R.W., "The Resistance of Metals to Cyclic Deformation," ASTM STP 467, ASTM, Philadelphia, Pa., 1970, pp. 3-34.

55. Manson, S.S., "Fatigue: A Complex Subject - Some Simple Approximations," Exp. Mech., Vol. 5, No. 7, 1965, pp. 193-225.

56. Miner, M.A., Cumulative Damage in Fatigue, Journal of Applied Mechanics 12, Sept. 1945.

57. Morrow, J., "Cyclic Plastic Strain Energy and Fatigue of Metals," ASTM STP 378, ASTM, Philadelphia, Pa., 1965, p. 45.

58. Mott, N.F., "Fracture of Metals: Some Theoretical Considerations," Engineering 165, 1948.

59. Newman, Jr., J.C., "Stress Analysis of the Compact Specimen Including the Effects of Pin Loading," ASTM STP 560, 1974, pp. 105-121.

60. Orowan, E., Fundamentals of Brittle Behavior in Metals, Fatigue and Fracture of Metals, 1952, pp. 139-167.

61. Paris, .C. and Sih, G.C., "Stress Analysis of Cracks," Fracture Toughness Testing and Its Applications, ASTM STP 381, 1965, pp. 30-81.

62. Pettit, D., Krupp, W., Ryder, Jr. and Hoeppner, D., "Investigation of the Effects of Stress and Chemical Environments on the Prediction of Fracture in Aircraft Structural Materials," Lockheed, California, Report LR-26026, July 1973.

63. Popp, H.G. and Coles, A., "Subcritical Crack Growth Criteria for Inconel 718 at Elevated Temperatures," Proceedings of Air Force Conference on Fatigue and Fracture of Aircraft Structures and Materials, Miami Beach, Fla., Dec. 15-18, 1969.

64. Rice, J.R., "Mechanics of Crack Tip Deformation and Extension by Fatigue," ASTM STP 415, 1967, p. 247.

65. Ryder, J.T., Pettit, D.E., Krupp, W.E. and Hoeppner, D.W., "Evaluation of Mechanical Property Characteristics of IMI 685," Lockheed-California Co., Rye Canyon Research Laboratory, October 1973.

66. Sih, G., Paris, P. and Erdogan, F., "Crack Tip Stress Intensity Factors for Plane Extension and Plate Bending Problems," _Trans. ASME, J. of Applied Mechanics_, 1962.

67. Sih, G. and Paris, P.C., _The Stress Distribution and Intensity Factors for A Crack Tip in An Anisotropic Plate Subjected to Extension_, Lehigh Univ., Inst. of Research Report, Oct. 1961.

68. Sneddon, I.N., "The Distribution of Stress in the Neighborhood of A Crack in An Elastic Solid," _Proc. Royal Soc. London, Vol. A-187_, 1946.

69. Sullivan, A.M., "Crack Length Determination for the Compact Tension Specimen Using a Crack-Opening Displacement Calibration," NRL Report, June 1974.

70. Swedlow, J.L., Further Comment on the Association between Crack Opening and G_I, _International Journal of Fracture Mechanics 3_, 1967.

71. _____, Cruse, T.A. and Halpin, J.C., "Proceedings of the Colloquim on Structural Reliability," Carnegie-Mellon University, October 1973.

72. Timoshenko, S. and Goodier, J.N., _Theory of Elasticity_, 2nd ed., McGraw-Hill Book Company, 1951, pp. 197-204.

73. Walker, E.K., "The Effect of Stress Ratio During Crack Propagation and Fatigue for 2024-T3 and 7075-T6 Aluminum," _Effects of Environment and Complex Load History on Fatigue Life_, ASTM, STP 462, 1970, pp. 1-14.

74. Wessel, E.T., "State-of-the-Art of the WOL Specimen for K_{Ic} Fracture Toughness Testing," _Engineering Fracture Mechanics_, Vol. 1, 1968, pp. 77-101.

75. Williams, M.L., "On the Stress Distribution at the Base of a Stationary Crack," _Journal of Applied Mechanics 24_, 1957, pp. 109-114.

Appendix

Appendix 1

DELTA K, MPa√m

da/dN, in./cycle

da/dN, mm/cycle

DELTA K, ksi√in.

17-4PH
H1050
R = 0.05
f = 10 Hz.
Sine Wave
Ambient Air

DELTA K, MPa√m̅

DELTA K, ksi√in̅.

da/dN, in./cycle

da/dN, mm/cycle

17-4PH
H1050
R=0.05
One Minute Hold
Ambient Air

DELTA K, MPa√m

da/dN, in./cycle

da/dN, mm/cycle

17-4PH
H1050
R = 0.67
f = 10 Hz.
Sine Wave
Ambient Air

DELTA K, ksi√in.

DELTA K, MPa√m

DELTA K, ksi√in.

da/dN, in./cycle

da/dN, mm/cycle

17-4PH
H1050
R=0.67
One Minute Hold
Ambient Air

DELTA K, MPa√m

DELTA K, ksi√in.

17-4PH
H1100
R = 0.05
f = 10 Hz.
Sine Wave
Ambient Air

DELTA K, MPa√m

17-4PH
H1100
R : 0.67
f = 10 Hz.
Sine Wave
Ambient Air

DELTA K, ksi√in.

DELTA K, MPa√m

DELTA K, ksi√in.

da/dN, in./cycle

da/dN, mm/cycle

17-4PH
H1100
R=0.05
One Minute Hold
Ambient Air

DELTA K, MPa√m

da/dN, in./cycle

da/dN, mm/cycle

DELTA K, ksi√in.

15 - 5PH
H1100
R = 0.05
One Minute Hold
Salt Water

DELTA K, MPa√m

da/dN, in./cycle

da/dN, mm/cycle

DELTA K, ksi√in.

15-SPH
H1050
R=0.67
One Minute Hold
Ambient Air

DELTA K, MPa√m

da/dN, in./cycle

da/dN, mm/cycle

DELTA K, ksi√in.

15-5 PH
H1100
R = 0.05
f = 10 Hz
Sine Wave
Ambient Al

DELTA K, MPa√m

da/dN, in./cycle

da/dN, mm/cycle

15 - 5PH
H1100
R = 0.67
One Minute Hold
Salt Water

DELTA K, ksi√in.

DELTA K, MPa√m

da/dN, in./cycle

da/dN, mm/cycle

15 - SPH
H1100
R=0.05
One Minute Hold
Ambient Air

DELTA K, ksi√in.

DELTA K, MPa√m

da/dN, in./cycle

da/dN, mm/cycle

DELTA K, ksi√in.

15-5PH
H1050
R • 0.05
f • 10 Hz.
Sine Wave
Ambient Air

Appendix 2

Fatigue-Crack Growth Reduced Data

17-4 PH
  H 1050
  R = 0.05
  f = 10 Hz.
  Sine Wave
  Ambient Air

AVA	DN	Da/DN	ΔK	P
0.0037	2000	1.85	17.321	5.00
0.0014	2000	0.70	17.332	5.00
0.0037	2000	1.85	17.361	5.00
0.0020	2000	1.00	17.376	5.00
0.0025	2000	1.25	17.396	5.00
0.0011	2000	0.55	17.405	5.00
0.0027	2000	1.35	17.427	5.00
0.0032	2000	1.60	17.453	5.00
0.0061	2000	3.05	17.505	5.00
0.0129	2000	6.45	17.619	5.00
0.0059	2000	2.95	17.673	5.00
0.0075	2000	3.75	17.745	5.00
0.0243	26000	0.93	17.993	5.00
0.0047	4000	1.18	18.043	5.00
0.0061	4000	1.52	18.110	5.00
0.0064	4000	1.60	18.182	5.00
0.0037	4000	0.93	18.225	5.00
0.0058	4000	1.45	18.292	5.00
0.0137	4000	3.42	18.457	5.00
0.0051	4000	1.28	18.520	5.00
0.0109	4000	2.73	18.658	5.00
0.0128	4000	3.20	18.826	5.00
0.0044	4000	1.10	18.884	5.00
0.0157	4000	3.92	19.100	5.00
0.0090	4000	2.25	19.228	5.00
0.0098	4000	2.45	19.369	5.00
0.0109	4000	2.73	19.531	5.00
0.0143	4000	3.57	19.748	5.00
0.0132	4000	3.30	19.953	5.00
0.0120	4000	3.00	20.145	5.00
0.0109	4000	2.72	20.322	5.00
0.0080	4000	2.00	20.454	5.00
0.0153	4000	3.82	20.712	5.00
0.0124	4000	3.10	20.925	5.00

con't

0.0118	4000	2.95	21.131	5.00
0.0116	4000	2.90	21.337	5.00
0.0184	4000	4.60	21.670	5.00
0.0133	4000	3.32	21.915	5.00
0.0127	4000	3.18	22.153	5.00
0.0167	4000	4.18	22.471	5.00
0.0172	4000	4.30	22.804	5.00
0.0138	4000	3.45	23.076	5.00
0.0230	4000	5.75	23.538	5.00
0.0140	4000	3.50	23.824	5.00
0.0178	4000	4.45	24.194	5.00
0.0186	4000	4.65	24.587	5.00
0.0204	4000	5.10	25.027	5.00
0.0243	4000	6.08	25.565	5.00
0.0235	4000	5.87	26.098	5.00
0.0208	4000	5.20	26.583	5.00
0.0287	4000	7.17	27.273	5.00
0.0242	4000	6.05	27.877	5.00
0.0281	4000	7.03	28.606	5.00
0.0293	4000	7.32	29.404	5.00
0.0327	4000	8.17	30.347	5.00
0.0378	4000	9.45	31.517	5.00
0.0452	4000	11.30	33.051	5.00
0.0399	4000	9.98	34.555	5.00
0.0536	4000	13.40	36.845	5.00
0.1200	4000	30.00	43.475	5.00
0.0346	4000	8.65	45.886	5.00
0.1468	4000	36.70	59.616	5.00
0.3741	3860	96.92	139.163	5.00

Fatigue-Crack Growth Reduced Data

17-4 PH
  H 1050
  R = 0.05
  One Minute Hold-Time
  Ambient Air

AVA	DN	Da/DN	ΔK	P
0.0751	761	98.69	24.386	7.00
0.0011	10	110.00	24.399	7.00
0.0017	10	170.00	24.418	7.00
0.0005	10	50.00	24.424	7.00
0.0009	150	6.00	31.416	9.00
0.0008	100	8.00	31.428	9.00
0.0016	290	5.52	41.936	12.00
0.0005	30	16.67	48.937	14.00
0.0007	10	70.00	48.953	14.00
0.0008	10	79.99	48.972	14.00
0.0035	40	87.50	49.056	14.00
0.0034	20	170.00	49.139	14.00
0.0026	150	17.33	49.204	14.00
0.0002	270	0.74	49.209	14.00
0.0003	10	30.00	49.216	14.00
0.0009	10	89.99	35.171	10.00
0.0016	190	8.42	35.199	10.00
0.0032	420	7.62	42.309	12.00
0.0013	60	21.67	45.866	13.00
0.0007	120	5.83	45.883	13.00
0.0016	60	26.67	45.922	13.00
0.0002	120	1.67	45.926	13.00
0.0007	60	11.67	45.943	13.00
0.0014	120	11.67	45.978	13.00
0.0002	60	3.33	45.982	13.00
0.0020	140	14.29	46.032	13.00
0.0018	120	15.00	46.076	13.00
0.0010	180	5.56	46.101	13.00
0.0008	120	6.67	46.121	13.00
0.0010	120	8.33	46.147	13.00
0.0012	270	4.44	46.177	13.00
0.0010	180	5.56	46.202	13.00
0.0008	60	13.33	46.223	13.00
0.0002	70	2.86	46.228	13.00

con't

0.0042	1010	4.16	46.336	13.00
0.0019	140	13.57	46.386	13.00
0.0003	240	1.25	46.394	13.00
0.0003	120	2.50	46.402	13.00
0.0001	120	0.83	46.404	13.00
0.0036	220	16.36	46.500	13.00
0.0008	120	6.67	46.521	13.00
0.0007	200	3.50	53.700	15.00
0.0013	550	2.36	53.740	15.00
0.0039	60	65.00	53.863	15.00
0.0002	150	1.33	50.278	14.00
0.0007	30	23.33	50.299	14.00
0.0007	130	5.38	50.320	14.00
0.0022	230	9.57	50.385	14.00
0.0014	310	4.52	50.427	14.00
0.0009	160	5.63	50.454	14.00
0.0044	650	6.77	50.589	14.00
0.0087	470	18.51	50.860	14.00
0.0023	350	6.57	50.933	14.00
0.0085	610	13.61	51.202	14.00
0.0038	280	13.57	51.328	14.00
0.0051	250	20.40	51.498	14.00
0.0007	60	11.67	51.522	14.00
0.0111	690	16.09	51.905	14.00
0.0012	10	120.00	51.947	14.00
0.0057	210	27.14	52.149	14.00
0.0018	150	12.00	52.213	14.00
0.0034	300	11.33	52.336	14.00
0.0089	520	17.12	52.663	14.00
0.0019	60	31.67	52.734	14.00
0.0008	140	5.71	52.764	14.00
0.0065	150	43.33	53.009	14.00
0.0022	160	13.75	53.093	14.00
0.0037	330	11.21	53.235	14.00
0.0143	720	19.86	53.797	14.00
0.0053	140	37.86	54.010	14.00
0.0042	130	32.31	54.181	14.00
0.0022	120	18.33	54.271	14.00
0.0043	290	14.83	50.559	13.00
0.0025	540	4.63	50.655	13.00
0.0027	110	24.55	50.760	13.00
0.0020	140	14.29	50.838	13.00
0.0023	110	20.91	50.928	13.00
0.0024	150	16.00	51.022	13.00
0.0046	340	13.53	51.204	13.00
0.0091	540	16.85	51.569	13.00
0.0020	120	16.67	51.650	13.00
0.0004	200	2.00	51.666	13.00
0.0041	80	51.25	51.834	13.00

0.0018	120	15.00	51.908	13.00
0.0078	310	25.16	52.230	13.00
0.0110	600	18.33	52.693	13.00
0.0080	150	53.33	53.035	13.00
0.0118	680	17.35	53.547	13.00
0.0124	580	21.38	54.095	13.00
0.0025	100	25.00	54.207	13.00
0.0057	250	22.80	54.463	13.00
0.0058	170	34.12	54.726	13.00
0.0063	330	19.09	55.014	13.00
0.0107	430	24.88	55.509	13.00
0.0011	130	8.46	55.560	13.00
0.0054	120	45.00	55.812	13.00
0.0026	150	17.33	55.935	13.00
0.0020	60	33.34	56.029	13.00
0.0077	330	23.33	56.394	13.00
0.0038	110	34.55	56.576	13.00
0.0116	500	23.20	57.135	13.00
0.0008	70	11.43	57.173	13.00
0.0026	100	26.00	57.300	13.00
0.0005	40	12.50	57.324	13.00
0.0069	170	40.59	57.662	13.00
0.0053	120	44.16	62.378	14.00
0.0076	150	50.67	62.784	14.00
0.0091	250	36.40	63.275	14.00
0.0173	480	36.04	64.220	14.00
0.0052	120	43.33	64.508	14.00
0.0037	100	37.00	64.714	14.00
0.0063	190	33.16	65.065	14.00
0.0026	110	23.64	65.211	14.00
0.0084	200	42.00	65.685	14.00
0.0047	160	29.37	65.951	14.00
0.0212	530	40.00	67.170	14.00
0.0088	1190	7.39	67.684	14.00
0.0042	140	30.00	67.931	14.00
0.0094	200	47.00	68.486	14.00
0.0084	220	38.18	68.988	14.00
0.0042	120	35.00	69.240	14.00
0.0009	20	44.99	69.294	14.00
0.0226	560	40.36	70.673	14.00
0.0065	140	46.43	71.025	14.00
0.0020	110	18.18	71.199	14.00
0.0034	59	57.62	71.411	14.00
0.0041	60	68.34	71.669	14.00
0.0060	120	50.00	72.046	14.00
0.0062	170	36.47	72.440	14.00
0.0088	190	46.32	73.007	14.00
0.0298	600	49.67	74.956	14.00
0.0057	110	51.82	75.338	14.00
0.0254	470	53.40	77.056	14.00

con't

0.0132	270	50.74	78.019	14.00
0.0300	520	57.69	80.202	14.00
0.0449	680	66.03	83.685	14.00
0.0504	640	78.75	87.967	14.00
0.0134	170	78.82	87.186	14.00
0.0165	180	91.67	90.738	14.00
0.0190	150	126.43	92.604	14.00
0.0133	160	63.17	93.962	14.00
0.0117	220	93.63	96.229	14.00
0.00607	520	137.11	100.577	14.00
0.00811	60	161.89	103.566	14.00
0.01110	30	295.07	105.298	14.00
0.00053	50	66.00	107.765	14.00
0.00062	30	206.68	103.655	14.00
0.00029	40	96.67	109.076	14.00
0.00058	20	189.95	109.654	14.00
0.00069	40	172.45	110.625	14.00
0.00946	30	153.34	111.565	14.00
0.00987	40	217.54	112.711	14.00
0.00960	50	199.99	113.662	14.00
0.00105	40	264.92	115.385	14.00
0.00042	10	420.31	116.082	14.00
0.00069	50	230.43	117.249	14.00
0.00044	40	109.93	118.006	14.00
0.00057	30	174.52	118.914	14.00
0.00067	20	335.21	120.106	14.00
0.00069	20	344.92	121.359	14.00
0.0208	20	292.11	125.306	14.00
0.00091	30	303.34	127.115	14.00
0.00051	10	310.91	127.743	14.00
0.00062	20	309.93	129.018	14.00
0.0113	30	376.63	131.407	14.00
0.0083	30	276.67	133.216	14.00
0.0109	50	363.36	135.665	14.00
0.0192	40	482.58	140.264	14.00
0.0052	600	155.40	166.651	14.00

Fatigue-Crack Growth Reduced Data

17-4 PH
  H 1050
  R = 0.67
  f = 10 Hz.
  Sine Wave
  Ambient Air

AVA	DN	Da/DN	ΔK	P
0.0005	4000	0.90	8.507	7.00
0.0003	4000	0.08	8.511	7.00
0.0010	4000	0.25	8.515	7.00
0.0013	4000	0.32	8.520	7.00
0.0011	4000	0.28	10.761	9.00
0.0011	4000	0.28	10.762	9.00
0.0048	4000	1.20	10.995	9.00
0.0018	4000	0.45	11.004	7.00
0.0025	4000	0.62	11.018	9.00
0.0016	4000	0.40	11.032	9.00
0.0008	4000	0.20	11.032	9.00
0.0019	4000	0.48	11.044	9.00
0.0016	4000	0.40	11.054	9.00
0.0018	4000	0.45	11.064	9.00
0.0034	4000	0.85	11.085	9.00
0.0033	4000	0.78	11.097	9.00
0.0042	4000	1.05	11.125	9.00
0.0042	4000	1.50	11.170	9.00
0.0012	4000	0.30	11.178	9.00
0.0049	4000	1.22	11.210	9.00
0.0012	4000	0.30	11.218	9.00
0.0015	4000	0.38	11.228	9.00
0.0038	4000	0.95	11.255	9.00
0.0005	4000	0.13	11.256	9.00
0.0006	4000	0.15	11.260	9.00
0.0018	4000	0.45	11.273	9.00
0.0020	8000	0.25	11.287	9.00
0.0010	4000	0.25	11.294	9.00
0.0013	4000	0.33	11.303	9.00
0.0011	4000	0.28	11.310	9.00
0.0018	4000	0.45	11.325	9.00
0.0030	4000	0.75	11.344	9.00
0.0010	4000	0.25	11.351	9.00
0.0020	4000	0.50	11.365	9.00
0.0020	4000	0.50	11.380	7.00

con't

0.0008	4000	0.20	11.385	9.00
0.0034	4000	0.85	11.410	9.00
0.0060	8000	0.75	11.454	9.00
0.0022	8000	0.28	11.470	9.00
0.0021	8000	0.26	11.486	9.00
0.0051	8000	0.64	11.525	9.00
0.0005	8000	0.06	11.529	9.00
0.0075	8000	0.94	11.587	9.00
0.0018	8000	0.23	11.601	9.00
0.0040	8000	0.50	11.633	9.00
0.0016	8000	0.20	11.640	9.00
0.0029	8000	0.36	11.669	9.00
0.0073	8000	0.91	11.728	9.00
0.0046	8000	0.52	11.767	9.00
0.0029	8000	0.36	11.791	9.00
0.0033	8000	0.41	11.819	9.00
0.0055	8000	0.46	11.864	9.00
0.0115	8000	1.44	11.964	9.00
0.0078	8000	0.35	11.989	9.00
0.0018	8000	0.23	12.005	9.00
0.0011	8000	0.14	12.015	9.00
0.0023	8000	0.29	12.035	9.00
0.0027	8000	0.34	12.060	9.00
0.0062	8000	0.28	12.116	9.00
0.0033	8000	0.41	12.142	9.00
0.0023	8000	0.29	12.168	9.00
0.0054	8000	0.67	12.218	9.00
0.0047	8000	0.59	12.263	9.00
0.0041	8000	0.51	12.302	9.00
0.0045	8000	0.56	12.345	9.00
0.0006	8000	0.07	12.351	9.00
0.0079	8000	0.99	12.427	9.00
0.0067	8000	0.84	12.495	9.00
0.0102	8000	1.27	12.595	9.00
0.0026	8000	0.33	12.622	9.00
0.0048	8000	0.60	12.670	9.00
0.0055	8000	0.69	12.727	9.00
0.0041	8000	0.51	12.767	9.00
0.0050	8000	0.63	12.821	9.00
0.0078	8000	0.97	12.903	9.00
0.0043	8000	0.54	12.949	9.00
0.0037	8000	0.46	12.989	9.00
0.0039	8000	0.49	13.030	9.00
0.0061	8000	0.76	13.097	9.00
0.0035	8000	0.44	13.155	9.00
0.0088	8000	1.10	13.251	9.00
0.0047	8000	0.59	13.283	9.00
0.0058	8000	0.73	13.348	9.00
0.0115	8000	1.44	13.428	9.00
0.0072	8000	0.90	13.500	9.00

con't

0.0004	8000	0.64	15.512	9.00
0.0000	4000	1.25	15.700	9.00
0.0001	4000	1.28	15.759	9.00
0.0001	4000	1.60	16.908	11.00
0.0000	4000	1.25	16.980	11.00
0.0115	4000	2.88	17.148	11.00
0.0064	4000	1.60	17.242	11.00
0.0025	4000	1.82	17.353	11.00
0.0048	4000	1.70	17.425	11.00
0.0040	4000	1.00	17.485	11.00
0.0047	4000	1.18	17.555	11.00
0.0126	4000	3.15	17.747	11.00
0.0071	4000	1.77	17.856	11.00
0.0080	4000	2.00	17.929	11.00
0.0073	4000	1.82	18.093	11.00
0.0102	4000	2.55	18.253	11.00
0.0344	4000	8.60	18.805	11.00
0.0115	4000	2.83	18.994	11.00
0.0103	4000	2.57	19.165	11.00
0.0077	4000	1.93	19.295	11.00
0.0102	4000	2.56	19.462	11.00
0.0084	4000	2.10	19.611	11.00
0.0144	4000	3.60	19.861	11.00
0.0104	4000	2.60	20.044	11.00
0.0073	4000	1.84	20.124	11.00
0.0083	4000	2.08	20.323	11.00
0.0132	4000	3.30	20.564	11.00
0.0057	4000	1.42	20.669	11.00
0.0114	4000	2.85	20.881	11.00
0.0121	4000	3.03	21.111	11.00
0.0045	4000	1.12	21.197	11.00
0.0033	4000	0.83	17.595	9.00
0.0084	4000	2.10	17.509	9.00
0.0054	4000	1.35	17.616	9.00
0.0077	4000	1.92	17.742	9.00
0.0091	4000	2.28	17.892	9.00
0.0065	4000	1.63	18.060	9.00
0.0061	4000	1.52	18.104	9.00
0.0082	4000	2.05	18.244	9.00
0.0097	4000	2.42	18.412	9.00
0.0040	4000	1.00	18.483	9.00
0.0082	4000	2.05	18.629	9.00
0.0083	4000	2.02	18.775	9.00
0.0103	4000	2.58	18.965	9.00
0.0065	4000	2.12	19.174	9.00
0.0075	4000	2.38	19.306	9.00
0.0065	4000	1.62	19.452	9.00
0.0098	4000	2.45	19.626	9.00
0.0104	4000	2.60	19.856	9.00
0.0026	4000	2.25	20.005	9.00

con't

0.0103	4000	2.58	20.209	9.00
0.0137	4000	3.42	20.458	9.00
0.0085	4000	2.13	20.728	9.00
0.0091	4000	2.27	20.936	9.00
0.0125	4000	3.13	21.229	9.00
0.0097	4000	2.42	21.464	9.00
0.0137	4000	3.42	21.805	9.00
0.0147	4000	3.43	22.159	9.00
0.0105	4000	2.63	22.459	9.00
0.0154	4000	3.85	22.866	9.00
0.0060	4000	1.50	17.929	7.00
0.0116	4000	2.90	18.287	7.00
0.0101	4000	2.53	18.527	7.00
0.0102	4000	2.55	18.777	7.00
0.0133	4000	3.32	19.115	7.00
0.0118	4000	2.95	19.427	7.00
0.0100	4000	2.50	19.699	7.00
0.0102	4000	2.55	19.986	7.00
0.0095	4000	2.42	20.261	7.00
0.0076	4000	1.90	20.482	7.00
0.0124	4000	3.10	20.868	7.00
0.0147	4000	3.67	21.331	7.00
0.0100	4000	2.50	21.614	7.00
0.0092	8000	0.11	15.496	5.00
0.0118	8000	1.48	15.787	5.00
0.0211	4000	5.28	16.354	5.00
0.0077	4000	1.92	16.543	5.00
0.0120	4000	3.00	16.679	5.00
0.0075	4000	1.87	17.096	5.00
0.0063	4000	1.57	17.282	5.00
0.0082	4000	2.05	17.529	5.00
0.0081	4000	2.03	17.780	5.00
0.0067	4000	1.67	17.993	5.00
0.0075	4000	1.37	18.256	5.00
0.0098	4000	2.45	18.563	5.00
0.0091	4000	2.28	18.825	5.00
0.0122	4000	3.05	19.308	5.00
0.0090	4000	2.25	19.639	5.00
0.0094	4000	2.35	19.994	5.00
0.0124	4000	3.10	20.429	5.00
0.0017	4000	0.43	20.547	5.00
0.0031	4000	0.77	16.532	4.00
0.0069	4000	1.73	16.763	4.00
0.0057	4000	1.57	16.946	4.00
0.0071	4000	1.78	17.188	4.00
0.0060	4000	1.50	17.396	4.00
0.0080	4000	2.00	17.680	4.00
0.0076	4000	1.90	17.958	4.00
0.0122	4000	3.05	18.412	4.00
0.0085	4000	2.12	18.741	4.00

con't

0.0093	4000	2.33	19.110	4.00
0.0082	4000	2.05	19.444	4.00
0.0096	4000	2.40	19.846	4.00
0.0091	4000	2.27	20.238	4.00
0.0091	4000	2.27	20.641	4.00
0.0111	4000	2.77	21.147	4.00
0.0105	4000	2.62	21.642	4.00
0.0141	4000	3.53	22.331	4.00
0.0015	4000	0.38	22.406	4.00
0.0139	4000	3.47	23.117	4.00
0.0158	4000	3.95	23.961	4.00
0.0208	4000	5.20	25.132	4.00
0.0233	4000	5.83	26.529	4.00
0.0191	4000	4.78	27.745	4.00
0.0235	4000	5.87	29.353	4.00
0.0292	4000	7.30	31.455	4.00
0.0782	4000	19.55	38.032	4.00

Fatigue-Crack Growth Reduced Data

17-4 PH
  H 1050
  R = 0.67
  f = 10 Hz.
  Sine Wave
  Ambient Air

AVA	DN	Da/DN	ΔK	P
0.0019	565	3.36	18.606	14.00
0.0051	218	23.39	18.676	14.00
0.0007	305	2.30	18.686	14.00
0.0011	160	6.87	18.701	14.00
0.0013	682	1.91	18.719	14.00
0.0029	160	18.13	18.760	14.00
0.0010	72	13.89	18.774	14.00
0.0014	591	2.37	18.794	14.00
0.0041	842	4.87	18.852	14.00
0.0011	280	3.93	18.868	14.00
0.0011	740	1.49	18.883	14.00
0.0037	260	14.23	18.937	14.00
0.0032	90	35.56	18.984	14.00
0.0005	230	2.17	18.990	14.00
0.0029	640	4.53	19.033	14.00
0.0020	410	4.88	19.063	14.00
0.0024	440	5.45	19.097	14.00
0.0047	790	5.95	19.167	14.00
0.0003	330	0.91	19.171	14.00
0.0051	910	5.60	19.248	14.00
0.0035	370	9.46	19.301	14.00
0.0069	1150	6.00	19.406	14.00
0.0005	40	12.50	19.413	14.00
0.0015	30	50.00	19.437	14.00
0.0014	90	15.56	27.757	20.00
0.0025	110	22.73	27.857	20.00
0.0011	120	9.17	27.877	20.00
0.0005	190	2.63	27.888	20.00
0.0002	580	0.34	27.893	20.00
0.0052	380	13.68	28.009	20.00
0.0031	350	8.86	28.078	20.00
0.0042	650	6.46	28.173	20.00
0.0028	190	14.74	28.237	20.00
0.0018	100	18.00	28.278	20.00
0.0036	590	6.10	28.361	20.00

con't

0.0069	240	5.74	28.352	20.00
0.0040	650	6.15	28.474	20.00
0.0011	180	6.11	28.500	20.00
0.0015	230	6.52	28.535	20.00
0.0018	160	11.25	28.576	20.00
0.0035	1480	2.36	28.658	20.00
0.0102	660	15.45	28.900	20.00
0.0038	810	4.69	28.990	20.00
0.0017	520	3.65	29.036	20.00
0.0078	910	8.57	29.224	20.00
0.0032	360	8.89	29.302	20.00
0.0009	270	3.33	29.324	20.00
0.0034	600	5.67	29.408	20.00
0.0070	780	8.97	29.580	20.00
0.0067	750	8.93	29.747	20.00
0.0045	380	11.84	29.860	20.00
0.0086	1090	7.89	30.077	20.00
0.0035	310	11.29	30.166	20.00
0.0027	230	11.74	30.235	20.00
0.0047	760	6.18	30.355	20.00
0.0044	400	11.00	30.469	20.00
0.0013	270	4.81	30.502	20.00
0.0058	630	9.21	30.654	20.00
0.0057	700	8.14	30.802	20.00
0.0061	1020	5.98	30.963	20.00
0.0046	370	12.43	31.084	20.00
0.0115	1200	9.58	31.391	20.00
0.0032	310	10.32	31.478	20.00
0.0081	630	12.86	31.697	20.00
0.0116	360	32.22	32.014	20.00
0.0017	180	9.45	32.061	20.00
0.0008	330	2.42	32.083	20.00
0.0106	890	11.91	32.372	20.00
0.0061	460	13.26	32.548	20.00
0.0040	770	5.19	32.660	20.00
0.0056	450	12.44	32.818	20.00
0.0093	940	9.89	33.083	20.00
0.0047	410	11.46	33.218	20.00
0.0077	930	8.28	33.439	20.00
0.0036	370	9.73	33.544	20.00
0.0104	990	10.50	33.847	20.00
0.0021	160	13.13	33.909	20.00
0.0024	450	6.86	33.980	20.00
0.0035	160	21.87	34.083	20.00
0.0069	830	8.31	34.288	20.00
0.0071	260	27.31	34.500	20.00
0.0114	1100	10.36	34.845	20.00
0.0057	190	30.00	35.018	20.00
0.0053	400	13.25	35.181	20.00
0.0099	900	11.60	35.482	20.00

con't

0.0051	490	10.41	35.648	20.00
0.0064	730	8.77	35.846	20.00
0.0058	370	15.68	36.030	20.00
0.0072	400	18.75	36.269	20.00
0.0099	770	12.86	36.582	20.00
0.0025	300	8.33	36.668	20.00
0.0059	370	15.95	36.860	20.00
0.0080	620	12.90	37.125	20.00
0.0062	400	15.50	37.329	20.00
0.0011	370	2.97	37.566	20.00
0.0123	730	16.85	37.779	20.00
0.0115	650	17.69	38.175	20.00
0.0110	560	19.64	38.555	20.00
0.0012	460	2.61	38.597	20.00
0.0018	200	9.00	38.660	20.00
0.0098	690	14.20	39.007	20.00
0.0103	680	15.15	39.378	20.00
0.0162	760	21.32	39.974	20.00
0.0010	70	14.28	40.011	20.00
0.0041	220	18.64	40.165	20.00
0.0036	220	16.36	40.300	20.00
0.0025	80	31.25	40.395	20.00
0.0093	680	13.68	40.751	20.00
0.0072	380	18.57	40.953	20.00
0.0007	120	5.83	40.980	20.00
0.0070	310	22.58	41.296	20.00
0.0108	640	16.88	41.687	20.00
0.0058	390	14.87	41.924	20.00
0.0074	350	21.14	42.227	20.00
0.0142	670	21.19	42.824	20.00
0.0095	490	19.39	43.234	20.00
0.0065	230	28.26	43.519	20.00
0.0147	670	21.94	44.179	20.00
0.0053	250	21.20	44.423	20.00
0.0035	230	15.22	44.585	20.00
0.0036	190	18.95	44.763	20.00
0.0069	90	76.66	45.080	20.00
0.0013	160	8.13	45.142	20.00
0.0106	460	23.04	45.656	20.00
0.0011	100	11.00	45.710	20.00
0.0044	150	29.33	45.928	20.00
0.0039	190	20.53	46.123	20.00
0.0114	470	24.26	46.704	20.00
0.0134	570	23.51	47.410	20.00
0.0064	230	27.83	47.755	20.00
0.0009	70	12.86	47.804	20.00
0.0036	70	51.42	48.001	20.00
0.0036	130	27.69	48.200	20.00
0.0052	160	32.50	48.491	20.00
0.0055	160	34.37	48.804	20.00

con't

0.0144	590	24.41	49.645	20.00
0.0043	107	40.19	49.902	20.00
0.0011	33	33.33	49.969	20.00
0.0006	7	85.67	50.005	20.00
0.0002	17	11.76	50.017	20.00
0.0002	19	10.53	50.029	20.00
0.0008	7	114.23	50.078	20.00
0.0039	67	58.21	50.316	20.00
0.0006	33	18.19	50.353	20.00
0.0030	29	103.42	50.538	20.00
0.0006	10	60.03	50.575	20.00
0.0002	9	22.21	50.588	20.00
0.0003	24	12.50	50.606	20.00
0.0005	27	18.52	50.637	20.00
0.0038	141	26.95	50.876	20.00
0.0010	80	12.50	50.939	20.00
0.0050	70	71.44	51.257	20.00
0.0269	630	42.70	53.049	20.00
0.0052	80	65.00	53.412	20.00
0.0856	10	200.00	60.285	20.00

Fatigue-Crack Growth Reduced Data

17-4 PH
 H 1100
 R = 0.05
 f = 10 Hz.
 Sine Wave
 Ambient Air

AVA	DN	Da/DN	ΔK	P
0.0525	90000	0.69	24.248	7.00
0.0118	4000	2.95	24.377	7.00
0.0045	4000	1.12	24.429	7.00
0.0004	4000	0.10	24.433	7.00
0.0074	4000	1.85	24.521	7.00
0.0021	4000	0.53	24.546	7.00
0.0056	4000	1.40	24.616	7.00
0.0039	4000	0.97	24.665	7.00
0.0025	4000	0.62	24.697	7.00
0.0096	4000	2.40	24.824	7.00
0.0005	4000	0.13	24.831	7.00
0.0062	4000	1.55	21.356	6.00
0.0043	4000	1.07	21.408	6.00
0.0020	4000	0.50	21.432	6.00
0.0025	4000	0.62	21.463	6.00
0.0117	4000	2.93	21.610	6.00
0.0016	4000	0.40	21.631	6.00
0.0032	4000	0.80	21.673	6.00
0.0030	4000	0.75	21.713	6.00
0.0066	4000	1.65	21.801	6.00
0.0063	4000	1.57	21.888	6.00
0.0052	4000	1.30	21.961	6.00
0.0072	4000	1.80	22.064	6.00
0.0088	4000	2.20	22.193	6.00
0.0048	4000	1.20	22.264	6.00
0.0086	4000	2.15	22.396	6.00
0.0055	4000	1.37	22.481	6.00
0.0072	4000	1.80	22.595	6.00
0.0074	4000	1.85	22.715	6.00
0.0055	4000	1.37	22.805	6.00
0.0141	4000	3.53	23.042	6.00
0.0064	4000	1.60	23.152	6.00
0.0098	4000	2.45	23.324	6.00
0.0080	4000	2.00	23.467	6.00

0.0112	4000	2.80	23.671	6.00
0.0103	4000	2.57	23.863	6.00
0.0122	4000	3.05	24.095	6.00
0.0081	4000	2.02	24.252	6.00
0.0168	4000	4.20	24.583	6.00
0.0072	4000	1.80	24.728	6.00
0.0090	4000	2.25	24.912	6.00
0.0129	4000	3.22	25.179	6.00
0.0109	4000	2.72	25.408	6.00
0.0095	4000	2.38	25.611	6.00
0.0132	4000	3.30	25.897	6.00
0.0129	4000	3.22	26.180	6.00
0.0159	4000	3.98	26.536	6.00
0.0090	4000	2.25	26.740	6.00
0.0166	4000	4.15	22.602	5.00
0.0037	4000	0.92	22.674	5.00
0.0048	4000	1.20	22.767	5.00
0.0059	4000	1.48	22.883	5.00
0.0085	4000	2.12	23.050	5.00
0.0101	4000	2.53	23.252	5.00
0.0074	4000	1.85	23.400	5.00
0.0101	4000	2.53	23.605	5.00
0.0078	4000	1.95	23.764	5.00
0.0178	4000	4.45	24.133	5.00
0.0109	4000	2.72	24.362	5.00
0.0090	4000	2.25	24.553	5.00
0.0114	4000	2.85	24.797	5.00
0.0139	4000	3.47	25.100	5.00
0.0222	4000	5.55	25.591	5.00
0.0085	4000	2.13	25.783	5.00
0.0116	4000	2.90	26.047	5.00
0.0160	4000	4.00	26.418	5.00
0.0185	4000	4.62	26.856	5.00
0.0131	4000	3.28	27.173	5.00
0.0133	4000	3.32	27.500	5.00
0.0183	4000	4.57	27.961	5.00
0.0174	4000	4.35	28.411	5.00
0.0168	4000	4.20	28.858	5.00
0.0177	4000	4.42	29.343	5.00
0.0257	4000	6.43	30.075	5.00
0.0208	4000	5.20	30.696	5.00
0.0255	4000	6.37	31.494	5.00
0.0250	4000	6.25	32.321	5.00
0.0260	4000	6.50	33.235	5.00
0.0310	4000	7.75	34.405	5.00
0.0372	4000	9.30	35.941	5.00
0.0432	4000	10.80	37.938	5.00
0.0426	4000	10.65	40.170	5.00
0.0512	4000	12.80	43.264	5.00
0.0679	4000	16.97	48.208	5.00
0.0997	4000	24.92	57.683	5.00
0.0832	2000	41.60	68.188	5.00
0.2979	2340	127.32	135.796	5.00

Fatigue-Crack Growth Reduced Data

17-4 PH

  H 1100

  R = 0.05

  One Minute Hold-Time

  Salt Water

ΔK	Da/DN
30.61	6.40
31.08	8.53
31.59	7.41
32.07	10.78
37.86	15.86
38.66	13.49
39.28	16.56
39.92	25.77
40.75	17.29
46.32	16.77
47.33	21.87
48.23	16.07
49.41	23.14
51.51	23.38
68.08	66.56
70.65	31.66
73.14	49.39
76.77	76.78
80.97	24.91
86.12	85.85
92.41	184.68
97.73	91.52
103.2	226.7
108.6	213.3
115.9	290.9

Fatigue-Crack Growth Reduced Data

17-4 PH
  H 1100
  R = 0.67
  f = 10 Hz.
  Sine Wave
  Ambient Air

AVA	DN	Da/DN	ΔK	P
0.0085	3000	1.11		
0.0160	8000	2.04	15.960	13.00
0.0002	4000	0.17		
0.0006	4000	0.26	15.977	
0.5040	4000	1.00	16.037	13.00
0.0031	4000	0.27	16.058	13.00
0.0003	4000	0.50	16.088	13.00
0.0101	4000		16.121	13.00
	4000	1.29	16.203	15.00
	4000	0.20	16.237	13.00
0.0041	4000	1.05	16.278	13.00
	9000		16.500	
	9000		16.471	
0.0102	8000		16.785	
	8000			
	8000		16.960	
	8000			
			17.100	
			17.054	
	8000		17.823	
	8000			
	8000			
	8000			
0.0188			18.250	
			18.407	
			18.7003	
			19.175	
			19.761	

con't

0.0238	8000	2.98	20.774	13.00
0.0285	8000	3.56	21.290	13.00
0.0177	8000	2.21	21.618	13.00
0.0231	8000	2.89	22.054	13.00
0.0252	8000	3.15	22.543	13.00
0.0301	8000	3.76	23.144	13.00
0.0293	8000	3.66	23.748	13.00
0.0332	8000	4.15	24.460	13.00
0.0148	4000	3.70	24.785	13.00
0.0185	4000	4.62	25.207	13.00
0.0195	4000	4.88	25.662	13.00
0.0252	4000	6.30	26.272	13.00
0.0155	4000	3.88	26.661	13.00
0.0240	4000	6.09	27.285	13.00
0.0266	4000	6.65	28.012	13.00
0.0249	4000	6.23	28.732	13.00
0.0272	4000	6.80	29.366	13.00
0.0315	4000	7.87	30.603	13.00
0.0351	4000	8.77	31.862	13.00
0.0354	4000	8.85	33.260	13.00
0.0000	4000	0.00	33.260	13.00
0.0000	4000	0.00	25.585	10.00
0.0059	4000	1.47	25.774	10.00
0.0353	4000	8.83	26.981	10.00
0.0325	4000	8.12	28.210	10.00
0.0306	4000	7.65	29.483	10.00
0.0332	4000	8.30	31.009	10.00
0.0374	4000	9.35	32.928	10.00
0.0230	4000	5.75	34.226	10.00
0.0265	4000	6.62	28.675	8.00
0.0288	4000	7.20	30.209	8.00
0.0347	4000	8.68	32.251	8.00
0.0429	4000	10.73	35.102	8.00
0.0524	4000	13.10	39.135	8.00
0.1200	2000	60.00	51.136	8.00

Fatigue-Crack Growth Reduced Data

17-4 PH
H 1100
R = 0.05
One Minute Hold-Time
Ambient Air

AVA	DN	Da/DN	ΔK	P
0.3013	340	8.13	23.134	7.00
0.0012	370	4.44	24.208	7.00
0.0013	320	4.06	24.223	7.00
0.0007	130	5.38	31.155	9.00
0.0107	570	18.77	48.571	14.00
0.0048	410	11.71	34.896	16.00
0.0004	440	9.13	45.402	13.00
0.0037	550	6.98	45.543	13.00
0.0013	170	7.80	45.573	13.00
0.0025	270	8.62	45.634	13.00
0.0048	560	16.11	45.780	13.00
0.0064	570	11.23	45.744	13.00
0.0043	310	14.31	46.052	13.00
0.0052	150	16.84	46.143	13.00
0.0050	530	15.43	46.208	13.00
0.0056	620	9.03	46.433	13.00
0.0005	110	4.55	46.447	13.00
0.0039	170	24.17	53.487	15.00
0.0020	250	8.00	53.263	15.00
0.0045	360	12.90	50.308	14.00
0.0062	610	15.90	50.422	14.00
0.0123	1250	9.84	50.812	14.00
0.0042	240	12.90	50.951	14.00
0.0028	420	25.43	51.283	14.00
0.0023	650	11.69	51.536	14.00
0.0032	500	16.40	51.678	14.00
0.0037	250	14.80	51.561	14.00
0.0070	540	15.26	52.218	14.00
0.0036	260	13.15	52.452	14.00
0.0055	240	22.50	52.559	14.00
0.0153	870	18.65	53.173	14.00
0.0050	350	14.25	53.521	14.00
0.0045	530	11.84	53.571	14.00
0.0153	830	19.64	54.759	14.00
0.0153	630	21.11	54.800	14.00

con't

0.0069	680	10.15	55.098	14.00
0.0194	1250	15.52	55.954	14.00
0.0111	650	17.08	56.456	14.00
0.0184	760	24.21	57.310	14.00
0.0070	360	19.44	57.641	14.00
0.0278	1080	25.74	58.988	14.00
0.0155	620	25.00	59.761	14.00
0.0173	560	30.89	60.640	14.00
0.0130	670	18.84	61.314	14.00
0.0305	950	32.11	62.932	14.00
0.0147	510	28.82	63.731	14.00
0.0498	700	21.14	66.527	14.00
0.0334	1920	17.40	68.482	14.00
0.0225	375	60.00	69.837	14.00
0.0406	1090	37.25	72.368	14.00
0.0399	940	42.45	74.979	14.00
0.0386	730	52.05	77.599	14.00
0.0254	430	59.07	79.436	14.00
0.0641	970	66.08	84.450	14.00
0.0382	460	84.13	87.801	14.00
0.0052	580	8.97	42.283	4.50
0.0016	140	11.42	42.396	4.50
0.0033	160	20.63	42.629	4.50
0.0015	210	7.14	42.736	4.50
0.0033	240	13.75	42.972	4.50
0.0006	110	5.45	43.016	4.50
0.0045	540	8.33	43.343	4.50
0.0069	400	17.25	43.854	4.50
0.0051	510	10.00	44.239	4.50
0.0086	510	16.86	44.903	4.50
0.0017	129	13.17	45.795	4.50
0.0007	60	11.67	45.851	4.50
0.0094	580	16.21	46.626	4.50
0.0019	80	23.75	46.786	4.50
0.0007	70	10.00	46.844	4.50
0.0018	80	22.51	46.992	4.50
0.0009	50	17.99	47.073	4.50
0.0011	50	22.01	47.167	4.50
0.0005	10	49.97	47.210	4.50
0.0019	90	21.11	47.373	4.50
0.0008	60	13.34	47.441	4.50
0.0011	100	11.01	47.536	4.50
0.0098	540	18.15	48.397	4.50
0.0009	50	17.99	48.478	4.50
0.0009	80	11.25	48.558	4.50
0.0031	140	22.15	48.838	4.50
0.1542	315	489.00	166.600	10.20

Fatigue-Crack Growth Reduced Data

15-5 PH

H 1100

R = 0.05

One Minute Hold-Time

Salt Water

ΔK	Da/DN
30.34	14.67
30.93	15.29
31.64	18.15
32.34	13.91
32.89	13.34
33.32	16.84
33.97	18.40
34.63	15.35
40.66	30.06
41.49	29.13
42.63	28.07
43.??	27.71
44.75	32.78
45.91	41.85
46.91	26.74
53.40	42.43
54.94	33.86
56.73	48.36
58.82	44.90
61.38	48.33
64.25	49.41
68.22	70.7?
72.09	58.63
75.46	100.0
81.30	72.67
88.32	111.7
95.28	124.0
101.0	208.3
108.0	162.1
122.9	298.1
139.4	326.9
147.1	361.1

Fatigue-Crack Growth Reduced Data

15-5 PH
  H 1100
  R = 0.05
  f = 10 Hz.
  Sine Wave
  Ambient Air

AVA	DN	Da/DN	ΔK	P
0.0035	8000	0.44	25.149	7.00
0.0126	8000	1.57	25.299	7.00
0.0230	8000	2.88	25.603	7.00
0.0242	8000	3.02	25.966	7.00
0.0303	8000	3.79	26.480	7.00
0.0315	8000	3.94	27.082	7.00
0.0420	8000	5.25	27.983	7.00
0.0384	8000	4.80	28.896	7.00
0.0460	8000	5.75	30.090	7.00
0.0486	8000	6.08	31.454	7.00
0.0649	8000	8.11	33.419	7.00
0.0609	8000	7.61	35.400	7.00
0.2684	8000	33.55	61.409	9.00
0.0739	2000	36.95	67.329	9.00
0.0911	2000	45.55	76.739	9.00
0.1601	2000	80.05	102.212	9.00
0.1509	1000	150.90	143.022	9.00
0.0083	20	415.22	145.917	9.00
0.0085	20	424.91	148.965	9.00
0.0098	20	489.89	152.580	9.00
0.0090	20	450.24	156.005	9.00
0.0088	20	439.93	159.450	9.00
0.0164	20	819.79	166.129	9.00

Fatigue-Crack Growth Reduced Data

15-5 PH
  H 1050
  R = 0.67
  One Minute Hold-Time
  Ambient Air

AVA	DN	Da/DN	ΔK	P
0.0041	640	6.41	28.066	20.00
0.0020	220	9.09	28.112	20.00
0.0034	150	22.67	28.192	20.00
0.0016	420	3.81	28.230	20.00
0.0097	660	14.70	28.462	20.00
0.0051	740	6.89	28.586	20.00
0.0086	770	11.17	28.798	20.00
0.0038	450	8.44	28.893	20.00
0.0095	940	10.11	29.133	20.00
0.0016	220	7.27	29.174	20.00
0.0026	260	10.00	29.241	20.00
0.0077	820	9.39	29.440	20.00
0.0042	620	6.77	29.550	20.00
0.0070	650	10.77	29.736	20.00
0.0029	330	8.79	29.813	20.00
0.0051	530	9.62	29.950	20.00
0.0046	550	8.36	30.074	20.00
0.0052	250	20.80	30.216	20.00
0.0034	450	7.56	30.310	20.00
0.0069	680	10.15	30.500	20.00
0.0047	360	13.06	30.632	20.00
0.0129	1360	9.49	30.996	20.00
0.0106	1240	8.55	31.301	20.00
0.0067	570	11.75	31.496	20.00
0.0095	830	11.45	31.775	20.00
0.0023	260	8.85	31.843	20.00
0.0120	930	12.90	32.202	20.00
0.0047	370	12.70	32.344	20.00
0.0120	990	12.12	32.709	20.00
0.0018	160	11.25	32.765	20.00
0.0029	350	8.29	32.854	20.00
0.0056	160	35.00	33.027	20.00
0.0098	830	11.81	33.333	20.00
0.0018	260	6.92	33.390	20.00
0.0148	1100	13.45	33.860	20.00

con't

0.0022	190	11.58	33.930	20.00
0.0063	400	15.75	34.133	20.00
0.0103	900	11.44	34.467	20.00
0.0068	490	13.88	34.690	20.00
0.0090	730	12.33	34.988	20.00
0.0016	370	4.32	35.041	20.00
0.0092	400	23.00	35.348	20.00
0.0063	770	8.18	35.561	20.00
0.0056	300	18.67	35.751	20.00
0.0032	370	8.65	35.860	20.00
0.0077	620	12.42	36.125	20.00
0.0036	400	9.00	36.249	20.00
0.0047	370	12.70	36.413	20.00
0.0094	730	12.88	36.742	20.00
0.0073	700	10.43	37.000	20.00
0.0064	510	12.55	37.228	20.00
0.0053	460	11.52	37.419	20.00
0.0033	200	16.50	37.538	20.00
0.0072	690	10.43	37.800	20.00
0.0085	680	12.50	38.112	20.00
0.0128	760	16.84	38.589	20.00
0.0024	290	8.28	38.680	20.00
0.0056	300	18.67	38.892	20.00
0.0079	680	11.62	39.195	20.00
0.0056	280	20.00	39.411	20.00
0.0016	120	13.33	39.473	20.00
0.0069	310	22.26	39.743	20.00
0.0097	640	15.16	40.127	20.00
0.0063	390	16.15	40.386	20.00
0.0059	350	16.86	40.619	20.00
0.0114	670	17.02	41.088	20.00
0.0066	490	13.47	41.364	20.00
0.0053	230	23.04	41.588	20.00
0.0122	670	18.21	42.112	20.00
0.0041	250	16.40	42.291	20.00
0.0049	230	21.30	42.507	20.00
0.0047	190	24.74	42.716	20.00
0.0015	90	16.66	42.783	20.00
0.0031	160	19.38	42.922	20.00
0.0070	460	15.22	43.240	20.00
0.0034	100	34.00	43.396	20.00
0.0022	150	14.67	43.497	20.00
0.0042	190	22.11	43.693	20.00
0.0127	470	27.02	44.294	20.00
0.0119	570	20.88	44.873	20.00
0.0062	230	26.96	45.181	20.00
0.0065	200	32.50	45.484	20.00
0.0014	160	8.75	45.555	20.00
0.0031	160	19.37	45.713	20.00
0.0159	590	26.95	46.046	20.00

con't

0.0026	183	14.71	46.686	20.00
0.0087	206	42.23	47.159	20.00
0.0014	141	9.95	47.236	20.00
0.0031	150	20.67	47.408	20.00
0.0161	630	25.56	48.324	20.00
0.0063	230	27.39	48.694	20.00
0.0222	930	23.87	50.050	20.00
0.0166	420	39.52	51.122	20.00
0.0224	650	34.46	52.657	20.00
0.0064	220	29.09	53.115	20.00
0.0082	220	37.27	53.715	20.00
0.0474	990	47.88	57.513	20.00
0.0245	370	66.22	59.720	20.00
0.0146	70	208.55	61.124	20.00
0.0117	150	78.00	62.301	20.00

Fatigue-Crack Growth Reduced Data

15-5 PH

H 1100

R = 0.67

One Minute Hold-Time

Ambient Air

AVA	DN	Da/DN	ΔK	P
0.0011	70	29.00	29.695	20.00
0.0048	70	68.57	29.871	20.00
0.0042	420	10.00	29.932	20.00
0.0074	660	11.21	30.129	20.00
0.0100	740	13.51	30.398	20.00
0.0066	770	8.57	30.578	20.00
0.0071	450	15.78	30.773	20.00
0.0108	940	11.49	31.073	20.00
0.0045	220	20.45	31.199	20.00
0.0025	260	9.62	31.270	20.00
0.0116	820	14.15	31.600	20.00
0.0090	620	14.52	31.859	20.00
0.0085	650	13.08	32.106	20.00
0.0042	330	12.73	32.229	20.00
0.0070	530	13.21	32.435	20.00
0.0079	550	14.36	32.670	20.00
0.0038	250	15.20	32.783	20.00
0.0068	450	15.11	32.988	20.00
0.0102	680	15.00	33.298	20.00
0.0051	460	11.09	33.454	20.00
0.0181	1260	14.37	34.014	20.00
0.0189	1230	15.37	34.612	20.00
0.0084	580	14.48	34.881	20.00
0.0153	830	18.43	35.378	20.00
0.0050	330	15.15	35.542	20.00
0.0106	700	15.14	35.893	20.00
0.0085	910	9.34	36.178	20.00
0.0060	360	16.67	36.380	20.00
0.0146	270	54.07	36.880	20.00
0.0122	600	20.33	37.304	20.00
0.0097	780	12.44	37.646	20.00
0.0144	750	19.20	38.162	20.00
0.0066	380	17.37	38.401	20.00
0.0176	1090	16.15	39.052	20.00

con't

0.0067	310	21.61	39.505	20.00
0.0044	250	17.60	39.472	20.00
0.0129	740	17.43	39.968	20.00
0.0091	400	22.75	40.325	20.00
0.0059	270	21.85	40.560	20.00
0.0125	630	19.84	41.064	20.00
0.0186	700	26.57	41.836	20.00
0.0171	1020	16.76	42.570	20.00
0.0122	370	32.97	43.110	20.00
0.0267	1200	22.25	44.343	20.00
0.0076	310	24.52	44.707	20.00
0.0193	630	30.63	45.663	20.00
0.0306	360	85.00	47.274	20.00
0.0066	180	36.67	47.639	20.00
0.0090	330	27.27	48.147	20.00
0.0283	890	31.80	49.829	20.00
0.0205	460	44.56	51.135	20.00
0.0290	770	37.66	53.124	20.00
0.0172	450	38.22	54.390	20.00
0.0486	940	51.70	58.361	20.00

Fatigue-Crack Growth Reduced Data

15-5 PH
  H 1100
  R = 0.67
  One Minute Hold-Time
  Salt Water

ΔK	Da/DN
23.99	16.63
25.20	30.20
25.53	23.81
25.81	17.98
26.28	16.33
27.43	24.75
27.94	25.57
25.74	17.69
26.43	20.87
27.32	21.85
28.16	28.42
28.80	23.62
29.89	30.42
31.39	29.89
32.97	31.00
38.31	52.49
39.95	56.26
42.11	42.41
44.61	75.80

Fatigue-Crack Growth Reduced Data

15-5 PH
 H 1100
 R = 0.05
 One Minute Hold-Time
 Ambient Air

AVA	DN	Da/DN	ΔK	P
0.0031	10	110.00	24.399	7.00
0.0017	10	120.00	24.418	7.00
0.0005	10	50.00	24.424	7.00
0.0009	150	6.00	31.416	9.00
0.0008	100	8.00	31.428	9.00
0.0016	290	5.52	41.936	12.00
0.0005	30	16.67	48.937	14.00
0.0007	10	70.00	48.953	14.00
0.0008	10	79.99	48.972	14.00
0.0035	40	87.50	49.056	14.00
0.0034	20	170.00	49.139	14.00
0.0026	150	17.33	49.204	14.00
0.0002	270	0.74	49.209	14.00
0.0003	10	30.00	49.216	14.00
0.0009	10	89.99	35.171	10.00
0.0016	190	8.42	35.199	10.00
0.0032	420	7.62	42.309	12.00
0.0013	60	21.67	45.866	13.00
0.0007	120	5.83	45.883	13.00
0.0016	60	26.67	45.922	13.00
0.0002	120	1.67	45.926	13.00
0.0007	60	11.67	45.943	13.00
0.0014	120	11.67	45.978	13.00
0.0002	60	3.33	45.982	13.00
0.0020	140	14.29	46.032	13.00
0.0018	120	15.00	46.076	13.00
0.0010	180	5.56	46.101	13.00
0.0008	120	6.67	46.121	13.00
0.0010	120	8.33	46.147	13.00
0.0012	270	4.44	46.177	13.00
0.0010	180	5.56	46.202	13.00
0.0008	60	13.33	46.223	13.00
0.0002	70	2.86	46.228	13.00
0.0042	1010	4.16	46.336	13.00
0.0019	140	13.57	46.386	13.00

0.0003	240	1.25	46.394	13.00
0.0003	120	2.50	46.402	13.00
0.0001	120	0.83	46.404	13.00
0.0036	220	16.36	46.500	13.00
0.0008	120	6.67	46.521	13.00
0.0007	200	3.50	53.700	15.00
0.0013	550	2.36	53.740	15.00
0.0039	60	65.00	53.863	15.00
0.0002	150	1.33	50.278	14.00
0.0007	30	23.33	50.299	14.00
0.0007	130	5.38	50.320	14.00
0.0022	230	9.57	50.385	14.00
0.0014	310	4.52	50.427	14.00
0.0009	160	5.63	50.454	14.00
0.0044	650	6.77	50.589	14.00
0.0087	470	18.51	50.860	14.00
0.0023	350	6.57	50.933	14.00
0.0083	610	13.61	51.202	14.00
0.0038	280	13.57	51.328	14.00
0.0051	250	20.40	51.498	14.00
0.0007	60	11.67	51.522	14.00
0.0111	690	16.09	51.905	14.00
0.0012	10	120.00	51.947	14.00
0.0057	210	27.14	52.149	14.00
0.0018	150	12.00	52.213	14.00
0.0034	300	11.33	52.336	14.00
0.0089	520	17.12	52.663	14.00
0.0019	60	31.67	52.734	14.00
0.0008	140	5.71	52.764	14.00
0.0065	150	43.33	53.009	14.00
0.0022	160	13.75	53.093	14.00
0.0037	330	11.21	53.235	14.00
0.0143	720	19.86	53.797	14.00
0.0053	140	37.86	54.010	14.00
0.0042	130	32.31	54.181	14.00
0.0022	120	18.33	54.271	14.00
0.0043	290	14.83	50.559	13.00
0.0025	540	4.63	50.655	13.00
0.0027	110	24.55	50.760	13.00
0.0020	140	14.29	50.838	13.00
0.0023	110	20.91	50.928	13.00
0.0024	150	16.00	51.022	13.00
0.0046	340	13.53	51.204	13.00
0.0091	540	16.85	51.569	13.00
0.0020	120	16.67	51.650	13.00
0.0004	200	2.00	51.666	13.00
0.0041	80	51.25	51.834	13.00
0.0018	120	15.00	51.908	13.00
0.0078	310	25.16	52.230	13.00
0.0110	600	18.33	52.693	13.00

con't

0.0080	150	53.33	53.035	13.00
0.0118	680	17.35	53.547	13.00
0.0124	580	21.38	54.095	13.00
0.0025	100	25.00	54.207	13.00
0.0057	250	22.80	54.463	13.00
0.0058	170	34.12	54.726	13.00
0.0063	330	19.09	55.014	13.00
0.0107	430	24.88	55.509	13.00
0.0011	130	8.46	55.560	13.00
0.0054	120	45.00	55.812	13.00
0.0026	150	17.33	55.935	13.00
0.0020	60	33.34	56.029	13.00
0.0077	330	23.33	56.394	13.00
0.0038	110	34.55	56.576	13.00
0.0116	500	23.20	57.135	13.00
0.0008	70	11.43	57.173	13.00
0.0026	100	26.00	57.300	13.00
0.0005	40	12.50	57.324	13.00
0.0069	170	40.59	57.662	13.00
0.0053	120	44.16	62.378	14.00
0.0076	150	50.67	62.784	14.00
0.0091	250	36.40	63.275	14.00
0.0173	480	36.04	64.220	14.00
0.0052	120	43.33	64.508	14.00
0.0037	100	37.00	64.714	14.00
0.0063	190	33.16	65.065	14.00
0.0026	110	23.64	65.211	14.00
0.0084	200	42.00	65.685	14.00
0.0047	160	29.37	65.951	14.00
0.0212	530	40.00	67.170	14.00
0.0088	1190	7.39	67.684	14.00
0.0042	140	30.00	67.931	14.00
0.0094	200	47.00	68.486	14.00
0.0084	220	38.18	68.988	14.00
0.0042	120	35.00	69.240	14.00
0.0009	20	44.99	69.294	14.00
0.0226	560	40.36	70.673	14.00
0.0065	140	46.43	71.075	14.00
0.0020	110	18.18	71.199	14.00
0.0034	59	57.62	71.411	14.00
0.0041	60	68.34	71.669	14.00
0.0060	120	50.00	72.046	14.00
0.0062	170	36.47	72.440	14.00
0.0088	190	46.32	73.003	14.00
0.0298	600	49.67	74.956	14.00
0.0057	110	51.82	75.338	14.00
0.0251	470	53.40	77.056	14.00
0.0137	270	50.74	78.019	14.00
0.0300	520	57.69	80.202	14.00
0.0449	680	66.03	83.683	14.00

con't

0.0504	640	78.75	87.967	14.00
0.0134	170	78.82	89.186	14.00
0.0165	180	91.67	90.738	14.00
0.0190	150	126.66	92.604	14.00
0.0133	160	83.12	93.962	14.00
0.0217	220	98.64	96.279	14.00
0.0687	520	132.12	104.577	14.00
0.0081	50	161.99	105.666	14.00
0.0118	40	295.05	107.298	14.00
0.0033	50	66.00	107.765	14.00
0.0062	30	206.68	108.655	14.00
0.0029	30	96.67	109.076	14.00
0.0038	20	189.96	109.634	14.00
0.0069	40	172.46	110.665	14.00
0.0046	30	153.34	111.363	14.00
0.0087	40	217.54	112.711	14.00
0.0060	30	199.99	113.662	14.00
0.0106	40	264.95	115.385	14.00
0.0042	10	420.23	116.082	14.00
0.0069	30	230.00	117.249	14.00
0.0044	40	109.98	118.006	14.00
0.0052	30	173.32	118.914	14.00
0.0067	20	335.21	120.106	14.00
0.0069	20	344.92	121.359	11.00
0.0208	70	297.11	125.306	14.00
0.0091	30	303.34	127.115	14.00
0.0031	10	310.21	127.743	14.00
0.0062	20	309.93	129.018	14.00
0.0113	30	376.68	131.407	14.00
0.0083	30	276.67	133.216	14.00
0.0109	30	363.36	135.665	14.00
0.0195	40	487.58	140.264	14.00

Fatigue-Crack Growth Reduced Data

15-5 PH
  H 1050
  R = 0.05
  f = 10 Hz.
  Sine Wave
  Ambient Air

AVA	DN	Da/DN	ΔK	P
0.0134	8000	1.67	24.932	7.00
0.0182	8000	2.27	25.159	7.00
0.0138	8000	1.72	25.347	7.00
0.0222	8000	2.77	25.676	7.00
0.0212	8000	2.65	26.022	7.00
0.0323	8000	4.04	26.605	7.00
0.0321	8000	4.01	27.247	7.00
0.0356	8000	4.45	28.027	7.00
0.0464	8000	5.80	29.139	7.00
0.0532	8000	6.65	30.532	7.00
0.0591	8000	7.39	32.206	7.00
0.0652	8000	8.15	34.191	7.00
0.0833	8000	10.41	36.940	7.00
0.0910	8000	11.37	40.287	7.00
0.1223	8000	15.29	45.701	7.00
0.1844	8000	23.05	57.821	7.00
0.3680	5500	66.91	119.729	7.00
0.1771	290	610.70	172.000	7.00